

**Universidade de Brasília
Faculdade de Tecnologia
Departamento de Engenharia Mecânica**

**Development of a Robotic Additive
Manufacturing Cell Based on Laser Metal
Deposition Using Wire**

Brayan Stiven Figueroa Betancourth

DISSERTAÇÃO DE MESTRADO
PROGRAMA DE PÓS-GRADUAÇÃO EM SISTEMAS MECATRÔNICOS

Brasília
2025

**Universidade de Brasília
Faculdade de Tecnologia
Departamento de Engenharia Mecânica**

Desenvolvimento de uma Célula de Manufatura Aditiva Robotizada Baseada na Deposição de Metal a Laser Usando Arame

Brayan Stiven Figueroa Betancourth

Dissertação de Mestrado submetida ao Departamento de Engenharia Mecânica da Universidade Brasília como parte dos requisitos necessários para a obtenção do grau de Mestre

Orientador: Prof. Dr. Alberto José Alvares

Brasília
2025

F769d Figueroa Betancourth, Brayan Stiven.
Development of a Robotic Additive Manufacturing Cell Based
on Laser Metal Deposition Using Wire / Brayan Stiven Figueroa
Betancourth; orientador Alberto José Alvares. -- Brasília, 2025.
154 p.

Dissertação de Mestrado (Programa de Pós-Graduação em
Sistemas Mecatrônicos) -- Universidade de Brasília, 2025.

1. Célula de Manufatura Aditiva. 2. Robôs. 3. Deposição de
Metal à Laser. 4. Gêmeo Digital. I. Alvares, Alberto José, orient.
II. Título

**Universidade de Brasília
Faculdade de Tecnologia
Departamento de Engenharia Mecânica**

**Development of a Robotic Additive Manufacturing Cell
Based on Laser Metal Deposition Using Wire**

Brayan Stiven Figueroa Betancourth

Dissertação de Mestrado submetida ao Departamento de Engenharia Mecânica da Universidade Brasília como parte dos requisitos necessários para a obtenção do grau de Mestre

Trabalho aprovado. Brasília, 27 de Julho de 2025:

Prof. Dr. Alberto José Alvares,
UnB/FT/ENM
Orientador

Prof. Dr. Maksym Ziberov,
UnB/FT/ENM
Examinador interno

Prof. Dr. Rodrigo Santiago Coelho,
SENAI CIMATEC/FT
Examinador externo

Brasília
2025

*This work is dedicated to my mother Luz Marina,
my brothers Diego Orlando, Jhon Jairo, and José Julián.
They have given me unconditional support and motivation
in my education and life project.*

Acknowledgements

I primarily thank my family for their unwavering support, encouragement, and understanding throughout the development of this endeavor.

I deeply thank Professor Alberto Alvares for the invaluable guidance provided during the development of this work.

I am grateful to the Postgraduate Program in Mechatronic Systems at the University of Brasília for offering the necessary conditions for the elaboration of this work.

I thank the Coordenação de Aperfeiçoamento de Pessoal de Nível Superior (CAPES) for awarding the master's scholarship.

I am grateful to the Fundação de Apoio à Pesquisa do Distrito Federal (FAPDF) and the Conselho Nacional de Desenvolvimento Científico e Tecnológico (CNPq) for funding the development of this project.

*“Science is the highest pursuit of
human intellect, the relentless
quest for truth that defines our
progress and shapes our destiny.”
(Brayan S. Figueroa)*

Abstract

In modern manufacturing, the integration of technologies such as Digital Twin (DT) and Additive Manufacturing (AM) is essential for optimizing production and process efficiency. Wire-Based Laser Metal Deposition (LMD-Wire) offers advantages such as flexibility in producing complex parts and cost reduction, but challenges like operation simulation, fault detection, and optimizing the lifespan of parts still limit its adoption. This study proposes the development of a Robotic Additive Manufacturing Cell (RAMC) using LMD-Wire, integrated with a CAD/CAPP/CAM system based on Digital Twins, in accordance with ISO 23247, ensuring interoperability across digital manufacturing levels. The RAMC physically integrates components such as the metal cell, the KUKA KR70 R2100 robot, and the MELTIO Engine, logically coordinating them to optimize workflow and ensure precise execution of operations. The CAD/CAPP/CAM systems in the RAMC are crucial for manufacturing. The CAD develops the design of the parts, the CAPP generates the KRL (Kuka Robot Language) code, which is transferred to the CAM phase for execution. The KRL code adjusts the robot parameters, ensuring the accuracy and quality of the metal parts. The integration of Digital Twins enables real-time monitoring, simulation of deposition strategies, and failure anticipation, promoting a more efficient and coordinated manufacturing process. Validation scenarios demonstrated the potential of the RAMC, highlighting the importance of Digital Twins in optimizing LMD-Wire, especially in the production of complex parts. The use of Digital Twins facilitates real-time simulation and monitoring, improving the quality and reliability of the parts. Furthermore, intelligent monitoring and control strategies in a connected digital environment enhance traceability and flexibility in the production of complex parts, meeting the demands of Industry 4.0. However, challenges remain, such as modeling parameters for complex geometries and expanding interoperability with other industrial standards. In conclusion, this study contributes to the advancement of Robotic Additive Manufacturing with LMD-Wire, integrating CAD/CAPP/CAM with Digital Twins to optimize production and quality control, and highlights the need for further research to refine digital modeling and expand the application of Additive Manufacturing in industry. Additionally, it paves the way for the creation of innovative solutions that can enhance competitiveness and sustainability in manufacturing.

Keywords: Additive Manufacturing Cell. Robots. Laser Metal Deposition. Digital Twin.

Resumo

Na manufatura moderna, a integração de tecnologias como Gêmeo Digital (DT) e Manufatura Aditiva (AM) é essencial para otimizar a produção e a eficiência dos processos. A Deposição de Metal a Laser baseado em Arame (LMD-Wire) oferece vantagens como flexibilidade na produção de peças complexas e redução de custos, mas desafios como simulação de operações, detecção de falhas e otimização do ciclo de vida das peças ainda limitam sua adoção. Este estudo propõe o desenvolvimento de uma Célula de Manufatura Aditiva Robotizada (RAMC) utilizando LMD-Wire, integrada a um sistema CAD/CAPP/CAM baseado em Gêmeos Digitais, em conformidade com a ISO 23247, garantindo interoperabilidade entre os níveis da manufatura digital. A RAMC integra fisicamente componentes como a célula metálica, o robô KUKA KR70 R2100 e o sistema MELTIO Engine, coordenando-os logicamente para otimizar o fluxo de trabalho e garantir a execução precisa das operações. Os sistemas CAD/CAPP/CAM na RAMC são cruciais para a fabricação. O CAD desenvolve o projeto das peças, o CAPP gera o código KRL (Kuka Robot Language), que é transferido para a fase CAM para execução. O código KRL ajusta os parâmetros do robô, assegurando a precisão e qualidade das peças metálicas. A integração de Gêmeos Digitais permite monitoramento em tempo real, simulação das estratégias de deposição e antecipação de falhas, promovendo uma manufatura mais eficiente e coordenada. Os cenários de validação demonstraram o potencial da RAMC, evidenciando a importância dos Gêmeos Digitais na otimização do LMD-Wire, especialmente na produção de peças complexas. O uso dos Gêmeos facilita a simulação e o monitoramento em tempo real, melhorando a qualidade e confiabilidade das peças. Além disso, estratégias inteligentes de monitoramento e controle em um ambiente digital conectado aprimoram a rastreabilidade e a flexibilidade na produção de peças complexas, atendendo às exigências da Indústria 4.0. Desafios persistem, como a modelagem de parâmetros para geometrias complexas e a ampliação da interoperabilidade com outras normas industriais. Em conclusão, este estudo contribui para o avanço da Manufatura Aditiva Robotizada com LMD-Wire, integrando CAD/CAPP/CAM com Gêmeos Digitais para otimizar a produção e controle de qualidade, e destaca a necessidade de mais pesquisas para refinar a modelagem digital e expandir a aplicação da Manufatura Aditiva na indústria. Além disso, abre caminhos para a criação de soluções inovadoras que possam aumentar a competitividade e a sustentabilidade na manufatura.

Palavras-chave: Célula de Manufatura Aditiva. Robôs. Deposição de Metal à Laser. Gêmeo Digital.

List of Figures

Figure 1 – Additive Manufacturing Processes. Adapted from (RODRIGUEZ, E.; ALVARES, A.; RIANO, 2025)	23
Figure 2 – Classification of Metal Additive Manufacturing Processes (AMPOWER, 2024).	25
Figure 3 – Resolution vs Feature Size in Metal AM Processes (RAMLAB, 2024a).	26
Figure 4 – Laser Metal Deposition Process (RAMLAB, 2024b).	29
Figure 5 – Diagrams of Melt Pool using Continuous and Pulsed Lasers (GHANADI; PASEBANI, 2024).	31
Figure 6 – Schematic representation of bead geometry in LMD-wire (GHANADI; PASEBANI, 2024).	32
Figure 7 – Diagrams of Bead for Stable Print Profiles and Overhang Angles. Adapted from (MELTIO, 2022a).	33
Figure 8 – Defects associated with the LMD-wire process. Adapted from (MELTIO, 2023a).	35
Figure 9 – Deposition Strategies. Adapted from (MELTIO, 2024).	39
Figure 10 – Evolution of the Robotic Additive Manufacturing Cell (RAMC) through sequential development phases.	47
Figure 11 – Robotic Additive Manufacturing System (FIGUEROA, B. S.; ÁLVARES, 2025b).	49
Figure 12 – IDEF0 Diagram: Methodology for the development of a RAMC.	50
Figure 13 – IDEF0 Diagram: Main activities of the RAMC.	52
Figure 14 – IDEF0 Diagram: Physical and Logical Integration Activities.	53
Figure 15 – IDEF0 Diagram: Physical Integration Activities.	55
Figure 16 – IDEF0 Diagram: Robot Installation Activities.	56
Figure 17 – IDEF0 Diagram: Print Table Positioning Activities.	58
Figure 18 – IDEF0 Diagram: Meltio System Installation Activities.	59
Figure 19 – IDEF0 Diagram: Robot/Meltio Integration Activities.	61
Figure 20 – IDEF0 Diagram: Logical Integration Activities.	62
Figure 21 – IDEF0 Diagram: CAD/CAPP/CAM System Activities.	64
Figure 22 – IDEF0 Diagram: CAD System Activities.	65
Figure 23 – IDEF0 Diagram: CAPP System Activities.	67
Figure 24 – IDEF0 Diagram: Part Slicing Activities.	68
Figure 25 – IDEF0 Diagram: CAM System Activities.	70
Figure 26 – IDEF0 Diagram: Digital Twin - Simulation (Planning) Activities.	71
Figure 27 – IDEF0 Diagram: 3D Printing Activities (CAM Execution).	74
Figure 28 – IDEF0 Diagram: CAM Operation Activities.	75

Figure 29 – IDEF0 Diagram: CAM Monitoring Activities.	76
Figure 30 – IDEF0 Diagram: Digital Twin - RAMC Real-Time Activities.	78
Figure 31 – IDEF0 Diagram: Digital Twin - Meltio Monitoring (IIoT) Activities.	79
Figure 32 – IDEF0 Diagram: Digital Twin - Meltio Monitoring (IIoT) Activities.	80
Figure 33 – Robotic Additive Manufacturing Cell LMD-Wire.	82
Figure 34 – Additive Manufacturing Cell Cabin.	82
Figure 35 – KUKA KR70 R2100 Robot Installation.	83
Figure 36 – Positioning of the Printing Table.	84
Figure 37 – Installation of the Meltio Engine System.	85
Figure 38 – Installation of the Safety System.	86
Figure 39 – Integration of Robot/Meltio.	86
Figure 40 – Overview of Meltio Controller Macros and KRL Programming for Macros Activation.	87
Figure 41 – Signal switching between Meltio and KUKA controllers.	88
Figure 42 – CAM Model RAMC in KUKA.SIM: Offline DT Simulation.	90
Figure 43 – CAM Model RAMC in RoboDK: Real-Time DT Monitoring.	90
Figure 44 – CAD Model RAMC in Rhinoceros 7 and Grasshopper: Offline DT Simu- lation.	91
Figure 45 – CAPP Algorithm with Grasshopper: DT Programming.	92
Figure 46 – Simplify3D and G-Code to KRL Converter.	93
Figure 47 – CAD/CAPP/CAM model RAMC Meltio Space.	94
Figure 48 – CAM Process Pipeline for Execution Phase - CAM.	95
Figure 49 – Setup RAMC.	96
Figure 50 – Toolpath Execution RAMC.	97
Figure 51 – Monitoring of the RAMC.	97
Figure 52 – Recorded Key LMD-wire Process Parameters.	98
Figure 53 – Representative Defects in LMD-Wire Process.	99
Figure 54 – Framework DT Architecture Proposal Based on ISO 23247 (ALVARES, A. J.; RODRIGUEZ, E.; FIGUEROA, B., 2025)	100
Figure 55 – KUKA iiQoT Dashboard (ALVARES, A. J.; RODRIGUEZ, E.; FIGUEROA, B., 2025).	104
Figure 56 – Meltio Dashboard (ALVARES, A. J.; RODRIGUEZ, E.; FIGUEROA, B., 2025).	105
Figure 57 – MQTT Flows Developed for Digital Twin Framework Architecture (AL- VARES, A. J.; RODRIGUEZ, E.; FIGUEROA, B., 2025).	106
Figure 58 – Digital twin of the cell during real-time 3D printing (ALVARES, A. J.; RODRIGUEZ, E.; FIGUEROA, B., 2025).	109
Figure 59 – Node-Red flows to generate a 2D Dashboard of the Kuka robot and store the robot’s kinematic parameters.	111

Figure 60 – Ishikawa Diagram associated with defects in parts printed using the LMD-wire process (ALVARES, A. J.; FIGUEROA, B. S., et al., 2025).	112
Figure 61 – Printed Parts and Meltio Standard Part Case Study 1.	113
Figure 62 – Capability Reports of the Parts in Case Study 1.	115
Figure 63 – Gravia Part Case Study 2.	117
Figure 64 – Wall Parts Case Study 3.	118
Figure 65 – Printed Parts and Metallographic Specimen Preparation.	119
Figure 66 – Microstructural Analysis of Printed Specimens.	120
Figure 67 – Microhardness Measurement Regions.	121
Figure 68 – Flowchart of Connections for Safety System.	137
Figure 69 – XG11.1 Port Pinout and Description.	138
Figure 70 – Electrical Connection Diagram for Safety System.	138
Figure 71 – Diagram of Connections for Robot/Meltio Integration.	139
Figure 72 – XG12 Port Pinout and Description.	139
Figure 73 – PLC routine on KUKA SmartPAD to disable deposition outputs in T1 mode.	140
Figure 74 – Installed packages on the KUKA KR C5 controller.	141
Figure 75 – Declaration of internal variables in the KUKA smartPAD interface for MQTT communication.	142

List of Tables

Table 1 – Bead Parameters.	33
Table 2 – Benchmark CAD/CAPP/CAM Systems Robotic Additive Manufacturing.	42
Table 3 – Comparative Table of Correlated Works.	46
Table 4 – Parameters of the G-Code to KRL Converter Interface.	93
Table 5 – Robot Data from the Robotic Additive Manufacturing Cell Collected from KUKA via MQTT.	106
Table 6 – Pseudocode for the Robot Data Connection and Publishing.	107
Table 7 – Pseudocode for Robotic Motion Control RoboDK.	108
Table 8 – Pseudocode for the Node-RED Flow.	110
Table 9 – Deposition Parameters of Parts Case Study 1.	113
Table 10 – Consolidated Measurement of the Parts.	114
Table 11 – Process capability analysis of Printed parts	116
Table 12 – Deposition Parameters of Gravia Part Case Study 2.	117
Table 13 – Deposition Parameters of Wall Parts Case Study 3.	118
Table 14 – Microstructural analysis of the printed specimens	121
Table 15 – Microhardness measurements of the printed specimens.	122
Table 16 – Implementation Costs of the RAMC (in BRL and USD)	146
Table 17 – Parâmetros de deposição de todos os casos de estudo.	152

List of abbreviations and acronyms

6σ	Quality Management Methodology.....	15
C_p	Process Capability Index.....	15
C_{pk}	Corrected Process Capability Index.....	15
AM	Additive Manufacturing.....	15
AWS	Amazon Web Services.....	15
CAD	Computer-Aided Design.....	15
CAM	Computer-Aided Manufacturing.....	15
CAPP	Computer-Aided Process Planning.....	15
CFD	Computational Fluid Dynamics.....	15
CI	Confidence Interval.....	15
CL-WAAM	Curved Layer Deposition in Wire and Arc Additive Manufacturing.....	15
CMT	Cold Metal Transfer.....	15
CNC	Computer Numerical Control.....	15
DCDCE	Data Collection and Device Control Entity.....	15
DED	Direct Energy Deposition.....	15
DED-Powder	Powder-Based Direct Energy Deposition.....	15
DED-Wire	Wire-Based Direct Energy Deposition.....	15
DMD	Direct Metal Deposition.....	15
DT	Digital Twin.....	15
DTE	Digital Twin Entity.....	15
DThE	Digital Thread Entity.....	15
DTUE	Digital Twin User Entity.....	15
DWD	Direct Wire Deposition.....	15
EBAM	Electron Beam Additive Manufacturing.....	15
FEA	Finite Element Analysis.....	15
G-code	Geometric Code for CNC Machines.....	15
GMA-AM	Gas Metal Arc Additive Manufacturing.....	15

GTA-AM	Gas Tungsten Arc Additive Manufacturing	15
HTTP	Hypertext Transfer Protocol	15
I/O	Input/Output	15
IDEF0	Integration Definition for Function Modeling	15
IIoT	Industrial Internet of Things	15
IoT	Internet of Things	15
KRL	KUKA Robot Language	15
L-DED	Laser-Directed Energy Deposition	15
LBDMD	Laser-Based Direct Metal Deposition	15
LC	Laser Consolidation	15
LENS	Laser Engineered Net Shaping	15
LMD	Laser Metal Deposition	15
LMD-Powder	Powder-Based Laser Metal Deposition	15
LMD-Wire	Wire-Based Laser Metal Deposition	15
MAM	Metal Additive Manufacturing	15
MQTT	Message Queuing Telemetry Transport	15
NMAM	Non-Metal Additive Manufacturing	15
OME	Observable Manufacturing Elements	15
OPC DA	Open Platform Communications Data Access	15
OPC UA	OPC Unified Architecture	15
RAMC	Robotic Additive Manufacturing Cell	15
RAMI	Reference Architectural Model Industry	15
SDM	Shape Deposition Manufacturing	15
SLM	Selective Laser Melting	15
STL	STereoLithography	15
TCP	Tool Center Point	15
TCP/IP	Transmission Control Protocol / Internet Protocol	15
TS	Travel Speed	15
WAAM	Wire Arc Additive Manufacturing	15
WFS	Wire Feed Speed	15

Contents

1	INTRODUCTION	19
1.1	Contextualization	19
1.2	Problem Definition	20
1.3	Justification	21
1.4	Objectives of the Dissertation	21
1.4.1	General Objective	21
1.4.2	Specific Objectives	21
1.5	Structure of the Dissertation	22
2	LITERATURE REVIEW	23
2.1	Metal Additive Manufacturing	23
2.1.1	Directed Energy Deposition (DED)	25
2.1.1.1	Powder-Based Directed Energy Deposition (DED-Powder)	26
2.1.1.2	Wire-Based Directed Energy Deposition (DED-Wire)	27
2.1.2	DED over Welding-Based AM Processes	28
2.1.2.1	Precision and Geometric Control:	28
2.1.2.2	Materials and Part Properties:	28
2.1.2.3	Efficiency and Material Waste:	28
2.1.2.4	Specialized Applications and Flexibility:	28
2.2	Laser Metal Deposition (LMD)	28
2.2.1	Process Overview	29
2.2.2	Critical Parameters	29
2.2.3	Types of Lasers	31
2.2.4	Modeling and Simulation	31
2.2.4.1	Bead Geometry	32
2.2.4.2	Comparison of LMD and CMT Deposition Processes	34
2.2.5	Types of Defects in Parts	34
2.3	Slicing Strategies	35
2.3.1	Constant Deposition Rate	36
2.3.2	Variable Deposition Rate	38
2.3.3	Slicing Strategies Meltio Space	38
2.3.3.1	Planar Horizontal Slicing	38
2.3.3.2	Planar Angled Slicing	38
2.3.3.3	Planar Along Curve Slicing	39
2.3.3.4	Revolved Surface Slicing	39

2.3.3.5	Radial Slicing	40
2.3.3.6	Radial 360 Slicing	40
2.3.3.7	cladding Slicing	40
2.3.3.8	Non-Planar Surface Slicing	40
2.3.3.9	Conical Fields Slicing	40
2.3.3.10	Sweep Slicing	41
2.4	CAD/CAPP/CAM Systems for Robotic Additive Manufacturing . .	41
2.5	Digital Twin ISO 23247	42
2.6	Correlated Works	43
2.7	Stepwise Development of the Robotic Additive Manufacturing Cell	47
3	METHODOLOGICAL PROPOSAL FOR THE DEVELOPMENT OF A ROBOTIC ADDITIVE MANUFACTURING CELL	48
3.1	Introduction	48
3.2	Robotic Additive Manufacturing System	48
3.3	Robotic Additive Manufacturing Cell	49
3.4	Physical and Logical Integration	51
3.4.1	Physical Integration	54
3.4.1.1	Cabin Assembly of the RAMC	54
3.4.1.2	Robot Installation	54
3.4.1.3	Print Table Positioning	57
3.4.1.4	Installation of the Meltio Engine System	57
3.4.1.5	Installation of the Safety System	57
3.4.1.6	Robot/Meltio Integration	60
3.4.2	Logical Integration	60
3.5	CAD/CAPP/CAM System	63
3.5.1	CAD	63
3.5.2	CAPP	66
3.5.2.1	Importing the CAD Model	66
3.5.2.2	Slicing the Part	66
3.5.2.3	Generating the KRL Program	69
3.5.3	CAM	69
3.5.3.1	Digital Twin - Simulation (CAM Planning)	69
3.5.3.2	3D Printing (CAM Execution)	72
3.5.3.2.1	CAM Operation	72
3.5.3.2.2	CAM Monitoring	73
4	DEVELOPMENT OF A ROBOTIC ADDITIVE MANUFACTURING CELL	81
4.1	Introduction	81

4.2	Physical Integration	81
4.2.1	Assembly of the Additive Manufacturing Cell Cabin	82
4.2.2	Robot Installation	83
4.2.3	Positioning of the Printing Table	83
4.2.4	Installation of the Meltio Engine System	84
4.2.5	Installation of the Safety System	85
4.2.6	Integration of Robot/Meltio	86
4.3	Logical Integration	87
4.4	CAD/CAPP/CAM Systems	89
4.4.1	KUKA.SIM	89
4.4.2	RoboDK	89
4.4.3	Rhino3D CAD	91
4.4.4	Grasshopper CAPP	91
4.4.5	Simplify3D and G-Code to KRL Converter CAPP	92
4.4.6	Meltio Space CAD/CAPP/CAM	93
4.4.7	Execution Phase - CAM	94
4.4.7.1	Setup - RAMC	95
4.4.7.2	Toolpath Execution - RAMC	96
4.4.7.3	Monitoring - RAMC	97
4.4.7.4	Quality Control - RAMC	98
5	DIGITAL TWIN SYSTEM DEVELOPMENT	100
5.1	Introduction	100
5.2	DT Architecture Proposal Based on ISO 23247	100
5.2.1	DT KUKA IIQoT - Condition-Based Maintenance	101
5.2.2	DT Meltio Dashboard	101
5.2.3	DT Robotic Additive Manufacturing Cell	102
5.3	Results of the Implemented DT Architecture of the RAMC	103
5.3.1	First Digital Twin: KUKA iiQoT	103
5.3.2	Second Digital Twin: Meltio Dashboard	104
5.3.3	Third Digital Twin: Robotic Additive Manufacturing Cell	105
5.3.3.1	3D Movement Simulation Flow	107
5.3.3.2	Node-RED Dashboard and Firestore Storage Flow	109
6	CASE STUDIES: VALIDATION AND EXPERIMENTS	112
6.1	Introduction	112
6.2	Visual Defect Analysis of Printed Parts	112
6.2.1	Case Study 1: Printed Parts	113
6.2.1.1	Capability Analyses of the printed Parts	114
6.2.2	Case Study 2: Gravia Part	117

6.2.3	Case Study 3: Wall Parts	118
6.3	Metallographic and Mechanical Characterization	119
6.3.1	Metallographic Preparation of Test Specimens	119
6.3.2	Microstructural Analysis	120
6.3.3	Microhardness Analysis	121
7	CONCLUSIONS AND FUTURE WORKS	123
7.1	Analysis of Achieved Objectives	124
7.2	Remaining Challenges and Future Research Directions	124
7.3	Future Work Recommendations	125
7.4	Final Remarks	126
	REFERENCES	127
	APPENDIX	136
	APPENDIX A – DIAGRAMS ASSOCIATED WITH THE PHYSICAL AND LOGICAL INTEGRATION OF THE RAMC	137
A.1	Safety System Connection Diagrams	137
A.2	DB15 Cable Connection Diagrams for Controllers	139
A.3	Safety Logic Integration for Deposition Modes	140
A.4	Installed Packages on the KUKA Controller	141
A.5	MQTT Configuration on the KUKA Controller	142
	APPENDIX B – CODES FOR THE DIGITAL TWIN SYSTEM	143
B.1	MQTT Publisher	143
B.2	RoboDK 3D Environment	143
B.3	Node-RED Flow	143
	APPENDIX C – RESEARCH DISSEMINATION THROUGH PEER- REVIEWED PUBLICATIONS DURING THE MAS- TER’S PROGRAM	144
C.1	Journal Articles	144
C.2	Book Chapters	145
C.3	Conference Papers	145
	APPENDIX D – IMPLEMENTATION COST OF THE ROBOTIC AD- DITIVE MANUFACTURING CELL	146
	APPENDIX E – RESUMO ESTENDIDO EM LÍNGUA PORTUGUESA	147

1 Introduction

1.1 Contextualization

Metal Additive Manufacturing (MAM) enables the production of complex metallic components through the layer-by-layer deposition of feedstock, typically in the form of powders or wires such as aluminum, titanium, or stainless steel, melted by a laser or an electron beam (ALVARES, A.; LACROIX, et al., 2023a). When combined with robotic automation, this approach becomes robotic MAM, where robotic arms control the deposition trajectory, access intricate geometries across multiple axes, and ensure efficient production with minimal human intervention (MORITZ et al., 2020). The field is further supported by international standards, including ISO/ASTM 52900, which defines fundamental terminology, and ISO/ASTM 52901, which specifies requirements for parts, providing a unified framework for quality and comparability (ISO/ASTM, 2017a,b).

The advantages of robotic MAM are diverse and significant. Automation reduces labor costs and increases manufacturing speed by eliminating the need for human intervention in the process. However, the ability to print complex metallic objects opens new possibilities for design and component optimization, leading to lighter, more efficient products tailored to specific market needs.

This technology has applications in a wide range of industrial sectors, including aerospace, automotive, medical, and defense. For example, in the aerospace industry, it is used to produce lighter and more resistant structural components for aircraft, while in the medical industry, it is employed in the manufacturing of custom implants and advanced medical devices (NGO et al., 2018).

However, robotic MAM faces significant challenges. Initial investment costs can be high, as both 3D printing equipment and robotic systems are expensive. In addition, ensuring the quality and integrity of printed parts requires rigorous evaluation to guarantee their suitability for final use, including the development of specific quality standards and certification for this technology (GIBSON et al., 2022).

The implementation of digital twins (DTs) in robotic MAM offers a variety of advantages that can profoundly transform the way production processes are conceived, executed, and optimized. DTs provide a virtual representation of the entire manufacturing process, from component modeling to final printing, allowing for detailed and accurate analysis of each stage of the process. This enables simulation of scenarios and the identification of potential bottlenecks or problems before they occur in reality, resulting in a significant reduction in production costs and development time (SHAO; HELU, 2020). Furthermore, DTs

allow for immersive visualization of the manufacturing process, enabling a more complete and intuitive understanding of the interactions between the different components of the robotic additive manufacturing cell (RAMC).

Another important benefit of DTs in robotic MAM is the ability to perform remote monitoring and predictive maintenance of equipment. Real-time virtual models enable constant monitoring of the performance of robots, 3D printers, and other devices, early identifying possible failures or wear that could lead to unplanned production interruptions. This allows for the implementation of preventive maintenance strategies, such as replacing worn parts before they fail, minimizing downtime, and reducing costs associated with corrective maintenance (LIU et al., 2022).

Despite its advantages, the implementation of DTs in robotic MAM presents notable challenges. A key issue is the integration of real-time monitoring and control systems, given the variety of devices and technologies in the RAMC (FIGUEROA, B. S.; ÁLVARES, 2025a). This demands interoperable communication standards and robust security protocols to ensure data integrity and confidentiality. Moreover, analyzing DT-generated data requires specialized knowledge in data science and statistics, which may be a barrier for some organizations. Even so, the potential for process optimization, cost reduction, and quality improvement makes DT implementation a promising strategy.

1.2 Problem Definition

The rapid advancement of manufacturing technologies has increased the demand for efficient, cost-effective methods to produce high-precision components. Among these, additive manufacturing (AM) stands out for its flexibility in creating complex geometries, material efficiency, and reduced lead times (RASIYA; SHUKLA; SARAN, 2021). A specific AM technique, Wire-Based Laser Metal Deposition (LMD-Wire), shows great potential for producing metallic parts with intricate designs (DASS; MORIDI, 2022). However, challenges persist in simulation operation, fault detection, and optimizing the service life of the produced parts (ARREGUI et al., 2018) (MONTROYA-ZAPATA et al., 2023).

In addition, the integration of Digital Twin (DT) technologies into robotic additive manufacturing systems has opened new possibilities for real-time monitoring, predictive maintenance, and process optimization (FIGUEROA, B. S.; ARAÚJO; ALVARES, A., 2023). Despite these advancements, there is still a gap in the effective integration of these technologies in a seamless and interoperable manner, aligned with industrial standards, particularly in the context of MAM processes (CABRAL; GASCA; ALVARES, A. J., 2023).

This study addresses these challenges by developing a RAMC using LMD-Wire, integrated with a CAD/CAPP/CAM system based on DTs, in compliance with ISO 23247 standards (ISO, 2021). This integration aims to optimize the production of high-precision

metallic parts while simultaneously improving monitoring, simulation, and failure prevention during the manufacturing process.

1.3 Justification

The proposed research is highly relevant due to the growing demand for manufacturing systems capable of producing complex parts with high precision and reduced costs (MOTTA; DEMIR; PREVITALI, 2018). The adoption of LMD-Wire combined with DT technologies offers significant potential to optimize metallic part production, enhancing the efficiency and reliability of manufacturing operations. Their integration can also reduce waste, improve material utilization, and minimize production errors—key aspects in advancing toward Industry 4.0 objectives (ALVARES, A.; LACROIX, et al., 2023a).

The study aligns with global trends toward digitizing manufacturing processes and the development of intelligent and interconnected production systems. By focusing on the application of DTs in a robotic MAM environment, the research addresses the need for greater interoperability between various systems, improving the flexibility, reliability, and overall performance of manufacturing processes (ALVARES, A. J.; LACROIX; MARON, et al., 2023) (ALVARES, A. J.; RODRIGUEZ, E.; FIGUEROA, B., 2025).

This research will contribute to the advancement of knowledge in the field of robotic MAM and DTs, providing valuable insights into their practical implementation and optimization. The results obtained could be applied across a wide range of industries, including aerospace, automotive, and medical, where the production of complex, high-precision metallic parts is crucial (GUAGLIONE; BENNI; PREVITALI, 2024).

1.4 Objectives of the Dissertation

1.4.1 General Objective

To develop a robotic additive manufacturing cell through the implementation and monitoring of real-time digital twins, enabling the additive manufacturing of planar and non-planar parts within an integrated physical and digital environment.

1.4.2 Specific Objectives

- Design and integrate the physical and logical systems of the KUKA KR70 R2100 robot with the MELTIO LMD engine.
- Develop a real-time Digital Twin using RoboDK.

- Implement and evaluate Digital Twin monitoring through KUKA iiQoT and Meltio Dashboard.
- Explore the role of real-time digital twins in process monitoring, data acquisition, and optimization.
- Validate the feasibility of additive manufacturing of planar and non-planar parts within the proposed robotic cell.

1.5 Structure of the Dissertation

Chapter 2 provides a review of the literature on additive manufacturing in Industry 4.0, highlighting the most relevant related studies.

Chapter 3 proposes a methodology for the development of a robotic additive manufacturing cell based on the laser metal deposition process using welding wire.

Chapter 4 demonstrates the physical and logical integration of the robotic additive manufacturing cell, which is based on the laser metal deposition process using welding wire.

Chapter 5 describes the development of Digital Twins for the robotic additive manufacturing cell, designed in accordance with the ISO 23247 standard.

Chapter 6 details three distinct case studies focused on the validation and experiments of the robotic additive manufacturing cell.

Chapter 7 presents the conclusions, contributions, future research directions, and suggestions for future work aimed at the evolution of the Robotic Additive Manufacturing Cell.

Appendix A includes the diagrams associated with the physical and logical integration of the Robotic Additive Manufacturing Cell.

Appendix B contains the programming codes developed for the implementation of a Digital Twin system in a robotic additive manufacturing cell.

Appendix C gathers the peer-reviewed scientific publications derived from the experimental results, proposed methodologies, and academic activities conducted during the master's program.

Appendix D outlines the financial structure related to the implementation of the Robotic Additive Manufacturing Cell, including acquisition, transportation, and installation costs, with values expressed in BRL and USD.

Appendix E provides an extended summary of this master's dissertation in Portuguese, offering a comprehensive overview of its objectives, methodology, key developments, experimental results, and final considerations.

2 Literature Review

2.1 Metal Additive Manufacturing

In the context of the current manufacturing landscape and the advent of Industry 4.0, AM, commonly known as 3D printing, represents a significant advancement in fabrication technology (FIGUEROA, B. S.; RIAÑO, et al., 2024). This innovative approach facilitates the production of intricate geometries and customized components that were previously difficult to achieve (RASIYA; SHUKLA; SARAN, 2021). AM encompasses a variety of processes tailored to specific materials, including both metallic and non-metallic types (SRIVASTAVA et al., 2022). Figure 1 illustrates these classifications, highlighting the distinct methodologies used for each material category. Furthermore, the figure provides a comprehensive overview of the specific processes associated with each type, particularly highlighting that LMD-Wire operates as a sub-process of directed energy deposition (DED).

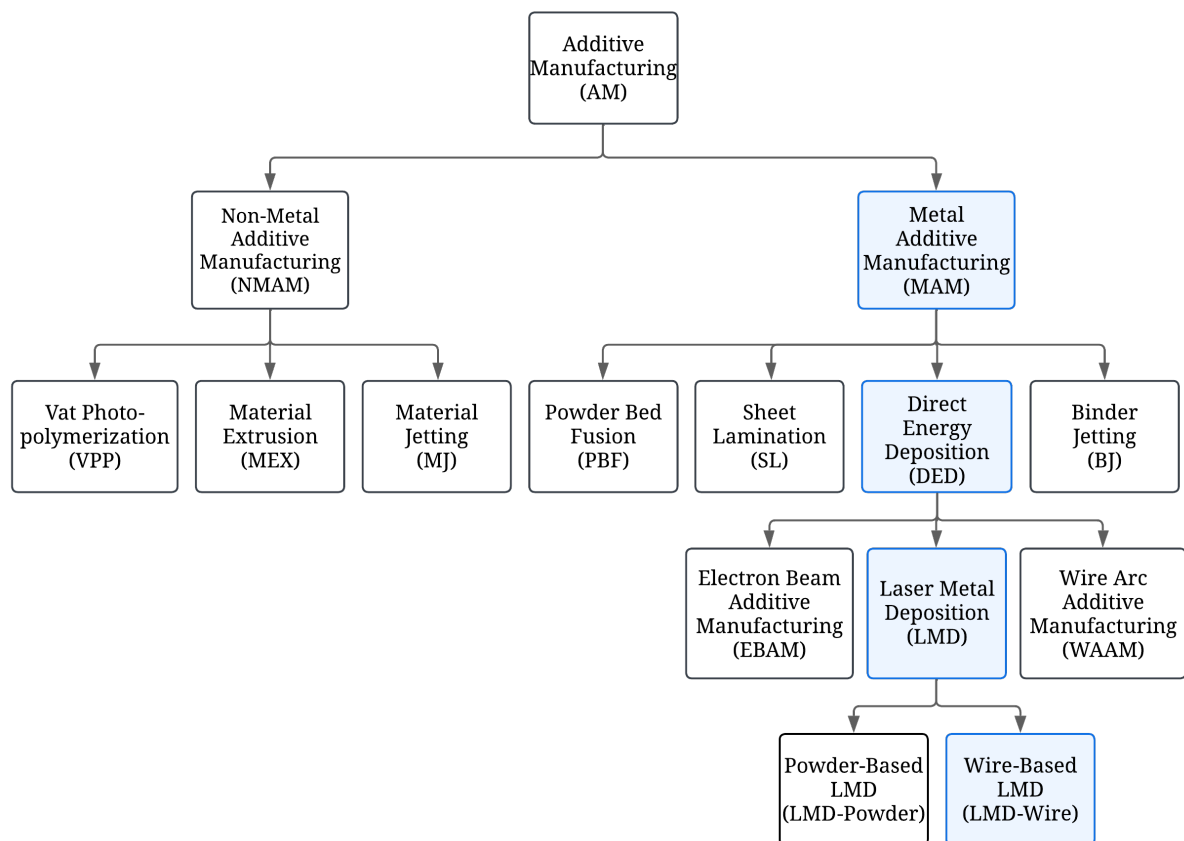


Figure 1 – Additive Manufacturing Processes. Adapted from (RODRIGUEZ, E.; ALVARES, A.; RIANO, 2025)

MAM represents a prominent facet of AM that has significantly transformed the conception and production of metallic parts. This process, also referred to as metal 3D printing, consists of creating three-dimensional objects through the layer-by-layer deposition of metallic feedstock, typically provided in the form of powders or wires, according to a digital model (WONG; HERNANDEZ, 2012) (SAMES et al., 2018).

Essentially, MAM distinguishes itself from traditional subtractive manufacturing methods such as turning or milling by incrementally building components rather than removing material from a solid block (LALEH et al., 2023) (NGO et al., 2018). This paradigm shift allows for the fabrication of parts with internal channels, lattice structures, and customized features that would be unfeasible or prohibitively expensive with conventional techniques. In addition to enhanced design freedom, MAM also offers shorter lead times, reduced material waste, and the possibility of consolidating multiple components into a single part, thereby improving overall production efficiency (DEBROY; WEI, H. L., et al., 2018). Moreover, the field is guided by international standards such as ISO/ASTM 52900, which provides the fundamental terminology, and ISO/ASTM 52901, which defines requirements for purchased parts. These standards collectively establish a unified framework that ensures quality assurance, comparability, and interoperability across diverse applications and industrial sectors (ISO/ASTM, 2017a) (ISO/ASTM, 2017b).

The process begins with the creation of a digital model of the desired object, which is sliced into extremely thin horizontal layers using specialized CAD software (BRACKETT; ASHCROFT; HAGUE, 2011). Next, an AM machine deposits metal material in the form of powder or wire, following the instructions from the digital model. The consolidation of these layers is achieved through the application of energy, which can be provided by lasers, electron beams, electric arcs, or even inert gases, depending on the specific process used (KÖRNER, 2016).

MAM offers significant benefits. It enables the production of customized parts that are tailored to specific customer needs or applications, while reducing material waste and eliminating the need for expensive tooling. This innovative technique also provides unprecedented design freedom, allowing the creation of lighter and more material-efficient components (HETTESHEIMER; HIRZEL; ROSS, 2018). Furthermore, it enables on-demand production and small batch manufacturing, enhancing flexibility and agility in supply chain management. MAM is highly adaptable to various metal alloys such as stainless steels, titanium, aluminum, copper, and superalloys, allowing for the production of components with customized mechanical properties for diverse industrial applications. According to (AMPOWER, 2024), Figure 2 classifies the MAM processes based on the forms of the material and the deposition techniques.



Figure 2 – Classification of Metal Additive Manufacturing Processes (AMPOWER, 2024).

2.1.1 Directed Energy Deposition (DED)

DED is a fundamental technique in MAM. In this process, metal powder or wire is locally melted and deposited in layers onto a substrate to build three-dimensional parts. The energy required to melt the material is supplied by a controlled energy source, such as a laser, electric arc, or electron beam (DEBROY; WEI, H., et al., 2018).

During the DED process, the path of the energy beam is controlled by a three-dimensional digital model, which directs the selective melting of the metal material to create the desired geometry of the part (DASS; MORIDI, 2017). As each layer is deposited and melted, the deposition head moves to apply the next layer of material. This deposition and melting process is repeated layer by layer until the part is fully formed.

To ensure reliability and facilitate adoption in critical applications, normative frameworks have been established for additive manufacturing with metallic feedstock (RODRIGUEZ, N. et al., 2018). In particular, the AWS D20.1 standard provides qualification and certification criteria for additive processes with metals, establishing guidelines for process validation, material requirements, and operator qualification in safety-critical industries such as aerospace and defense (AWS, 2019). Figure 3, adapted from (RAMLAB, 2024a), illustrates the relationship between resolution, part complexity, and cost for different metal AM processes, emphasizing the advantages of DED in terms of scalability and process flexibility.

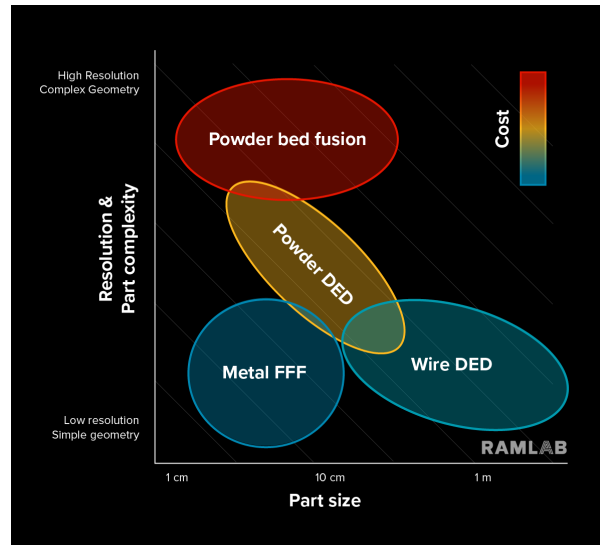


Figure 3 – Resolution vs Feature Size in Metal AM Processes (RAMLAB, 2024a).

2.1.1.1 Powder-Based Directed Energy Deposition (DED-Powder)

DED-Powder is a variant of the DED process used in MAM. In this method, metallic powder is continuously supplied to a deposition area, where it is selectively melted by a directed energy beam, such as a laser or an electron beam (RIZA et al., 2014). This process is guided by a three-dimensional digital model, which directs the energy beam to melt the powder layer by layer to build up the desired part geometry (IMRAN et al., 2011).

DED-Powder offers significant advantages, including the ability to produce parts with high density and precision. It supports a wide range of metal materials and is particularly useful for the manufacture of large components, the repair and modification of existing parts (MALUKHIN; EHMANN, 2005). The technique is commonly employed in demanding applications, such as aerospace and energy sectors, where high performance and intricate details are required.

Within the DED-Powder process, the following techniques are applied:

- **Direct Metal Deposition (DMD):** A technique in which a laser melts a bed of metal powder to form the desired part.
- **Laser Engineered Net Shaping (LENS):** A technique that uses a laser to melt metal powder, which is deposited in layers onto the substrate.
- **Laser Cladding:** A technique that uses a laser to melt a metal coating onto a surface to enhance its properties.
- **Laser Consolidation (LC):** A process where a laser is used to melt layers of metal powder, consolidating them to form the final part.

- **Shape Deposition Manufacturing (SDM):** The method uses multiple materials to create layers that are machined to form the desired part.
- **Laser Metal Deposition (LMD):** Method that uses a laser beam to melt a bed of metal powder to form the desired part.

2.1.1.2 Wire-Based Directed Energy Deposition (DED-Wire)

DED-Wire is a specialized variant of the DED technique used in MAM. In this process, a metallic wire is continuously fed through a deposition head, which is guided by a three-dimensional digital model. The wire is melted by a directed energy beam, such as a laser or electric arc, as it is deposited in layers onto a substrate (DING, D. et al., 2015). This layer-by-layer deposition allows the precise creation of complex geometries and large parts (AHN, D.-G., 2021).

DED-Wire offers several advantages, including high deposition rates and the ability to use a wide range of metal materials. The process is particularly suitable for the manufacturing of parts with intricate details and large dimensions, providing flexibility for various industrial applications (GENG et al., 2017). Its efficiency in material use and adaptability to different geometries make it a valuable technique for producing high-performance components.

Within the DED-Wire process, the following techniques are applied:

- **Direct Wire Deposition (DWD):** A technique that uses an electric arc to melt metallic wire, depositing it in layers onto a substrate.
- **Wire Arc Additive Manufacturing (WAAM):** A technique in which metallic wire is melted by an electric arc between the wire and the substrate, forming the part.
- **Gas Metal Arc Additive Manufacturing (GMA-AM):** Derived from Gas Metal Arc Welding (MIG/MAG), this approach uses an electric arc between the wire and the substrate, shielded by inert or active gases, to melt and deposit the material.
- **Gas Tungsten Arc Additive Manufacturing (GTA-AM):** Derived from Gas Tungsten Arc Welding (TIG), this method employs a tungsten electrode to generate the arc, with inert gas shielding, and may incorporate filler wire for deposition.
- **Laser Metal Deposition (LMD):** A technique that uses a laser beam to melt metallic wire as it is deposited in layers onto the substrate.

2.1.2 DED over Welding-Based AM Processes

DED presents significant advantages over welding-based AM processes, particularly in precision, material control, and flexibility. DED excels in producing complex geometries with high detail, due to its superior precision and control. It also offers advanced material management, improving the mechanical properties and performance of the final components. Furthermore, DED's efficient material usage and on-demand production capabilities contribute to reduced waste and overall cost-effectiveness ([GRADL, 2022](#)).

2.1.2.1 Precision and Geometric Control:

DED provides superior precision and control over part geometry through a three-dimensional digital model, allowing for complex geometries and fine details. In contrast, welding-based techniques such as WAAM, GTA-AM and GMA-AM produce parts with generally less precision and control over shape and surface finish.

2.1.2.2 Materials and Part Properties:

DED allows for precise control over a broad range of metal materials, ensuring high-performance properties and exact specifications. Conversely, welding-based techniques may have less precise control over material properties and can negatively affect material quality as a result of residual stresses and defects formed during cooling.

2.1.2.3 Efficiency and Material Waste:

DED reduces material waste and enhances manufacturing efficiency by producing parts directly from a digital model and enabling on-demand production and repairs. Welding-based techniques often result in more material waste, require additional processing, and generally have lower efficiency in material use and production time.

2.1.2.4 Specialized Applications and Flexibility:

DED excels in high-precision and high-performance applications, such as aerospace, medical, and energy sectors, because of its flexibility with materials and geometries. Welding-based techniques, while effective for general applications, may fall short in high-precision or specialized requirements.

2.2 Laser Metal Deposition (LMD)

LMD is a sophisticated technique within the DED category of MAM processes. This process employs a high-energy laser beam to selectively melt metallic powder or wire, which is then deposited precisely onto a substrate to build up the part in successive layers

(MELTIO, 2023). LMD is acclaimed for its ability to fabricate complex geometries and high-quality components with meticulous control over material properties and structural integrity (ARREGUI et al., 2018).

2.2.1 Process Overview

LMD starts with a focused, high-energy laser beam that melts metallic feedstock, either powder or wire, delivered to the melt pool through a controlled feeding system. The molten metal is deposited onto the substrate layer by layer. A protective gas is also used to shield the melt pool from oxidation and contamination, ensuring a clean deposition process, as shown in Figure 4, which illustrates the interaction between the laser beam, powder feeder, shielding gas and melt pool.

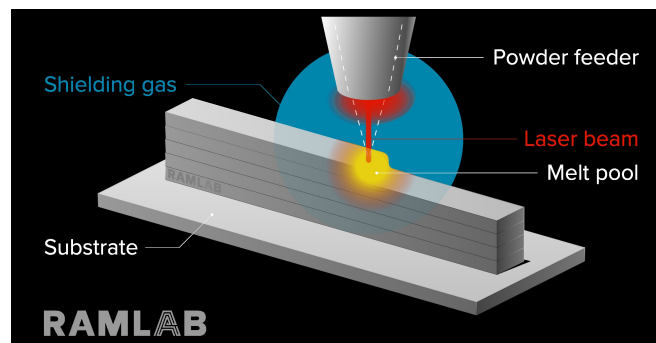


Figure 4 – Laser Metal Deposition Process (RAMLAB, 2024b).

The LMD process is managed by advanced control systems. Laser and feedstock movement are regulated through Computer Numerical Control (CNC) systems or robot programming, depending on the setup (DASS; MORIDI, 2022). CNC systems offer high precision for laser path and deposition control, while robotic systems use specific programming languages for complex geometries.

A digital model guides the deposition process, ensuring accurate alignment of each layer. The commands for the CNC or robot direct the laser, feedstock delivery, and protective gas flow. Real-time adjustments to parameters such as laser power, scan speed, and feed rate are made on the basis of sensor feedback monitoring the deposition.

Advanced control systems with real-time monitoring enable LMD to achieve high precision and repeatability, making it suitable for producing complex high-quality components with stringent performance requirements.

2.2.2 Critical Parameters

The critical parameters in LMD encompass the essential process variables that must be meticulously regulated to attain the desired manufacturing outcomes. These parameters,

including laser power, scanning speed, deposition rate, material feed rate, and layer dimensions, are instrumental in governing of energy input, material flow, and thermal conditions throughout the deposition process (AZARNIYA et al., 2019; BERNAUER; SIGL, et al., 2024). Effective management of these parameters is imperative to ensure consistent material deposition, minimize the occurrence of defects, and enhance the mechanical properties of the resultant components. Proper control over these variables facilitates the achievement of high-quality and reliable results in LMD applications (ZAPATA et al., 2022).

- **Laser Power:** The energy delivered to the material, crucial for fusion and penetration. Incorrect power levels can cause structural defects.
- **Scanning Speed:** The rate at which the laser traverses the material surface, impacting heat distribution and deposition rate.
- **Deposition Rate:** The rate at which material is added to the substrate, which must be coordinated with other parameters for uniform deposition.
- **Material Feed Rate:** The quantity of material supplied to the laser, which should be synchronized with the laser power and scanning speed to ensure consistent deposition.
- **Layer Overlap:** The degree of overlap between successive layers during deposition, essential for maintaining homogeneity and structural integrity.
- **Layer Height:** The thickness of each deposited layer, which must be controlled to achieve the desired component geometry and mechanical properties.
- **Layer Width:** The width of each deposited layer affects the overall build-up of the component and its thermal and mechanical characteristics.
- **Shielding Atmosphere:** The type of gas used to protect the melt pool from oxidation and contamination is critical to maintain material quality.
- **Substrate Temperature:** The initial temperature of the base material before deposition, influencing the adhesion and thermal behavior of the deposited layers.
- **Scanning Strategy:** The pattern followed by the laser during deposition, which affects the uniformity of heat distribution and the final quality of the component.
- **Focal Distance:** The distance between the laser lens and the material surface, which must be accurately adjusted to achieve optimal focus and efficiency.
- **Cooling Time Between Layers:** The interval allowed cooling between successive layers, influencing the formation of residual stresses and the overall microstructure of the component.

2.2.3 Types of Lasers

In LMD, the selection of the appropriate laser type is a critical factor for optimizing process efficiency, material interaction, and the quality of the manufactured part. Continuous-wave lasers generate a constant energy beam that produces a stable melt pool; however, this condition may lead to excessive heat input and defect formation, particularly when fabricating complex geometries, as illustrated in Figure 5. This can lead to issues such as deformations and cracks. In contrast, pulsed lasers deliver energy in short bursts, offering better control over heat accumulation and improving thermal distribution and microstructure quality. The choice between continuous and pulsed lasers should be based on the specific needs of the application, including the desired precision, material type, and structural properties of the final component (GHANADI; PASEBANI, 2024).

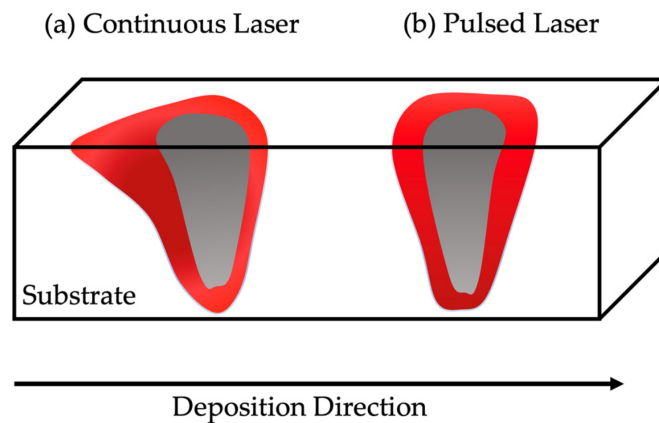


Figure 5 – Diagrams of Melt Pool using Continuous and Pulsed Lasers (GHANADI; PASEBANI, 2024).

Among laser types used in LMD, fiber lasers are known for high precision and efficiency, ideal for metallic materials; diode lasers offer high energy efficiency, suitable for surface coatings and repairs; CO₂ lasers generate powerful infrared light, effective for cutting and welding various materials; Nd lasers are versatile for welding and cutting, available in continuous or pulsed modes; disk lasers provide high beam quality for complex components; and excimer lasers, though less common, are used for micromachining and semiconductor manufacturing (DEMIR, 2018) (MEDRANO et al., 2009) (SHI et al., 2018).

2.2.4 Modeling and Simulation

The LMD process is frequently analyzed and optimized through sophisticated computational techniques to accurately predict thermal behavior, material flow, and the properties of the final component. Advanced modeling approaches, including Computational Fluid Dynamics (CFD) and Finite Element Analysis (FEA), are employed to simulate critical aspects such as melt pool dynamics, thermal gradients, and residual stresses (SEDIGHI; NABAVI; FARSHIDIANFAR, 2024).

2.2.4.1 Bead Geometry

The schematic representation of the bead geometry, shown in Figure 6, emphasizes its principal dimensions: width (W), height (H), and depth (D). These geometric characteristics are directly influenced by the deposition process parameters, which govern the final morphology and overall quality of the deposited material.

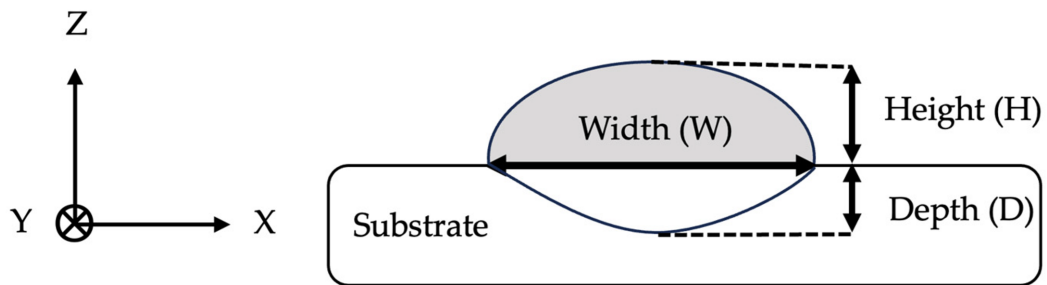


Figure 6 – Schematic representation of bead geometry in LMD-wire (GHANADI; PASEBANI, 2024).

Process parameters critically influence the geometry of the bead by controlling the thermal cycle during deposition and solidification. Key factors such as laser power, wire feed speed (WFS), travel speed (TS), and focal position regulate heat input, cooling rates, and material flow dynamics. Increasing laser power leads to wider beads, but reduces height due to greater remelting and lower solidification rates. Higher TS decreases bead height and has a marginal effect on width due to limited melt pool volume. Variations in WFS impact bead height and width depending on material properties, energy distribution, and deposition stability (SHAIKH et al., 2020) (ZAPATA et al., 2022).

Bead characteristics such as dilution, aspect ratio, and contact angle are crucial for process optimization. The dilution, defined as the mixing ratio between the deposited material and the substrate, increases with the laser power and TS while decreasing with WFS (BRANDL et al., 2011). A controlled dilution level (20–30%) ensures structural integrity and minimizes defects (CAIAZZO; ALFIERI, 2021). The aspect ratio, representing the width-to-height ratio of the bead, is directly proportional to laser power and TS but inversely related to WFS. An optimal aspect ratio above three is recommended to prevent defects. The contact angle, which affects wetting and adhesion, should remain below 80° to avoid porosity and ensure strong bonding between adjacent beads (ABIOYE; FOLKES; CLARE, 2013).

Optimizing process parameters is essential for achieving stable bead geometry and high-quality deposition. Excessive deposition rates can result in cylindrical beads with high contact angles, leading to pore formation in multi-bead structures. By carefully adjusting laser power, TS, and WFS, the bead shape can be tailored to more stable geometries such as semi-circular, parabolic, or ellipsoidal profiles (AKBARI; DING, Y.; KOVACEVIC, 2017). These shapes promote uniform material distribution, reduce defects, and enhance the mechanical properties of the deposited layers, ensuring a reliable and repeatable process.

Table 1 presents the bead parameters for printing based on the type of part, including layer height, layer width, robot speed, and feeder speed. These parameters are essential to determine the optimal settings for different types of piece, ensuring effective printing and quality control (MELTIO, 2022a).

Table 1 – Bead Parameters.

Type	Layer Height	Layer Width	Robot Speed	Feeder Speed
Hollow (1 Perimeter)	0.6	2	10	15.28
Hollow (2 Perimeters)	0.8	1.5	10	15.28
Hollow (3 Perimeters) Solid-Infill	1.2	1	10	15.28
Solid Refrigerated Base	1	1	5	6.37

according to MELTIO (2022a) To achieve optimal printing results, lower power is applied to thin walls to avoid excessive temperatures and potential material sagging. In contrast, thicker walls with additional perimeters can accommodate higher power due to the increased mass relative to the laser power, enhancing the energy density. Figure 7a illustrates the printing substrate, layers, and measurements of the height and width of the layer, providing a visual reference for stable print profiles. Regarding overhangs, Figure 7b demonstrates how overhang angles are influenced by substrate characteristics and layer structure. Printable overhangs are defined by angles greater than 65° from the horizontal plane and less than 25° from the vertical axis; angles beyond these require support material. Although steeper overhangs can be achieved under specific conditions, this may lead to surface or material defects. The LMD process enables the creation of larger overhangs at lower layer heights by maintaining a constant bead width, thereby reducing the percentage of overhanging material per layer.

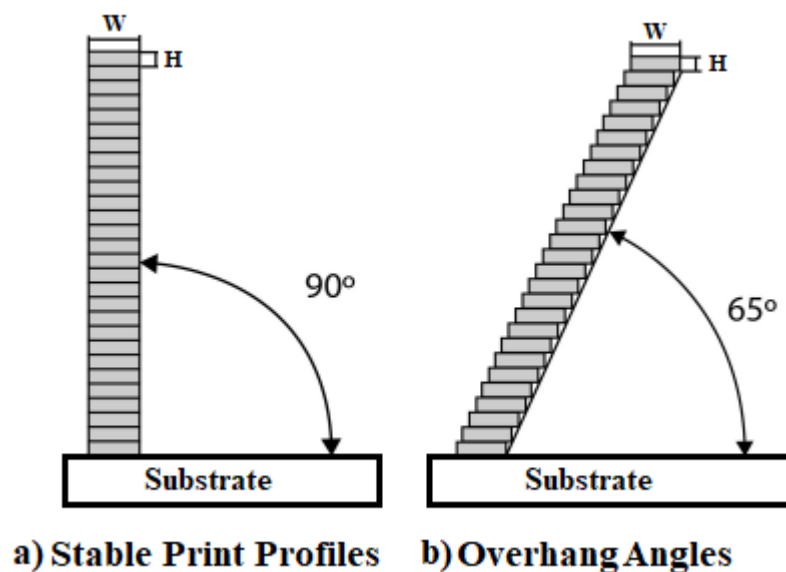


Figure 7 – Diagrams of Bead for Stable Print Profiles and Overhang Angles. Adapted from (MELTIO, 2022a).

Effective overhang printing is better achieved with methods other than 3-axis printing to avoid poor surface quality due to insufficient control. Aligning the tool perpendicularly to the slicing plane simplifies the process, and a 150 mm safety distance should be maintained to avoid collisions, with work-holding solutions used if necessary for proper clearance. The Meltio Engine tool can print overhangs up to 65° from the horizontal plane using 3-axis motion. However, a 6-axis robotic arm offers better alignment by following the trajectory of the part, while adding an external axis improves freedom and maintains tool verticality, improving surface quality and accuracy (MELTIO, 2022a).

2.2.4.2 Comparison of LMD and CMT Deposition Processes

The Cold Metal Transfer (CMT) process, developed by Fronius, employs controlled droplet transfer for welding, effectively minimizing heat input during material application. This approach, highlighted in a video by Cavitar (2023), highlights droplet formation in the welding process, underscoring its role in managing heat and maintaining stability. However, while suitable for certain uses, the CMT technique can pose challenges related to droplet transfer precision in advanced manufacturing environments.

In contrast, LMD process utilized by Meltio features a continuous application method that avoids droplet formation altogether. The video presented by Meltio (2023b) effectively illustrates this approach, demonstrating how the laser directly melts metal wire onto the substrate, thereby enhancing control and minimizing thermal distortion compared to CMT. This continuous method facilitates greater precision and efficiency, making LMD more appropriate for complex applications where consistent material quality is essential.

LMD process offers distinct advantages over CMT as a result of its continuous metal deposition, which eliminates droplet formation and enhances precision. LMD employs focused laser application, resulting in reduced spatter and minimal thermal distortion, thereby significantly improving material quality. This method is particularly advantageous in advanced manufacturing contexts, where intricate detail and consistency are crucial, positioning LMD as the preferred technique for complex fabrications. Its ability to achieve high-quality results makes it an optimal choice for applications requiring meticulous accuracy and repeatability.

2.2.5 Types of Defects in Parts

Based on the classification proposed by Meltio (2023a), the following taxonomy presents the LMD defect categories identified by visual inspection.

Necking Defect: Refers to the phase in which the melt pool becomes significantly thinner before it reaches the substrate, typically preceding dripping. This reduction in material leads to insufficient deposition, causing poor bonding between layers. As a result,

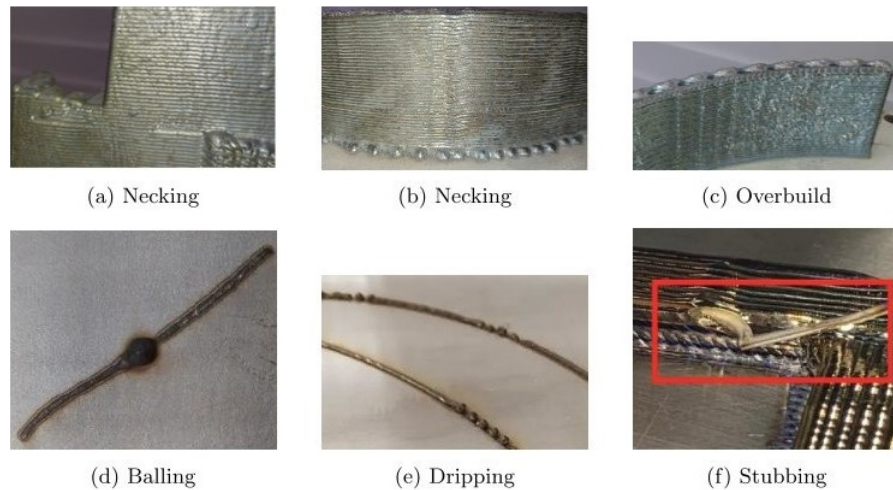


Figure 8 – Defects associated with the LMD-wire process. Adapted from (MELTIO, 2023a).

surface tension issues arise, creating uneven, wavy exterior surfaces and misaligned layer lines, which may affect both the appearance and structural soundness of the printed part.

Overbuilding Defect: This defect is observed when layers are deposited higher than the programmed height, usually due to an imbalance in the energy distribution. Such variations cause uneven layer thickness, where the material is positioned higher than intended, reducing contact between the print head and the workpiece. This may embed the melt pool in the substrate, weakening the laser's effectiveness and distorting the overall structure.

Balling Defect: Occurs when the material melts prematurely, forming a large, bright ball of molten metal in mid-air before it contacts the build plate. This defect leads to material solidifying away from its intended deposition point, resulting in poor layer adhesion and an irregular surface finish.

Dripping Defect: Arises when the wire temporarily loses contact with the build plate, causing the molten material to drip without adhering properly. Though not always detrimental, severe dripping can create uneven deposition, complicating the print and making it difficult to proceed without introducing further imperfections.

Stubbing Defect: Happens when there is insufficient energy to melt the wire properly, resulting in poor bonding with the substrate. In extreme cases, the wire may exit the melt pool and bend away from its path, potentially putting excessive stress on the print head. This can lead to process failure with the risk of damaging the printing equipment.

2.3 Slicing Strategies

The Slicing strategies are grouped into two fundamental approaches. The first approach maintains a constant deposition rate by applying a uniform feeder speed throughout the process. The second approach features a variable deposition rate, dynamically adjusting

the feeder speed or tool movement along the trajectory ([MELTIO, 2022a](#)).

2.3.1 Constant Deposition Rate

According to [MELTIO \(2022a\)](#), constant deposition is a printing strategy designed to maintain a consistent amount of material extruded throughout the part. To achieve this, several key parameters are computed. The volume of deposited material is determined using the formula provided in Equation 2.1. The mass of the material is calculated based on Equation 2.2. The feeder speed necessary to ensure constant deposition is derived from Equation 2.3. The deposition rate per hour is regulated according to Equation 2.4, and the coating rate is determined using Equation 2.5. The energy density applied is evaluated using Equation 2.6. These calculations facilitate the precise and efficient management of the deposition process during printing.

$$\text{Volume} = \text{LayerHeight} \times \text{LayerWidth} \times \text{ToolpathLength} \quad [\text{mm}^3] \quad (2.1)$$

Where:

Volume: Volume of deposited material [mm^3].

LayerHeight: Height of each deposited layer [mm].

LayerWidth: Width of the deposited layer [mm].

ToolpathLength: Total length of the toolpath [mm].

$$\text{Mass} = \text{Volume} \times \text{Material Density} \quad [\text{g}] \quad (2.2)$$

Where:

Mass: Total weight of the deposited material [g].

Volume: Volume of deposited material [mm^3].

Material Density: Density of the material used [g/mm^3].

$$\text{Feeder Speed} = \frac{\text{PrintSpeed} \times \text{LayerHeight} \times \text{LayerWidth}}{\pi \times \text{WireRadius}^2} \quad [\text{mm/s}] \quad (2.3)$$

Where:

Feeder Speed: Feeder speed [mm/s].

PrintSpeed: Printing speed along the toolpath [mm/s].

LayerHeight: Height of the deposited layer [mm].

LayerWidth: Width of the deposited layer [mm].

WireRadius: Radius of the wire used for deposition [mm].

$$\frac{\text{kg}}{\text{h}} = \text{Feeder Speed} \times \pi \times \text{WireRadius}^2 \times \rho \times \frac{3600}{1000} \quad [\text{Kg/h}] \quad (2.4)$$

Where:

kg/h: Deposition rate per hour [kg/h].

Feeder Speed: Feeder speed [mm/s].

WireRadius: Radius of the wire used for deposition [mm].

ρ : Material density [g/mm³].

$$\frac{\text{dm}^2}{\text{h}} = \text{Robot Speed} \times \text{Layer Width} \times \frac{3600}{1000} \quad [\text{dm}^2/\text{h}] \quad (2.5)$$

Where:

dm²/h: Coating rate per hour [dm²/h].

Robot Speed: Robot speed along the toolpath [mm/s].

Layer Width: Width of the deposited layer [mm].

$$\text{Energy Density} = \frac{\text{Laser Power}}{\text{Feeder Speed} \times \pi \times \text{WireRadius}^2} \quad [\text{J/mm}^3] \quad (2.6)$$

Where:

Energy Density: The energy applied per unit volume [J/mm³].

Laser Power: Power of the laser used in the deposition process [W].

Feeder Speed: Speed at which the wire is fed into the deposition process [mm/s].

WireRadius: Radius of the wire being deposited [mm].

2.3.2 Variable Deposition Rate

As outlined by MELTIO (2022a), applying a variable deposition rate can be achieved by keeping the feeder speed constant while adjusting the robot speed. Faster robot speeds result in less material being deposited, while slower speeds increase deposition. To ensure precision, the material volume and robot speed are calculated for each point along the trajectory using the equation 2.7. This method also allows for smoother printing of curved sections by varying the layer height based on proximity to the next layer, while ensuring vertical build direction and avoiding head-component collisions.

$$\text{PrintSpeed} = \frac{\text{BasePrintSpeed} \times \text{Base Layer Height}^2}{\text{Layer Height}^2} \quad (2.7)$$

Where:

PrintSpeed: Adjusted printing speed [mm/s].

BasePrintSpeed: Printing speed corresponding to the base layer height [mm/s].

Base Layer Height: Reference base layer height [mm].

Layer Height: Current layer height [mm].

2.3.3 Slicing Strategies Meltio Space

As described by MELTIO (2024), the slicing strategies for the LMD process are divided into 10, as illustrated in Figure 9, which have been incorporated into the software called Meltio Space.

2.3.3.1 Planar Horizontal Slicing

Planar slicing divides a part into layers using horizontal planes with constant spacing, which can result in segmentation of the surface into curved areas and limit the handling of overhangs. In this method, the tool remains vertical or is aligned perpendicular to the cutting plane if it is not horizontal. Key features include the use of 2 to 4 perimeters for solid parts printed from the inside out, a 100% fill orientation that rotates 45 degrees per layer, a simple toolpath, a constant layer height, and consistent layer orientation.

2.3.3.2 Planar Angled Slicing

Angular planar slicing divides a part into layers using planes that are inclined at a constant angle relative to the horizontal. This method helps to manage overhangs and can improve surface finish by aligning the layers with the contours of the part. The tool remains

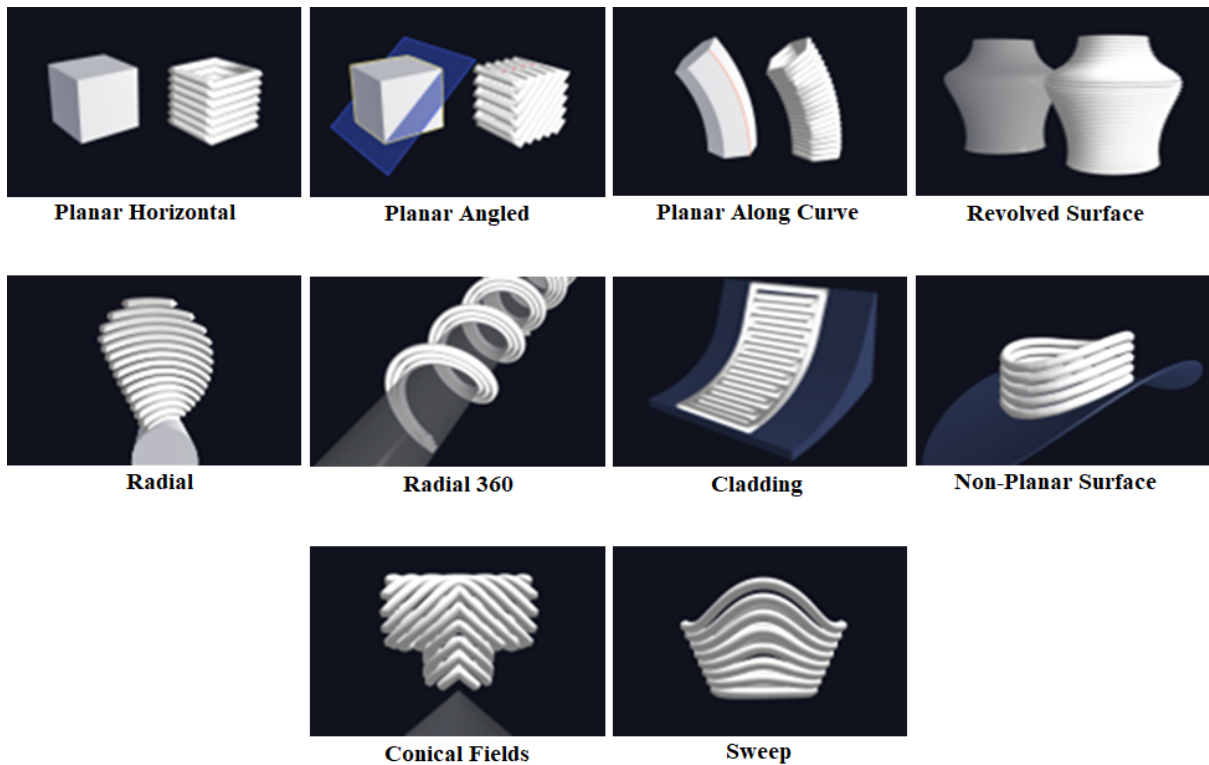


Figure 9 – Deposition Strategies. Adapted from (MELTIO, 2024).

perpendicular to the inclined cutting plane. Key features include the use of 2 to 4 perimeters for solid parts printed from the inside out, a 100% fill orientation that rotates by a specified angle per layer, a simple toolpath, a constant layer height, and consistent orientation of the layers with respect to the angular slicing planes.

2.3.3.3 Planar Along Curve Slicing

The variable layer height based on the distance to the next layer enables smooth printing of curved sections. The slicing planes are calculated based on the guide geometry of each section. the positioner and robot axes are used to maintain vertical build direction, with careful attention required to avoid collisions between the head and components. Within the variable deposition feed rate, there is great potential for application in pipes or curved tubes.

2.3.3.4 Revolved Surface Slicing

This slicing method is designed for rotary symmetrical parts, involving constant layer height and deposition rate. The slicing is specifically for revolved surfaces, with the tool orientation kept tangent to the surface. Using a rotary tilting table is recommended to minimize extensive tool reorientations, while maintaining the deposition head vertically ensures the best quality.

2.3.3.5 Radial Slicing

Radial slicing uses radial layers to slice a part, primarily for printing on cylindrical substrates. It is optimized for features that cover only part of a cylinder. The tool remains normal to the cylinder at every point. To create solid parts, use parameters similar to those in planar slicing: 2 to 4 perimeters, printed from inside out with 100% infill, and Alternately angled 45° per layer. This method maintains a constant layer height, ensuring a consistent deposition rate. A 2-axis part positioner minimizes excess movement of the deposition head and keeps the Meltio Deposition head vertical.

2.3.3.6 Radial 360 Slicing

This method uses coordinated motion between the robot and the positioner, maintaining a constant layer height, deposition rate, and robot speed. Radial slicing involves layers that are "wrapped around" a radial surface, making it ideal for features that twist or twine around a cylindrical substrate. It supports the printing of complex angles and has no size limitations for rotary symmetrical parts, depending on the robot's capacity. The printed features can be hollow, a capability not available with subtractive technology, and can benefit from the use of corrosion or abrasion-resistant materials on the exterior.

2.3.3.7 cladding Slicing

This slicing method generates one or several layers on top of an existing surface. It is specifically available for B-Rep 3D models, such as step files. Cladding is used to add material to a preexisting surface, enabling the enhancement or modification of the model's features with additional layers.

2.3.3.8 Non-Planar Surface Slicing

Non-planar slicing deals with three-dimensional geometries, like double curvature surfaces. It involves offsetting the original surface by a constant layer height, similar to planar slicing, but applied successively. The tool remains perpendicular to the offset surface, with constant layer height, deposition rate, and robot speed. Using a positioner or external axis keeps the deposition tool vertical, reduces the movement of the robot wrist, and enhances surface quality. For solid parts, the same parameters as for planar slicing can be used.

2.3.3.9 Conical Fields Slicing

This slicing method is designed for parts with a conical substrate. It is particularly useful for printing complex overhangs in multiple directions. By adapting the slicing to the conical shape, this method effectively manages challenging geometries, allowing for the accurate creation of intricate features on conical surfaces.

2.3.3.10 Sweep Slicing

This slicing method generates toolpaths that follow the outer shape of a part by interpolating between the start and end points defined by the user. It effectively maps out the tool's trajectory along the part's profile, allowing for precise and controlled material deposition that adheres to the specified contours.

2.4 CAD/CAPP/CAM Systems for Robotic Additive Manufacturing

The material deposition strategies using robotic LMD-Wire are classified based on the geometry of the piece to be created. These deposition strategies are categorized into different **slicing** techniques and can be:

1. **Planar (Part1)**: A strategy that uses flat layers to build the piece.
2. **Multi-planar (Part2)**: A strategy that employs multiple planes for material deposition.
3. **Non-planar (Part3)**: A strategy that allows deposition on non-flat surfaces, accommodating complex geometries.
4. **Segmented (Part4)**: Divides the piece into segments to facilitate deposition.
5. **Angled Printing (Part5)**: A strategy that enables deposition at specific angles to create inclined shapes.
6. **Radial Printing (Part6)**: Uses a radial pattern around an axis for deposition.
7. **Cladding (Part7)**: A strategy that adds layers on top of an existing surface.
8. **Revolved Printing, Hollow Parts (Part8)**: A strategy for printing hollow parts using a rotational pattern.
9. **Contour with 1 or more Material Deposition Cords (Part9)**: A strategy that follows a contour with one or more deposition cords.
10. **Solid (Part10)**: A strategy that creates solid pieces without internal voids.

Table 2 outlines the key software platforms used for CAD, CAPP, and CAM (Computer-Aided Design, Process Planning, and Computer-Aided Manufacturing) in the context of Robotic AM with ABB and Kuka robots. It aligns these platforms with the various part types and slicing methods discussed earlier. In particular, the specific architecture referenced in this context utilizes the Kuka KR70 R2100 robot without the inclusion of a 2-degree-of-freedom positioning table.

Table 2 – Benchmark CAD/CAPP/CAM Systems Robotic Additive Manufacturing.

Software Platform	Part1	Part2	Part3	Part4	Part5	Part6	Part7	Part8	Part9	Part10	Cost (Euro)
SKM	Yes	Yes	Yes	Yes	Yes	Yes	Yes	Yes	Yes	Yes	45000
ADAXIS	Yes	Yes	Yes	Yes	Yes	Yes	Yes	Yes	Yes	Yes	7500
Ai Build	Yes	Yes	Yes	Yes	Yes	Yes	Yes	Yes	Yes	Yes	27000
Meltio	Yes	No	No	No	No	No	No	No	Yes	Yes	Free
Gcode/Rapid/KRL											
ABB Studio	Yes	No	No	No	No	No	No	No	No	No	5000
Kuka.Sim	No	No	No	No	No	No	No	No	No	No	8000
MasterCam Aplus	Yes	Yes	Yes	No	No	No	No	Yes	Yes	Yes	7500
OpenMind	Yes	Yes	Yes	Yes	Yes	Yes	Yes	Yes	Yes	Yes	43000
Siemens NX	Yes	Yes	Yes	Yes	Yes	Yes	Yes	Yes	Yes	Yes	50000
Grasshopper/Rhino	Yes	Yes	Yes	Yes	Yes	Yes	Yes	Yes	Yes	Yes	1000
Simplify3D	Yes	No	No	No	No	No	No	No	Yes	Yes	300
RoboDK	Yes	No	No	No	No	No	No	No	Yes	Yes	1500
Meltio Space	Yes	Yes	Yes	Yes	Yes	Yes	Yes	Yes	Yes	Yes	7500

In addition, several CAD/CAM software providers have integrated with Meltio Engine's Software Partner ecosystem for hybrid and robotic platforms. These include SKM DCAM from SKM Informatik, AdaOne from Adaxis, AiSync from AiBuild, Esprit from Hexagon, Fusion 360 from Autodesk, Aplus+Mastercam from Camufacturing and Mastercam, Hypermill from OpenMind, SiemensNX from Siemens, Hy5CAM from 1ATechnologies, RobotStudio 3D Printing PowerPack from ABB, and SprutCAM X from SprutCam ([MELTIO, 2022b](#)). In August 2023, Meltio also introduced Meltio Space, a new CAD/CAM software designed to integrate with the Meltio Engine (head), offering an intuitive path generation tool.

2.5 Digital Twin ISO 23247

ISO 23247 provides a framework and architecture for the creation of DTs using automation and integration systems. DTs hold significant potential in advancing smart manufacturing. Therefore, ISO 23247 proposes a structure that facilitates context-dependent implementations and supports the composition and reuse of DT components ([SHAO; HELU, 2020](#)) ([LIU et al., 2022](#)).

ISO standard 23247 was developed by ISO Technical Committee TC 184/SC 4 to standardize the architecture to implement DTs in Industry 4.0. This standard outlines a framework for building DTs and integrating data from various sources in four layers ([ISO, 2021](#)) ([CABRAL; GASCA; ALVARES, A. J., 2023](#)). These layers are composed of: Observable Manufacturing Elements (OME), Data Collection and Device Control Entity (DCDCE), Digital Twin (DT) management, and the user domain. The OME layer includes all physical elements for monitoring and control, while the DCDCE layer handles data collection and device control, ensuring synchronization with digital entities ([ALVARES, A. J.; LACROIX; MARON, et al., 2023](#)). The DT domain manages and optimizes the overall system through the

modeling and synchronization of OMEs, providing services such as monitoring, simulation, and analysis. The user domain utilizes the services and applications offered by Digital Twin (FIGUEROA, B. S.; ARAÚJO; ALVARES, A., 2023).

ISO 23247 is aligned with the RAMI 4.0 model and introduces a Business Model with six layers: Asset, Integration, Communication, Information, Functional, and Business. Although the RAMI 4.0 framework does not yet have a specific standard for the DT dimension, the development of AP 238 (STEP-NC) by STEP Tools and ISO/TC 184/SC 4 led to ISO 23247, establishing standards for information exchange and interoperability of the system (ALVARES, A. J.; LACROIX; LIMA MARON, et al., 2023).

2.6 Correlated Works

Yaoyu Ding, Dwivedi, and Kovacevic (2017) describes a LMD system developed at Southern Methodist University's RCAM. This system incorporates a six-axis robotic arm equipped with a two-axis tilt and rotary positioning mechanism, facilitating multidirectional deposition. Using a hybrid slicing technique, it effectively converts overhanging geometries to a flat base, leading to reduced production times and the successful fabrication of intricate components, such as propellers.

Liang et al. (2018) reports on a study investigating WAAM that employs GMA-AM to deposit aluminum alloys. The research examines droplet transfer behaviors via arc voltage and acoustic emission signals, demonstrating that the interaction between arc voltage and current ($U \times I$) has a significant impact on droplet dynamics. A cubic polynomial regression model is introduced, indicating that higher droplet transfer frequencies lead to smaller droplet sizes and higher deposition rates.

Motta, Demir, and Previtali (2018) discusses a study on the coaxial LMD technique utilizing AISI 308 stainless steel, implemented with an ABB robot that has six degrees of freedom. This research emphasizes the mechanisms behind defect formation and identifies stable processing conditions by employing high-speed imaging to observe dynamic behaviors. The optimized melting parameters achieved during the process enable the production of high-aspect ratio components characterized by lower porosity and smoother surfaces.

Moritz et al. (2020) outlines a study examining the effects of cryogenic milling with carbon dioxide on titanium Ti-6Al-4V specimens produced through LMD. This investigation evaluates tool wear and surface integrity relative to dry machining and conventional coolant methods. The results indicate that cryogenic milling achieves superior surface quality with lower roughness and significantly reduced tool wear, promoting effective metallurgical bonding when additional layers are applied using LMD. This method highlights the potential of cryogenic milling in hybrid manufacturing by providing clean surfaces that negate the need for additional cleaning steps while improving tool lifespan.

[Hu et al. \(2022\)](#) investigates a region-based path planning strategy for curved layer deposition in WAAM using a robotic arm with six degrees of freedom. This method mitigates gravitational influences and ensures consistent bead geometry by segmenting complex surfaces into smaller subregions and generating adaptable paths. Compared to conventional techniques, this approach decreases surface waviness and the stair-step effect, making it particularly suitable for producing and repairing intricate, wear-resistant components like forging dies and turbine blades.

[Dugar et al. \(2022\)](#) explores a hybrid manufacturing approach that merges CAD/CAM techniques with WAAM for AlSi5 aluminum alloy, resulting in improved productivity compared to conventional powder-based 3D printing methods. The research highlights the use of a KUKA KR150-2 robotic arm, which possesses six degrees of freedom, to optimize CMT parameters for turbine blade production. The findings indicate a mean deviation of -0.76 mm between virtual simulations and actual outcomes. Mechanical assessments reveal favorable tensile properties, indicating that this hybrid approach serves as a cost-effective and efficient substitute for Selective Laser Melting (SLM) in the creation of intricate components.

[Gibson et al. \(2022\)](#) examines the use of 5-axis Hot-Wire LMD with an 8-axis industrial robot, equipped with a 6-axis arm and a 2-degree-of-freedom positioner. This approach enhances both geometric complexity and print quality through coordinated movements for Ti-6Al-4V components. The research presents various slicing techniques and demonstrates the successful printing of unsupported overhangs at angles of 35° and 45°. It further assesses the control of layer heights and toolpath velocities, culminating in the production of three geometries, including a significant part exceeding 500 mm in height and weighing 44 kg.

[Bernauer, Meinzing, et al. \(2023\)](#) details the development of a localized shielding gas nozzle intended for laser metal deposition, which was evaluated using a KUKA robot that features six degrees of freedom. This nozzle is designed to optimize gas flow and includes internal cooling, achieved through AM. The test with stainless steel wire showed that it effectively prevented oxide formation while maintaining control over melt pool temperatures, thus improving both the quality and efficiency of deposition.

[Montoya-Zapata et al. \(2023\)](#) presents a path-planning strategy for LMD using a six-axis KUKA robot, focusing on the fabrication of revolute workpieces through iso-radial slicing. The approach leverages the multi-axis capabilities of the robot to deposit non-planar layers, reducing the need for support structures. By exploiting the isometry between cylindrical surfaces and 2D parametric space, the system ensures homogeneous bead spacing and consistent metal deposition. Experimental validation on spur and helical gears confirms the suitability of the method for industrial applications.

[Rao \(2024\)](#) presents an online monitoring system based on the Grey model OGM (1,N) for WAAM using a robotic arm, which tracks weld bead height and depth in real time. This system utilizes fewer training samples to optimize process parameters, achieving RMSE

values of 2.52 for height and 0.23 for depth without requiring extensive training time.

[Kushwaha and Basak \(2024\)](#) explores LMD, examining the effects of coaxial powder and wire feedstock deposition to produce stainless steel 316L parts. Using the MELTIO M450 system, the research compares microstructure and microhardness, finding powder-fed specimens with deeper melt pools and faster cooling, while wire-fed parts have smoother surfaces and fewer oxide inclusions. This study highlights key insights into feedstock selection and process parameters for efficient LMD manufacturing.

[Guaglione, Benni, and Previtali \(2024\)](#) investigates the performance of hybrid components manufactured via LMD-Wire, employing a six-axis IRB 4600 robot and a two-axis IRBP A-250 positioner. The study explores continuous, interrupted, and combined manufacturing strategies to assess microstructural integrity and mechanical properties. The results show that fully dense components (>99.9%) can be achieved across all deposition scenarios, with tensile strength influenced by process conditions. The findings highlight the potential of W-LMD for industrial-scale fabrication and repair, especially in heat-sensitive alloys, enabling efficient integration of additive processes with conventional manufacturing.

[Bernauer, Leitner, et al. \(2024\)](#) developed a layer height control system for LMD-Wire, employing a six-axis KR 60 robot, a DKP 400 two-axis positioner, and a 4 kW TruDisk 4001 laser. The system maintained a consistent layer height through closed-loop control using a laser line scanner to acquire height profiles after each layer. The weld beads were segmented and individual feed rates were adjusted per segment. The method effectively compensated for disturbances within a few layers, improving dimensional accuracy and contributing to the automation of LMD processes. This approach improves the reliability of wire-based AM in industrial applications.

[Cai et al. \(2024\)](#) proposed a monitoring method for process stability in robotic LMD-Wire, utilizing an six-axis ABB IRB 4600 robot and an IPG YLS-4000 laser (1080 nm). The approach estimates the intersection point-to-top-layer distance (IPTD) using coaxial visual sensing and a multi-modal deep learning model that integrates molten pool image features and process parameters. A ResNet-18-based CNN demonstrated the highest classification accuracy (99.75%) and superior convergence. Multimodal regression models outperformed single-modal ones, validating the effectiveness of the method. This contributes to automated, stable LMD-Wire for complex metal parts.

In contrast to the correlated works summarized in Table 3, this work presents a robotic additive manufacturing cell (RAMC) that integrates a six-axis KUKA KR70 R2100 robot with the MELTIO Engine, operating with a 1.2 kW lfiber laser source for LMD-Wire. While the developed RAMC has the capability to fabricate both planar and non-planar geometries, the present work focuses on planar deposition in three case studies involving metallic components designed via Rhino3D/Grasshopper and Meltio Space. These parts were used to evaluate geometric accuracy, defects, and mechanical performance through dimensional analysis and Metallographic and Mechanical Characterization. The RAMC also implements a DT architecture compliant with ISO 23247, enabling real-time monitoring, process simulation, traceability, and predictive failure analysis. Furthermore, the system adopts a CAD/CAPP/CAM-integrated workflow for automated toolpath generation using the KUKA Robot Language (KRL). For operator safety, the cell includes 980 nm laser filtering windows, an exhaust system, and an interlocked door mechanism to prevent exposure during laser operation. This comprehensive setup enhances deposition precision, operator safety and interoperability of the system, aligning with the industry 4.0 standards for smart manufacturing.

Table 3 – Comparative Table of Correlated Works.

Authors	Year	Process	Machine	Part Type	Laser Power [kW]	DT
(DING, Y.; DWIVEDI; KO-VACEVIC)	(2017)	LMD	Robot (8-Axis)	Planar	4	No
(LIANG et al.)	(2018)	WAAM	3D Printer	Planar	No	No
(MOTTA; DEMIR; PREVITALI)	(2018)	LMD	Robot (6-Axis)	Planar and Non-Planar	3	No
(MORITZ et al.)	(2020)	LMD	Robot (6-Axis)	Planar	2	No
(HU et al.)	(2022)	WAAM	Robot (6-Axis)	Planar and Non-Planar	No	No
(DUGAR et al.)	(2022)	CMT	Robot (6-Axis)	Planar	No	No
(GIBSON et al.)	(2022)	LMD	Robot (8-Axis)	Planar	20	No
(BERNAUER; MEINZINGER, et al.)	(2023)	LMD	Robot (6-Axis)	Planar	4	No
(MONTOLYA-ZAPATA et al.)	(2023)	LMD	Robot (6-Axis)	Planar	6	No
(RAO)	(2024)	WAAM	Robot (6-Axis)	Planar	No	No
(KUSHWAHA; BASAK)	(2024)	LMD	3D Printer	Planar	1.2	No
(GUAGLIONE; BENNI; PREVITALI)	(2024)	LMD	Robot (8-Axis)	Planar	3	No
(BERNAUER; LEITNER, et al.)	(2024)	LMD	Robot (8-Axis)	Planar	4	No
(CAI et al.)	(2024)	LMD	Robot (6-Axis)	Planar	4	No
This Work	2025	LMD	Robot (6-Axis)	Planar and Non-Planar	1.2	Yes

2.7 Stepwise Development of the Robotic Additive Manufacturing Cell

The flow diagram in Figure 10 depicts the sequential evolution of the RAMC, encompassing the integration of physical and logical components, software systems, and validation activities. The process began with the reception of the KUKA KR70 R2100 robot and the Meltio Engine, alongside training for proper installation and operation. Physical integration followed, consisting of six tasks: cabin assembly, robot installation, table positioning, Meltio Engine installation, safety system integration, and robot–Meltio synchronization. Logical integration then validated the bidirectional communication between the robot and Meltio controllers. Subsequently, the CAD/CAPP/CAM system was developed through design, process planning, and manufacturing stages, generating optimized slicing strategies and executable KUKA KRL codes. Finally, case studies validated the RAMC through visual defect inspection, metallographic analysis, and microhardness testing. Together, the diagram outlines the structured pathway by which the RAMC was implemented and validated for industrial AM.

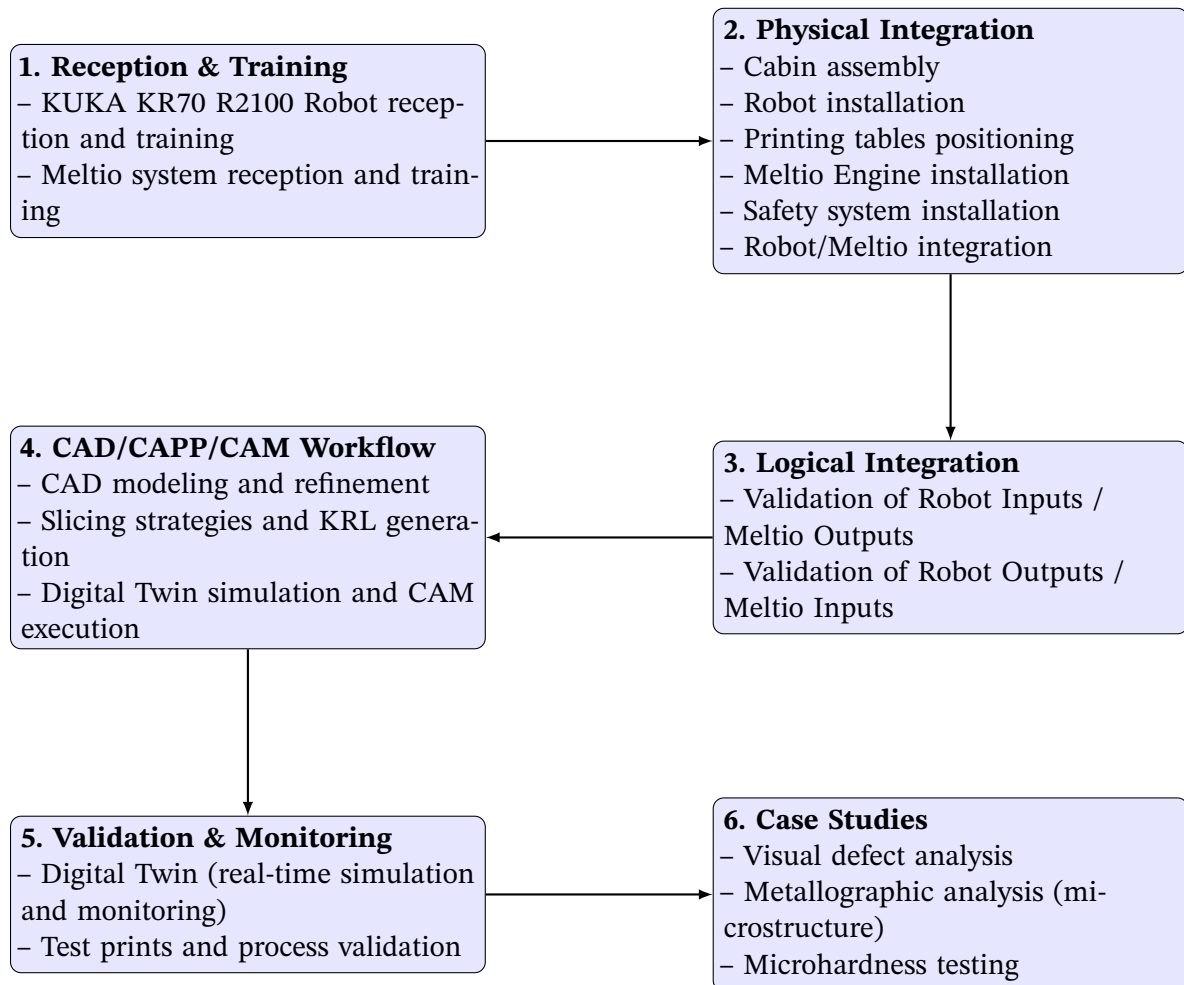


Figure 10 – Evolution of the Robotic Additive Manufacturing Cell (RAMC) through sequential development phases.

3 Methodological Proposal for the Development of a Robotic Additive Manufacturing Cell

3.1 Introduction

This chapter presents a methodological proposal based on the IDEF0 model for the development of a Robotic Additive Manufacturing Cell (RAMC) based on the Wire-Based Laser Metal Deposition Process (LMD-Wire). Initially, diagrams related to physical and logical integration activities, the physical assembly of RAMC components, and physical and logical integration between components and the control system are presented. Finally, diagrams related to the development and implementation activities of the CAD/CAPP/CAM system (Computer-Aided Design, Computer-Aided Process Planning, and Computer-Aided Manufacturing) based on a Digital Twin (DT) and printing of metal parts are presented. This methodology covers from the physical integration of components, logical integration, design, planning, digital twin simulation, real-time monitoring to the printing of the final part.

3.2 Robotic Additive Manufacturing System

Figure 11 illustrates a comprehensive architecture for the RAMC, seamlessly integrated within a CAD/CAPP/CAM system. The workflow begins with a diverse array of inputs, such as printing parameters, logical signals, argon gas supply, robot calibration weight, cooling liquid, STL geometry files, and printing wire. These inputs are systematically processed within the RAMC, which comprises a secure metal cabin that houses the KUKA KR70 R2100 robotic system and the Meltio Engine, all governed by a sophisticated safety system alongside precision printing tables.

The integration of these components facilitates the transformation of digital models into actionable commands for the robot, adhering to deposition strategies that align with the ISO 23247 standards. The outputs of this intricate process include the final printed part, comprehensive process data, and DTs of the KUKA, RoboDK, and Meltio systems. These DTs enable real-time monitoring and data analysis through user-friendly 2D panels and cloud services, significantly improving process control, optimization, and overall operational efficiency. By leveraging this integrated architecture, the RAMC not only improves productivity, but also ensures the consistent quality of AM outputs.

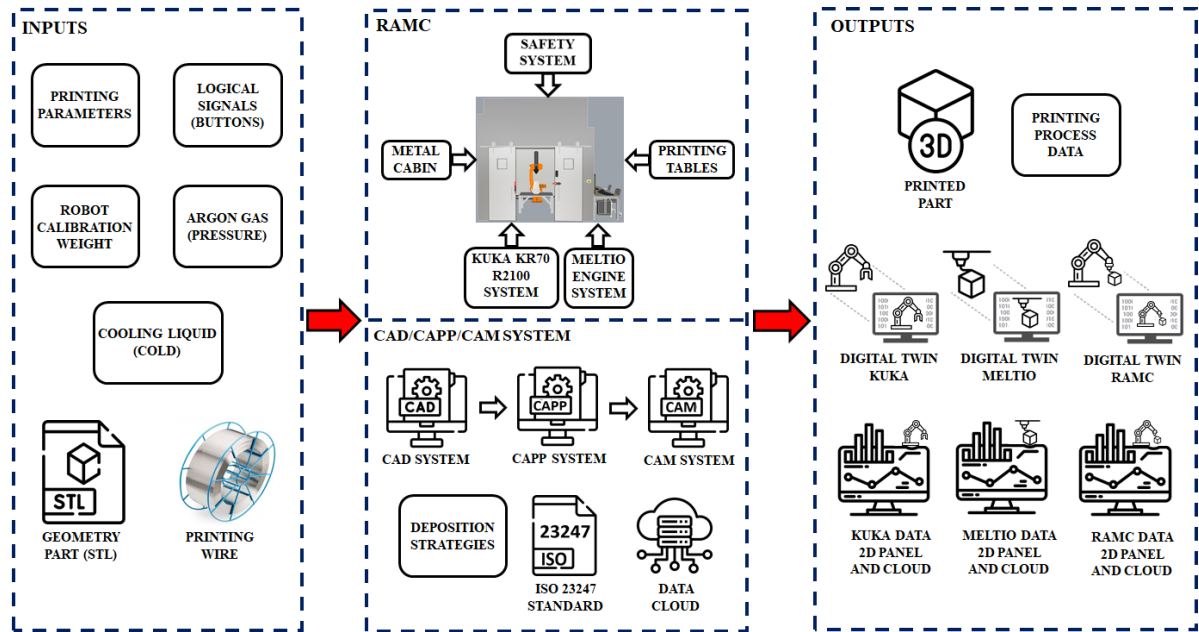


Figure 11 – Robotic Additive Manufacturing System (FIGUEROA, B. S.; ÁLVARES, 2025b).

3.3 Robotic Additive Manufacturing Cell

RAMC has been meticulously modeled using the IDEF0 methodology, which is recognized for its structured approach to represent complex systems and processes (FIGUEROA, B. S.; ÁLVARES, 2024). Figure 12 illustrates level 0 of the IDEF0 model, which encompasses all inputs, controls, mechanisms, outputs, and functionalities relevant to the development of this Cell. This comprehensive depiction facilitates a thorough understanding of the interactions among various components, thus clarifying the operational framework essential for the effective functioning of the cell.

The architecture of the IDEF0 model is intentionally designed to promote clarity and enhance communication among stakeholders involved in the project. By providing a detailed breakdown of inputs and outputs, the model fosters collaboration and ensures that all parties maintain a shared understanding of the project objectives and requirements. This visualization not only serves as an aid to comprehension, but also acts as a foundational framework for continuous improvement, allowing for iterative refinements based on stakeholder insights.

The IDEF0 model is accessible via the URL <https://tinyurl.com/mrcc2vra>, providing a resource to navigate the proposed activities. This model outlines key components, allowing users to analyze the dynamics of the functionalities of the RAMC. Employing the IDEF0 methodology enhances stakeholder communication and ensures comprehensive coverage of critical elements, aligning the project with industry standards. This structured approach is essential for identifying bottlenecks and optimization areas that ultimately improve productivity and quality in manufacturing operations.

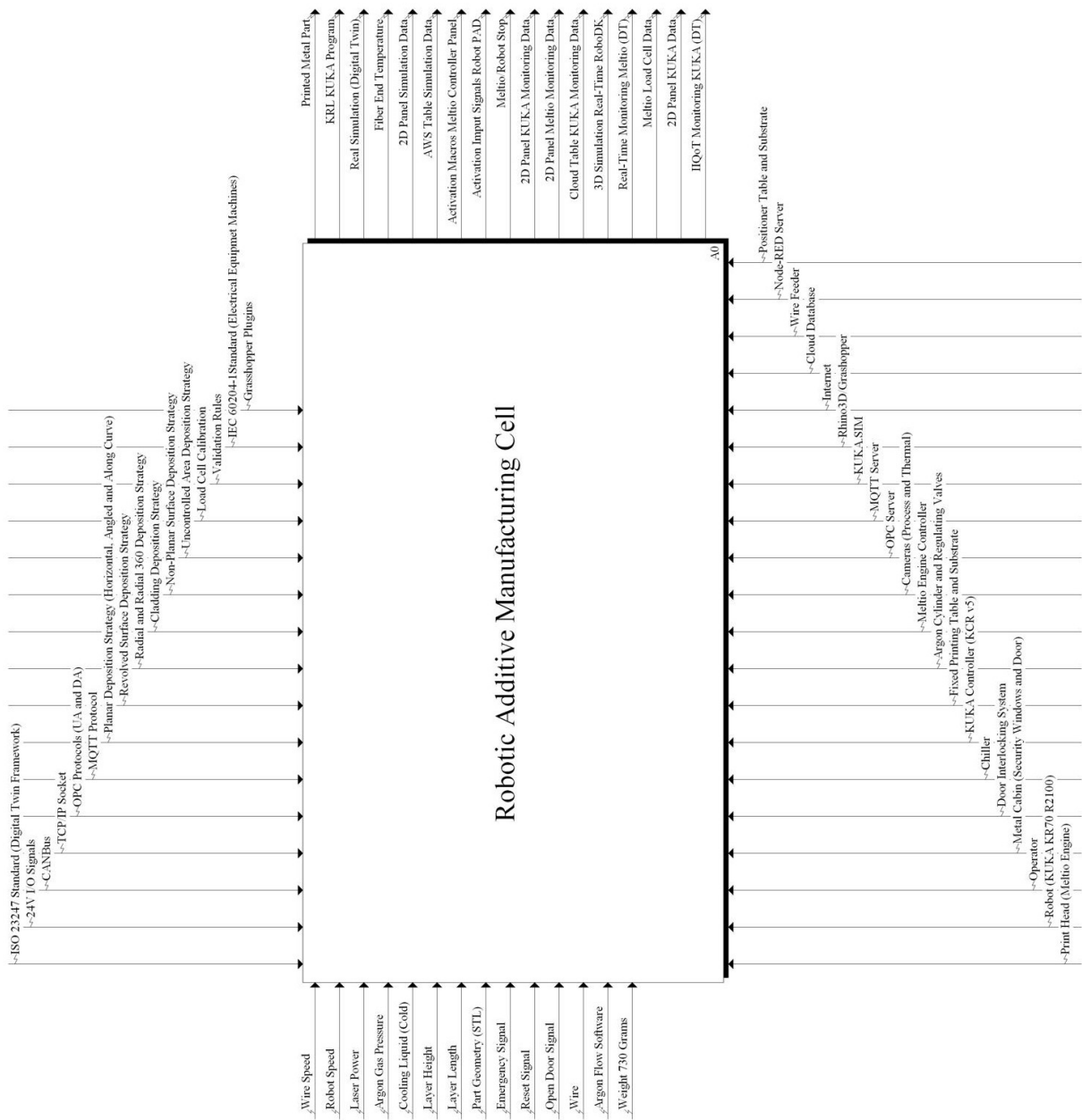


Figure 12 – IDEF0 Diagram: Methodology for the development of a RAMC.

Figure 13 illustrates the stratification of the system into two layers associated with the integration of RAMC:

1. Physical and Logical Integration.
2. CAD/CAPP/CAM System.

This activity focuses on the comprehensive interaction between hardware and software components within the RAMC. It encompasses the reception of various signals and inputs, which generate crucial outputs, including safety stop signals for the system, positional data for both the robot and the printing table, and activation signals that interface with the CAD/CAPP/CAM system. The CAD/CAPP/CAM System activity processes inputs such as printing parameters and part geometries, yielding outputs that consist of real-time simulations, the generation of printing code, the actual printed metal part, and continuous monitoring of relevant variables and data.

3.4 Physical and Logical Integration

Figure 14 depicts the IDEF0 model pertinent to these physical and logical integration activities, highlighting two critical activities essential for the seamless integration of the RAMC:

1. Physical Integration: Physical connection of RAMC components.
2. Logical Integration: Logical connection for process coordination.

The Physical Integration activity is essential for the operation of the RAMC, as it manages key inputs such as pressurized argon gas, cooling fluids, wire feedstock, reset signals, emergency stop commands, and door-opening indicators. Proper handling of these inputs enables critical outputs, including the secure positioning of the printing head, precise alignment of the printing tables and robot, and the generation of return signals and macro activations. This coordinated flow of information is fundamental to ensuring safety and efficiency in the manufacturing environment.

The outputs from the Physical Integration activity serve as vital inputs for the Logical Integration activity. This stage uses return signals and macro activations to initiate input signals in the Programmable Automation Controller (PAD) and to activate specific macros on the Meltio controller panel. Through this coordination, the Logical Integration enhances the RAMC's operational performance. This dual-layered integration ensures safe, efficient operation and supports a streamlined AM process, improving productivity and quality in complex metal part production.

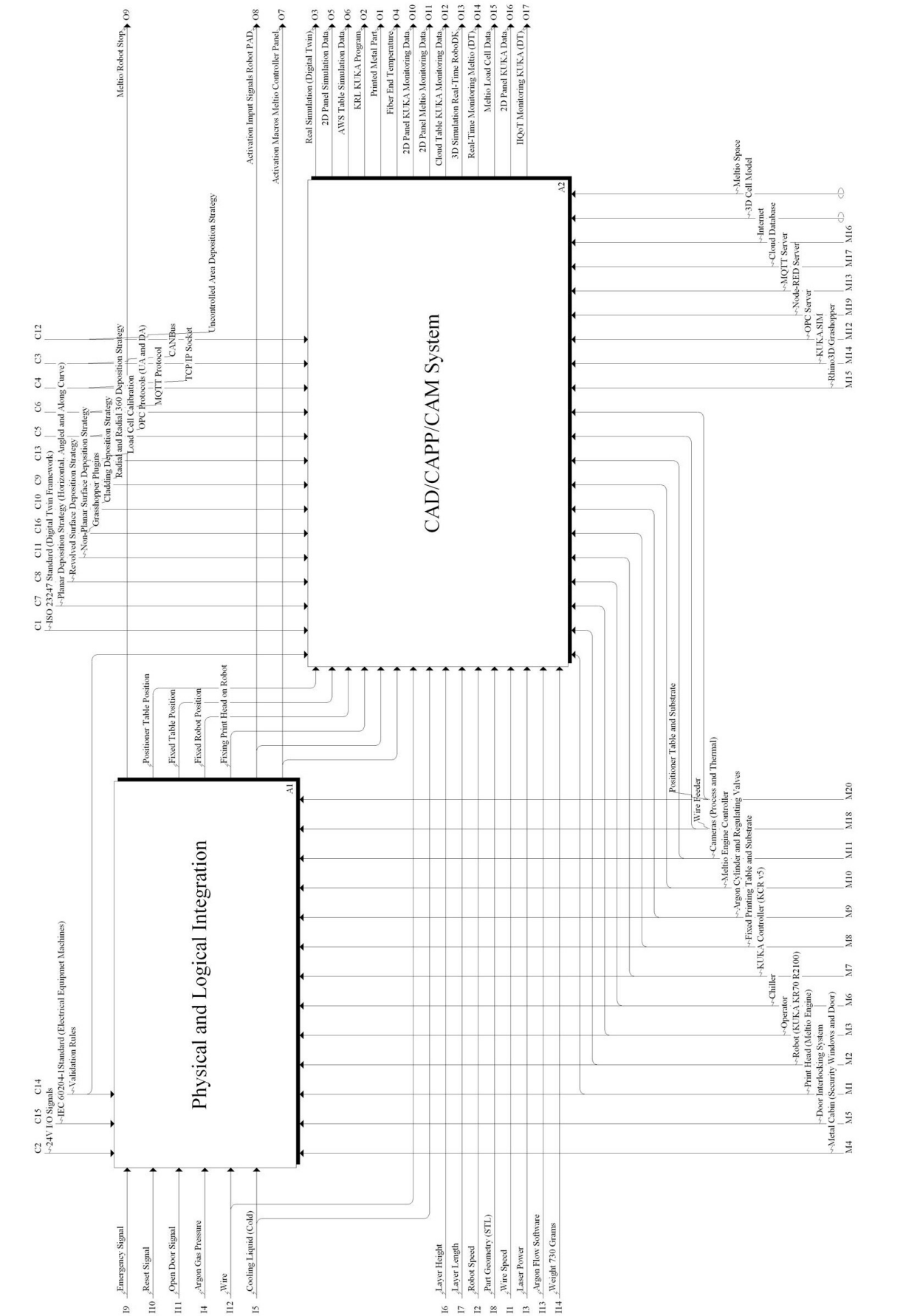


Figure 13 – IDEF0 Diagram: Main activities of the RAMC.

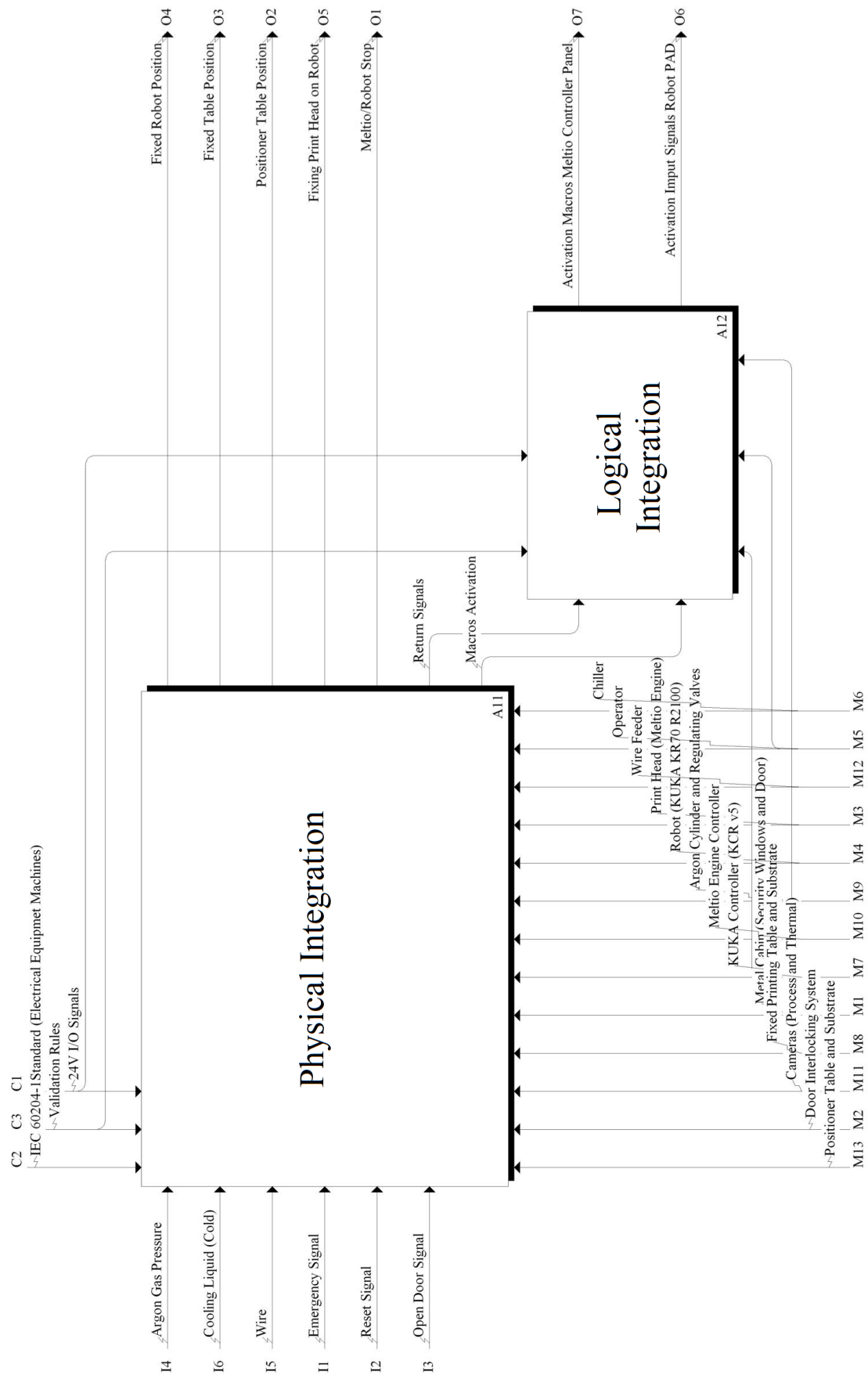


Figure 14 – IDEF0 Diagram: Physical and Logical Integration Activities.

3.4.1 Physical Integration

Figure 15 shows the IDEF0 model concerning Physical Integration activities, consisting of six tasks that facilitate the physical, electrical, and mechanical connections required for the RAMC:

1. Assembly of the Additive Manufacturing Cell cabin.
2. Installation of the robot.
3. Positioning of the printing tables.
4. Installation of the Meltio Engine System.
5. Installation of the Safety System.
6. Robot/Meltio Integration.

The RAMC's physical system activities are interconnected and handle both external inputs and the inputs/outputs of other activities. Each task incorporates mechanisms for seamless integration, with controls established on validation rules, electrical standards, and 24V input/output signals. The outputs generated from these tasks serve as inputs for subsequent activities, facilitating the production of essential outputs for the operation of the RAMC and its logical integration.

3.4.1.1 Cabin Assembly of the RAMC

The Cabin Assembly activity of the RAMC processes emergency signals, reset signals, and door opening signals from external buttons. The cabin comprises components and tools for its metal structure, an exhaust fan, cameras for process visualization and thermal imaging, safety windows, and a door. The resulting output is the AM Metal Cabin, which supports the subsequent robot installation and safety system installation activities.

3.4.1.2 Robot Installation

Figure 16 presents the IDEF0 model for the Robot Installation activity, which encompasses two tasks that utilize the AM Metal Cabin output from the cabin assembly activity as input. The robot fixation task aims to secure the robot within the workspace using screws, the robot's metal base, and acetic silicone, resulting in the robot being fixed in position. The robot controller assembly task involves connecting electrical cables, leading to the establishment of the robot's emergency stops, digital outputs, and digital inputs.

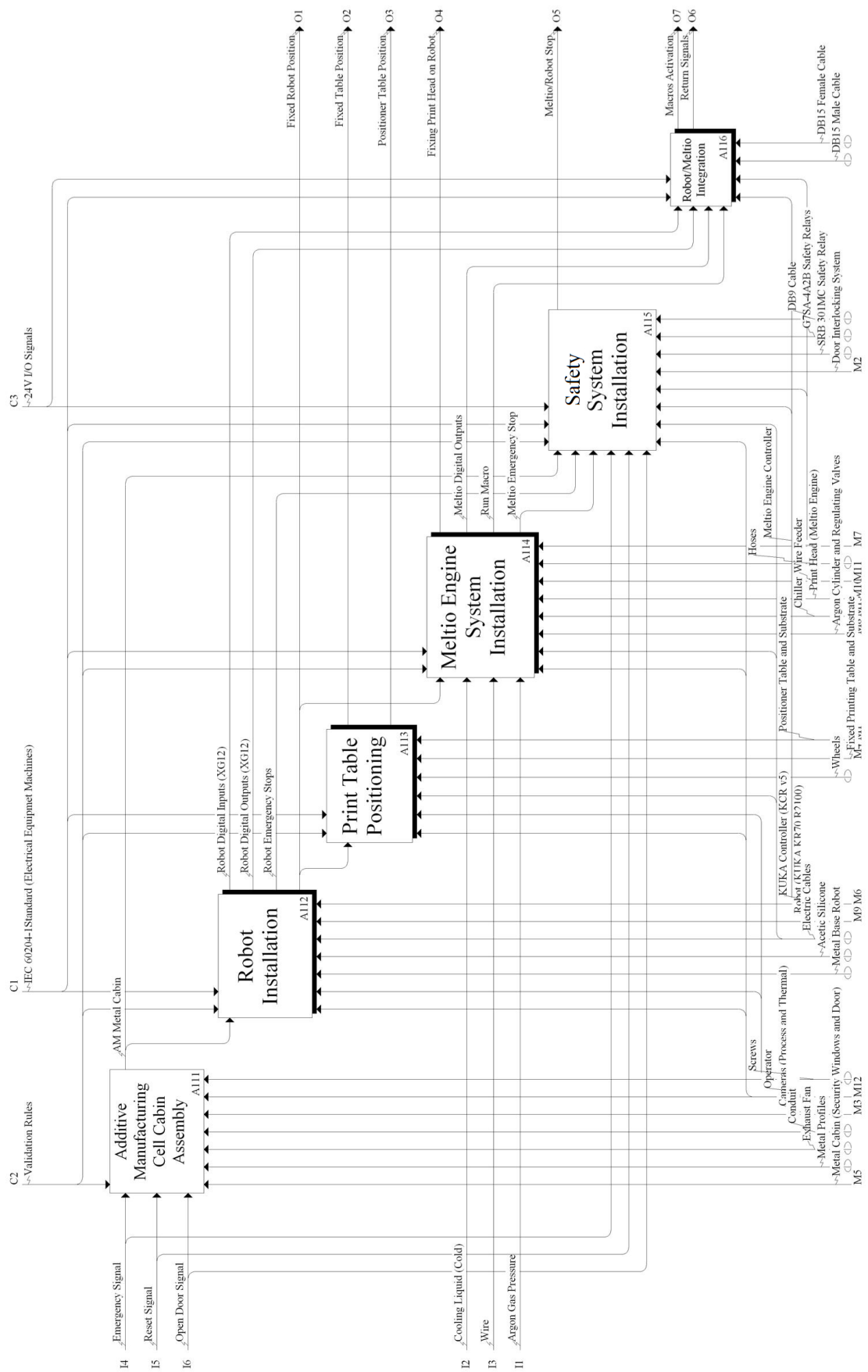


Figure 15 – IDEF0 Diagram: Physical Integration Activities.

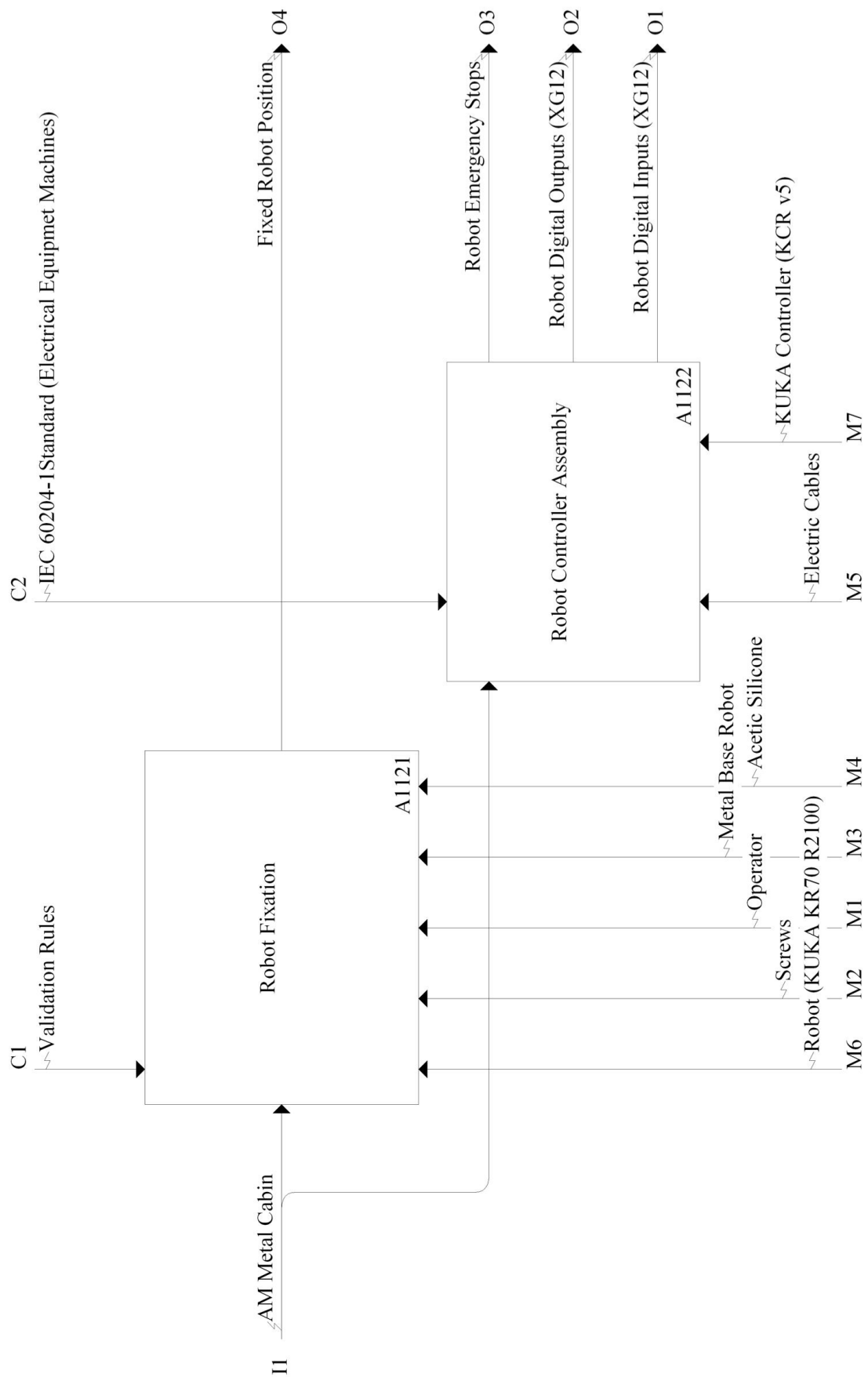


Figure 16 – IDEF0 Diagram: Robot Installation Activities.

3.4.1.3 Print Table Positioning

Figure 17 illustrates the IDEF0 model for the Print Table Positioning activity, comprising two stages that rely on the robot's fixed position as input. Fixed Printing Table Positioning task utilizes a stable table with a metal substrate, wheels, grounding electrical cables, and screws to achieve the fixed position of the print table. The Positioning Print Table task employs a positioning table with two degrees of freedom, screws, and grounding electrical cables to determine the final position of the table.

3.4.1.4 Installation of the Meltio Engine System

Figure 18 presents the IDEF0 model corresponding to the Meltio System Installation activity, consisting of seven tasks:

1. Attaching the Printhead to the Robot: The printhead is attached to the robot considering its fixed position.
2. Assembling the Cooling System: The cooling system is assembled to cool the printhead.
3. Assembling the Gas System: The argon gas system is assembled to create a protective atmosphere against oxidation of the metal part during the printing process.
4. Assembling the Wire Feeding System.
5. Connecting the Fibers: Responsible for activating the laser in the printhead from the controller.
6. Electrical Connections of the Printed Circuit Board: Physical electrical connections of the printed circuit board for the printhead system.
7. Integrating the Meltio System.

The activities outlined in Figure 18 ensure the functionality of the Meltio system, relying on inputs such as the robot's fixed position, cold cooling liquid, pressurized argon gas, and wire, and producing outputs that include the attachment of the printhead to the robot, digital outputs of Meltio, Run Macro, and the emergency stop of the meltio system.

3.4.1.5 Installation of the Safety System

The Safety System Installation activity receives inputs from emergency, reset, and door opening signals, as well as outputs from the AM metal cabin from the RAMC cabin assembly, the robot's emergency stops from the robot installation, and the Meltio system's emergency stop. This task also incorporates the implementation of screws, DB9 cables, SBR301MC safety relays, G7SA-1A2B safety relays, the KUKA controller and the Meltio Engine controller, culminating in the shutdown of the Meltio/Robot system.

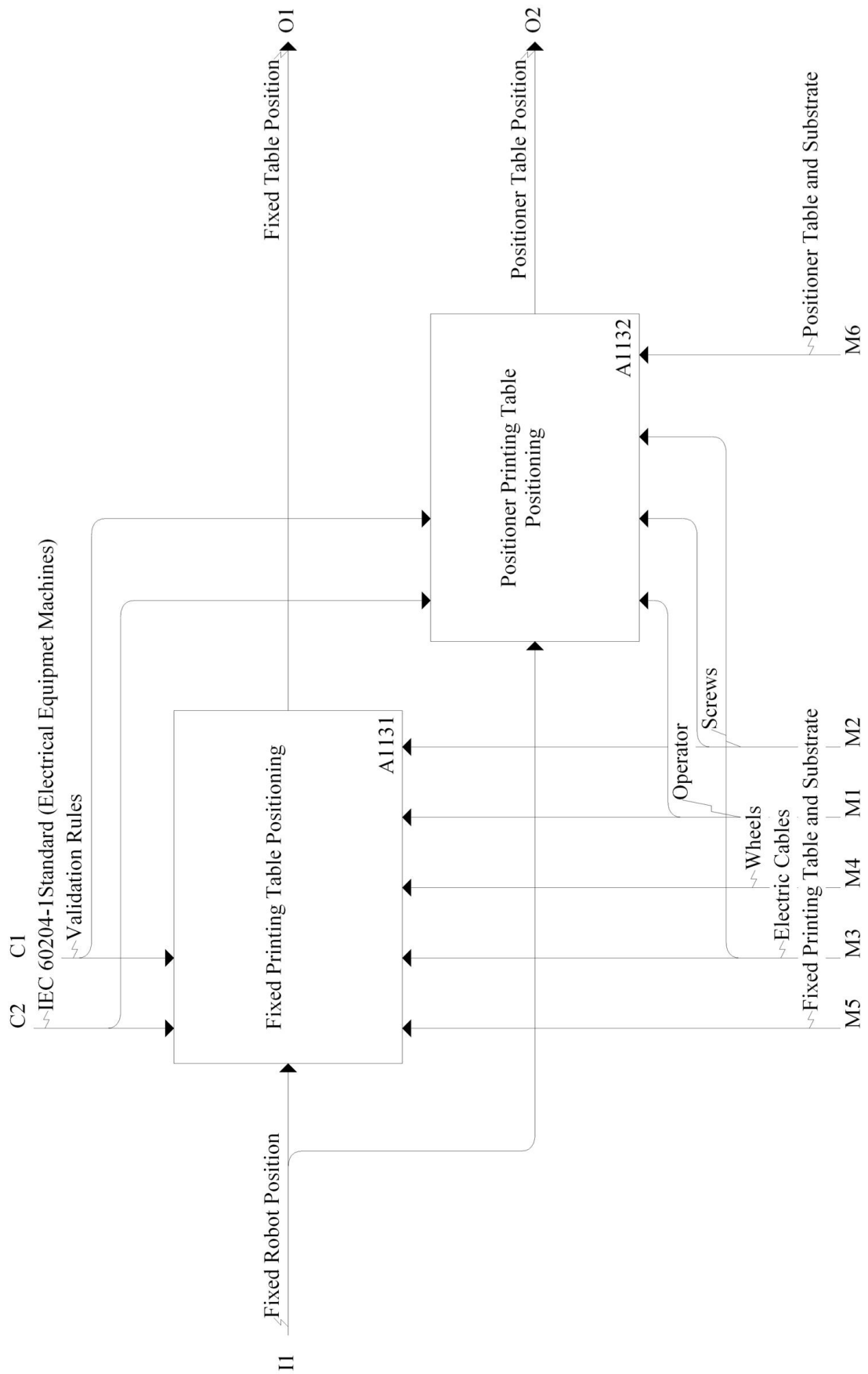


Figure 17 – IDEF0 Diagram: Print Table Positioning Activities.

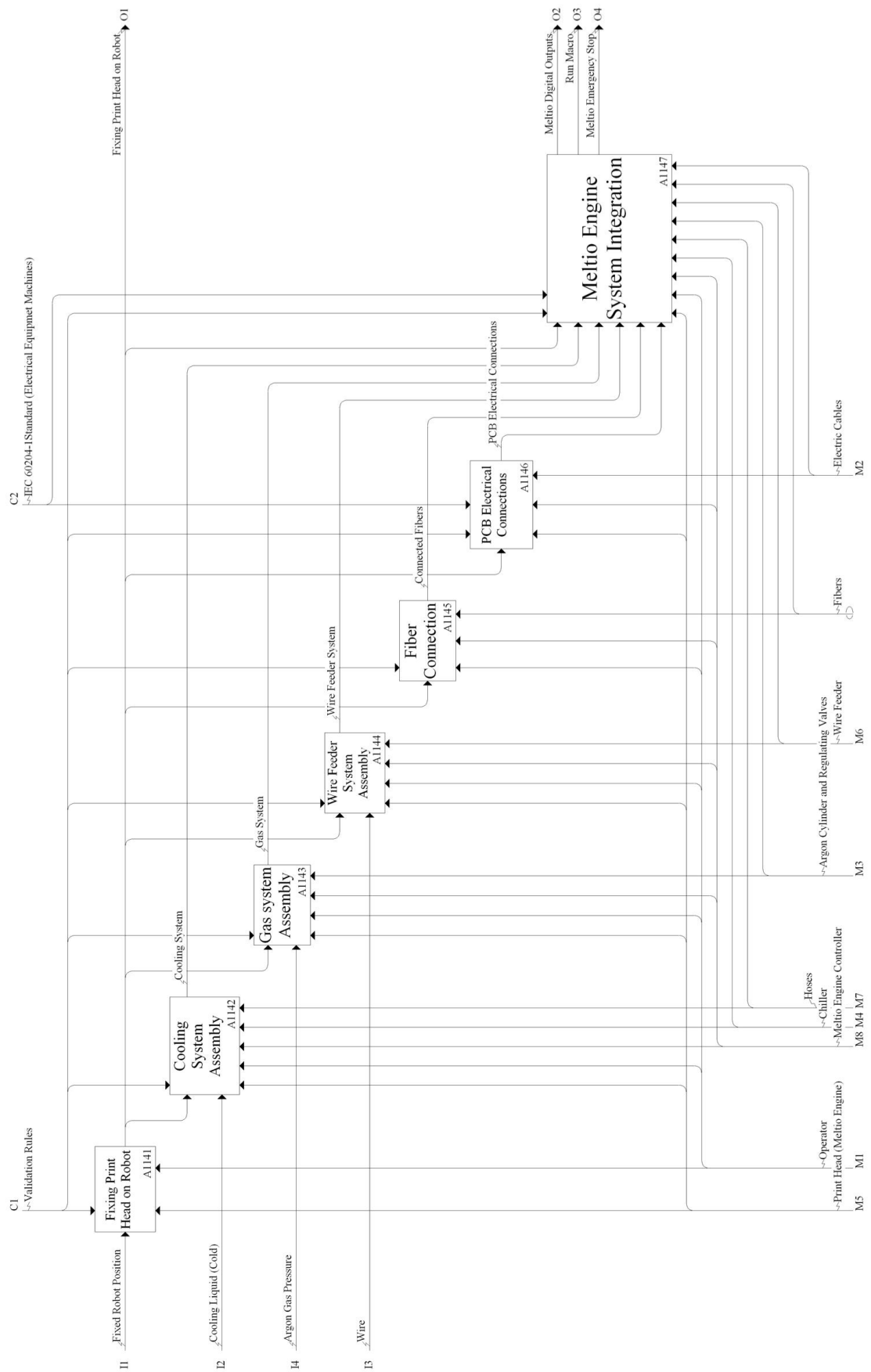


Figure 18 – IDEF0 Diagram: Meltio System Installation Activities.

3.4.1.6 Robot/Meltio Integration

Figure 19 presents the IDEF0 model related to the Robot/Meltio Integration activity, which consists of two stages that utilize the outputs of the preceding activities.

The Robot Outputs/Meltio Inputs Integration task incorporates the robot's digital outputs and Run Macro, utilizing a male DB15 cable, the robot controller, and the Meltio Engine controller, resulting in the activation of macros. Meanwhile, the Robot Inputs/Meltio Outputs Integration task processes the robot's digital inputs and Meltio's digital outputs, employing a female DB15 cable, the robot controller, and the Meltio Engine controller, producing signal returns.

These signal returns and macro activations establish a crucial connection that facilitates the logical integration of the system, allowing the outputs of these activities to feed into the logical integration processes.

3.4.2 Logical Integration

Figure 20 presents the IDEF0 model corresponding to the Logical Integration activity, comprising two essential tasks to align the logical framework with the physical components of the RAMC:

1. Validation of Robot Inputs/Meltio Outputs Integration.
2. Validation of Robot Outputs/Meltio Inputs Integration.

The Validation of Robot Inputs/Meltio Outputs Integration task takes as input the return of signals from physical integration, utilizing the robot controller and Meltio Engine controller, resulting in the activation of input signals on the robot control panel. Conversely, the Validation of Robot Outputs/Meltio Inputs Integration task processes the activation of macros from physical integration, using the robot controller and Meltio Engine controller, leading to macro activations on the Meltio controller panel.

This logical interaction streamlines the connection between control processes and physical integration, enabling the transmission of instructions from the controllers to the physical elements, thereby facilitating task execution.

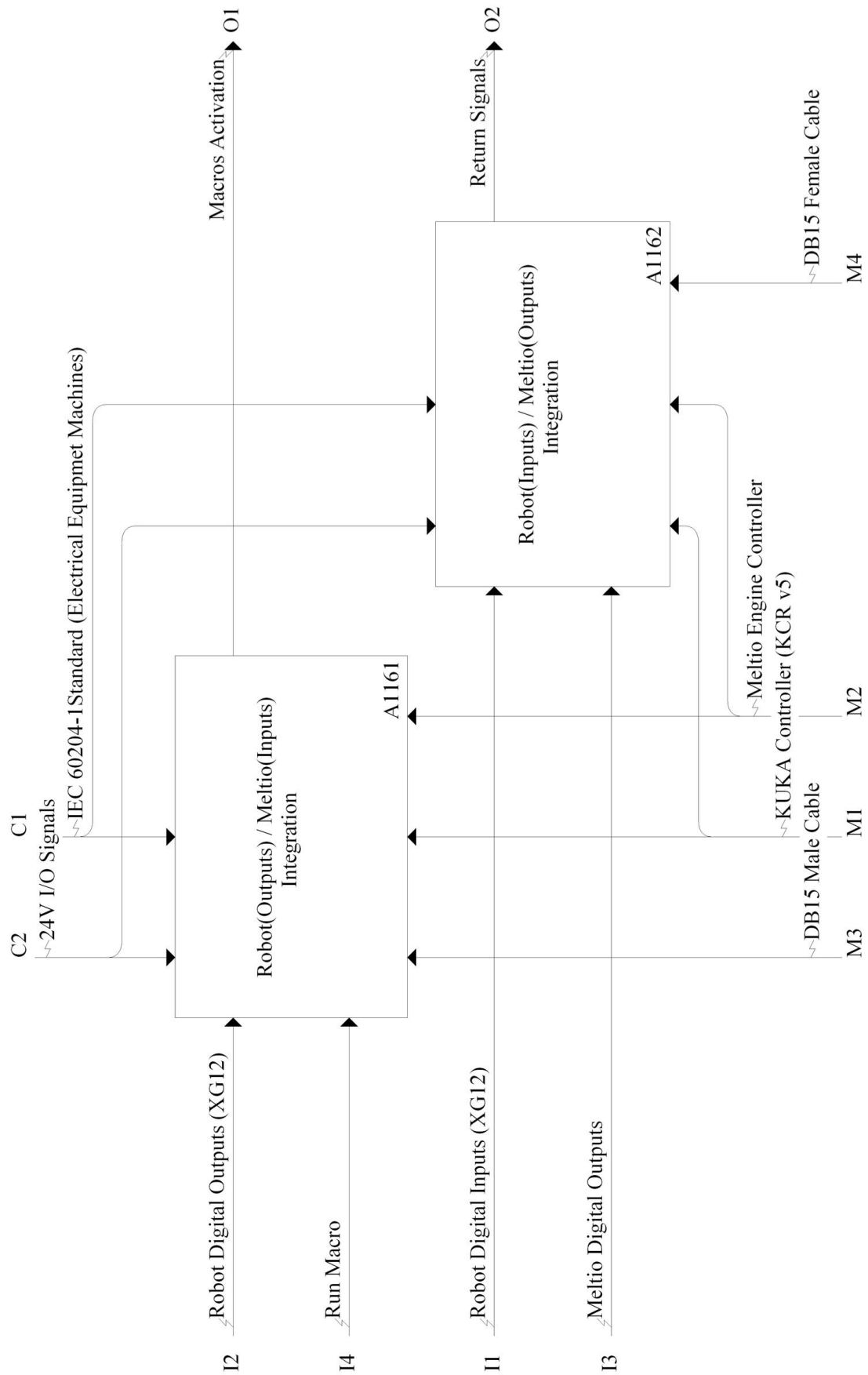


Figure 19 – IDEF0 Diagram: Robot/Meltio Integration Activities.

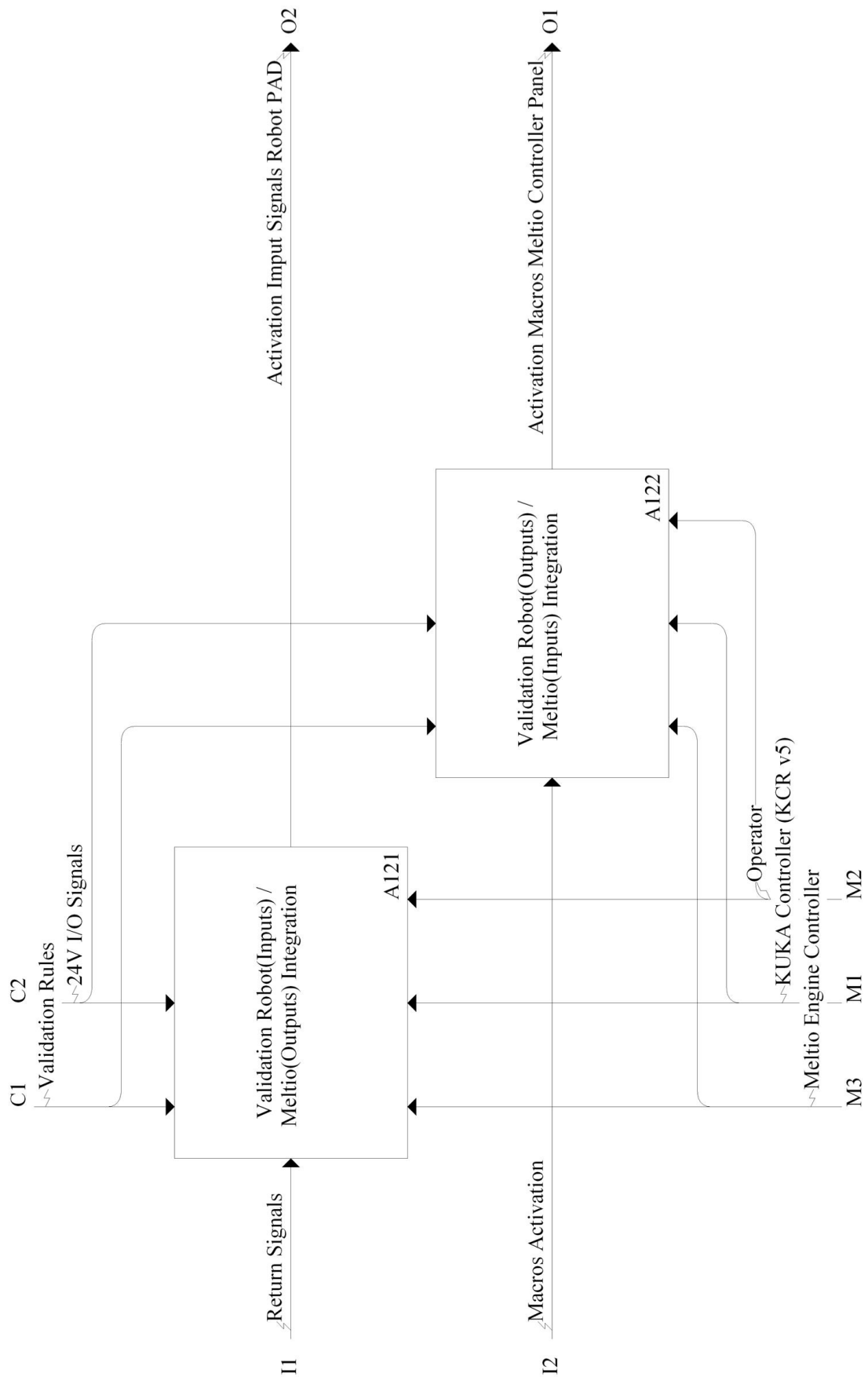


Figure 20 – IDEF0 Diagram: Logical Integration Activities.

3.5 CAD/CAPP/CAM System

Figure 21 presents the IDEF0 model for developing the CAD/CAPP/CAM System, which encompasses three key activities:

1. CAD: Computer-Aided Design.
2. CAPP: Computer-Aided Process Planning.
3. CAM: Computer-Aided Manufacturing.

The system accepts inputs from the printing parameters, coolant, wire, and weight for robot calibration. It also integrates data from the Physical and Logical Integration activity, which includes the attachment of the printing head, activation of input signals on the control panel, and positioning of the printing tables and robot. The resulting outputs include the DT simulation, monitoring of variables in 2D, KUKA KRL program, fiber temperature, the printed metal part, and the referencing of Base and Tool, which subsequently feeds into the CAPP system.

3.5.1 CAD

Figure 22 illustrates the IDEF0 model related to the CAD activity, which consists of three tasks:

1. Importing the STL file.
2. Generating the base model.
3. Adjusting and refining the model.

The import activity receives the geometry of the part in STL format and produces an imported file within the CAD system. This file serves as input for generating the base model, which occurs in the CAD environment. The adjustment and refining activity processes the base model, resulting in the final CAD model in STL format. The activities share resources such as the CAD system, internet connectivity, and operator intervention.

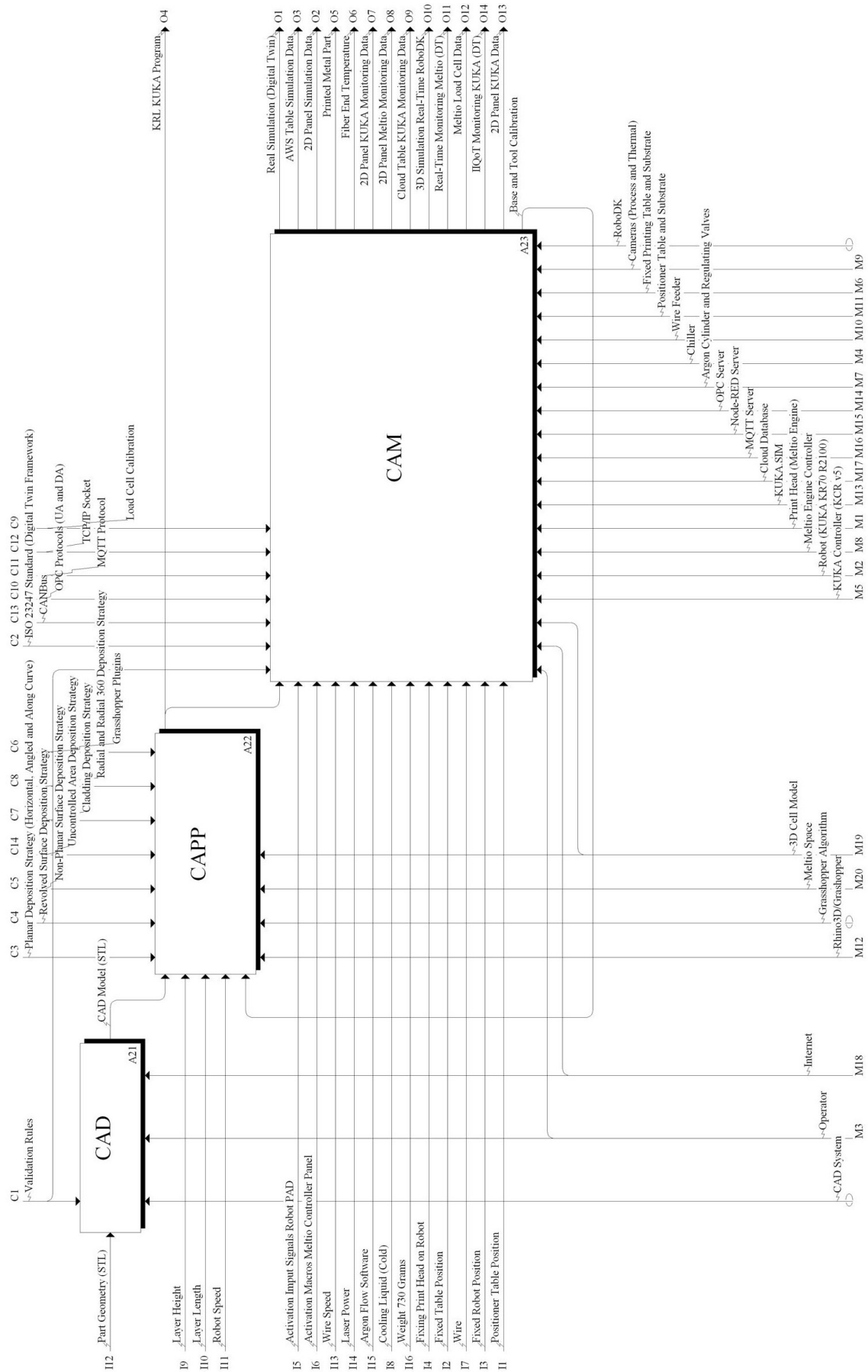


Figure 21 – IDEF0 Diagram: CAD/CAPP/CAM System Activities.

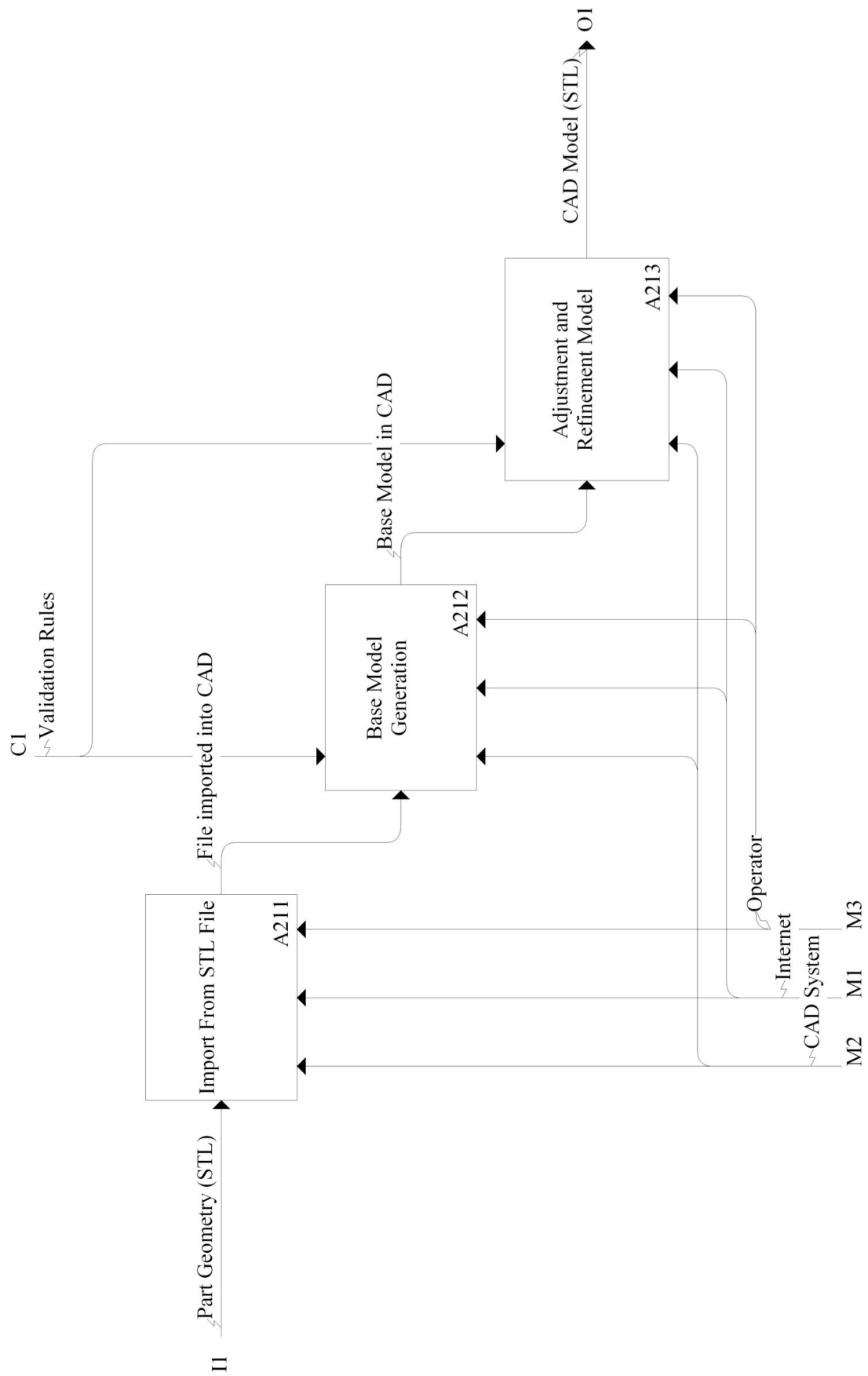


Figure 22 – IDEF0 Diagram: CAD System Activities.

3.5.2 CAPP

Figure 23 presents the IDEF0 model related to the CAPP activity, which includes three activities:

1. Importing the CAD Model.
2. Slicing the Part.
3. Generating the KRL Program.

The CAPP activity receives the CAD model in STL format from the CAD activity, along with adjustments for the tool origin from the CAM activity and external parameters such as robot speed, layer height, and width. This activity conducts print planning and generates the KUKA KRL code.

3.5.2.1 Importing the CAD Model

The CAD model import activity takes the CAD model in STL format from the CAD activity, importing it into the Rhinoceros/Grasshopper and Meltio Space software, resulting in a CAD model ready for processing.

3.5.2.2 Slicing the Part

Figure 24 illustrates the IDEF0 model that defines the ten slicing strategy activities involved in generating the toolpaths for the part. These activities include **Horizontal Planar**, **Angular Planar**, and **Planar Along the Curve**, which are based on conventional planar approaches. In addition, more advanced activities such as **Radial**, **Radial 360**, and **Coating** are considered, along with **Conical Field**, **Sweep**, **Surface of Revolution**, and **Non-Planar Surface** methods. Each activity represents a specific slicing operation designed to enhance material deposition across complex geometries, supporting the overall manufacturing strategy of the RAMC.

These activities take as input the CAD model of the part for the slicing process, utilizing the Rhinoceros/Grasshopper and Meltio Space software, along with the 3D models of the cell and tables. The output is associated with the appropriate slicing strategy for deposition on the fixed table or the 2-degree-of-freedom positioning table.

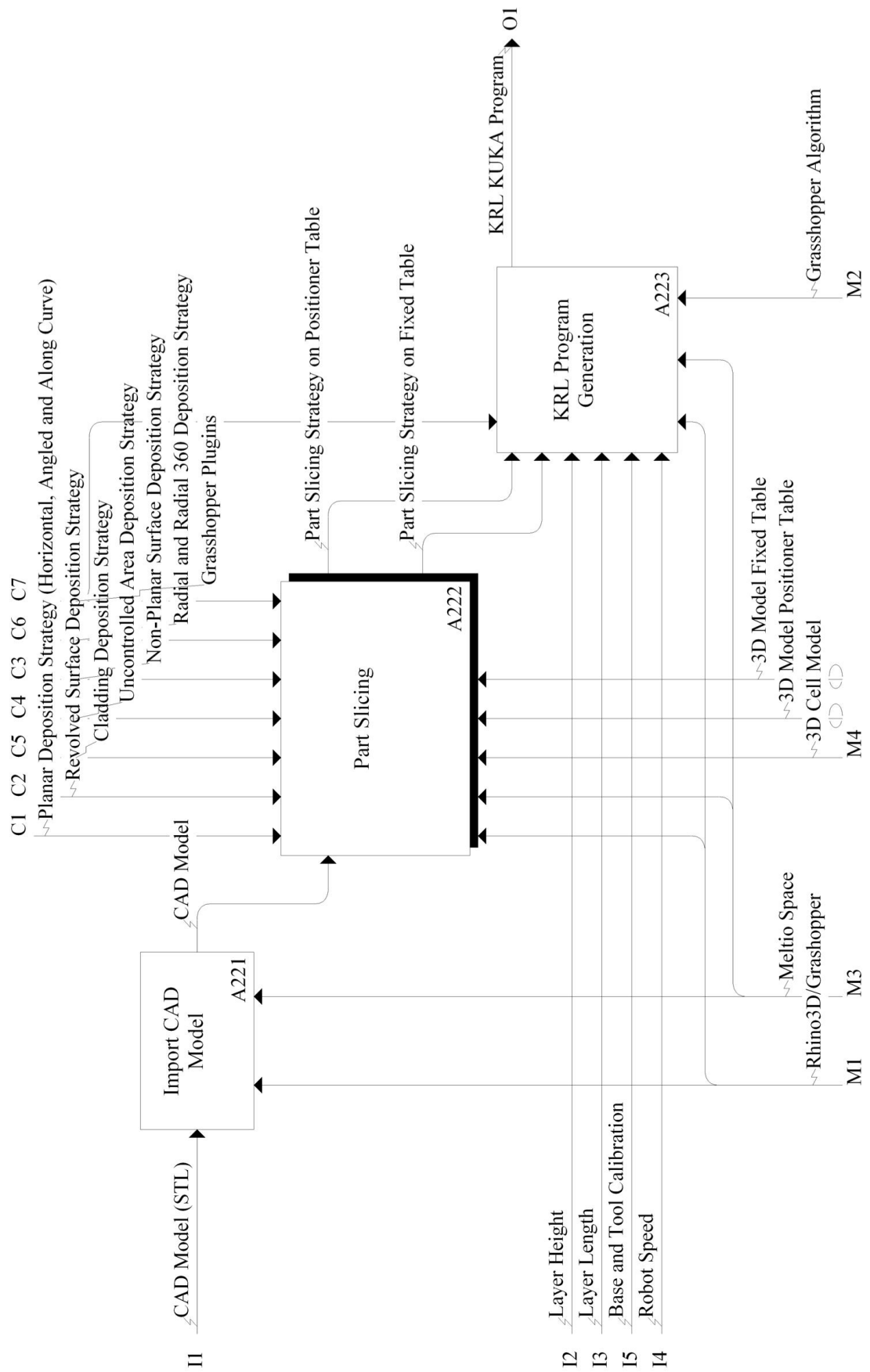


Figure 23 – IDEF0 Diagram: CAPP System Activities.

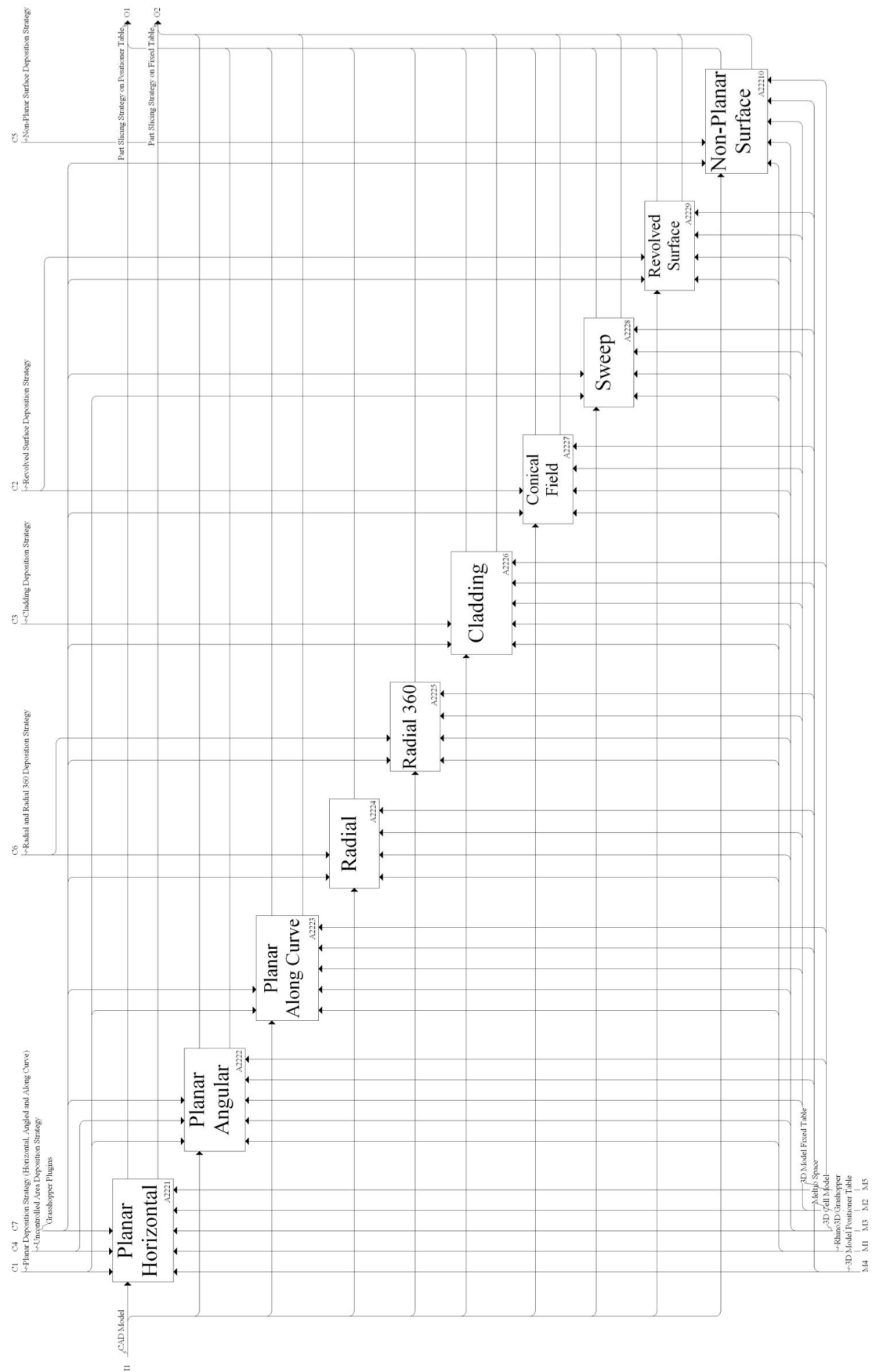


Figure 24 – IDEF0 Diagram: Part Slicing Activities.

3.5.2.3 Generating the KRL Program

The KRL Program Generation activity receives as inputs the part slicing strategies for either a fixed or positioning table, along with parameters for robot speed, layer height, and width, and the Base and Tool zeroing from the CAM activity. It utilizes Meltio Space and Rhinoceros/Grasshopper software, with a Grasshopper algorithm containing the printing parameters and robot speed, resulting in the generation of a KUKA KRL program as output.

3.5.3 CAM

Figure 25 presents the IDEF0 model associated with the CAM activity, which includes two activities:

1. Digital Twin - Simulation (CAM Planning).
2. 3D Printing (CAM Execution).

Both activities depend on the KUKA KRL program generated in the CAPP activity. The Digital Twin - Simulation activity utilizes a digital twin for real-time simulation and monitoring of variables on a 2D panel and AWS table. The 3D printing activity incorporates various printing parameters, results from physical and logical integration, and produces data such as final fiber temperatures and robot joint metrics.

3.5.3.1 Digital Twin - Simulation (CAM Planning)

Figure 29 illustrates the IDEF0 model for the CAM monitoring activity, which involves three activities:

1. Importing the KUKA KRL Program.
2. Simulation.
3. Sending Process Data to the Cloud.
4. Cloud Monitoring.

In the KUKA KRL Program Import activity, the program generated by the CAPP activity is imported into the KUKA.SIM environment. Subsequently, a simulation is performed with the 3D model of the cell, resulting in a DT real simulation and processing and control data as output. This data is then sent to the process data sending activity, resulting in the data being uploaded to the cloud. In the following step, the data are monitored, resulting in the monitoring of variables on a 2D panel and an AWS table.

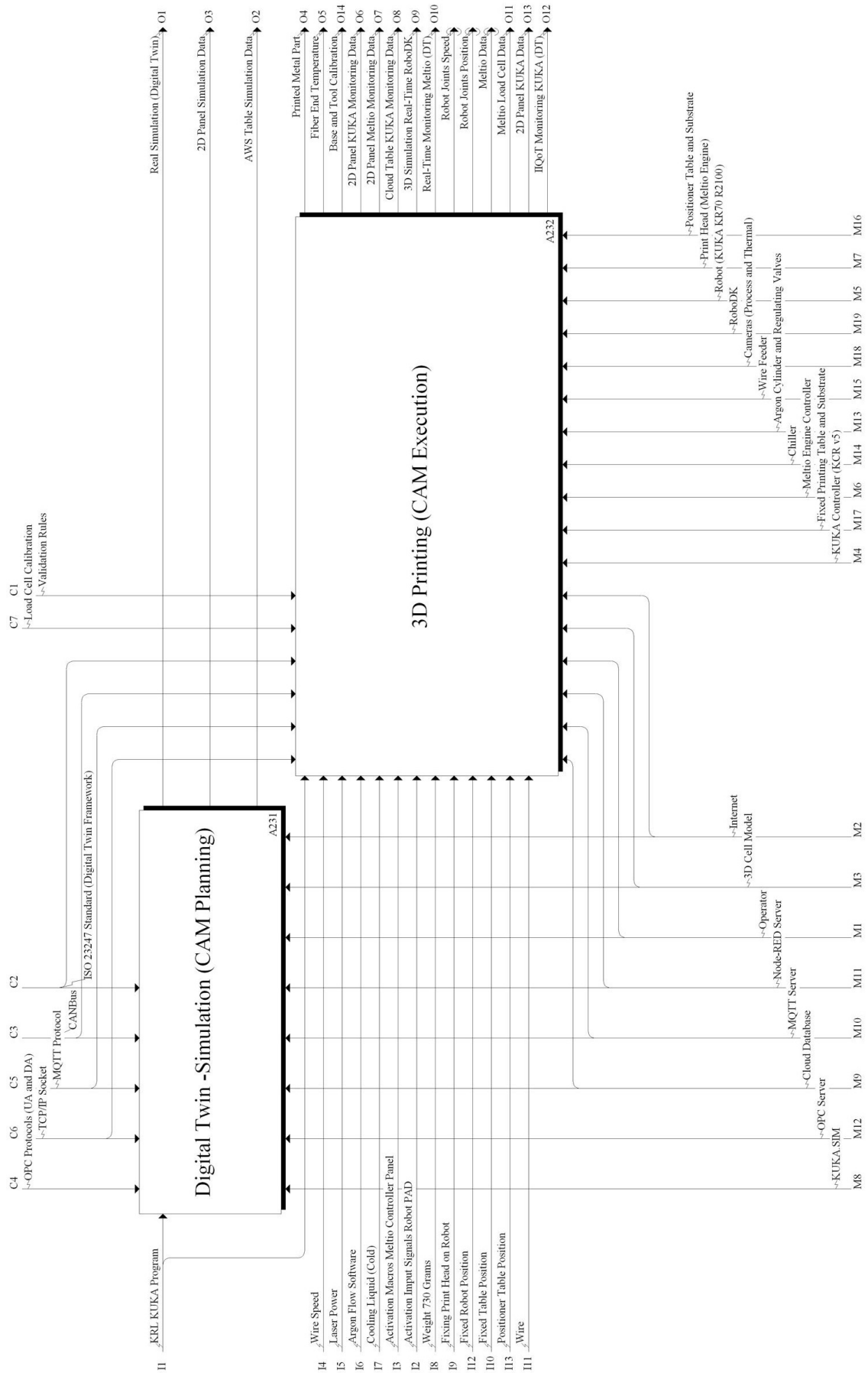


Figure 25 – IDEF0 Diagram: CAM System Activities.

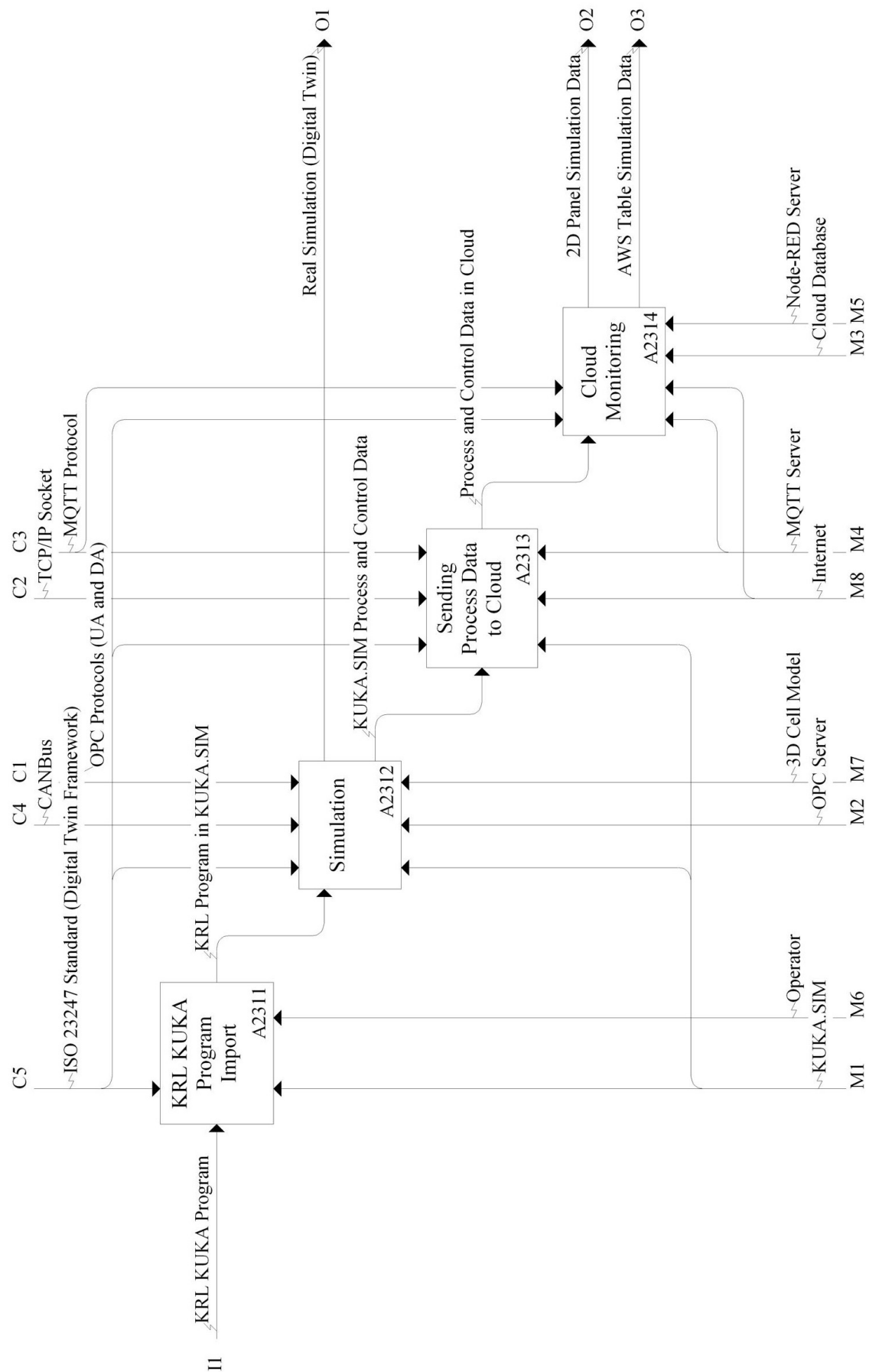


Figure 26 – IDEF0 Diagram: Digital Twin - Simulation (Planning) Activities.

3.5.3.2 3D Printing (CAM Execution)

Figure 27 presents the IDEF0 model related to the 3D Printing (CAM Execution) activity, which comprises two activities.

1. CAM Operation.
2. CAM Monitoring.

The CAM Operation activity accepts as inputs the generated KUKA KRL program, various printing parameters, outputs from physical and logical integration, and necessary external supplies for the operational process. Its outputs include the temperatures of the fiber ends, the printed metallic component, the adjustment of the Base Tool origin, readings from the Meltio load cell, Meltio Data, KUKA Data, Robot Joint Motor Temperature, along with the speed and position of the robot joints.

The CAM Monitoring activity processes Meltio Data, KUKA Data, motor temperature, speed, and position of the robot joints, all of which are generated by the CAM Operation activity. Outputs from this activity consist of a 3D Real-Time Simulation in RoboDK, real-time monitoring of the Meltio Engine, a Cloud table for KUKA monitoring data, DT IIQoT Monitoring, a 2D panel displaying monitored Meltio information, a 2D panel for KUKA data observations, and an additional 2D panel focused on KUKA data.

3.5.3.2.1 CAM Operation

Figure 28 illustrates the IDEF0 model associated with the CAM Operation activity, which includes four distinct processes:

1. TCP Base Tool Zeroing.
2. Laser Zeroing.
3. Fiber Cooling.
4. 3D Printing of the Part.

The TCP Base Tool Zeroing activity utilizes inputs such as the fixed table position, the positioning of the print table, the attachment of the print head to the robot, and a weight of 730 grams, leading to the zeroing of the Base and Tool.

The Laser Zeroing activity relies on the output from the TCP Base Tool Zeroing, along with inputs like wire, laser power, and the attachment of the print head to the robot, resulting in the alignment of the laser.

The Fiber Cooling activity incorporates inputs including the fixation of the print head to the robot and a cold cooling liquid, producing cooled fibers.

The 3D Printing of the Part activity combines inputs from the aligned laser as determined in the Laser Zeroing, the cooled fibers obtained from the Fiber Cooling, the generated KUKA KRL program derived from the CAPP activity, wire speed, argon flow rate, laser power, wire, activation of macros on the Meltio control panel, and the triggering of input signals on the robot control PAD. Its outputs encompass the Printed Metal Part, Fiber End Temperature, Robot Joint Speed, Robot Joint Temperature, Meltio Data, Meltio Load Cell Data, KUKA Data, and Robot Joint Motor Temperature.

3.5.3.2.2 CAM Monitoring

Figure 29 depicts the IDEF0 model related to the CAM Monitoring activity, which consist of three primary processes:

1. Digital Twin - RAMC Real-Time.
2. Digital Twin - KUKA Monitoring (IIoT).
3. Digital Twin - Meltio Monitoring.

The Digital Twin - RAMC Real-Time activity processes inputs such as the robot joint position, joint speed, and motor temperature. Its outputs consist of a 2D panel displaying KUKA Monitoring Data, a Cloud Table for KUKA Monitoring, and a 3D Real-Time Simulation in RoboDK.

The Digital Twin - KUKA Monitoring (IIoT) activity utilizes KUKA Data as its input, yielding outputs that include a 2D panel showcasing KUKA Data and DT IIQoT Monitoring.

The Digital Twin - Meltio Monitoring activity relies on Meltio Data as its input, producing outputs that encompass a 2D panel for Meltio Monitoring Data and DT Real-Time Monitoring for Meltio.

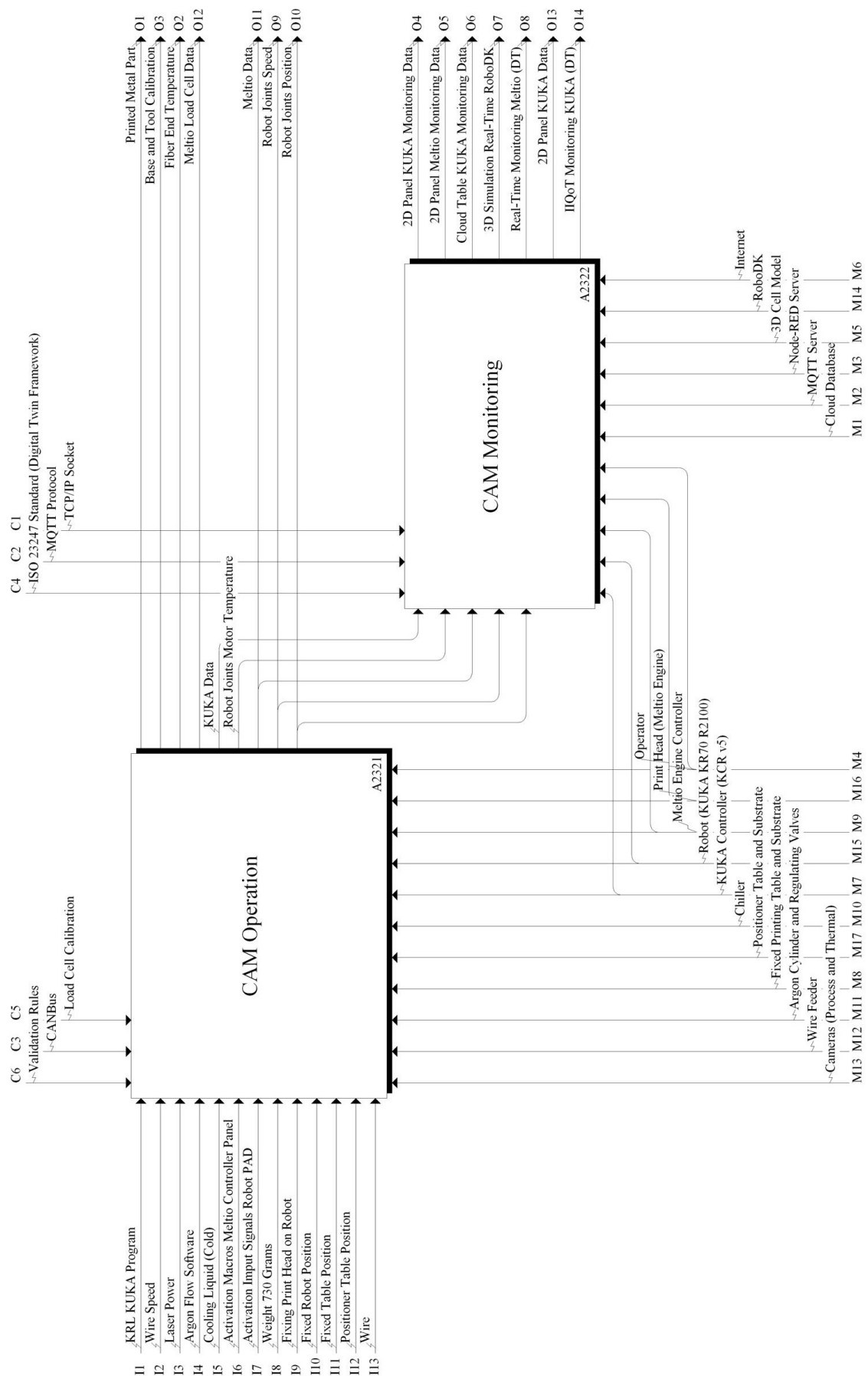


Figure 27 – IDEF0 Diagram: 3D Printing Activities (CAM Execution).

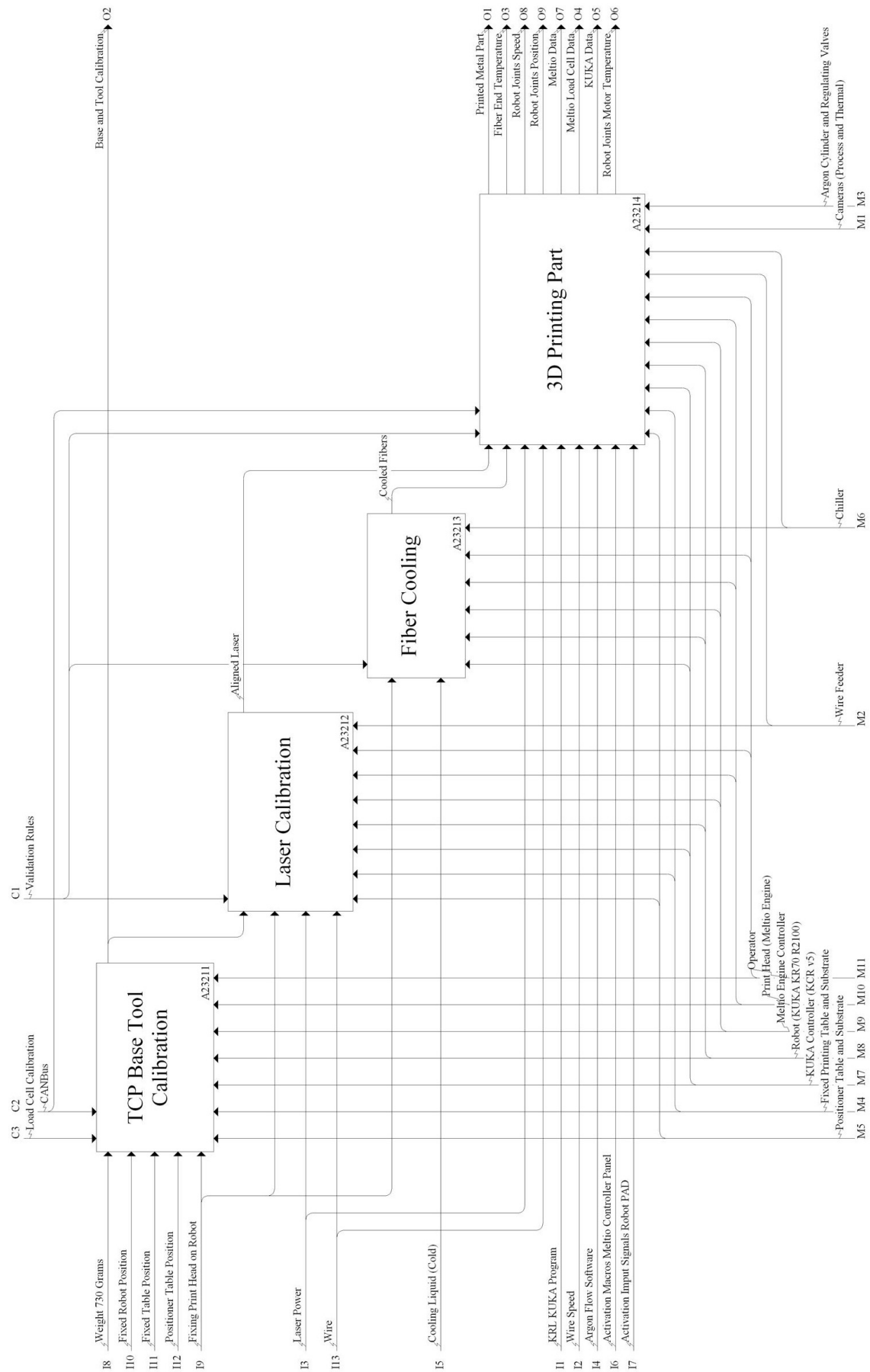


Figure 28 – IDEF0 Diagram: CAM Operation Activities.

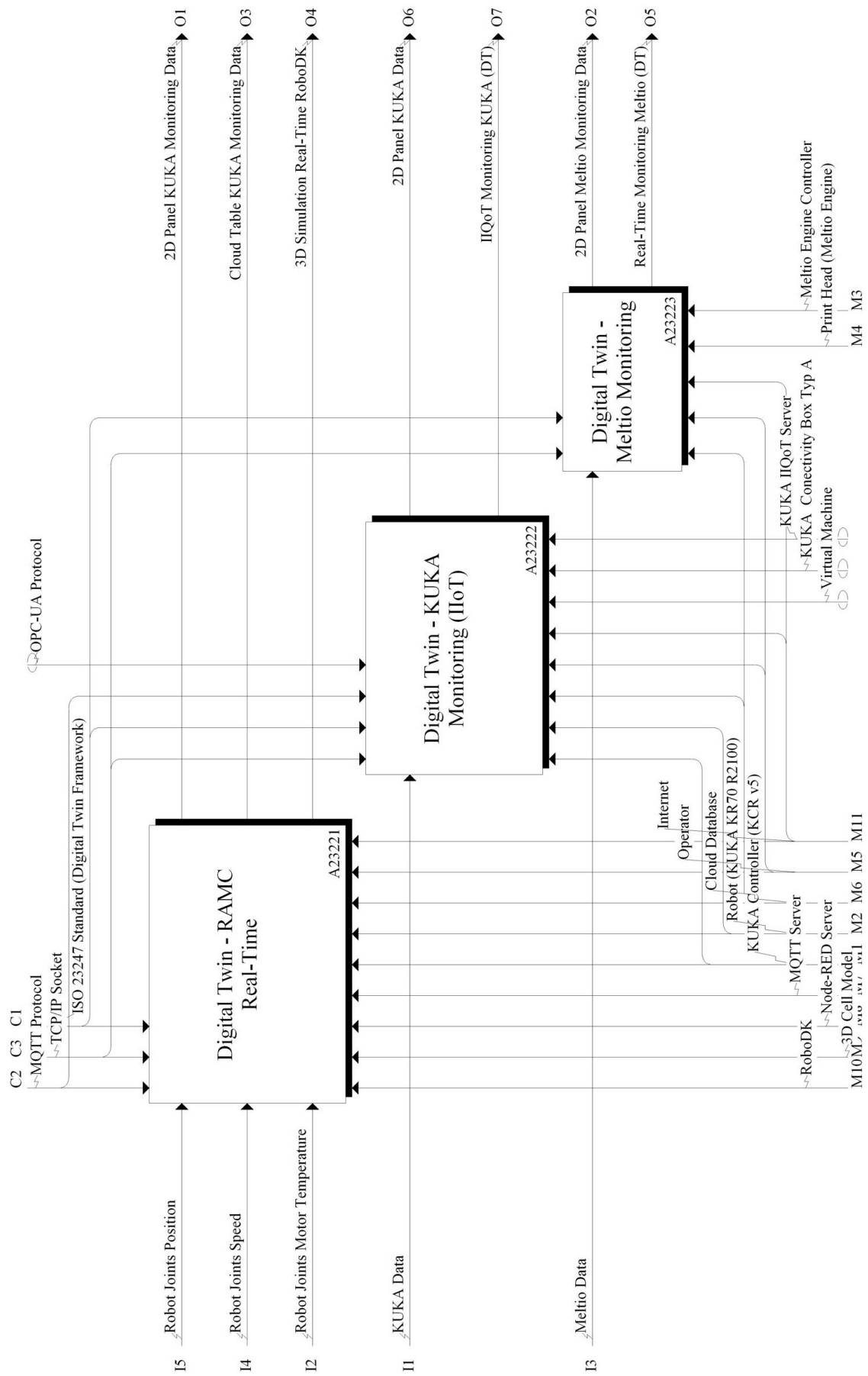


Figure 29 – IDEF0 Diagram: CAM Monitoring Activities.

Digital Twin - RAMC Real-Time

Figure 30 presents the IDEF0 model connected to the Digital Twin - RAMC Real-Time activity, consisting of five specific processes.

1. Importing KUKA Data into RoboDK.
2. Importing KUKA Data into Node-Red.
3. Real-time Monitoring with RoboDK.
4. Sending Monitored KUKA Data to Cloud.
5. KUKA Data Monitoring in Cloud.

The Importing KUKA Data into RoboDK process collects joint motor temperature, joint speed, and positional data of the robot, integrating them into the RoboDK platform and Node-RED Server. These data are then processed to enable real-time 3D simulations using a digital model of the cell along with a 2D KUKA monitoring panel, all integrated within the Real-Time Monitoring framework. The Sending Monitored KUKA Data to the Cloud activity takes joint motor temperature, joint speed, and positional data as its inputs, which are then sent to the cloud. This information acts as the foundation for the KUKA Data Monitoring in the Cloud process, which produces the Cloud Table for KUKA Monitoring Data.

Digital Twin - KUKA Monitoring (IIoT)

Figure 31 illustrates the IDEF0 model associated with the Digital Twin – Meltio Monitoring (IIoT) activity, comprising two main processes. The first, *Importing KUKA Data to the KUKA IIQoT Server*, takes KUKA-generated data as input and sends it to the IIQoT platform. The second, *KUKA Real-Time Data Monitoring within IIQoT*, processes this data to enable real-time digital twin visualization, resulting in outputs such as DT IIQoT-based KUKA Monitoring and a dedicated 2D panel for KUKA data.

Digital Twin - Meltio Monitoring

Figure 32 depicts the IDEF0 model associated with the Digital Twin – Meltio Monitoring activity, which also involves two main processes. The first, *Importing Meltio Monitoring Data to the Meltio Server*, uses Meltio-generated data as input and sends it to the cloud-based server. The second, *Real-Time Monitoring of Meltio Data in the Meltio Server*, processes this data to enable real-time monitoring of the Meltio system, resulting in outputs such as the Meltio DT and a dedicated 2D panel for Meltio Monitoring Data.

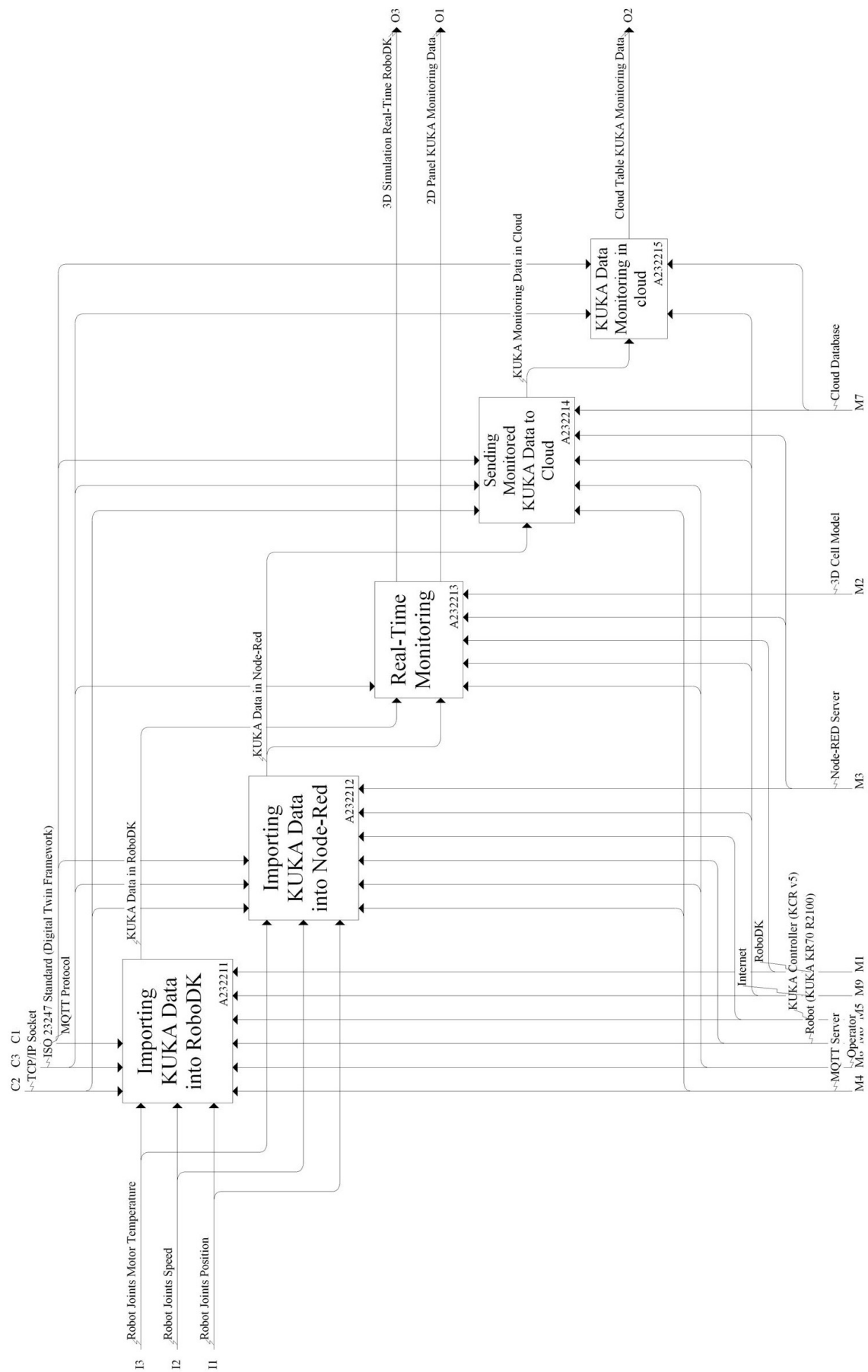


Figure 30 – IDEF0 Diagram: Digital Twin - RAMC Real-Time Activities.

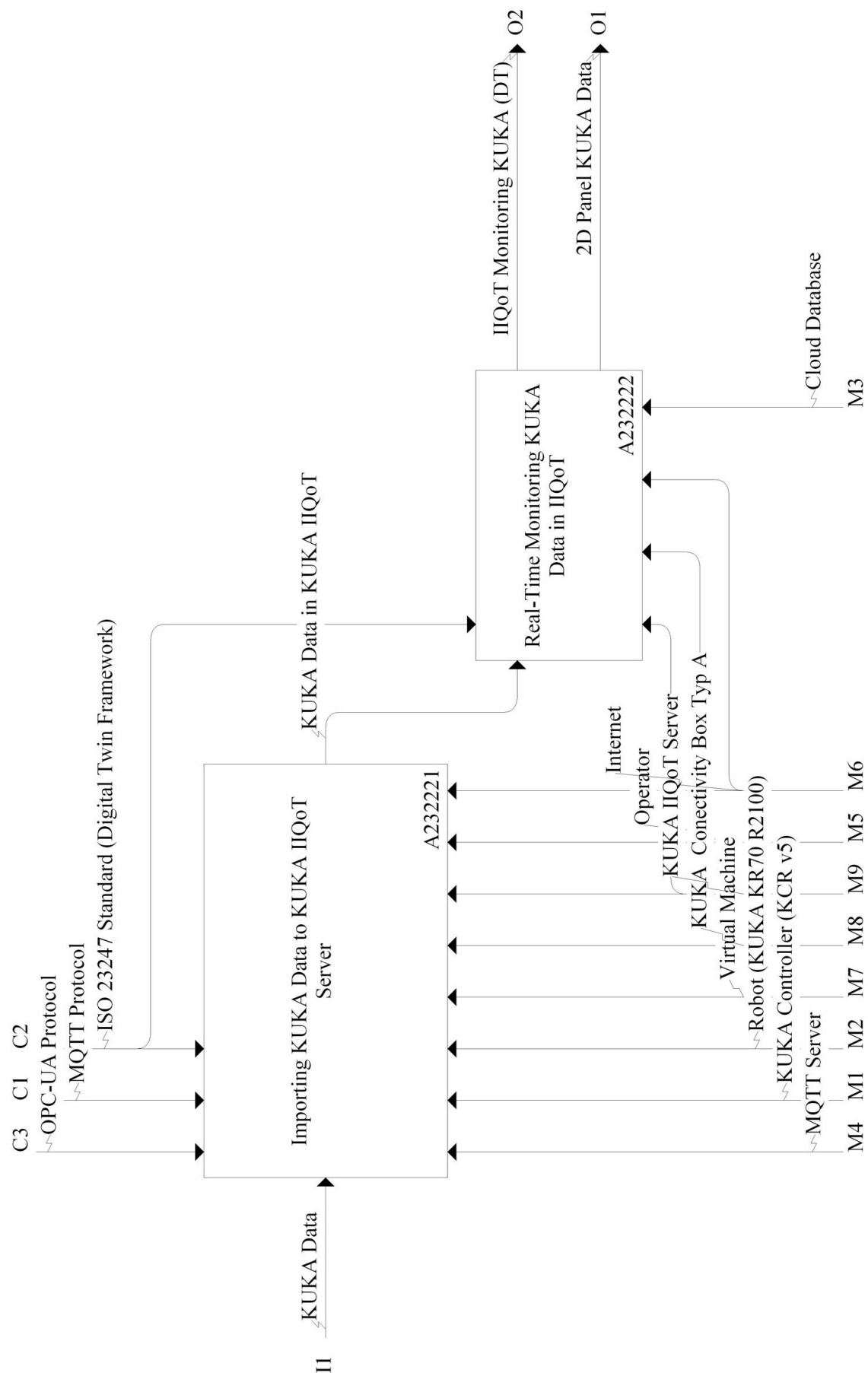


Figure 31 – IDEF0 Diagram: Digital Twin - Meltio Monitoring (IIoT) Activities.

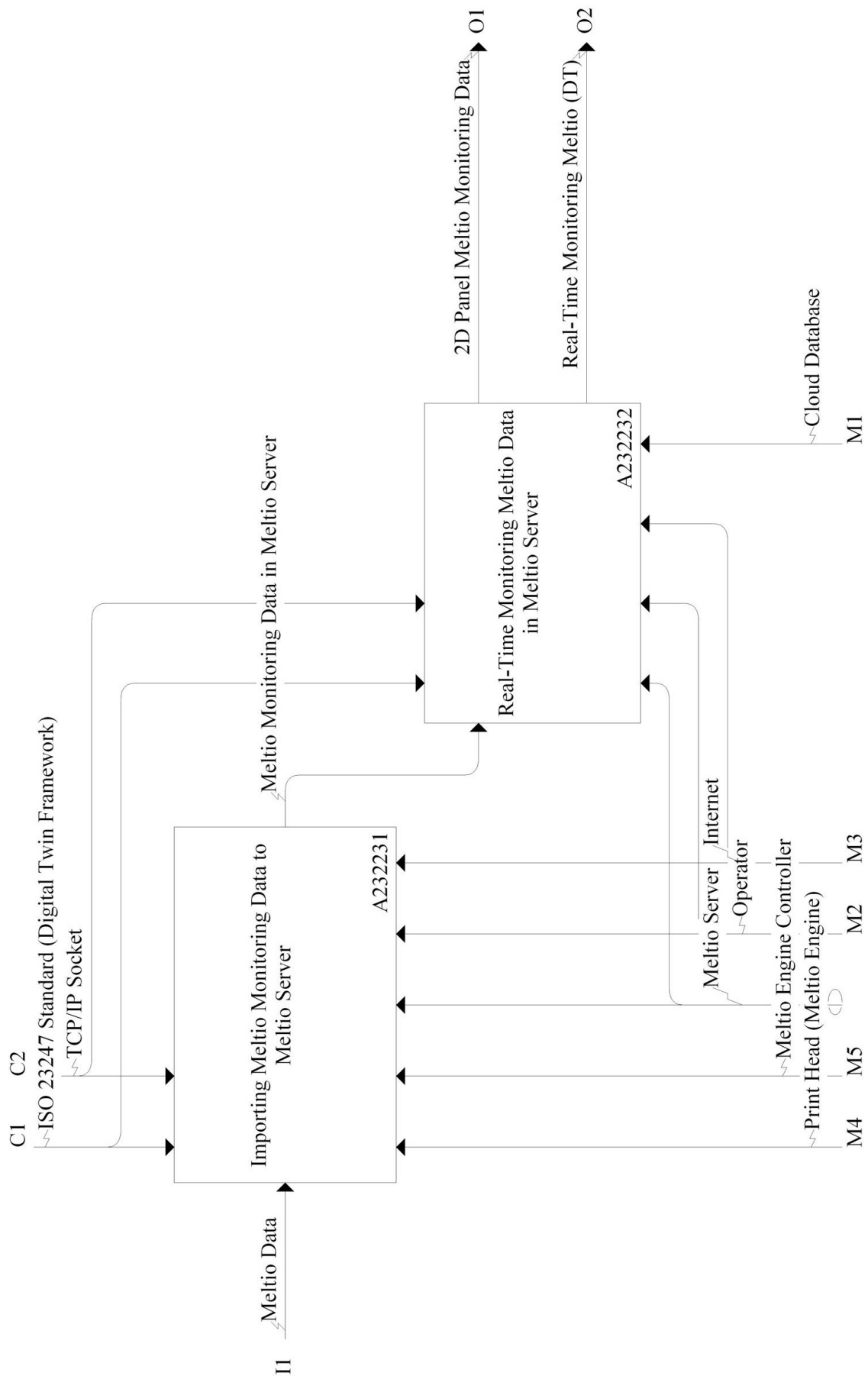


Figure 32 – IDEF0 Diagram: Digital Twin - Meltio Monitoring (IIoT) Activities.

4 Development of a Robotic Additive Manufacturing Cell

4.1 Introduction

This chapter delineates the development of a Robotic Additive Manufacturing Cell (RAMC) utilizing the Wire-Based Laser Metal Deposition process, following the proposed IDEF0-based methodology. It emphasizes the physical assembly and logical integration of the RAMC components, detailing their interconnections and interactions with the control system. The chapter offers a comprehensive analysis of the integration activities, highlighting the physical setup and the logical coordination essential for effective operation. In addition, it addresses the implementation of the CAD/CAPP/CAM system to facilitate planning and execution, ensuring a streamlined workflow and enhancing overall process efficiency (FIGUEROA, B. S.; ÁLVARES, 2025a).

4.2 Physical Integration

Figure 33 illustrates the RAMC utilizing the LMD-Wire process, detailing its key components (ÁLVARES, A. J.; ZHU, et al., 2023). Figure 33 (A) presents the internal setup, including the robotic arm with the Meltio Engine deposition head, the printing table with a substrate, the thermal chamber, the process visualization camera and the wire feeder that supplies stainless steel 316LSi. Figures 33 (B) and 33 (C) show the external configuration, featuring the KUKA KC5 controller, the Meltio Engine controller, processing computers, gas cylinders, and the chiller system for thermal management. The RAMC integrates a safety system to ensure operational reliability and personnel protection, in accordance with international standards for industrial and collaborative robots (ISO, 2025a) (ISO, 2025b) (ISO, 2016).

Moreover, the integration process includes the critical connection between the robotic arm and the Meltio system, which is vital to facilitate coordinated operation and achieve the desired printing accuracy. The methodology employed in this integration is meticulously structured to ensure efficient assembly while adhering to established validation protocols and electrical standards. This includes the proper configuration of 24V I/O signals, which are essential to ensure the operational functionality and reliability of the RAMC (ÁLVARES, A.; LACROIX, et al., 2023b). In general, this thorough integration approach significantly enhances the ability of the system to produce high-quality additive components, thereby advancing the effectiveness and versatility of AM technology across various industries.

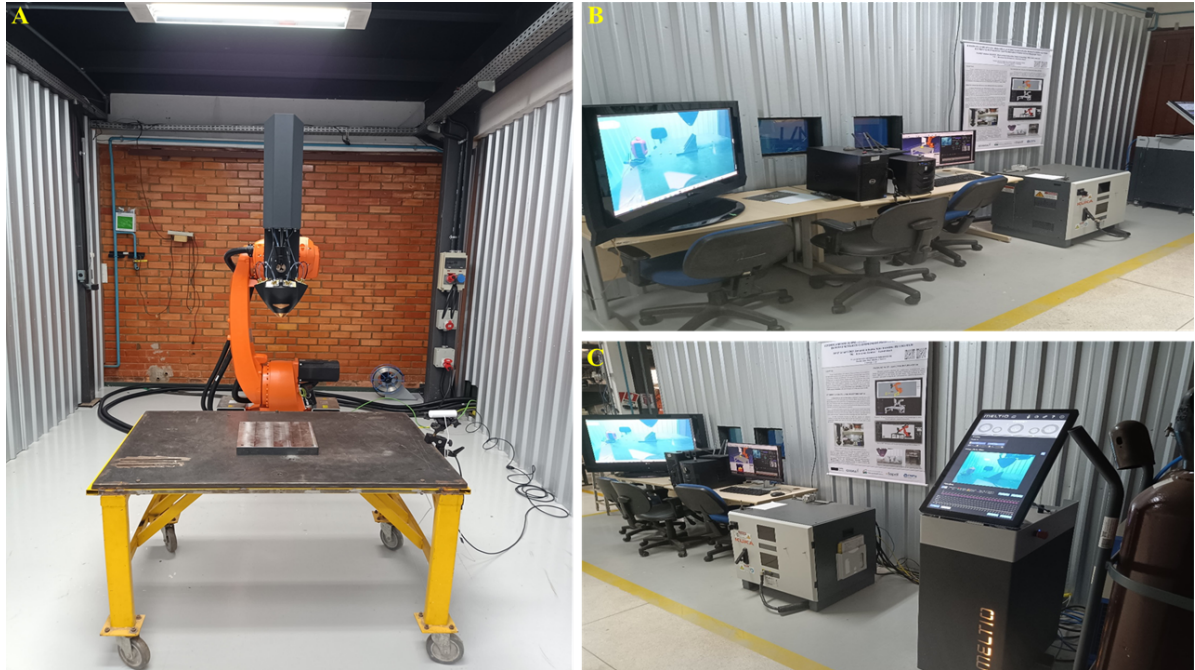


Figure 33 – Robotic Additive Manufacturing Cell LMD-Wire.

4.2.1 Assembly of the Additive Manufacturing Cell Cabin

The cabin was constructed within a metal structure measuring 4.75 x 5 x 3.5 meters. This fully enclosed cabin, as illustrated in Figure 34, is equipped with four laser safety windows featuring a 980 nm filter to ensure optimal protection for the operator. The internal and external views of the cabin are shown in Figures 34 (A) and 34 (B), respectively. Furthermore, the cabin includes an exhaust fan, depicted in Figure 34 (C), which facilitates effective gas removal. Additionally, it is fitted with cameras for process visualization and thermal imaging.

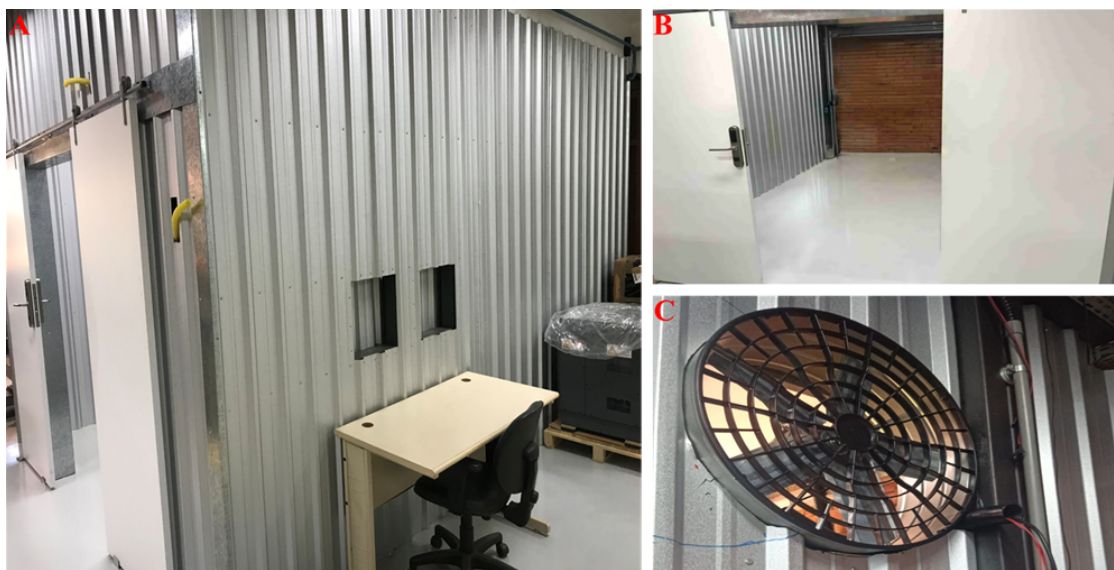


Figure 34 – Additive Manufacturing Cell Cabin.

4.2.2 Robot Installation

Upon completion of the cabin assembly, the Robot Installation activity is conducted. This activity consists of two primary tasks. The first task, robot fixation, involves securing the KUKA KR70 R2100 robot within the workspace using screws, a metal base, and acetic silicone, ensuring a stable and fixed position, as shown in Figure 35 (A). The second task, robot controller assembly, consists of installing the KUKA KC5 controller and connecting the electrical cables to establish the emergency stop systems, digital outputs, and digital inputs, enabling full operational control of the system, as illustrated in Figure 35 (B).

To carry out this activity, KUKA Roboter provided specialized technical training. This training encompassed detailed procedures for robot fixation and controller assembly, ensuring that technical personnel acquired the necessary competencies to perform a precise installation in accordance with industrial standards. In addition, training covered the configuration and connection process between the robot and its controller, as depicted in Figure 35 (C), focusing on the integration of control and safety systems to ensure proper operation.



Figure 35 – KUKA KR70 R2100 Robot Installation.

4.2.3 Positioning of the Printing Table

The Fixed Print Table Positioning activity was conducted using a fixed table with a height of 680 mm. This table was equipped with a metallic substrate measuring 300 x 300 x 35 mm, which served as the foundation for metal deposition during the printing process, as shown in Figure 36. The substrate was designed to minimize thermal deformations and residual stresses, ensuring dimensional stability and adhesion throughout the AM process. Moreover, the table features wheels for mobility, which allows for easy repositioning within the workspace. To ensure operational safety, it was equipped with grounding electrical cables, preventing potential electrical discharges, and screws to securely attach the substrate, further enhancing stability and precision during fabrication.



Figure 36 – Positioning of the Printing Table.

4.2.4 Installation of the Meltio Engine System

Following the completion of the preceding activities, the installation of the Meltio System was conducted, encompassing seven key tasks: attaching the printhead to the robot, assembling the cooling system to ensure proper cooling of the printhead, setting up the argon gas system to create a protective atmosphere against metal oxidation during printing, assembling the wire feeding system, connecting the fibers responsible for activating the laser in the printhead to the controller, establishing the electrical connections for the printed circuit board associated with the printhead system, and finally integrating the Meltio system. These tasks are illustrated in Figure 37.

Figure 37 (A) presents the Meltio printhead installed on the end effector of the KUKA KR70 R2100 robot, along with its respective fiber connections, material feeding tubes, power supply and other components. Figure 37 (B) shows the physical connection of the printhead, chiller, gas tanks, and wire feeder to the Meltio Engine controller. Figure 37 (C) illustrates the electrical connections on the printhead PCB for control purposes. Figure 37 (D) depicts the wire feeder along with 316L SI wire inside the RAMC. Finally, Figure 37 (E) presents the Meltio Engine system integrated on the outside of the RAMC

To achieve this installation, Meltio provided specialized training, the company that supplied the system. This training ensured that technical personnel were equipped with the necessary expertise to perform installation and integration tasks according to the system's specifications and operational standards.



Figure 37 – Installation of the Meltio Engine System.

4.2.5 Installation of the Safety System

The safety system has been designed to optimize operational safety within the RAMC. This system consists of safety relays, specifically the SBR301MC and G7SA-1A2B models, which receive signals from control panels located both inside and outside the cell, as well as from the KUKA robot controller and the Meltio Engine controller. The implementation of this safety mechanism, which uses B9 cables, ensures that the cell operates only when the access door is securely closed and when the signals from the control buttons confirm a safe operational state. These components are illustrated in Figure 38.

Figure 38 (A) shows the electrical connections between the relays and the controllers. Figure 38 (B) displays the control panel with the reset, emergency and door open buttons, which interact with the circuit and the electronic lock of the door. Finally, Figure 38 (C) presents the electronic lock of the access door.

The safety system connections are detailed in the Appendix A.1, which includes both the flow diagram and the electric diagram. This system is responsible for generating a stop command to the Meltio/Robot system if the pre-established safety conditions are not met. This approach enables effective signal monitoring, ensuring the maintenance of safety protocols and the protection of personnel and equipment. The integration of this system optimizes operational efficiency and minimizes risks in the manufacturing environment.



Figure 38 – Installation of the Safety System.

4.2.6 Integration of Robot/Meltio

The integration of the Robot system with the Meltio controller was achieved using DB15 cables to ensure precise and reliable connections. Appendix A.2 presents the connection diagrams between the DB15 cables and the controllers. Figure 39 (A) shows the KUKA KC5 controller, which features the X12 port that defines the inputs and outputs of the robot. Figure 39 (B) illustrates the male DB15 cable with its respective connections, and Figure 39 (C) shows the female DB15 cable with its corresponding connections. This configuration facilitates not only the activation of macros but also the return of signals, ensuring effective communication and coordination between both systems. These cables interact to exchange signals between the robot and the Meltio Engine system, enabling the activation of output and input functions within the printing process.

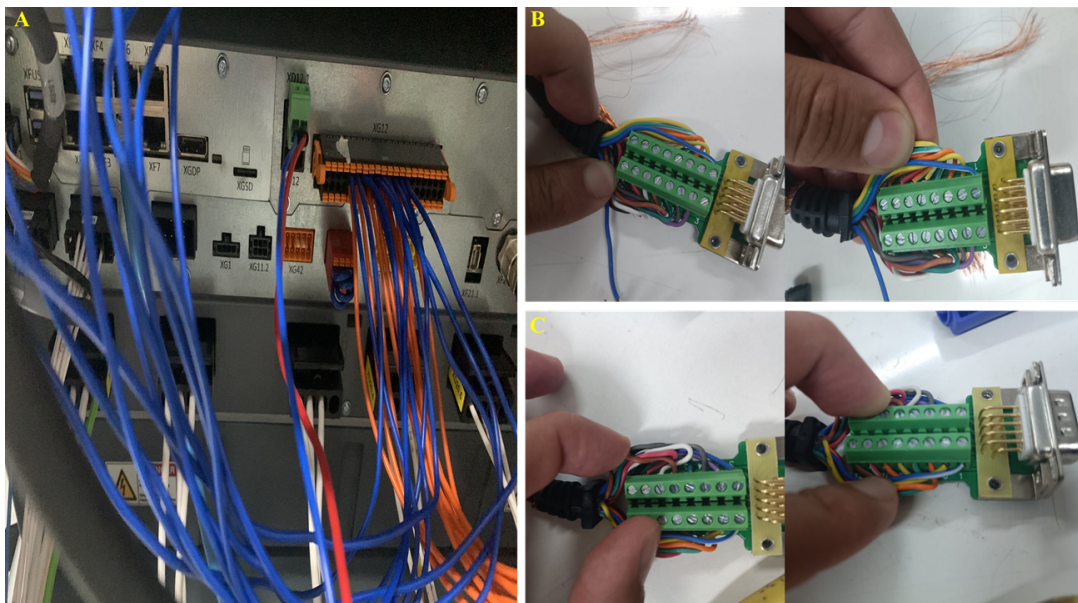


Figure 39 – Integration of Robot/Meltio.

4.3 Logical Integration

Validation tests were conducted to verify the signal exchange between the Meltio controller and the KUKA robot. These tests ensure the proper integration of input and output signals, enabling the robot to trigger and control the Meltio system macros. The process involves two main tasks: confirming that the robot correctly interprets signals from the Meltio controller, and verifying that Meltio executes actions based on signals from the robot. This bidirectional communication ensures reliable interaction between both systems, improving the synchronization between robotic motion and material deposition. The implementation also considers the ISO 11554 standard, which defines methods for laser performance testing and characterization, providing a framework to validate the correct operation of the laser system during integration (ISO, 2022).

Figure 40 (A) displays the graphical interface of the macro command system within the Meltio controller, where predefined macros are activated based on the operational requirements of the process. These macros automate critical stages of the AM workflow, including Initialize Print, Start Deposition, and End Deposition, thus streamlining process execution and enhancing system reliability. Figure 40 (B) provides an excerpt of the KUKA Robot Language (KRL) code used to print a part. This code specifies the structured sequence of commands sent by the robot to the Meltio controller, which triggers the corresponding macros at precise moments during the operation. Proper execution of these signals ensures synchronized coordination between the motion of the robot and the deposition process, enabling efficient, repeatable, and highly accurate AM.

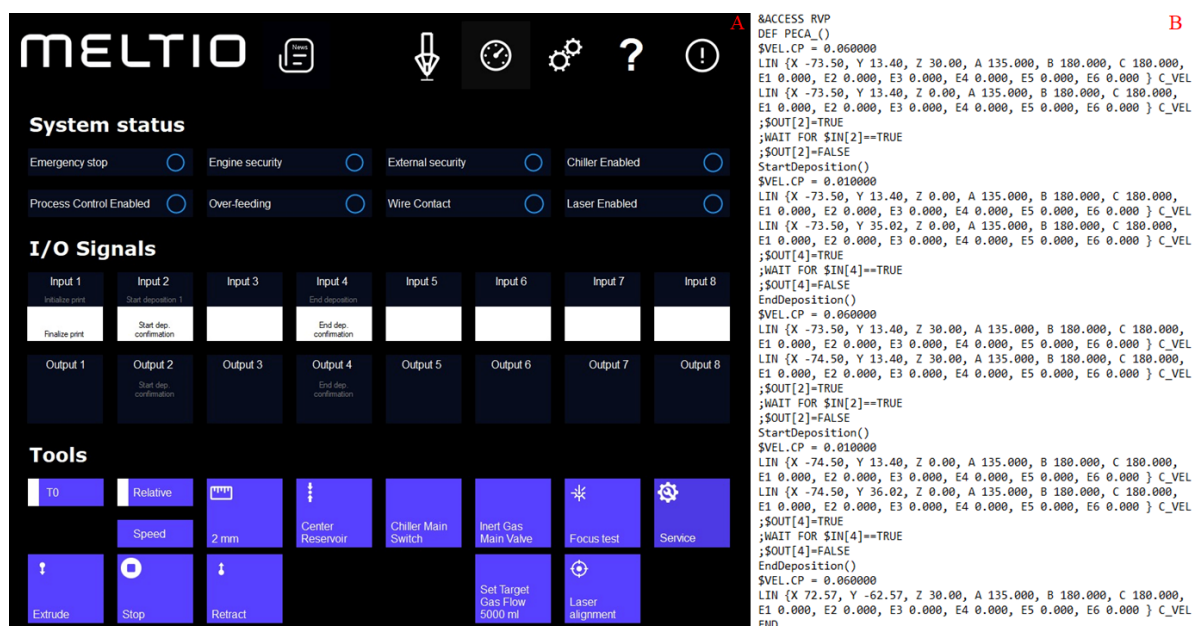


Figure 40 – Overview of Meltio Controller Macros and KRL Programming for Macros Activation.

Figure 41 illustrates the 24-volt signal exchange between the KUKA controller and the Meltio Engine during the AM process. Three primary signals are shown: Initialize Print (blue), Start Deposition (green), and End Deposition (red). The Initialize Print signal activates the Meltio Engine, performing safety checks, starting the chiller system, and enabling the pre-defined argon flow. After initialization, the KUKA controller sends the Start Deposition signal by raising it to 24 volts. Upon receiving this command, the Meltio Engine initiates filament extrusion and laser activation, then quickly returns the signal to zero volts, typically within 50 milliseconds. The End Deposition signal follows the same protocol: the KUKA controller raises it to 24 volts to indicate the end of deposition, and the Meltio system deactivates it almost instantly. These signals act as brief control pulses rather than sustained activations. The figure represents them as discrete ON/OFF states, clearly illustrating the transitions that control each process stage.

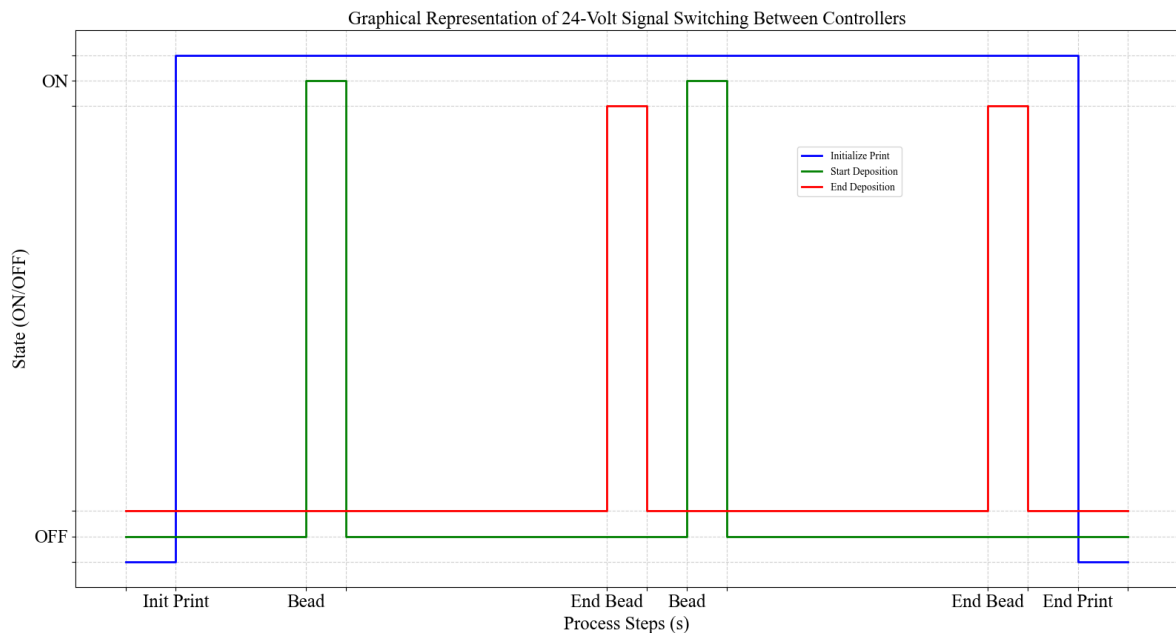


Figure 41 – Signal switching between Meltio and KUKA controllers.

To ensure safe execution of deposition routines, a supervisory logic was implemented using the internal PLC of the KUKA KR C5 controller. This logic continuously monitors the robot's operating mode and prevents the activation of components related to the deposition when operating in the T1 mode (manual with reduced speed). Specifically, if the robot is in T1, the PLC logic automatically disables the output signals $\$OUT[1]$, $\$OUT[2]$ and $\$OUT[4]$, which are responsible for triggering the laser and wire feed commands. This mechanism ensures that no deposition activity occurs during the programming, testing, or maintenance stages, thereby avoiding potential hazards or process interruptions. In contrast, normal deposition routines are permitted in T2 (manual full-speed) and AUTOMATIC modes, where system conditions and safety interlocks are fully validated. The implemented logic improves safety and reliability, as shown in Code 4.1 and Appendix A.3.

Code 4.1 – Routine to Disable Outputs in T1 Mode for Safe Execution.

```

1 WAIT FOR NOT ($POWER_FAIL)
2
3 BASISTECH PLC
4 BACKUPMANAGER PLC
5 USER PLC
6
7 IF $T1 THEN
8     $OUT[1] = FALSE
9     $OUT[2] = FALSE
10    $OUT[4] = FALSE
11 ENDIF
12
13 KUKA_BR
14 ENDLOOP

```

4.4 CAD/CAPP/CAM Systems

The CAD/CAPP/CAM systems utilized in the RAMC are essential for optimizing the manufacturing process. The CAM system consists of two main phases: Planning and Execution. In the Planning phase, the KRL code is generated, which includes defining crucial parameters for the manufacturing process. The Execution phase involves transmitting this KRL code to the Kuka robot controller, configuring the Meltio Engine and chiller, setting up the substrate on the deposition table, calibrating the TCP Base Tool, and ensuring effective monitoring and quality control of the metal part's printing process.

4.4.1 KUKA.SIM

The simulation and offline programming of the RAMC are conducted using KUKA.Sim, which enables precise validation of the robot's kinematics, motion planning, and workspace constraints. Within this environment, a detailed 3D model of the RAMC is implemented, incorporating all essential components, including the KUKA KR70 R2100 robot, the print head, the worktable, and a realistic 3D substrate. This comprehensive digital representation ensures accurate trajectory planning, collision detection, and optimization of deposition paths prior to execution. Figure 42 illustrates the RAMC setup within the KUKA.Sim environment, where the robotic movements and deposition process are simulated under controlled conditions to improve manufacturing efficiency. A full demonstration of this simulation workflow is provided in the video tutorial ([ALVARES, A., 2025c](#)).

4.4.2 RoboDK

The integration of process monitoring and DT functionalities is achieved through RoboDK, a software platform that facilitates advanced robot programming, simulation, and

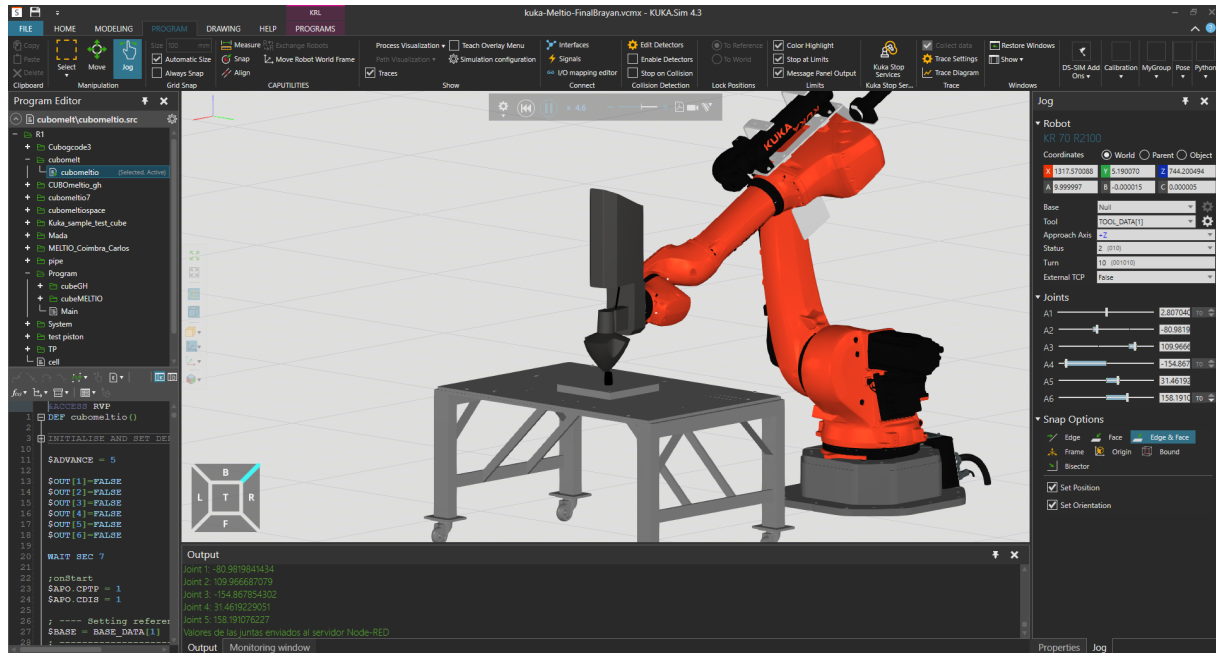


Figure 42 – CAM Model RAMC in KUKA.SIM: Offline DT Simulation.

control. A complete 3D model of the RAMC is developed within RoboDK, including the KUKA KR70 R2100 robot, the print head, the worktable, and the substrate, ensuring a realistic and interactive representation of the AM process. The software allows for toolpath generation, trajectory validation, and direct robot control, while also enabling real-time synchronization with external data sources for process monitoring. Figure 43 shows the RAMC simulation within RoboDK, showcases the execution of predefined deposition trajectories and the interaction between the robotic system and the printing process.

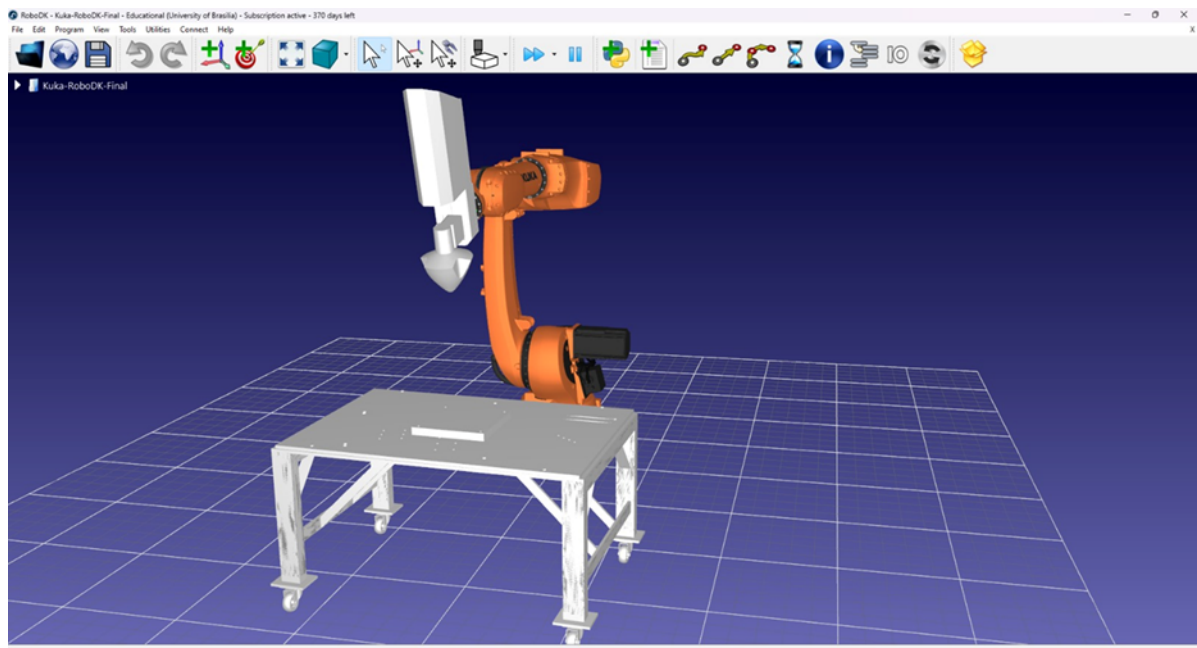


Figure 43 – CAM Model RAMC in RoboDK: Real-Time DT Monitoring.

4.4.3 Rhino3D CAD

CAD process of the RAMC was carried out in Rhinoceros 7, where a detailed 3D model of the cell was developed, comprising all essential components, including the KUKA KR70 R2100 robot, the laser deposition print head, the support table, and a geometrically accurate substrate. This digital model ensures correct spatial alignment and mechanical integration of the system, serving as a reference for simulation, trajectory planning, and manufacturing validation. Figure 44 presents the complete 3D representation of the RAMC within the Rhinoceros 7 environment.

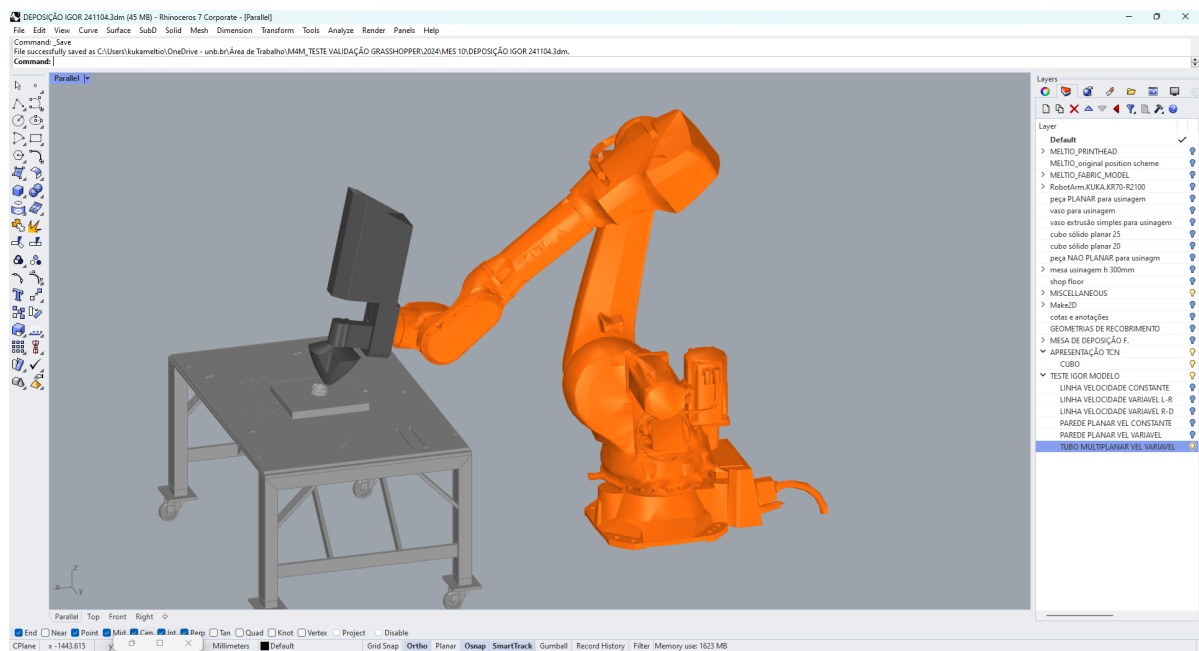


Figure 44 – CAD Model RAMC in Rhinoceros 7 and Grasshopper: Offline DT Simulation.

4.4.4 Grasshopper CAPP

CAPP system is developed using Grasshopper, integrated with Rhinoceros 7, and employs various plugins such as Robots and Pufferfish. This system plans the manufacturing process through block programming, leveraging the 3D design of the parts and deposition strategies. For each part, a unique code is created, considering the robot's kinematics and deposition parameters. The resulting code is then converted into KRL format for printing, as illustrated in Figure 45, which shows the generated code for both planar and non-planar parts within the Grasshopper environment.

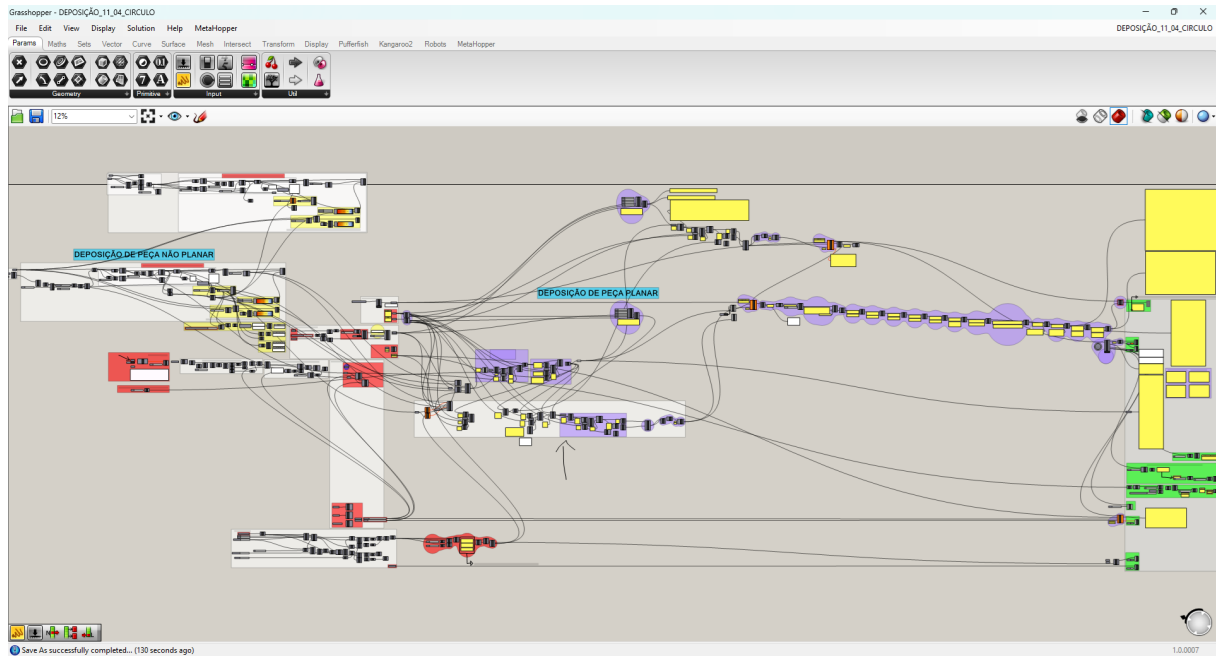
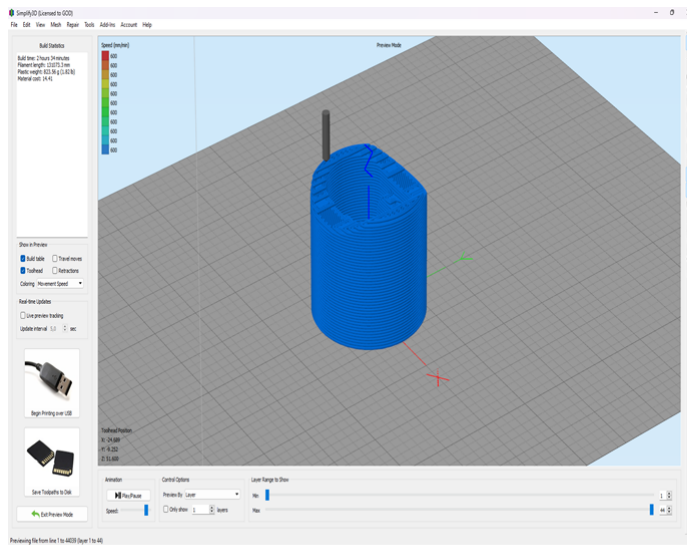


Figure 45 – CAPP Algorithm with Grasshopper: DT Programming.

4.4.5 Simplify3D and G-Code to KRL Converter CAPP

The AM workflow begins with the importation of the STL geometry into the Simplify3D environment, where a series of essential parameters specific to the Meltio print head must be defined. These include the layer height, bead width, retraction distance and speed, coasting distance, and wipe distance. Furthermore, the software allows for the configuration of the infill density, infill pattern, and support structures, depending on the part geometry and its functional requirements. Once all settings are defined, the slicing process generates a G-code file that contains the complete toolpath and deposition instructions. This file is then exported through a USB device, as illustrated in Figure 46a

The G-code is then processed by the Meltio-integrated G-code to KRL converter, which translates the instructions into KRL. This interface enables the configuration of tool and base frames, motion speeds, extended axis values (E1–E6), and macro-settings. The resulting KRL program will be executed by the robotic system to carry out the deposition process, which is limited to planar geometries. The main parameters of the converter interface are summarized in Table 4 and visually presented in Figure 46b. A complete overview of this process is presented in the video tutorial (ALVARES, A., 2025b).



a) Simplify3D



b) G-Code to KRL Converter

Figure 46 – Simplify3D and G-Code to KRL Converter.

Table 4 – Parameters of the G-Code to KRL Converter Interface.

Section	Parameter	Value / Input Example
Profile	Profile	kuka
Variables	\$TOOL	[16] {FRAME: X 254.83, Y 3.84, Z 192.61, A -90, B 0, C -90}
	\$BASE	[16] {FRAME: X 1484.74, Y -60.23, Z -60.23, A 0, B 0, C 0}
	SAPO_CDIS	1
Homing	\$TOOL	[16] {A1 0, A2 -90, A3 90, A4 0, A5 0, A6 0}
	\$BASE	[16] {X 0.00, Y 0.00, Z 10, A -90, B 0, C 180, S'B110', T'B110010'}
Speed	Home	0.01
	1st aprox	0.01
	Layer Change	0.01
	Print	0.01
LIN Variables	A	-90
	B	0
	C	180
	E1, E2, E3, E4, E5, E6	0
Main Program	Start Program	InitDeposition()
	End Program	ResetDeposition()
Interrupts	Interrupt	0
	WHEN/DO	[]
GCODE Template	M101	StartDeposition()
	M103	EndDeposition()
LIN Template	LIN Temp	LIN{X 0, Y 0, Z 0, A -90, B 0, C 180, E1 0, E2 0, E3 0, E4 0, E5 0, E6 0} C_DIS

4.4.6 Meltio Space CAD/CAPP/CAM

In this process, the part is sliced within the Meltio Space software, where the .stl or .step file is initially loaded. Deposition parameters are configured, including layer height, width, material type, and part specifications, such as solid, hollow, or perimeter configurations. The 3D cell model is included in this step to ensure accurate simulation and visualization of the additive process. Additional settings, such as the percentage of filling, the geometry, and the overall geometry of the part, are also defined. Once these parameters are established, the slicing of the part is generated, as depicted in Figure 47. The slicing data

are then processed by the internal system within Meltio Space to produce KRL code. This method supports the development of highly complex parts, including planar (horizontal, angular, and along the curve), revolved surfaces, radial, radial 360, cladding, non-planar surfaces, conical fields, and sweep configurations, among others.

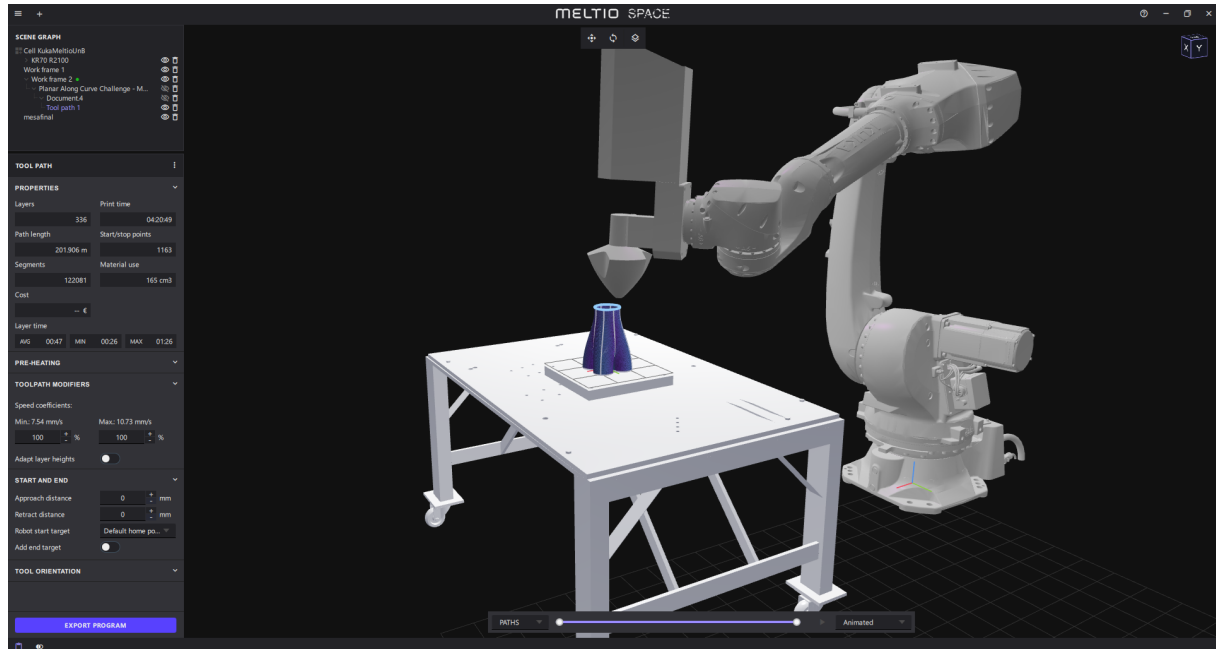


Figure 47 – CAD/CAPP/CAM model RAMC Meltio Space.

4.4.7 Execution Phase - CAM

The Execution Phase in CAM comprises four essential stages: setup, toolpath execution, monitoring, and quality control. This phase ensures the accurate implementation of manufacturing processes in accordance with predefined design parameters. During setup, the machine environment is prepared through referencing and calibration procedures that establish the operational framework. Toolpath execution involves the controlled motion of the system along programmed trajectories, enabling precise material deposition.

Monitoring supports continuous supervision of the process to detect deviations and maintain operational stability, while quality control confirms that the manufactured components meet the expected dimensional and structural requirements. Together, these stages contribute to the consistency, reliability, and repeatability of AM operations. As illustrated in Figure 48, the CAM process pipeline provides a structured workflow that connects design intent with production outcomes.

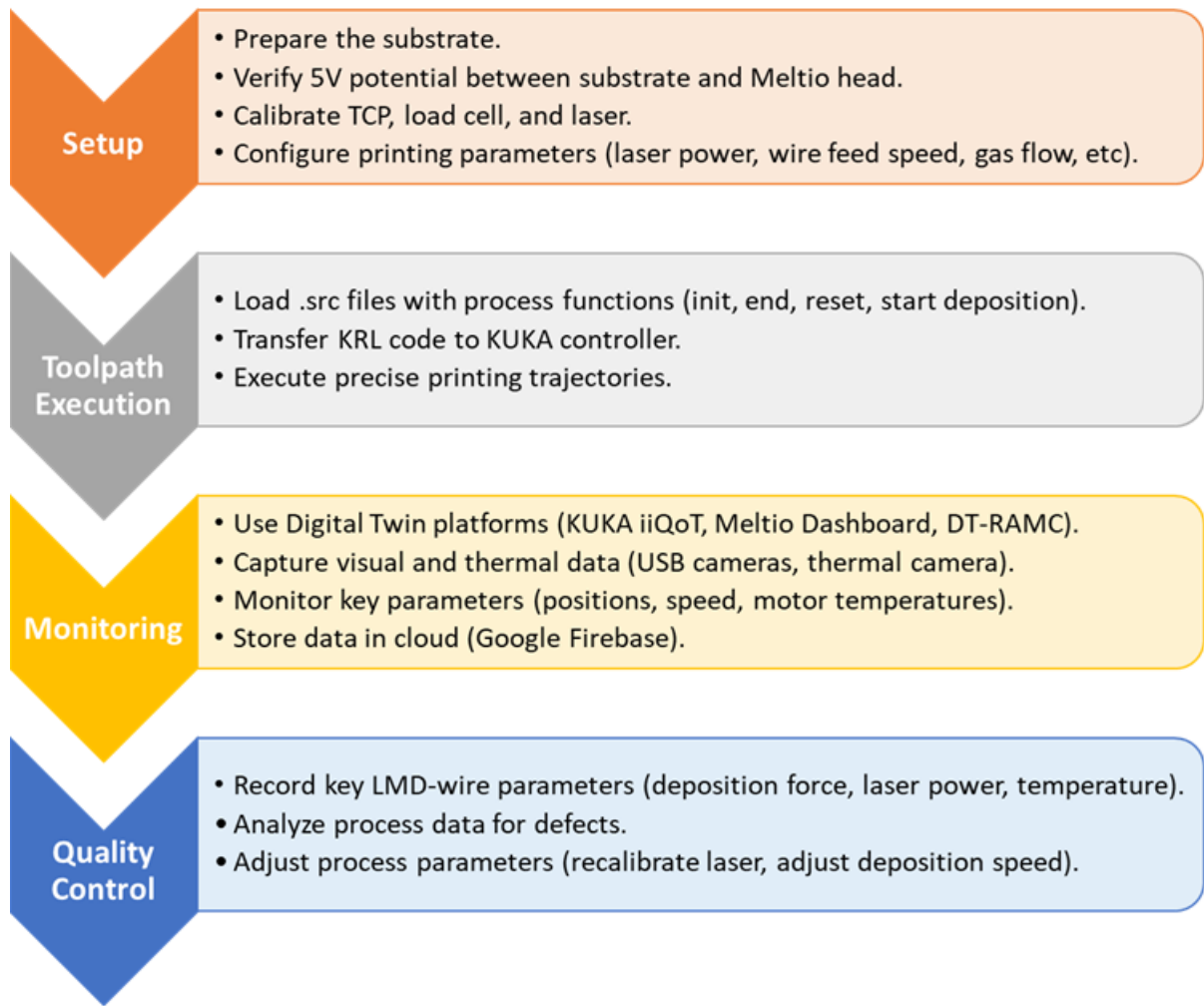


Figure 48 – CAM Process Pipeline for Execution Phase - CAM.

4.4.7.1 Setup - RAMC

The Setup phase in metallic 3D printing using the Meltio system begins with securing the substrate, measuring 300x300x35 mm, to the printing table. This specific thickness is selected to minimize thermal expansion and deformation, thereby ensuring thermal stability throughout the process. Additionally, it is critical to confirm that a 5V potential is maintained between the substrate and the Meltio deposition head, as this ensures proper material deposition.

Following this, the load cell calibration is performed using a reference weight of 730 grams, considering the positions of both the robot and the printing table, as illustrated in Figure 49 (A). Next, laser calibration is performed by positioning the nozzle at a height of 6 mm. For optimal deposition, each laser beam must be precisely focused so that 50% is directed toward the substrate and 50% toward the metal wire, forming a hexagonal pattern, as shown in Figure 49 (B). Subsequently, the Tool Center Point (TCP) configuration is established, which defines the origin from which the printing process will start, independent of the reference weight, as presented in Figure 49 (C). To prevent overheating and ensure

the longevity of the lasers, the fiber cooling system's temperature is set to 18°C. Finally, the Meltio controller is configured with essential printing parameters, including wire feed speed, argon flow rate, and laser power, ensuring precise control over the deposition process. The setup procedure aligns with the recommendations provided in AWS D20.1 for additive manufacturing using directed energy deposition processes (AWS, 2019).

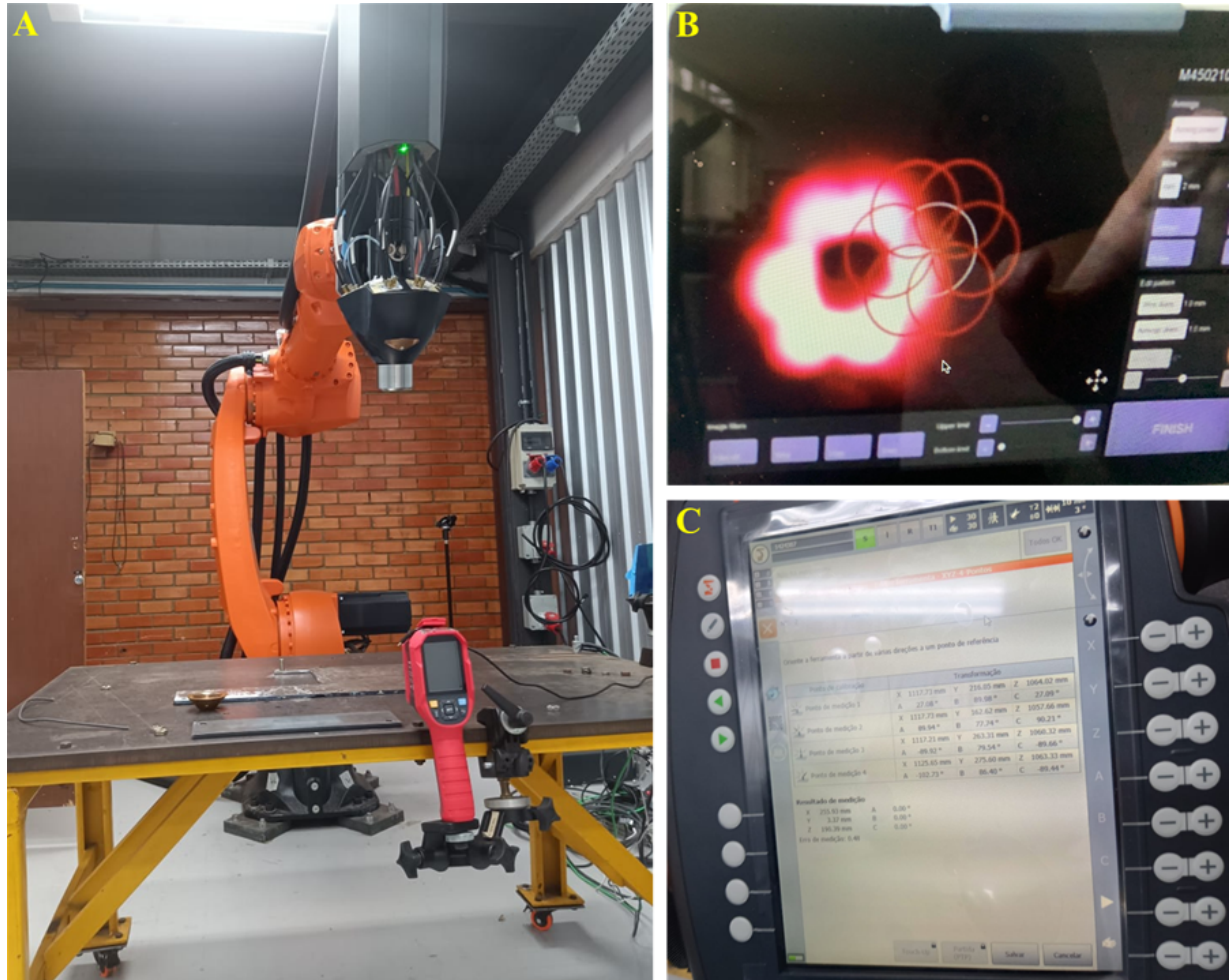


Figure 49 – Setup RAMC.

4.4.7.2 Toolpath Execution - RAMC

The toolpath execution involved the implementation of .src files containing specific functions such as init deposition, end deposition, reset deposition, and start deposition. These files were transferred to the KUKA controller and accessed through the teach pendant interface, as illustrated in Figure 50 (A). The Meltio controller was configured with the corresponding macros to ensure synchronized operation. The robot trajectories, previously defined in the KRL code, were uploaded via USB and executed through the KUKA pendant, as shown in Figure 50 (B). This configuration enabled the AM process to proceed with high accuracy and full compliance with the defined operational parameters.

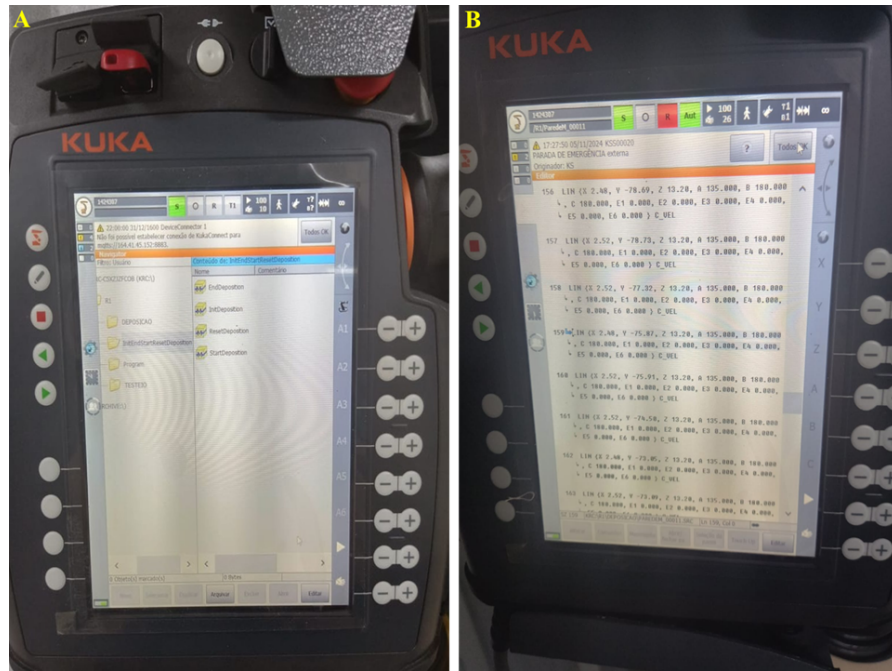


Figure 50 – Toolpath Execution RAMC.

4.4.7.3 Monitoring - RAMC

The process was monitored using three DT platforms: KUKA iiQoT, Meltio Dashboard, and DT-RAMC. Visual and thermal data were collected using two USB cameras with optical filters and a thermal imaging camera, enabling image capture for post-process analysis. Key parameters such as joint positions, velocities, and motor temperatures were continuously stored in a cloud-based database. Real-time monitoring was conducted via 2D and 3D dashboards to ensure effective control and feedback, as illustrated in Figure 51. Figure 51(A) shows the main process visualization, while Figure 51(B) displays the DT environment and thermal monitoring interface, as demonstrated in the accompanying video tutorial showing the DT functionality (ALVARES, A., 2025a).

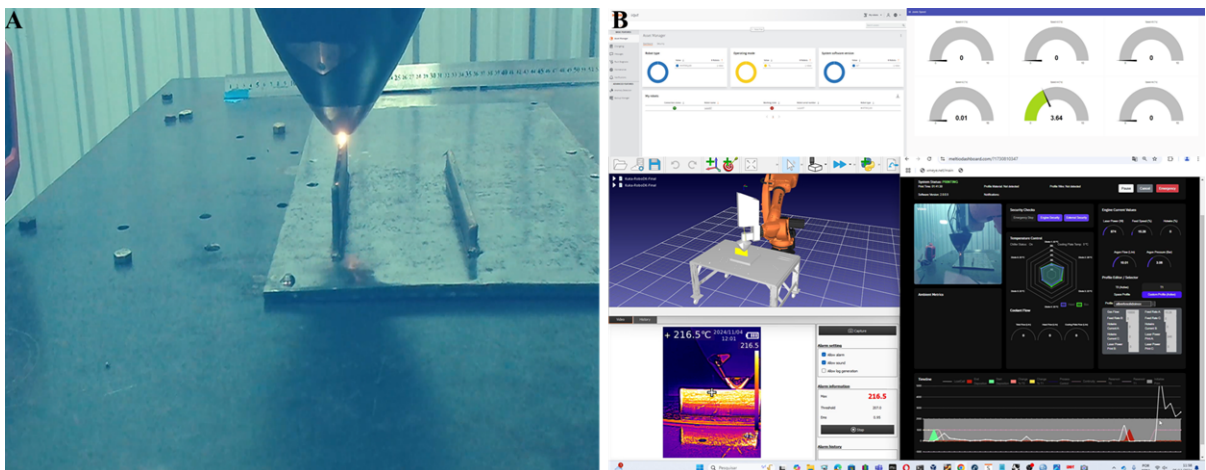


Figure 51 – Monitoring of the RAMC.

4.4.7.4 Quality Control - RAMC

Figure 52 displays the user interface of the Meltio controller, which provides real-time monitoring and control of system parameters at the end of the AM process. Figure 52 (B) shows the directory in which the files containing key process parameters and configurations are stored for the current printing. Figure 52 (C) presents the contents of the *Sensors.csv* file, which records the sensor readings collected by the Meltio controller during the active printing process, including the wire deposition speed, laser power, and laser temperatures. These data are essential for real-time monitoring, process control, and subsequent analysis to ensure quality of parts and facilitate corrective actions when necessary.

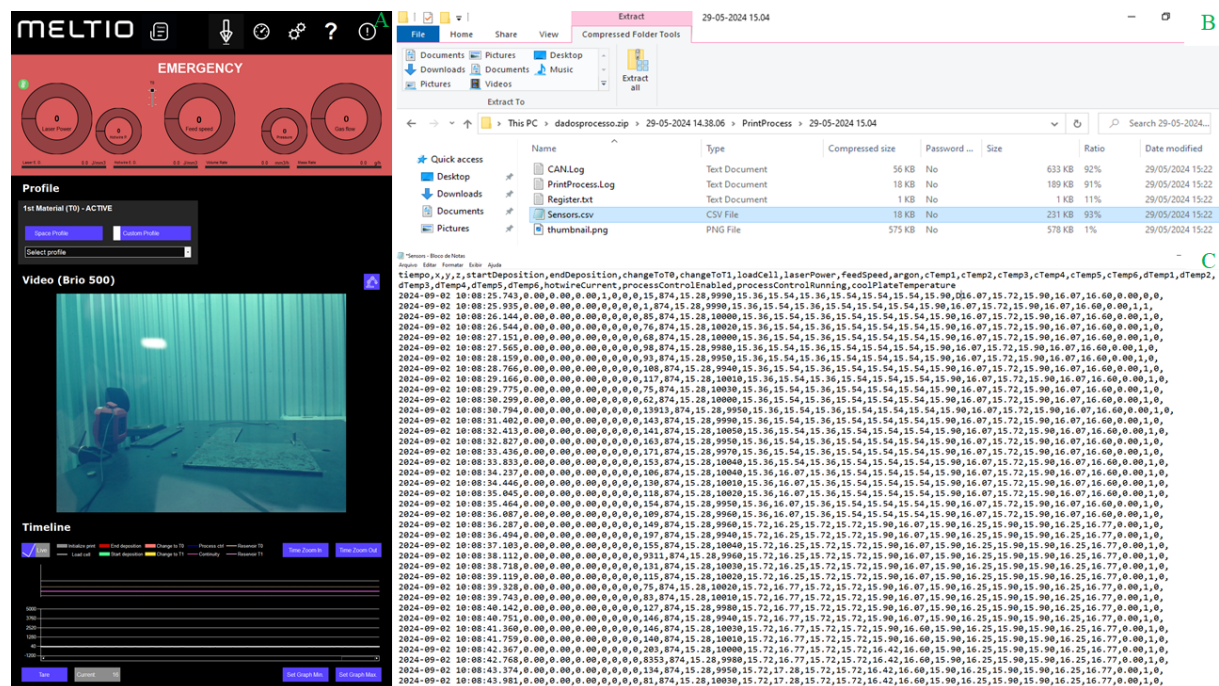


Figure 52 – Recorded Key LMD-wire Process Parameters.

Figure 53 illustrates the occurrence of defects that can compromise the integrity of additively manufactured parts if the process parameters are not adequately controlled. Process data, such as wire deposition force and laser power recorded in the *Sensors.csv* file, serve as essential resources for identifying variations in energy input that may lead to these defects. Stubbing, shown in Figure 53 (A), arises when the energy input is not enough to fully melt the feedstock material, leading to poor layer bonding and surface irregularities. This defect is primarily caused by an imbalance between laser power, wire feed speed, and travel speed, which prevents proper fusion between successive layers. Real-time monitoring of these parameters is crucial for dynamically adjusting deposition conditions and preventing stubbing formation.

Balling, depicted in Figure 53 (B), is the result of premature solidification of molten material before it can fully fuse with the substrate, generating excessive surface roughness and potential porosity. This phenomenon typically occurs when the energy input is too low or thermal conditions fluctuate excessively, preventing proper wetting and spreading of the melt pool. Identifying these deviations enables corrective actions, such as optimizing process parameters to achieve a stable energy distribution and mitigate the occurrence of balling. Overbuilding, illustrated in Figure 53 (C), occurs due to a mass imbalance between the deposited material and the energy available for fusion, leading to excessive accumulation and dimensional inaccuracies. This defect is often associated with inconsistencies in the wire feed rate or excessive energy input, resulting in uncontrolled material accumulation. Using real-time process data, adjustments can be made to maintain deposition stability, ensuring geometric accuracy and minimizing the need for extensive post-processing.

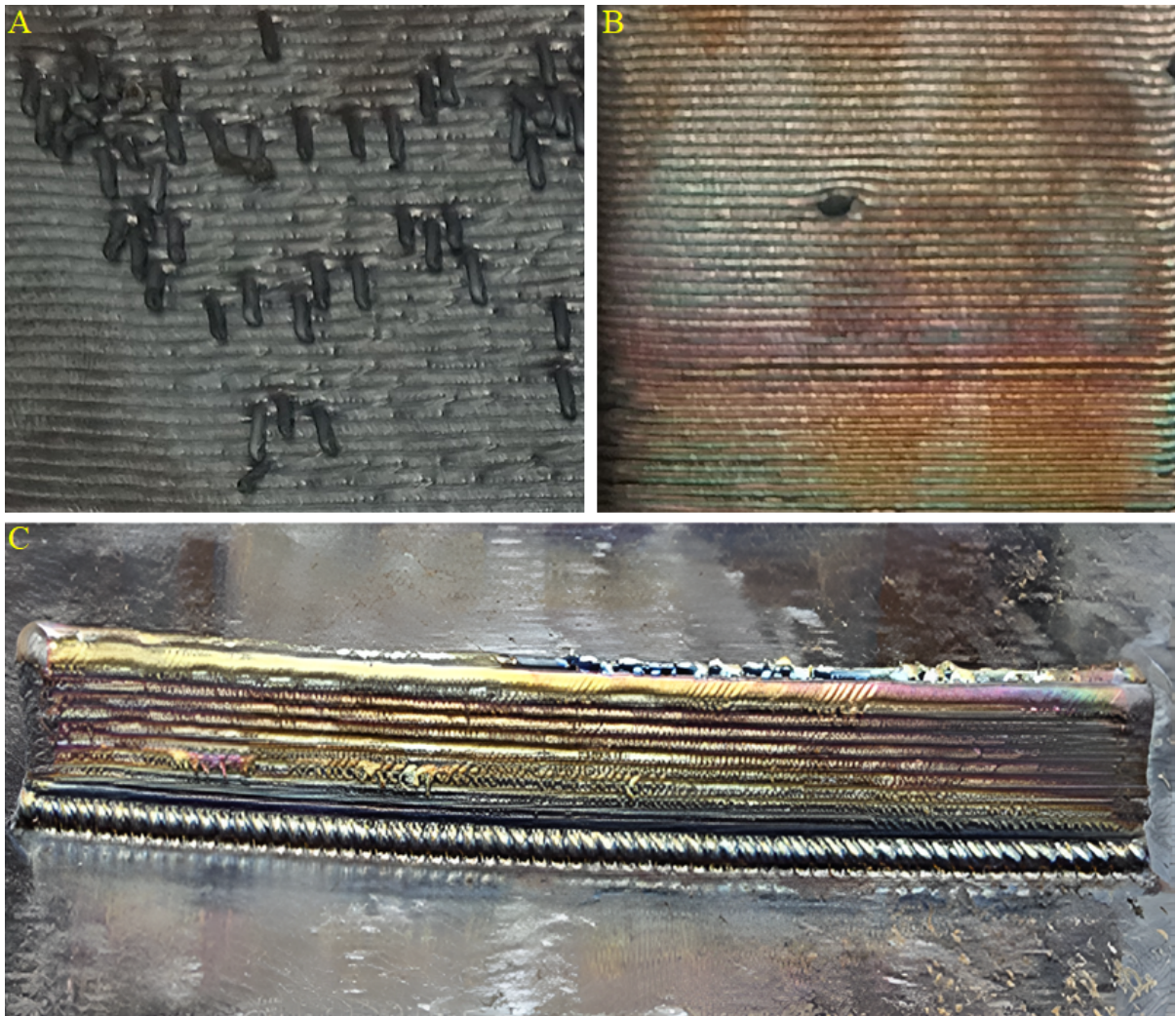


Figure 53 – Representative Defects in LMD-Wire Process.

5 Digital Twin System Development

5.1 Introduction

This chapter details the development of three distinct Digital Twins for a Robotic Additive Manufacturing Cell (RAMC), aligned with ISO 23247 standards. The first Digital Twin (DT) focuses on predictive maintenance for the KUKA iiQoT robot, utilizing Industrial Internet of Things (IIoT) technology to enhance performance and operational status. The second Digital Twin, Meltio Dashboard, provides real-time data visualization of the Meltio AM process, ensuring both efficiency and quality. The third Digital Twin serves as a real-time 3D simulation model, enabling data visualization and cloud storage for RAMC processes, allowing for comprehensive analysis and optimization.

5.2 DT Architecture Proposal Based on ISO 23247

Figure 54 illustrates the architecture proposed for the implementation of a DT according to the ISO 23247 standard developed in this work. This proposal integrates the five application domains—DThE, OME, DCDCE, DT, and DTUE—synchronized with each other, as outlined in ISO 23247-5. The primary objective is to enable 2D monitoring via a dashboard and 3D simulation of the RAMC in real-time. The architecture also incorporates KUKA iiQoT for predictive maintenance and Meltio Dashboard for visualization of printing data.

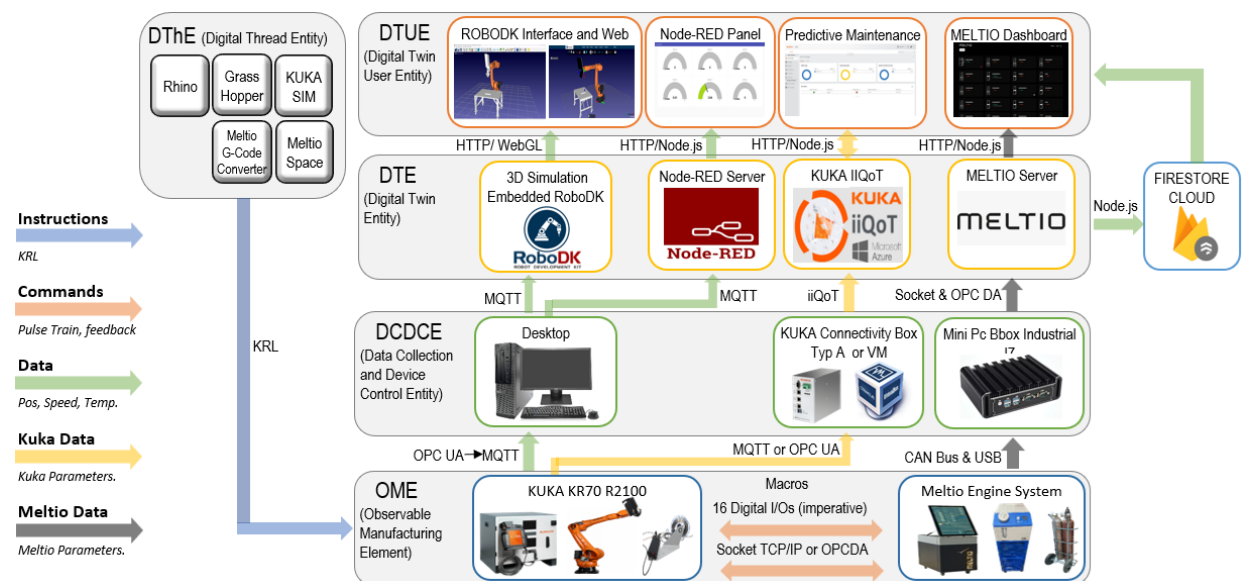


Figure 54 – Framework DT Architecture Proposal Based on ISO 23247 (ALVARES, A. J.; RODRIGUEZ, E.; FIGUEROA, B., 2025)

DThE (Digital Thread Entity) domain encompasses the CAD/CAPP/CAM systems, including CAD software such as Rhino3D, CAPP tools such as Grasshopper, and the Meltio G-Code Converter, as well as CAM systems such as KUKA.sim and Meltio Space. The primary objective of this layer is to generate KRL code, which includes instructions for printing and robot movement. This KRL code is then transmitted to the physical OME layer for execution (ISO, 2024).

5.2.1 DT KUKA iiQoT - Condition-Based Maintenance

OME (Observable Manufacturing Element): This layer includes the tangible components of the RAMC, encompassing all visible elements, such as actuators. It specifically integrates the KUKA KR 70 R2100, which comprises both the KUKA KR 70 R2100 robot and the KUKA KC5 controller. This layer processes KRL code, which contains printing commands to manage the physical devices. It also provides data from the robot's controller, detailing all operational parameters. The information is transmitted to the DCDCE layer via MQTT publisher or OPC UA.

DCDCE (Data Collection and Device Control Entity): This layer is tasked with the collection and regulation of data from the elements within the OME layer. In this setup, parameters from the KUKA system are received and processed through the KUKA Connectivity Box Type A or a designated virtual machine based on Linux. After processing, these parameters are sent to the DTE layer via KUKA iiQoT.

DTE (Digital Twin Entity): This layer represents the DT, which uses specialized software for its functionality. In this arrangement, KUKA parameters are processed on the KUKA iiQoT server and within the cloud infrastructure, enabling a two-way data exchange with the DTUE layer through HTTP/Node.js protocols.

DTUE (Digital Twin User Entity): This layer acts as the user interface for the DT, responsible for visualizing the data received from the DTE layer. Facilitates the two-way communication of KUKA parameters from KUKA iiQoT, displaying these parameters on a predictive maintenance dashboard, thereby enabling user interaction and monitoring.

5.2.2 DT Meltio Dashboard

OME (Observable Manufacturing Element): This layer includes tangible components of the RAMC, specifically highlighting the Meltio system, which comprises the Meltio controller, chiller, and argon gas tanks essential for managing the metal deposition process. It is responsible for executing control commands received for the operation of the deposition equipment and relaying specific Meltio parameters to the DTE layer.

DTE (Digital Twin Entity): This layer represents the DT, which uses specialized software to function effectively. In this setup, the Meltio parameters are gathered and processed

within the Meltio server and cloud infrastructure, after which they are communicated to the DTUE layer via HTTP/Node.js.

DTUE (Digital Twin User Entity): This layer acts as the user interface for the DT, tasked with visualizing data received from the DTE layer. It includes the Meltio Dashboard, which receives parameters from the Meltio system and graphically displays the printing data for user interaction and analysis.

5.2.3 DT Robotic Additive Manufacturing Cell

OME (Observable Manufacturing Element): This layer comprises the tangible components of the RAMC, including all observable elements such as actuators. It specifically integrates the KUKA KR 70 R2100, which includes the KUKA KR 70 R2100 robot, the KUKA KC5 controller, wire feeder, and wire, alongside the Meltio system, which consists of the Meltio controller, chiller, and argon gas tanks. This layer processes KRL code that contains printing instructions to manage physical devices. The interaction between these systems is enabled through digital I/O signals (imperative macros) and bidirectional communication via TCP/IP sockets or OPC DA. Moreover, this layer provides data on the position, speed, and temperature of the robot joints, obtained through OPC UA and converted to an MQTT publisher for transmission to the DCDCE layer.

DCDCE (Data Collection and Device Control Entity): This layer is tasked with collecting and controlling data from the components within the OME layer. It functions as a desktop system that utilizes the MQTT protocol in a subscriber role to collect and consolidate data, with respect to the position, speed, and temperature of the robot joints. In addition, it serves as an intermediary by processing and relaying this information to the DTE layer.

DTE (Digital Twin Entity): This layer embodies the actual DT, leveraging the appropriate software for its functionality. Here, data related to the position, speed, and temperature of the robot joints are received through an MQTT subscriber and processed within RoboDK alongside a 3D cell model to create real-time 3D simulations. This simulation data is then sent to the DTUE layer via HTTP/WebGL. Furthermore, the information is also processed through a Node-RED server flow, which subsequently forwards the data to the DTUE layer via HTTP/Node.js. Additionally, this layer transmits data to Firestore Cloud using Node.js, where it is stored in a cloud-based database and later made available to the DTUE layer.

DTUE (Digital Twin User Entity): This layer functions as the user interface for the DT, responsible for displaying data received from the DTE layer to the user. It acquires data via HTTP/WebGL from the RoboDK simulation within the DTE layer and visualizes it as a real-time 3D simulation within the RoboDK interface and RoboDK Web. Moreover, data sent by the Node-RED server through HTTP/Node.js are received and graphically represented on a 2D dashboard within the Node-RED panel.

5.3 Results of the Implemented DT Architecture of the RAMC

5.3.1 First Digital Twin: KUKA iiQoT

The configuration process for the KUKA iiQoT system involves multiple steps, including setting up a virtualized environment to facilitate secure deployment, installing necessary applications, and defining configuration files to enable communication between the robot controller and the monitoring platform. The virtual machine runs a Linux-based operating system, such as Ubuntu, where the required software components are installed to establish a stable interface between the iiQoT platform and the robot controller. The iiQoT system operates using OPC UA as its primary communication protocol, ensuring secure and standardized data exchange.

Once the virtualized environment is prepared, the iiQoT application must be configured to establish seamless data exchange with the KUKA controller. Unlike other industrial monitoring solutions that require complex network configurations, the integration of KUKA iiQoT is streamlined by using a preissued license file from KUKA Robotics. This file must be placed in the directory "C:\KRC\ROBOTER\Config\User\Common\OpcUa\AccessConfig\" on the robot controller. By doing so, the system gains the necessary permissions to access and transmit operational data via OPC UA, facilitating real-time monitoring and predictive maintenance.

The final step in the deployment process consists of integrating the iiQoT system with the KUKA controller. This involves verifying the correct installation of the OPC UA server on the robot controller and ensuring that the iiQoT platform can retrieve and process the collected data. Once the integration is complete, the system continuously monitors the robot's operational status, allowing for real-time analysis of performance indicators and failure modes. The data collected are stored in the KUKA cloud infrastructure, which is hosted on Microsoft Azure, allowing remote access, advanced analytics, and integration with predictive maintenance systems. This approach improves condition-based maintenance strategies by taking advantage of cloud computing for scalable and efficient data management (KUKA, 2025).

Figure 55 displays the interface of the KUKA iiQoT monitoring system. This system is specifically designed for condition-based maintenance, enabling the diagnosis of failure modes in KUKA robots. Additional details on its usage can be found in the video available at (ALVARES, A., 2024).

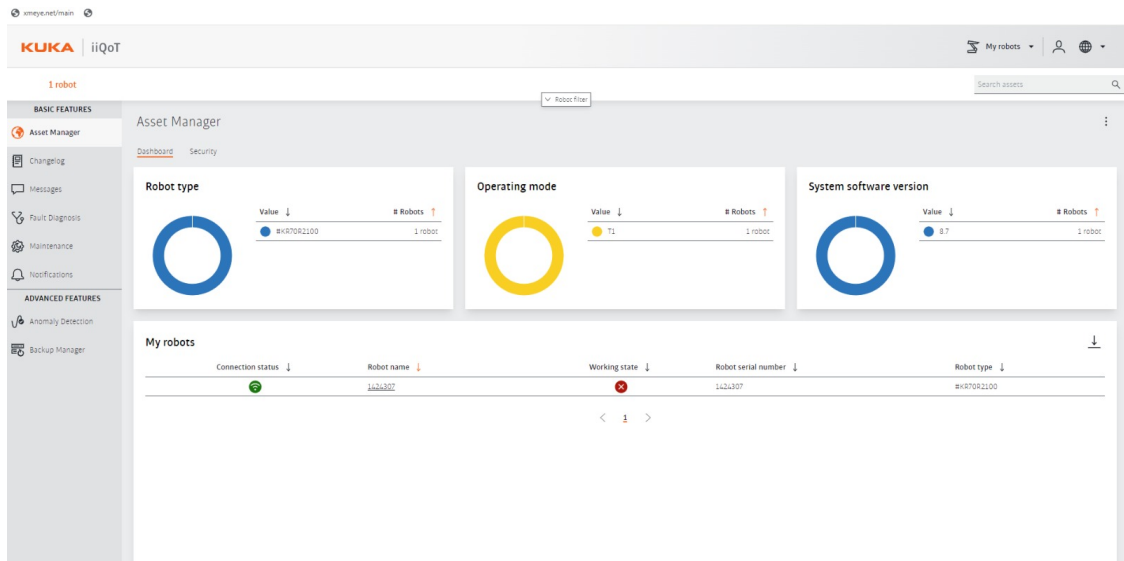


Figure 55 – KUKA iiQoT Dashboard (ALVARES, A. J.; RODRIGUEZ, E.; FIGUEROA, B., 2025).

5.3.2 Second Digital Twin: Meltio Dashboard

The Meltio Dashboard configuration process requires the establishment of a network connection between the Meltio controller and the monitoring interface. Initially, a request must be submitted to Meltio to obtain a dedicated IP address and an available port for access to the dashboard. Once these credentials are assigned, the Meltio controller must be connected to the network by manually configuring its IP address and port settings. The controller transmits process data via OPC DA and socket communication to the Meltio server, where the data is processed and stored. The dashboard interface is then accessed through HTTPS using a Node.js-based web application, enabling real-time interaction with the system.

The Meltio Dashboard retrieves and visualizes operational parameters from the Meltio server, which collects data from the Meltio controller through an embedded Mini PC Bbox Industrial i7. The system continuously monitors and displays key process variables such as laser power, fiber temperature, gas flow rate, wire feed speed, and load cell measurements. Additionally, it integrates real-time imaging from the visualization camera, allowing for enhanced process supervision.

Figure 56 illustrates the interface of the Meltio Dashboard, a monitoring system developed by Meltio that is accessible via the dashboard link (MELTIO, 2024). This dashboard provides real-time insights into the printing parameters, enhancing the operator's ability to monitor the process effectively. More details on its usage and features can be found in the video available at (ALVARES, A., 2024).

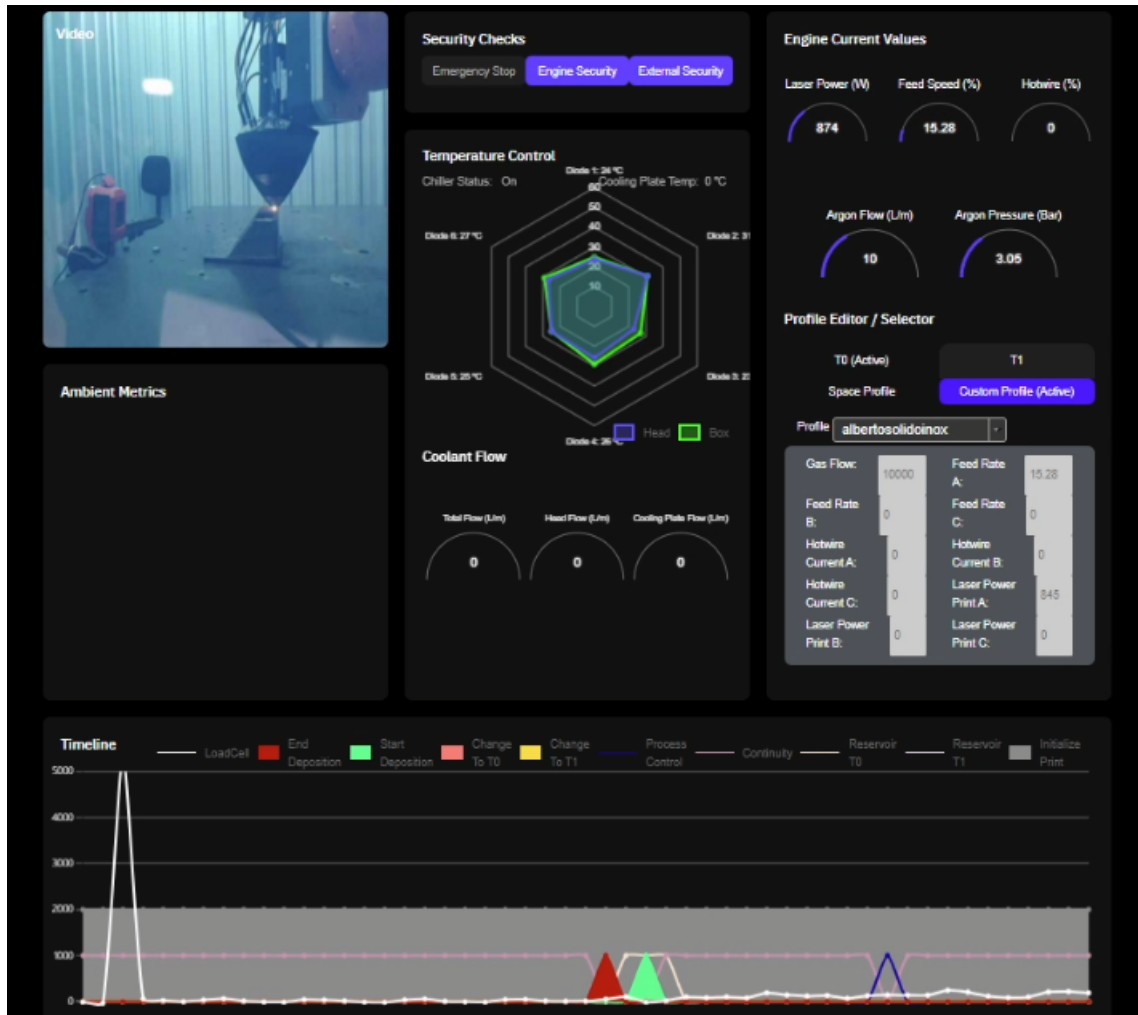


Figure 56 – Meltio Dashboard (ALVARES, A. J.; RODRIGUEZ, E.; FIGUEROA, B., 2025).

5.3.3 Third Digital Twin: Robotic Additive Manufacturing Cell

The implemented DT architecture facilitates two distinct data flows: the first focuses on 3D movement simulation during the printing process (FIGUEROA, B. S., 2024), while the second relates to the Node-RED dashboard and data storage in Firestore Cloud. Both data flows leverage information published by the MQTT publisher and are interconnected through a common MQTT broker. The real robotic cell, along with these data flows, is depicted in the diagram presented in Figure 57.

Table 5 summarizes the key variables collected from the KUKA KRC5 system using MQTT and TCP/IP sockets, including their collection methods, descriptions, and corresponding MQTT topics. These variables encompass the robot's operational status, joint positions, speeds, motor temperatures, and timestamps for synchronization during data transmission. The process of establishing the connection and publishing the robot data via MQTT is detailed in the pseudocode presented in Table 6. A comprehensive description of the data acquisition implementation, including MQTT configurations and scripts, is provided in Appendix B.1.

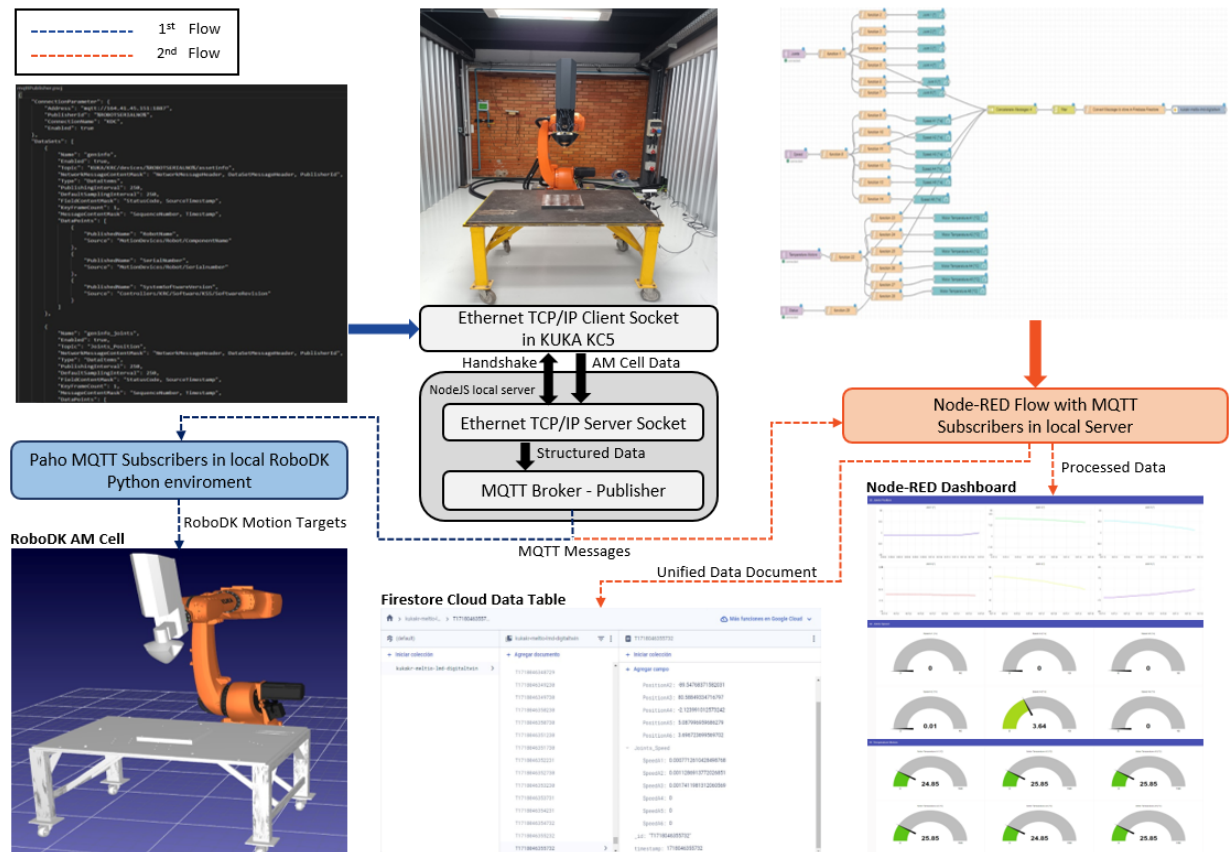


Figure 57 – MQTT Flows Developed for Digital Twin Framework Architecture (ALVARES, A. J.; RODRIGUEZ, E.; FIGUEROA, B., 2025).

Table 5 – Robot Data from the Robotic Additive Manufacturing Cell Collected from KUKA via MQTT.

Variable	Collection Method	Description	MQTT Topic
Status	The KUKA KRC5 system sends a "TRUE" message upon initialization and "FALSE" upon termination to indicate connection status.	Indicates whether the adapter is online with the KUKA KRC5 controller.	"Status"
Joints Position	The KUKA system retrieves the "ActualPosition" variable for each joint.	Represents the angular position of the six joints (1 to 6) in degrees.	"Joints_Position"
Joints Speed	The KUKA system retrieves the "ActualSpeed" variable for each joint.	Indicates the angular speed of each joint in degrees per second.	"Joints_Speed"
Joint Motor Temperature	Accesses the "MotorTemperature" variable for each joint's motor.	Displays the motor temperature for each joint in Kelvin.	"Motor_Temperature"
Timestamp	Created in JavaScript for data transmission reference.	Provides an instantaneous timestamp for the current data cycle.	"Timestamp"

Table 6 – Pseudocode for the Robot Data Connection and Publishing.

Pseudocode for Robot Data Connection
START
DEFINE Connection AS STRUCTURE
Address ← "mqtt://BROKER_ADDRESS:PORT"
PublisherId ← "%ROBOTSERIALNO%"
ConnectionName ← "KDC"
Enabled ← TRUE
END STRUCTURE
DEFINE DataSets AS LIST
ADD DataSets: STRUCTURE
"Joints_Position", ["A1", "A2", "A3", "A4", "A5", "A6"], "ActualPosition"
"Joints_Speed", ["A1", "A2", "A3", "A4", "A5", "A6"], "ActualSpeed"
"Motor_Temperature", ["A1", "A2", "A3", "A4", "A5", "A6"], "MotorTemperature"
"Status", ["Status"], "InMotion"
END

5.3.3.1 3D Movement Simulation Flow

The second flow of the DT architecture was designed to develop an application capable of simulating the movements of the RAMC in near real-time. This simulation relies on continuously updating the positions and velocities of the six robotic joints, ensuring an accurate representation of the motion dynamics of the robot. By integrating data-driven control, the DT enhances the monitoring and predictive capabilities of the system, improving operational efficiency and decision-making in robotic processes.

Within the RoboDK environment, a Python script was developed using the Paho MQTT library to communicate with the robotic system. The script subscribes to MQTT topics that provide real-time joint positions and velocities, enabling precise movement control. Positions are received in degrees, while velocities are in degrees per second and converted to radians per second for accurate motion planning. This ensures that the virtual model closely replicates the physical behavior of the robot.

To streamline the motion control process, Table 8 presents the pseudocode outlining the fundamental steps for processing MQTT data and executing robotic commands within RoboDK. This structured algorithm guarantees efficient interpretation of incoming messages, parsing of relevant joint parameters, and the appropriate execution of motion commands. In addition, it incorporates error handling mechanisms to manage unexpected interruptions in data transmission. A comprehensive description of the complete implementation, including the Python script, MQTT configurations, and data flow structure, is provided in Appendix B.2, offering an in-depth view of the system's architecture and operational logic.

Table 7 – Pseudocode for Robotic Motion Control RoboDK.

```

Pseudocode for Robotic Motion Control RoboDK
BEGIN
  INITIALIZE RoboDK API
  DEFINE FUNCTION SetSpeeds(speeds)
    SET robot joint speed
  END FUNCTION

  DEFINE FUNCTION MoveRobot(target_position)
    MOVE robot to target_position
  END FUNCTION

  robot ← SELECT robot in RoboDK
  IF robot NOT found THEN
    TERMINATE process
  END IF

  DEFINE FUNCTION OnMessage(topic, data)
    IF topic == "Position" THEN
      target_position ← PARSE data
      MoveRobot(target_position)
    ELSE IF topic == "Speed" THEN
      speeds ← PARSE data
      SetSpeeds(speeds)
    END IF
  END FUNCTION

  SUBSCRIBE to "Joints_Position" and "Joints_Speed"
END

```

The code initializes the RoboDK API using Robolink(), allowing interaction with robotic elements in the simulation. It defines functions to set joint speeds and command the robot to move to specific joint positions. The user selects a robot and identifies the fixed printing table within the RoboDK environment, while an MQTT message handler processes topics such as "Joints_Position" and "Joints_Speed," extracting necessary data and updating the robot's movements in real time through the specified MQTT broker. To ensure seamless communication, the implementation relies on a Python script that connects to the MQTT broker and processes incoming data via an Ethernet TCP/IP client socket, allowing real-time adjustments of the robot position and speed. This setup provides a high-fidelity simulation of the dynamics of the RAMC, accurately reflecting the trajectory of the KUKA robot during operation.

The 3D assets used in the DT model include standard RAMC components, such as the KUKA KR70 R2100 model, the fixed printing table model and the Meltio Engine head model, all integrated within the RoboDK library, as shown in Figure 57. To simulate the movement of the RAMC, MQTT subscribers receive data published through the broker, capturing key parameters such as the current position and speed of the six joints (expressed in degrees and degrees per second), joint angular speeds (converted to radians per second for precise control) and commands to manage the robot movements during the simulation. Figure 58 illustrates the 3D DT of the cell in operation, depicting a real-time print of a part.

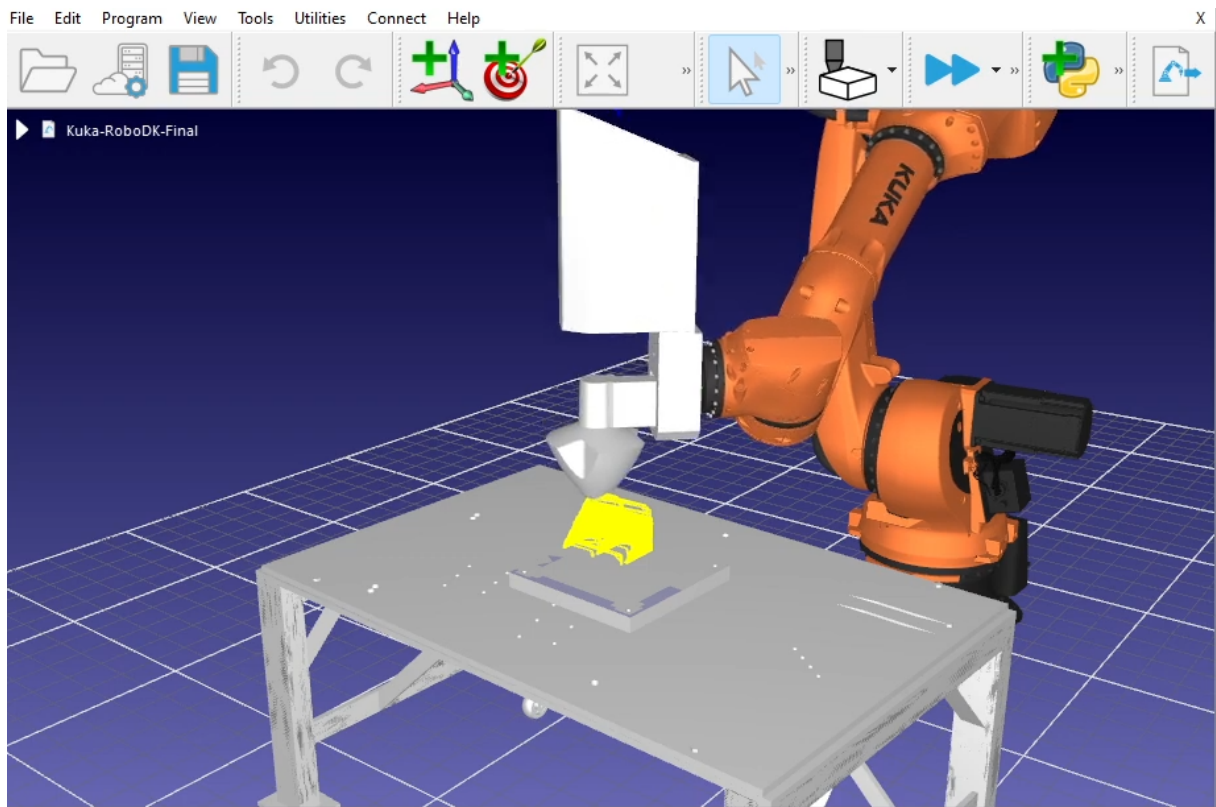


Figure 58 – Digital twin of the cell during real-time 3D printing (ALVARES, A. J.; RODRIGUEZ, E.; FIGUEROA, B., 2025).

5.3.3.2 Node-RED Dashboard and Firestore Storage Flow

The second flow of the implemented DT architecture operates on a local Node-RED server, processing data published by the MQTT broker across five topics related to the parameters of the RAMC, as detailed in Table 5. Each message from the MQTT topics is received by a corresponding Node-RED subscriber and structured into a unified format, including position in degrees, speed in degrees per second, and temperature in degrees Celsius, before being transmitted to Firestore Cloud for secure storage.

The core logic of this flow is outlined in the pseudocode presented in Table 8, which details the structured process of subscribing to MQTT topics, extracting key data points such as joint positions, speeds, and motor temperatures, and formatting them for integration with the cloud database. Additionally, the same subscribers direct data to a customized Node-RED dashboard, visualizing these key parameters in real time and allowing operators to monitor critical metrics and respond promptly to deviations. The complete Node-RED implementation, including the developed flow logic and data handling mechanisms, is provided in Appendix B.3, ensuring real-time access and historical data analysis.

Table 8 – Pseudocode for the Node-RED Flow.

Pseudocode for Node-RED Flow
START
DEFINE Data AS STRUCTURE
Joints ← LIST ["A1", "A2", "A3", "A4", "A5", "A6"]
Speed ← LIST ["A1", "A2", "A3", "A4", "A5", "A6"]
MotorTemperature ← LIST ["A1", "A2", "A3", "A4", "A5", "A6"]
Status ← LIST ["System Status"]
END STRUCTURE
CONNECT TO MQTT Broker "mqtt://BROKER_ADDRESS:PORT"
SUBSCRIBE TO Topics:
"robot/joints/position"
"robot/joints/speed"
"robot/motors/temperature"
"robot/status"
RECEIVE Data from MQTT Topics
PROCESS Data using Functions
FOR EACH Joint IN Joints DO
APPLY Function to Extract Position
END FOR
FOR EACH SpeedValue IN Speed DO
APPLY Function to Extract Speed
END FOR
FOR EACH TempValue IN MotorTemperature DO
APPLY Function to Extract Temperature
END FOR
APPLY Function to Extract System Status
CONCATENATE Messages
FILTER Data
CONVERT Data Format for Firebase Firestore
PUBLISH Data to "kukakr-meltio-lmd-digitaltwin"
END

The data stored in Firestore Cloud can be leveraged to generate graphs and trend analyses, offering valuable insight into the operational performance of the RAMC. This analytical capability enables process optimization and data-driven decision-making, ultimately improving efficiency and system reliability. The Node-RED flow diagram, along with examples of the visualizations generated, is presented in Figure 57. By seamlessly integrating real-time monitoring with cloud storage, this data architecture establishes a robust foundation for both immediate operational control and long-term strategic analysis within the DT framework.

Figure 59 provides a detailed representation of the DT, showcasing real-time monitoring of key parameters such as position, speed, and temperature on a 2D dashboard. In addition, it illustrates the functional nodes and their interconnections within the Node-RED platform, along with a snapshot of the structured data stored in Google Firebase. This visualization highlights the seamless integration between the monitoring system and cloud storage, reinforcing the role of the DT in enhancing process transparency and control.

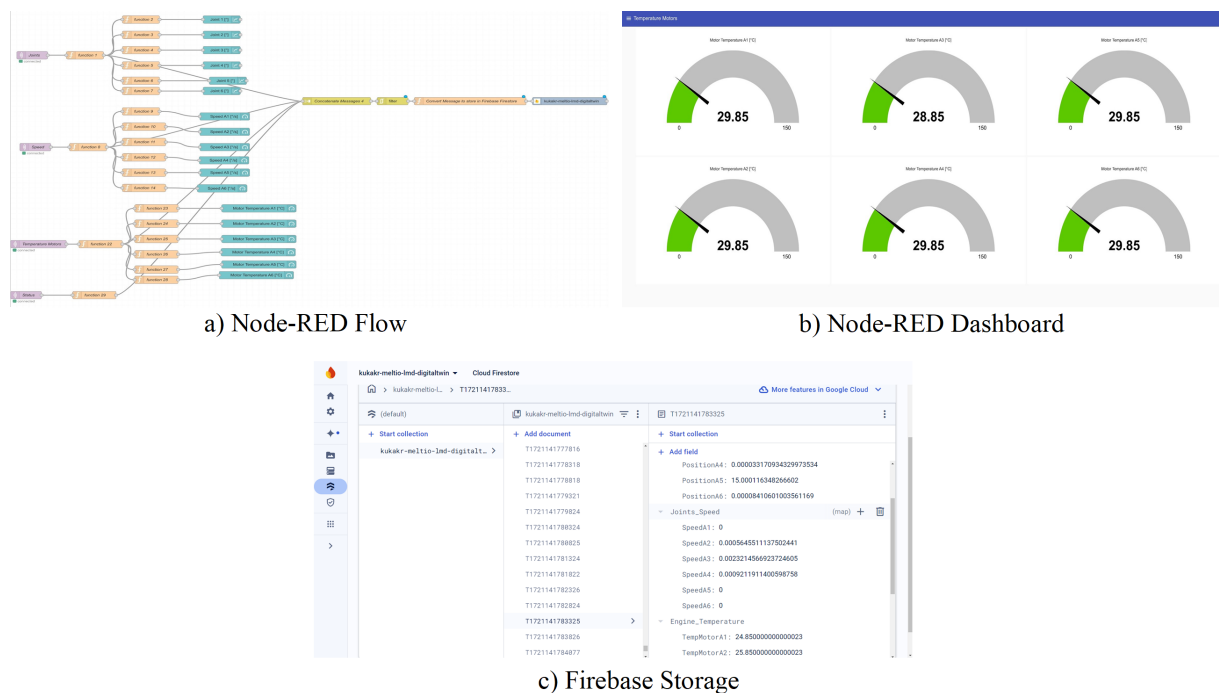


Figure 59 – Node-Red flows to generate a 2D Dashboard of the Kuka robot and store the robot's kinematic parameters.

6 Case Studies: Validation and Experiments

6.1 Introduction

This chapter presents a series of case studies analyzing printed parts produced with the Robotic Additive Manufacturing Cell (RAMC). The first analysis focuses on the visual assessment of defects present in the printed parts. The second analysis involves a metallographic examination, incorporating evaluations of microstructure and microhardness.

6.2 Visual Defect Analysis of Printed Parts

This section presents three case studies focused on the visual analysis of defects in printed parts. The first involves six cubes fabricated with varying deposition parameters to evaluate their influence on defect formation. The second examines a structural support component, based on a Gravia model, to assess imperfections that may impact structural integrity. The third analyzes a printed wall, emphasizing surface defects. Figure 60 shows the Ishikawa (fishbone) diagram related to defects observed in parts printed using the LMD-wire process with Meltio Engine Robots. The diagram outlines the causes of each defect and their recommended solutions, with the red left side highlighting defect sources and the green right side showing possible corrective actions.

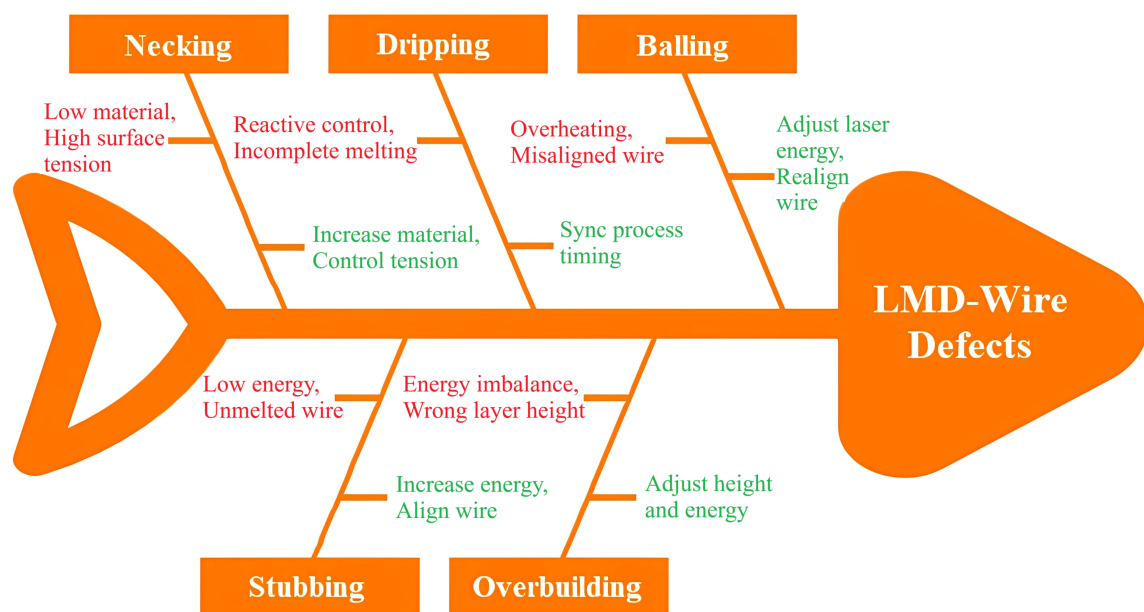


Figure 60 – Ishikawa Diagram associated with defects in parts printed using the LMD-wire process (ALVARES, A. J.; FIGUEROA, B. S., et al., 2025).

6.2.1 Case Study 1: Printed Parts

In Case Study 1, six cubic samples were produced with varying deposition parameters to investigate their effect on process stability and part quality. Table 9 (Part 1 to Part 6) details the parameter sets, including laser power, wire and print speed, gas flow, layer dimensions, slicing software, and deposition strategies. As shown in Figure 61a, these variations were deliberately introduced to compare how different parameter configurations influence surface finish, dimensional accuracy, and defect formation. Figure 61b presents the Meltio standard part, which served as the reference model for evaluating deposition performance. Parts 1 to 3 employed rectilinear infill with different laser powers, Parts 4 and 5 introduced overlapping strategies, and Part 6 incorporated a raft and alternative slicing software. This systematic design enabled a structured analysis of defects, deviations, and overall deposition quality.

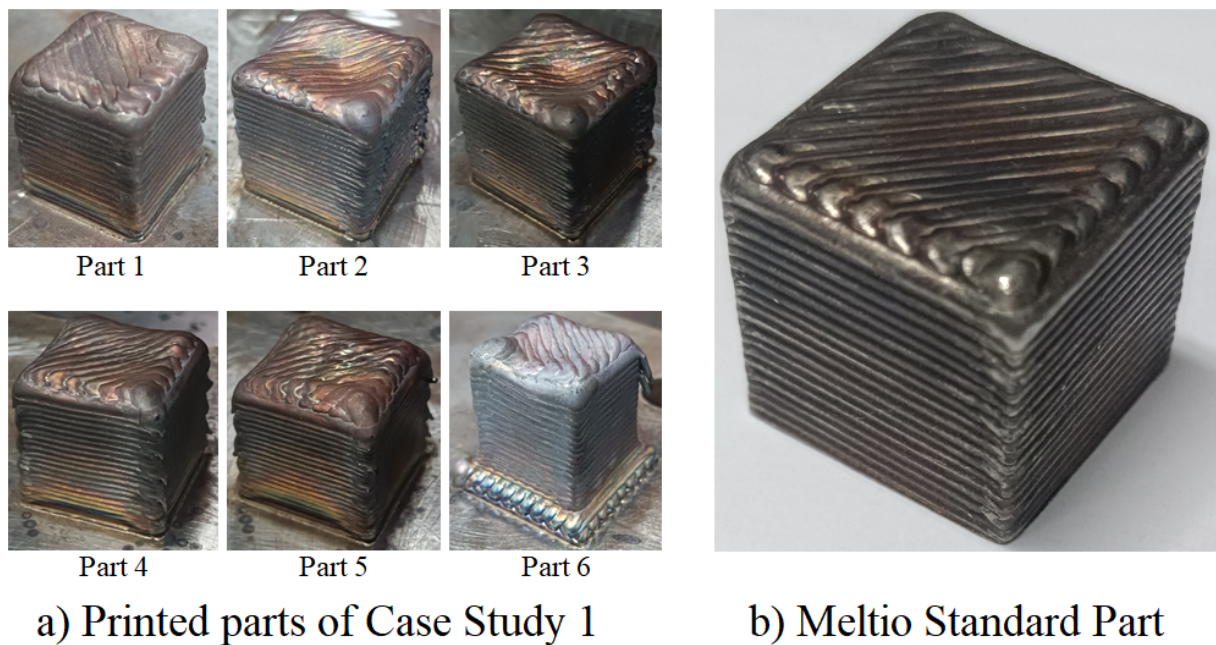


Figure 61 – Printed Parts and Meltio Standard Part Case Study 1.

Table 9 – Deposition Parameters of Parts Case Study 1.

Part	Laser Power [W]	Wire Speed [mm/s]	Print Speed [mm/s]	Gas Flow [ml/min]	Layer Height [mm]	Layer Width [mm]	3D Slicing Software	Deposition Strategy
Part 1	850	15.3	10	12000	1.2	1	Grasshopper	Rectilinear infill
Part 2	800	15.3	10	12000	1.2	1	Grasshopper	Rectilinear infill
Part 3	860	15.3	10	12000	1.2	1	Grasshopper	Rectilinear infill
Part 4	860	15.3	10	12000	1.2	1	Grasshopper	Rectilinear + 0.1 mm Overlap
Part 5	860	15.3	10	12000	1.2	1	Grasshopper	Rectilinear + 0.2 mm Overlap
Part 6	845	15.28	10	10000	1.2	1	Meltio Space	Rectilinear infill + 2 mm Raft

6.2.1.1 Capability Analyses of the printed Parts

To assess the dimensional accuracy of the printed parts, 15 measurements were conducted along the X and Y axes of each specimen using a Mitutoyo digital caliper, while measurements along the Z axis were excluded due to material loss during the extraction process. The detachment of specimens, performed using cutting discs due to the large substrate size, resulted in partial material removal, compromising the reliability of Z-axis measurements. For the process capability analysis, a tolerance limit of ± 0.5 mm was established as a reference for evaluating manufacturing accuracy and stability. The measurement results, consolidated in Table 10, include systematic error values, process capability indices (C_p and C_{pk}), and six-sigma values. The systematic error was computed in absolute terms, eliminating negative values, and exhibited a range between 0.01 mm and 0.54 mm, indicating a tendency for undersizing in certain cases.

Table 10 – Consolidated Measurement of the Parts.

Measurement	Part 1 (X,Y)	Part 2 (X,Y)	Part 3 (X,Y)	Part 4 (X,Y)	Part 5 (X,Y)	Part 6 (X,Y)	Meltio (X,Y)	Part
1	19.49, 19.58	26.01, 26.03	25.99, 26.06	24.81, 24.86	24.93, 25.03	20, 20.25	24.71, 24.96	
2	19.48, 19.41	25.97, 26.08	26, 26.01	24.82, 24.85	24.86, 25	19.99, 20.2	24.71, 24.98	
3	19.25, 19.4	25.98, 26	26.16, 25.72	24.85, 24.98	24.91, 25.07	19.91, 20.3	24.69, 25.01	
4	19.18, 19.38	26.02, 25.99	26.04, 25.74	24.74, 24.76	24.92, 24.98	19.84, 20.18	24.71, 24.94	
5	19.31, 19.23	26.03, 25.94	25.71, 25.72	24.54, 24.73	24.91, 24.89	19.86, 20.13	24.7, 24.99	
6	19.37, 19.18	25.96, 25.97	25.71, 25.71	24.47, 24.5	24.87, 24.98	19.85, 20.06	24.77, 25.19	
7	19.25, 19.28	25.8, 25.89	25.69, 25.73	24.45, 24.51	24.74, 24.84	19.87, 19.99	24.89, 25.01	
8	19.5, 19.44	25.84, 25.98	25.72, 25.91	24.41, 24.54	24.72, 24.83	19.94, 20	24.9, 24.94	
9	19.55, 19.49	25.9, 25.98	25.77, 26.03	24.46, 24.69	24.69, 24.84	19.92, 19.98	24.9, 24.96	
10	19.49, 19.78	25.72, 25.97	25.99, 26.27	24.66, 24.64	24.67, 24.8	20.08, 19.93	24.92, 25.01	
11	19.64, 19.77	25.87, 26.17	26.12, 26.22	24.82, 24.66	24.65, 24.84	20.07, 19.95	24.91, 25	
12	19.5, 19.63	26, 26.15	26.22, 26.22	24.99, 24.78	24.74, 24.85	19.96, 19.98	24.92, 25	
13	19.52, 19.51	26.13, 26.18	26.37, 26.15	25.03, 24.8	24.87, 24.9	20.07, 19.94	24.79, 25.01	
14	19.47, 19.52	26.2, 26.13	26.38, 26.13	25.04, 24.78	24.9, 24.88	20.1, 19.92	24.8, 24.96	
15	19.88, 19.5	26.16, 26.13	25.79, 25.9	25.14, 24.73	24.82, 24.95	20.01, 19.93	24.9, 24.89	
Final Mean	19.46, 19.47	25.97, 26.04	25.98, 25.97	24.75, 24.72	24.81, 24.91	19.96, 20.05	24.81, 24.99	
Design Value	20, 20	25, 25	25, 25	25, 25	25, 25	20, 20	25, 25	
Systematic Error	0.54, 0.53	0.97, 1.04	0.98, 0.97	0.25, 0.28	0.19, 0.09	0.04, 0.05	0.19, 0.01	
Standard Dev	0.17, 0.17	0.13, 0.09	0.24, 0.21	0.24, 0.14	0.10, 0.08	0.09, 0.13	0.09, 0.07	
6 σ	1.02, 1.02	0.78, 0.54	1.44, 1.26	1.44, 0.84	0.60, 0.48	0.54, 0.78	0.54, 0.42	
C_p	1.13, 0.99	1.70, 4.14	0.89, 0.89	1.43, 2.0	2.15, 2.65	2.19, 3.39	3.21, 2.48	
C_{pk}	-0.09, -0.05	-1.61, -4.47	-0.85, -0.84	0.71, 0.88	1.35, 2.18	2.03, 3.05	2.02, 2.43	
CI _{95%} [Min,Max]	[0.059,1.021], [0.049,1.011]	[0.654,1.286], [0.724,1.356]	[0.342,1.618], [0.332,1.608]	[0.306,0.806], [0.276,0.836]	[0.066,0.446], [0.166,0.346]	[0.276,0.356], [0.266,0.366]	[0.038,0.418], [0.218,0.238]	

In addition, Figure 62 presents the capability analysis performed using Minitab for each part along the X and Y axes, providing a graphical representation of the process performance. These analyses illustrate key statistical indicators such as the process mean, standard deviation, and distribution relative to the defined tolerance limits of ± 0.5 mm. The computed capability indices, including C_p and C_{pk} , offer insights into process stability and centering, where C_p quantifies the overall process capability, while C_{pk} assesses how well the mean aligns with the nominal dimension. The confidence interval at 95% (CI) further enhances the reliability of these estimations by defining a range within which the true mean is expected to lie. The 6 σ range provides an additional measure of process dispersion, indicating

whether dimensional variability remains within acceptable thresholds. By integrating these statistical analyses, Figure 62 enables a comprehensive evaluation of dimensional accuracy and process consistency.

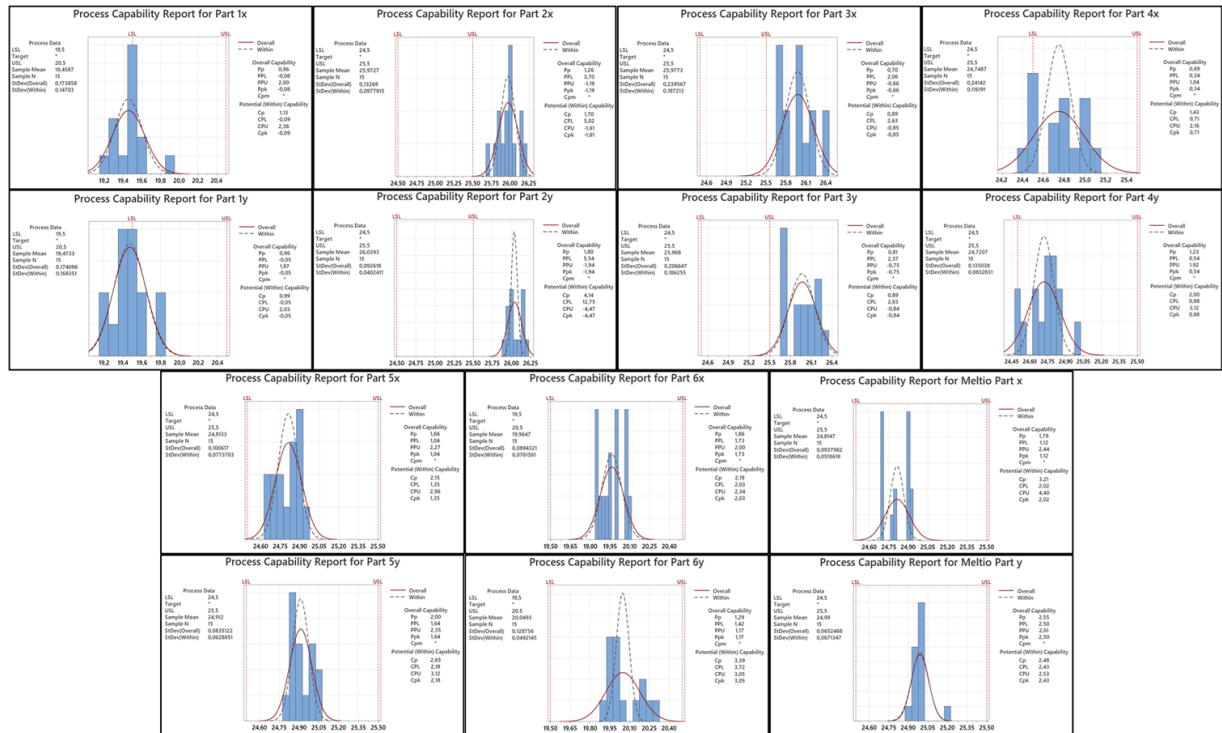


Figure 62 – Capability Reports of the Parts in Case Study 1.

Furthermore, Table 11 provides a structured overview of each printed part, detailing its geometric characteristics and deviations identified through dimensional analysis. The description includes systematic error values, highlighting whether the parts exhibit consistent undersizing or oversizing trends. Additionally, process variability is reported, reflecting fluctuations in dimensions across multiple measurements. These metrics, derived from statistical evaluations, facilitate a comprehensive understanding of how each part deviates from its nominal design, contributing to the assessment of manufacturing consistency.

Moreover, the table integrates critical capability analysis parameters obtained from the statistical evaluations, including the capability indices (C_p , C_{pk}), the 6σ range, and the 95% confidence interval (CI). The C_p and C_{pk} indices indicate whether the manufacturing process is capable of producing parts within the defined tolerance limits, while the 6σ range quantifies the total spread of variations. The 95% confidence interval further enhances the reliability of these evaluations by estimating the precision of the measurements. By consolidating these key indicators, the table serves as a comprehensive reference for understanding the dimensional accuracy and process stability of each printed part, supporting continuous improvements in manufacturing precision.

Table 11 – Process capability analysis of Printed parts

Part	Description
Part 1	The process capability for this part demonstrates a moderate level of variability, as indicated by the standard deviation. The 95% confidence interval (CI) for the mean provides an estimate of the range in which the true population mean is expected to lie, reflecting the measurement uncertainty. The C_p value suggests that the process has a reasonable capability, but the negative C_{pk} indicates a significant shift from the nominal value, increasing the risk of non-conforming parts. Additionally, the 6σ range highlights the total dispersion relative to specification limits.
Part 2	The statistical analysis reveals a high C_p value, signifying a process with low variability relative to tolerance limits. However, the negative C_{pk} value suggests a misalignment of the process mean, increasing the likelihood of defective parts. The 95% CI indicates the reliability of the estimated mean and helps quantify the degree of uncertainty. The 6σ range confirms the dispersion within the process, further emphasizing the need for corrective adjustments to improve centering.
Part 3	This part presents a C_p value close to 1, indicating that the process barely meets specification requirements. The negative C_{pk} reveals an off-center process, which may lead to increased defect rates. The 95% CI suggests a broader range of possible true mean values, reflecting higher uncertainty. The 6σ calculation confirms the extent of variation in the process, indicating the necessity for tighter control mechanisms.
Part 4	This part exhibits an improved C_p value, suggesting that the process has the potential to meet specifications. Unlike previous cases, the C_{pk} value is positive, indicating better alignment of the process mean with the nominal value. The 95% CI is narrower, signifying increased measurement precision and reduced uncertainty. The 6σ range confirms a stable process with controlled variability.
Part 5	With a high C_p and a positive C_{pk} , this part demonstrates strong process capability and centering. The 95% CI is relatively small, reflecting greater reliability in the estimated mean. The standard deviation is low, suggesting minimal variation in production measurements. The 6σ value indicates that the process operates well within acceptable limits.
Part 6	The process capability analysis for this part highlights optimal control, as reflected by its high C_p and C_{pk} values. The 95% CI suggests a high level of confidence in the estimated mean, reinforcing process stability. The 6σ range confirms that variability remains well within acceptable thresholds, reducing the probability of defects. The low standard deviation further supports the consistency of the process.
Meltio Part	The final part presents acceptable process capability values, though minor adjustments are necessary for further optimization. The difference between C_p and C_{pk} suggests that while the process has low variability, it is not perfectly centered. The 95% confidence interval reflects the expected range for the mean, providing insight into the estimation's reliability. The 6σ value confirms controlled process dispersion, reinforcing stability while identifying potential areas for improvement.

6.2.2 Case Study 2: Gravia Part

In Case Study 2, a structural support for industrial application was printed for the company Gravia, as shown in Figure 63. The component, modeled in Rhino3D and manufactured with 316 LSi stainless steel wire of 1 mm diameter, was produced following the deposition parameters summarized in Table 12. These parameters comprise laser power, wire feed speed, print speed, shielding gas flow, layer geometry, slicing software, and deposition strategy. The assessment emphasized surface finish, dimensional accuracy, and deposition consistency, with particular attention to the uniformity of material distribution and the identification of irregularities that could compromise structural integrity.

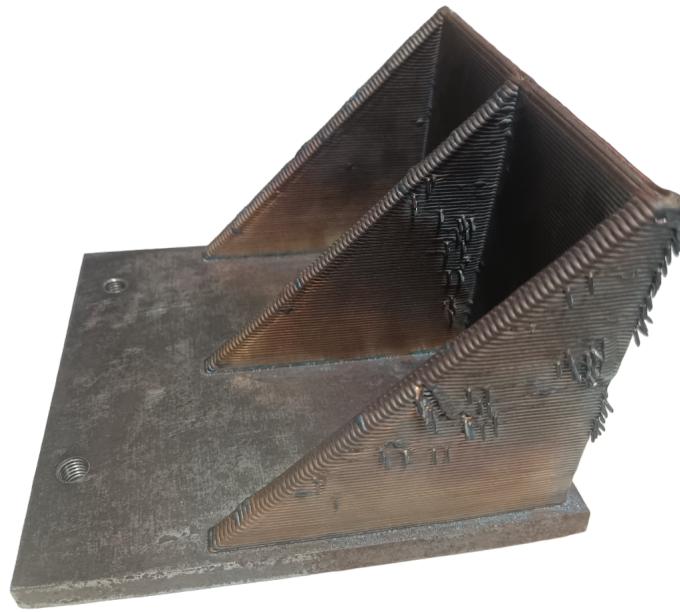


Figure 63 – Gravia Part Case Study 2.

Table 12 – Deposition Parameters of Gravia Part Case Study 2.

Part	Laser Power [W]	Wire Speed [mm/s]	Print Speed [mm/s]	Gas Flow [ml/min]	Layer Height [mm]	Layer Width [mm]	3D Slicing Software	Deposition Strategy
Gravia	874	15.28	10	10000	1.2	1	Meltio Space	Linear infill

The analysis revealed the presence of defects, specifically stubbing and balling, which were identified through visual inspection and classified according to the criteria outlined in Figure 60. These irregularities, commonly associated with variations in the laser-material interaction, were primarily attributed to improper laser calibration, as observed in the first case study. The results emphasize the critical impact of process parameters on final part quality, underscoring the necessity of precise laser calibration to mitigate defects and enhance the reliability of the printed part.

6.2.3 Case Study 3: Wall Parts

In Case Study 3, two wall specimens with identical geometry ($100 \times 180 \times 3$ mm) were printed using 316 LSi stainless steel wire of 1 mm diameter, as illustrated in Figure 64. The deposition parameters and strategies applied in each case are summarized in Table 13. Both walls were manufactured with a linear infill supported by a 2 mm raft, while differing in their deposition speeds.

The first wall (Figure 64a) was produced with a robot speed that induced mass imbalance, preventing uniform molten material deposition. This instability caused lack of fusion and eventually led to an interruption of the process. According to the classification criteria in Figure 60, these defects were primarily attributed to inadequate parameter selection, which compromised deposition stability and material flow, negatively impacting both dimensional accuracy and structural integrity.

In contrast, the second wall (Figure 64b) was printed with optimized deposition speeds combined with laser recalibration. These adjustments improved deposition uniformity, enhanced layer adhesion, and minimized surface irregularities, thereby demonstrating the importance of precise process control and deposition strategy in achieving consistent manufacturing results.

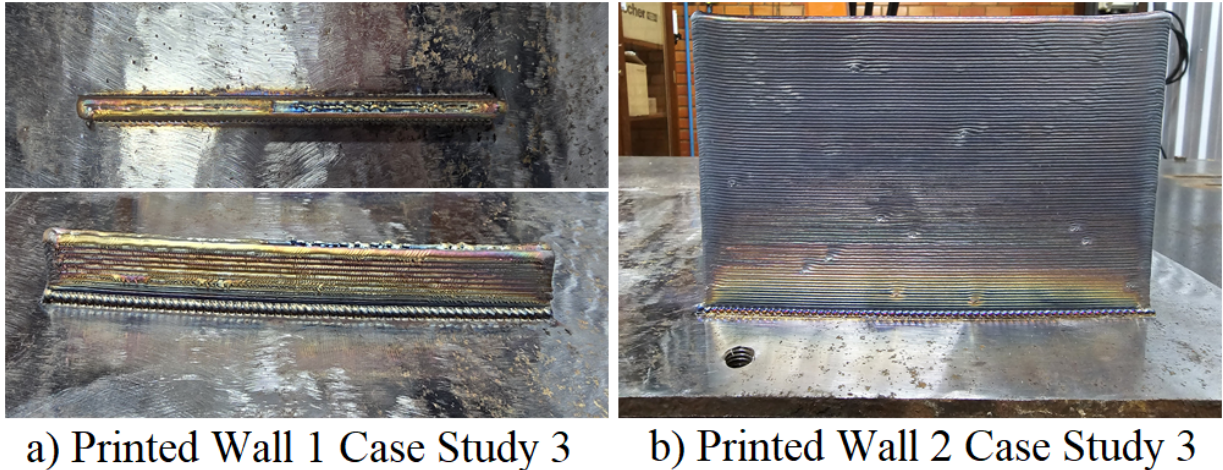


Figure 64 – Wall Parts Case Study 3.

Table 13 – Deposition Parameters of Wall Parts Case Study 3.

Part	Laser Power [W]	Wire Speed [mm/s]	Print Speed [mm/s]	Gas Flow [ml/min]	Layer Height [mm]	Layer Width [mm]	3D Slicing Software	Deposition Strategy
Wall 1	845	15.28	7.5	10000	1.2	1	Meltio Space	Linear infill + 2 mm Raft
Wall 2	845	15.28	10	10000	1.2	1	Meltio Space	Linear infill + 2 mm Raft

6.3 Metallographic and Mechanical Characterization

The six specimens analyzed in this study correspond to the printed parts presented in Case Study 1. The deposition parameters are detailed in Table 9 and were systematically varied to evaluate their influence on the microstructure and microhardness of the material. The printed parts consisted of 316 LSi stainless steel parts with varying geometries, as specified in Table 10, and are illustrated in Figure 65. These variations allowed for a comprehensive assessment of how different deposition conditions affect material properties.

6.3.1 Metallographic Preparation of Test Specimens

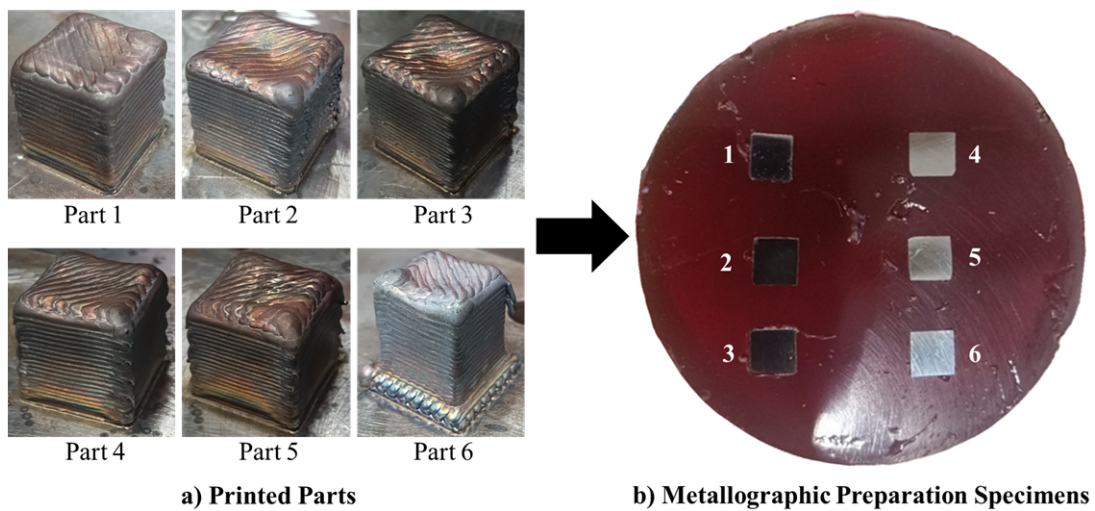


Figure 65 – Printed Parts and Metallographic Specimen Preparation.

To obtain standardized test specimens for metallographic and microhardness analysis, each printed part was sectioned into smaller specimens (5 x 5 x 5 mm) according to its original dimensions. The cutting process was carried out under controlled conditions to prevent thermal alterations in the microstructure, ensuring that the temperature did not exceed 50°C, in compliance with ASTM E3-11 (ASTM, 2017).

Following sectioning, the specimens underwent cold metallographic mounting using polyester resin brand *Crystal* with a polymerization ratio of 100 ml of resin per 1 ml of catalyst. This procedure facilitated handling during preparation and ensured structural integrity. Each mounted specimen was labeled accordingly to maintain traceability, as illustrated in Figure 65b. The sequential grinding process was then performed using water-cooled silicon carbide abrasive papers (220, 320, 400, 600, 800, and 1200 grit) in a rotary system operating at low speed with continuous water flow. Subsequently, the final polishing was performed using alumina abrasive paste, ensuring a reflective surface suitable for both microstructural and microhardness characterization.

6.3.2 Microstructural Analysis

The microstructural analysis was conducted after the specimens were chemically etched using aqua regia, a solution made of nitric acid (HNO_3) and hydrochloric acid (HCl) in a 1:3 volumetric ratio, in accordance with ASTM E407 (ASTM, 2015). The specimens were immersed in the solution for 30 seconds to reveal grain boundaries and phase distributions. Following etching, the specimens were rinsed with distilled water and ethanol before being dried with compressed air. The microstructural analysis was performed using an Olympus BX51 optical microscope, with objective lenses ranging from 5x to 100x magnification, enabling detailed observation of grain morphology, phase distribution, and possible defects.

The micrographs obtained from this analysis, as shown in Figure 66, reveal the characteristic dendritic morphology of 316LSI stainless steel processed through RAMC based on LMD-Wire, exhibiting variations depending on the thermal conditions and solidification dynamics during the AM process. The detailed analysis of these microstructures is summarized in Table 14, which presents the microstructural characteristics of the specimens extracted from the printed parts in Case Study 1.

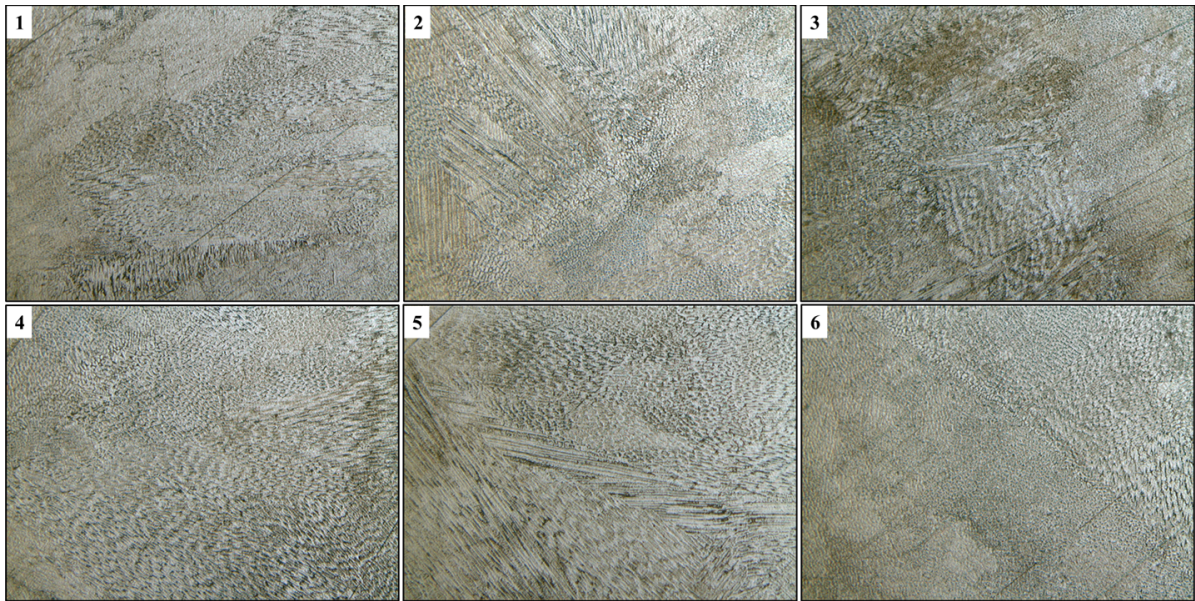


Figure 66 – Microstructural Analysis of Printed Specimens.

The observed microstructural differences demonstrate the influence of process parameters on grain refinement and phase distribution, which are key factors in the mechanical properties of the fabricated components. Variations in dendritic growth patterns suggest that deposition stability and thermal management significantly affect solidification dynamics. In addition, localized morphological changes, such as transitions from cellular to columnar growth, highlight the impact of thermal gradients and cooling rates, emphasizing the need for precise parameter selection to ensure optimal material properties.

Table 14 – Microstructural analysis of the printed specimens

Specimen	Description
1	Microstructure with dendritic structures oriented in a preferential direction. Areas of differentiated growth are observed, along with a possible discontinuity associated with microcracks or variations in solidification.
2	Well-defined dendritic pattern with multiple intersections, indicating thermal gradients during deposition. The homogeneous distribution suggests stable solidification without evident defects.
3	Variations in dendrite size and orientation, suggesting differences in cooling rates. Some areas exhibit a rough texture, possibly due to chemical segregation or fusion variations.
4	Homogeneous microstructure with well-oriented dendritic growth and no significant discontinuities, indicating a stable and controlled deposition process.
5	Combination of directional dendritic growth and regions with more equiaxed structures, reflecting thermal variations during the process. No evident cracks are identified, but differences in material homogeneity are observed.
6	Microstructure with fine and organized dendrites, showing a clear transition between regions of different morphology. The arrangement suggests moderate thermal fluctuations, influencing the residual stress distribution.

6.3.3 Microhardness Analysis

Microhardness measurements were performed to assess the mechanical properties of the printed specimens. As illustrated in Figure 67, five measurement regions (A, B, C, D, and E) were defined on each specimen's surface. The tests were carried out using the DuraScan equipment from EMCO TEST, with objective lenses of 10x and 40x. The Vickers microhardness evaluation was conducted in compliance with the NBR ISO 6507-1 standard (ISO, 2023), utilizing a pyramidal diamond indenter with a square base and a face angle of 136° , applying a load of 0.5 kgf.

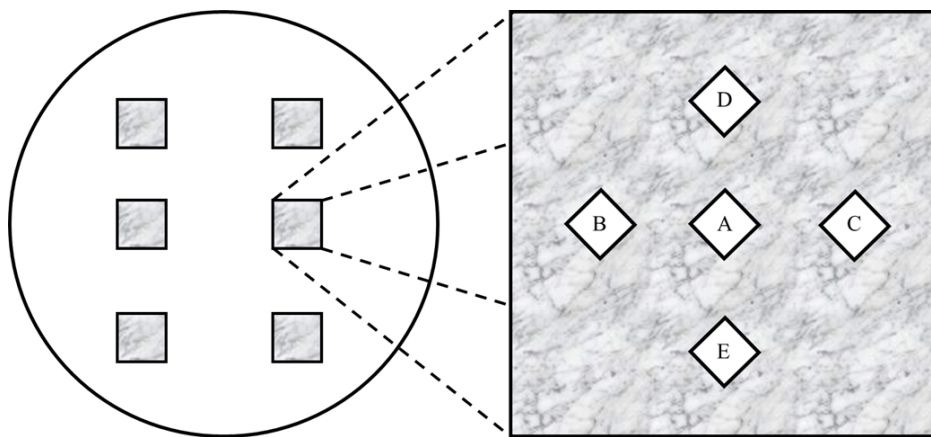


Figure 67 – Microhardness Measurement Regions.

The microhardness results, presented in Table 15, indicate variations in hardness values among the specimens, with Specimen 4 exhibiting the highest mean value (207.6 HV) and Specimen 1 the lowest (184.6 HV). Specimen 3 showed a range of microhardness values from 185 HV to 222 HV, indicating potential inhomogeneity, while Specimen 6 had the lowest individual value (173 HV), which could suggest weaker regions related to suboptimal heat dissipation or variations in the solidification rate.

Table 15 – Microhardness measurements of the printed specimens.

Specimen	A (HV)	B (HV)	C (HV)	D (HV)	E (HV)	Mean (HV)
1	164	177	197	194	191	184.6
2	188	197	203	212	203	200.6
3	191	185	196	191	222	197.0
4	219	199	212	199	209	207.6
5	206	185	212	216	199	203.6
6	206	194	180	173	183	187.2

The microhardness variations are associated with microstructural differences, where finer dendritic structures correspond to higher hardness values, whereas coarser structures or segregated regions result in lower values. This relationship underscores the influence of thermal gradients and cooling rates during the LMD-Wire process on the resulting mechanical properties of the material.

7 Conclusions and Future Works

This dissertation presented the development of a RAMC based on LMD-Wire, integrating advanced technologies such as DTs and CAD/CAPP/CAM systems. The research aimed to improve the efficiency, precision and automation of AM processes while addressing key challenges related to real-time monitoring, process simulation, and defect detection.

The IDEF0-based methodology was successfully applied, providing a structured framework for the development, integration, and operation of the RAMC. This methodology enabled the seamless integration of the components of the system, including mechanical, electrical and control elements, ensuring a smooth interaction between hardware and software. Furthermore, the use of CAD/CAPP/CAM tools optimized process planning and execution, contributing to a more efficient and automated manufacturing workflow.

Three DT models played a critical role in improving process supervision and system performance. The first DT enabled predictive maintenance of the KUKA iiQoT robot using industrial IoT technologies, which improved reliability and operational efficiency. The second DT, implemented as the Meltio Dashboard, provided real-time visualization of process parameters, ensuring better control and quality assurance in the AM process. The third DT established a real-time 3D simulation environment, enabling cloud-based data storage and visualization, which facilitated advanced process analysis and optimization. These DTs significantly improved traceability, decision-making, and defect prevention, aligning the RAMC with Industry 4.0 principles.

Experimental validation through three case studies confirmed the effectiveness of RAMC in AM applications. The first case study demonstrated the feasibility of the system by producing test parts and evaluating their dimensional accuracy and surface quality. The second analysis involved metallographic and microhardness analyzes, which validated the mechanical properties and microstructural characteristics of the deposited material. The results confirmed the stability and repeatability of the process, highlighting the reliability of the proposed system.

This research confirms that the integration of LMD-Wire technology, robotic automation, and DT models enables a more intelligent, flexible, and efficient approach to AM. These findings contribute to the advancement of robotic AM and digital production systems, laying the groundwork for further improvements in real-time process control, predictive analytics, and automated decision making. Moreover, a cost breakdown of the system's implementation is presented in the Appendix D, demonstrating the feasibility of deploying the proposed solution in industrial contexts.

In addition to the technical developments and experimental validations presented throughout this dissertation, the research activities conducted during the master's program resulted in several peer-reviewed scientific publications. These contributions supported the dissemination and validation of the proposed methodologies and findings within the academic and industrial communities. Publications include journal articles, book chapters, and conference papers documenting various aspects of research. A complete list of these publications is presented in Appendix C.

7.1 Analysis of Achieved Objectives

The objectives outlined at the start of this research were successfully achieved. The study confirmed the feasibility of integrating LMD-Wire technology with a robotic system, resulting in a fully functional RAMC, which was experimentally validated. The deployment of DT models enabled real-time process supervision, enhancing predictive maintenance, data traceability, and defect detection. Furthermore, the integration of ISO 23247-compliant DT architectures facilitated improved interoperability across various manufacturing levels, contributing to the advancement of the Industry 4.0 framework.

7.2 Remaining Challenges and Future Research Directions

Despite the significant progress made in this dissertation, several challenges remain that warrant further exploration. The following research directions are identified as critical for the continued advancement of RAMCs using LMD-Wire technology:

- Refine deposition modeling by enhancing predictive models to achieve higher precision in controlling complex geometries and accommodating material variability. Research should further integrate advanced machine learning algorithms to improve model adaptability and reduce uncertainties in predicting deposition behavior under diverse process conditions.
- Advance defect detection and mitigation through AI-driven feedback loops that enable real-time analysis for dynamic process adjustments. These systems should autonomously identify and mitigate defects such as porosity, warping, and thermal gradients by adjusting key parameters like laser power, scanning speed, and feed rate. The use of multi-sensor fusion and deep learning can significantly improve detection and prevention capabilities.
- Address scalability and robustness for industrial applications by overcoming challenges related to automation, integration, and robotic platform reliability in high-throughput

environments. Research should ensure the scalability of LMD-Wire systems for large-scale production and improve resilience to operational variations and environmental factors, including material inconsistencies.

- Increase system autonomy to minimize human intervention and enable real-time decision-making within LMD-Wire RAMCs. Further development of AI algorithms for autonomous process control is required to correct deviations independently. Additionally, frameworks for AI explainability and safety will be vital to ensure reliable and transparent integration in industrial environments.
- Integrate emerging technologies such as edge computing, federated learning, and blockchain to enhance digitalization in AM. Edge computing allows local data processing, reducing latency and dependence on central systems. Federated learning supports decentralized model training, improving privacy while sharing insights. Blockchain ensures secure, transparent, and immutable data exchange—critical for traceability, quality control, and compliance.

7.3 Future Work Recommendations

To further enhance the RAMC framework and expand its applicability, several key research directions have been identified. These areas focus on improving system intelligence, scalability, process efficiency, and integration with emerging Industry 4.0 technologies, ensuring continuous advancements in robotic AM.

- **Advanced AI Integration:** The implementation of machine learning models for predictive maintenance, anomaly detection, and adaptive control of deposition parameters. These advancements will enhance process stability, minimize variability, and improve overall manufacturing reliability.
- **Enhanced Digital Twin Capabilities:** Strengthening the integration of DTs with the IIoT to enable real-time analytics and autonomous decision-making. This includes the incorporation of hybrid simulation methodologies to improve predictive accuracy and system adaptability.
- **Multi-Material and Hybrid Manufacturing:** Investigating the feasibility of multi-material deposition and hybrid manufacturing techniques within the RAMC framework. This approach will facilitate the fabrication of functionally graded materials and composite structures, broadening the scope of applications in high-performance industries.
- **Scalability and Industrial Implementation:** Expanding the RAMC framework for large-scale industrial deployment to ensure robustness and reliability in commercial appli-

cations, particularly within aerospace and defense sectors. This requires optimizing process parameters for scalability and assessing long-term operational performance.

- **Real-Time Defect Mitigation:** Developing and validating closed-loop feedback control systems capable of dynamically adjusting deposition parameters to mitigate defects in real time. AI-driven optical and thermal monitoring technologies will be leveraged to enhance defect detection and correction efficiency.
- **Sustainability and Energy Efficiency:** Investigating energy-efficient algorithms and material optimization strategies to improve the sustainability of AM processes. These efforts align with green manufacturing initiatives by reducing material waste and minimizing energy consumption.
- **Development of a DeepSeek-Based Specialized Chatbot:** Implementing an open-source DeepSeek model to develop a specialized chatbot for the RAMC using LMD-wire. This chatbot will support the entire lifecycle of printed components, from design modeling to final inspection, enhancing digital thread integration and optimizing decision-making processes in manufacturing workflows.

7.4 Final Remarks

This research constitutes a significant advancement in the digitalization and automation of robotic AM using LMD-Wire technology. Through the integration of DTs, real-time monitoring, and advanced AI-driven control mechanisms, this work contributes to the evolution of Industry 4.0 principles and establishes a robust foundation for future innovations in robotic MAM.

The findings presented herein pave the way for further advancements in smart manufacturing, self-optimizing production systems, and cyber-physical integration. As automation and artificial intelligence continue to progress, the methodologies developed in this study can serve as a cornerstone for the development of more intelligent, adaptive, and efficient manufacturing environments. These advancements will ensure a high degree of precision, quality, and sustainability in the future of robotic AM.

References

- ABIOYE, T.; FOLKES, J.; CLARE, A. A parametric study of Inconel 625 wire laser deposition. **Journal of Materials Processing Technology**, Elsevier, v. 213, n. 12, p. 2145–2151, 2013. Cit. on p. 32.
- AHN, D.-G. Directed energy deposition (DED) process: state of the art. **International Journal of Precision Engineering and Manufacturing-Green Technology**, v. 8, n. 2, p. 703–742, 2021. Cit. on p. 27.
- AKBARI, M.; DING, Y.; KOVACEVIC, R. Process Development for a Robotized Laser Wire Additive Manufacturing. In: Volume 2: Additive Manufacturing; Materials. (International Manufacturing Science and Engineering Conference), v002t01a015. DOI: [10.1115/MSEC2017-2951](https://doi.org/10.1115/MSEC2017-2951). Available from: <<https://doi.org/10.1115/MSEC2017-2951>>. Cit. on p. 32.
- ALVARES, A.; LACROIX, I.; MARON, M.; FIGUEROA, B. Robotic additive manufacturing by laser metal deposition in the context of Industry 4.0: Manufatura aditiva robotizada por deposição de metal a laser no contexto da Indústria 4.0. **Concilium**, v. 23, n. 23, p. 79–103, 2023a. DOI: [10.53660/clm-2571-23u13](https://doi.org/10.53660/clm-2571-23u13). Cit. on pp. 19, 21.
- ALVARES, A. J.; FIGUEROA, B. S.; CABRAL, J. V. A.; LACROIX, I. Automated defect classification in additive manufacturing LMD-wire using deep learning. **Journal of the Brazilian Society of Mechanical Sciences and Engineering**, v. 47, p. 432, 2025. DOI: [10.1007/s40430-025-05740-5](https://doi.org/10.1007/s40430-025-05740-5). Cit. on p. 112.
- ALVARES, A. **Digital Twins - Kuka, Meltio, Node-Red**. 2025a. Available from: <<https://youtu.be/cloxBx9oEj4?si=xtSdqYmoak0dqGov>>. Cit. on p. 97.
- ALVARES, A. **Gerar Código KUKA KRL - Simplify3D - Convert Gcode-KRL**. 2025b. Available from: <<https://youtu.be/DpqIVARBODA?si=HyCgnJB7hZ7is0iJ>>. Cit. on p. 92.
- ALVARES, A. **Kuka.sim Simuladoe Célula**. 2025c. Available from: <https://youtu.be/_PQv2EOCZAc?si=G0Le0Tpoh6RDsQJ7>. Cit. on p. 89.
- ALVARES, A. **Peça Gravia - 5:30 Printing - 874 W - 2024 09 02 10 07 53**. 2024. Available from: <<https://youtu.be/GYeWsoT8GcY>>. Cit. on pp. 103, 104.
- ALVARES, A.; LACROIX, I.; MARON, M.; FIGUEROA, B. Robotic additive manufacturing by laser metal deposition in the context of industry 4.0: Manufatura aditiva robotizada por deposição de metal a laser no contexto da indústria 4.0. **Concilium**, v. 23, n. 23, p. 79–103, 2023b. Cit. on p. 81.

- ALVARES, A. J.; LACROIX, I.; LIMA MARON, M. A. de; FIGUEROA, B. S. Desenvolvimento de uma célula de manufatura aditiva robotizada baseada no processo deposição de metal à laser usando arame de soldagem. **Peer Review**, v. 5, n. 21, p. 17–39, 2023. Cit. on p. 43.
- ALVARES, A. J.; LACROIX, I.; MARON, M.; FIGUEROA, B. S.; ARAÚJO, L. Development of a Digital Twin for a Robotic Additive Manufacturing System Based on Laser Metal Deposition (LMD) Process. In: PROCEEDINGS of the 27th International Congress of Mechanical Engineering. 2023. Cit. on pp. 21, 42.
- ALVARES, A. J.; RODRIGUEZ, E.; FIGUEROA, B. Digital-Twin-Enabled Process Monitoring for a Robotic Additive Manufacturing Cell Using Wire-Based Laser Metal Deposition. **Processes**, v. 13, n. 8, 2025. ISSN 2227-9717. DOI: [10.3390/pr13082335](https://doi.org/10.3390/pr13082335). Cit. on pp. 21, 100, 104–106, 109.
- ALVARES, A. J.; ZHU, C.; SIMOES DA SILVA, L.; TANKOVA, T.; LACROIX, I.; FIGUEROA, B. S. Development of a Robotic Additive Manufacturing Cell Based on Laser Metal Deposition Process at the University of Coimbra and University of Brasilia. In: PROCEEDINGS of the 27th International Congress of Mechanical Engineering. 2023. Cit. on p. 81.
- AMPOWER. **File: -example/figuras/AM.png**. 2024. Available from: <https://ampower.eu/wp-content/uploads/2019/10/metal-additive-manufacturing-landscape-1.png>. Cit. on pp. 24, 25.
- ARREGUI, L.; GARMENDIA, I.; PUJANA, J.; SORIANO, C. Study of the Geometrical Limitations Associated to the Metallic Part Manufacturing by the LMD Process. **Procedia CIRP**, v. 68, n. 1, p. 363–368, 2018. Cit. on pp. 20, 29.
- ASTM. **ASTM E3-11(2017) - Standard Guide for Preparation of Metallographic Specimens**. 2017. ASTM Standard. Cit. on p. 119.
- ASTM. **ASTM E407-07(2015) - Standard Practice for Microetching Metals and Alloys**. 2015. ASTM Standard. Cit. on p. 120.
- AWS. **AWS D20.1/D20.1M:2019 - Specification for Fabrication of Metal Components using Additive Manufacturing**. Miami, USA: American Welding Society, 2019. Cit. on pp. 25, 96.
- AZARNIYA, A.; COLERA, X. G.; MIRZAALI, M. J.; SOVIZI, S.; BARTOLOMEU, F.; WITS, W. W.; YAP, C. Y.; AHN, J.; MIRANDA, G.; SILVA, F. S., et al. Additive manufacturing of Ti–6Al–4V parts through laser metal deposition (LMD): Process, microstructure, and mechanical properties. **Journal of Alloys and Compounds**, Elsevier, v. 804, p. 163–191, 2019. Cit. on p. 30.

- BERNAUER, C.; LEITNER, P.; ZAPATA, A.; GARKUSHA, P.; GRABMANN, S.; SCHMOELLER, M.; ZAEH, M. F. Segmentation-based closed-loop layer height control for enhancing stability and dimensional accuracy in wire-based laser metal deposition. **Robotics and Computer-Integrated Manufacturing**, Elsevier, v. 86, p. 102683, 2024. Cit. on pp. 45, 46.
- BERNAUER, C.; MEINZINGER, L.; ZAPATA, A.; ZHAO, X. F.; BAEHR, S.; ZAEH, M. F. Design and Investigation of a Novel Local Shielding Gas Concept for Laser Metal Deposition with Coaxial Wire Feeding. **Applied Sciences**, MDPI, v. 13, n. 8, p. 5121, 2023. Cit. on pp. 44, 46.
- BERNAUER, C.; SIGL, M. E.; GRABMANN, S.; MERK, T.; ZAPATA, A.; ZAEH, M. F. Effects of the thermal history on the microstructural and the mechanical properties of stainless steel 316L parts produced by wire-based laser metal deposition. **Materials Science and Engineering: A**, Elsevier, v. 889, p. 145862, 2024. Cit. on p. 30.
- BRACKETT, D.; ASHCROFT, I.; HAGUE, R. **Topology optimization for additive manufacturing**. University of Texas at Austin, 2011. Cit. on p. 24.
- BRANDL, E.; MICHAILOV, V.; VIEHWEGER, B.; LEYENS, C. Deposition of Ti-6Al-4V using laser and wire, part II: Hardness and dimensions of single beads. **Surface and Coatings Technology**, Elsevier, v. 206, n. 6, p. 1130–1141, 2011. Cit. on p. 32.
- CABRAL, J. V. A.; GASCA, E. A. R.; ALVARES, A. J. Digital twin implementation for machining center based on ISO 23247 standard. **IEEE Latin America Transactions**, p. 628–635, 2023. Cit. on pp. 20, 42.
- CAI, Y.; ZHANG, S.; WANG, Y.; CHEN, H.; XIONG, J. Monitoring process stability in robotic wire-laser directed energy deposition based on multi-modal deep learning. **Journal of Manufacturing Processes**, v. 128, p. 111–124, 2024. ISSN 1526-6125. DOI: <https://doi.org/10.1016/j.jmapro.2024.08.033>. Cit. on pp. 45, 46.
- CAIAZZO, F.; ALFIERI, V. Directed Energy Deposition of stainless steel wire with laser beam: Evaluation of geometry and affection depth. **Procedia CIRP**, Elsevier, v. 99, p. 348–351, 2021. Cit. on p. 32.
- CAVITAR. **Comparison of CAVILUX Laser Illumination in Different Imaging Setups - CMT Process**. 2023. Available from: <<https://youtu.be/ISbwJzM4Gb4>>. Cit. on p. 34.
- DASS, A.; MORIDI, A. Hybrid manufacturing of complex components: Full methodology including laser metal deposition (LMD) module development, cladding geometry estimation and case study validation. **Mechanical Systems and Signal Processing**, v. 179, n. 1, p. 109337, 2022. Cit. on pp. 20, 29.
- DASS, A.; MORIDI, A. State of the art in directed energy deposition: From additive manufacturing to materials design. **Coatings**, v. 9, n. 7, p. 418, 2017. Cit. on p. 25.

- DEBROY, T.; WEI, H.; ZUBACK, J.; MUKHERJEE, T.; ELMER, J.; MILEWSKI, J.; BEESE, A.; WILSON-HEID, A.; DE, A.; ZHANG, W. Additive manufacturing of metallic components – Process, structure and properties. **Progress in Materials Science**, v. 92, n. 1, p. 112–224, 2018. Cit. on p. 25.
- DEBROY, T.; WEI, H. L.; ZUBACK, J. S.; MUKHERJEE, T.; ELMER, J. W.; MILEWSKI, J. O.; BEESE, A. M.; WILSON-HEID, A. d.; DE, A.; ZHANG, W. Additive manufacturing of metallic components–process, structure and properties. **Progress in Materials Science**, v. 92, n. 1, p. 112–224, 2018. Cit. on p. 24.
- DEMIR, A. G. Micro laser metal wire deposition for additive manufacturing of thin-walled structures. **Optics and Lasers in Engineering**, v. 100, p. 9–17, 2018. Cit. on p. 31.
- DING, D.; PAN, Z.; CUIURI, D.; LI, H. Wire-feed additive manufacturing of metal components: technologies, developments and future interests. **The International Journal of Advanced Manufacturing Technology**, v. 81, n. 1, p. 465–481, 2015. Cit. on p. 27.
- DING, Y.; DWIVEDI, R.; KOVACEVIC, R. Process planning for 8-axis robotized laser-based direct metal deposition system: A case on building revolved part. **Robotics and Computer-Integrated Manufacturing**, v. 44, p. 67–76, 2017. ISSN 0736-5845. Cit. on pp. 43, 46.
- DUGAR, J.; IKRAM, A.; KLOBČAR, D.; PUŠAVEC, F. Sustainable Hybrid Manufacturing of AlSi5 Alloy Turbine Blade Prototype by Robotic Direct Energy Layered Deposition and Subsequent Milling: An Alternative to Selective Laser Melting? **Materials**, MDPI, v. 15, n. 23, p. 8631, 2022. Cit. on pp. 44, 46.
- FIGUEROA, B. S.; ÁLVARES, A. Development of a robotic additive manufacturing cell based on the LMD-Wire process. In: LECTURE Notes in Mechanical Engineering (LNME). Springer, 2025a. Cit. on pp. 20, 81.
- FIGUEROA, B. S.; ÁLVARES, A. Methodological approach to the development of a robotic additive manufacturing cell based on LMD-Wire. In: PROCEEDINGS of the XVI Ibero-American Congress of Mechanical Engineering (CIBIM). Springer, 2025b. Cit. on p. 49.
- FIGUEROA, B. S.; ÁLVARES, A. Metodología para el desarrollo de una célula de manufactura aditiva robótica basada en el sistema de deposición de metal por láser (LMD). In: ACTAS del XVI Congreso Iberoamericano de Ingeniería Mecánica (CIBIM). 2024. Cit. on p. 49.
- FIGUEROA, B. S.; RIAÑO, C. I.; PEÑA, C. A.; ÁLVARES, A. Artificial vision system for digital inspection of dimensional and geometric measurements in closed-loop manufacturing architecture. In: PROCEEDINGS of the 2024 IEEE Latin American Con-

- ference on Computational Intelligence (LA-CCI). 2024. P. 1. DOI: [10.1109/LA-CCI62337.2024.10814821](https://doi.org/10.1109/LA-CCI62337.2024.10814821). Cit. on p. 23.
- FIGUEROA, B. S.; ARAÚJO, L.; ALVARES, A. Development of a Digital Twin for a Laser Metal Deposition (LMD) Additive Manufacturing Cell. In: PROCEEDINGS of the Latin American Congress on Automation and Robotics. 2023. Cit. on pp. 20, 43.
- FIGUEROA, B. S. **Real-Time DT Additive Manufacturing Cell LMD - Structural Support**. 2024. Available from: <https://youtu.be/dv6h9anrcQU>. Cit. on p. 105.
- GENG, H.; LI, J.; XIONG, J.; LIN, X.; ZHANG, F. Geometric limitation and tensile properties of wire and arc additive manufacturing 5A06 aluminum alloy parts. **Journal of Materials Engineering and Performance**, v. 26, n. 1, p. 621–629, 2017. Cit. on p. 27.
- GHANADI, N.; PASEBANI, S. A Review on Wire-Laser Directed Energy Deposition: Parameter Control, Process Stability, and Future Research Paths. **Journal of Manufacturing and Materials Processing**, v. 8, n. 2, p. 1–48, 2024. Cit. on pp. 31, 32.
- GIBSON, B. T.; MHATRE, P.; BORISH, M. C.; ATKINS, C. E.; POTTER, J. T.; VAUGHAN, J. E.; LOVE, L. J. Controls and process planning strategies for 5-axis laser directed energy deposition of Ti-6Al-4V using an 8-axis industrial robot and rotary motion. **Additive Manufacturing**, Elsevier, v. 58, p. 103048, 2022. Cit. on pp. 19, 44, 46.
- GRADL, P. Principles of Directed Energy Deposition for Aerospace Applications. In: SEMINAR for WM Keck Center for 3D Innovation. 2022. Cit. on p. 28.
- GUAGLIONE, F.; BENNI, A. A.; PREVITALI, B. Exploring wire laser metal deposition of 316L stainless steel as a viable solution for combined manufacturing routes. **Progress in Additive Manufacturing**, Springer, p. 1–20, 2024. Cit. on pp. 21, 45, 46.
- HETTESHEIMER, T.; HIRZEL, S.; ROSS, H. B. Energy savings through additive manufacturing: An analysis of selective laser sintering for automotive and aircraft components. **Energy Efficiency**, v. 11, n. 1, p. 1227–1245, 2018. Cit. on p. 24.
- HU, Z.; HUA, L.; QIN, X.; NI, M.; LIU, Z.; LIANG, C. Region-based path planning method with all horizontal welding position for robotic curved layer wire and arc additive manufacturing. **Robotics and Computer-Integrated Manufacturing**, v. 74, p. 102286, 2022. ISSN 0736-5845. Cit. on pp. 44, 46.
- IMRAN, M. K.; MASOOD, S.; BRANDT, M.; BHATTACHARYA, S.; MAZUMDER, J. Direct metal deposition (DMD) of H13 tool steel on copper alloy substrate: Evaluation of mechanical properties. **Materials Science and Engineering: A**, v. 528, n. 9, p. 3342–3349, 2011. Cit. on p. 26.
- ISO. **ISO 10218-1:2025 - Robots and robotic devices – Safety requirements for industrial robots – Part 1: Robots**. Geneva, Switzerland: ISO, 2025a. Cit. on p. 81.

- ISO. **ISO 10218-2:2025 - Robots and robotic devices – Safety requirements for industrial robots – Part 2: Robot systems and integration**. Geneva, Switzerland: ISO, 2025b. Cit. on p. 81.
- ISO. **ISO 11554:2022 - Optics and Photonics – Lasers and Laser-Related Equipment – Test Methods for Laser Beam Power, Energy and Temporal Characteristics**. Geneva, Switzerland: ISO, 2022. Cit. on p. 87.
- ISO. **ISO 23247-1: Automation systems and integration—digital twin framework for manufacturing—Part 1: overview and general principles**. International Organization for Standardization Geneva, Switzerland, 2021. Cit. on pp. 20, 42.
- ISO. **ISO 23247-4:2021 Automation systems and integration — Digital twin framework for manufacturing — Part 5: Digital thread for digital twin, stage 60.60, disponível em: <https://www.iso.org/standard/87425.html>. Access: 23 sep. 2024. v. 1. Sept. 2024. Cit. on p. 101.**
- ISO. **ISO 6507-1:2023: Metallic materials — Vickers hardness test**. International Organization for Standardization Geneva, Switzerland, 2023. Cit. on p. 121.
- ISO. **ISO/TS 15066:2016 - Robots and robotic devices – Collaborative robots**. Geneva, Switzerland: ISO, 2016. Cit. on p. 81.
- ISO/ASTM. **ISO/ASTM 52901:2017 Additive manufacturing — General principles — Requirements for purchased AM parts**. International Organization for Standardization and ASTM International, Geneva, Switzerland, 2017a. Cit. on pp. 19, 24.
- ISO/ASTM. **ISO/ASTM 52901:2017 Additive manufacturing — General principles — Requirements for purchased AM parts**. International Organization for Standardization and ASTM International, Geneva, Switzerland, 2017b. Cit. on pp. 19, 24.
- KÖRNER, C. Additive manufacturing of metallic components by selective electron beam melting — a review. **International Materials Reviews**, v. 61, n. 5, p. 361–377, 2016. Cit. on p. 24.
- KUKA. **KUKA iiQoT – leveraging the Industrial IoT for a more transparent and efficient robot fleet**. 2025. Available from: <<https://www.kuka.com/en-us/products/robotics-systems/software/cloud-software/iiqot-robot-condition-monitoring>>. Cit. on p. 103.
- KUSHWAHA, A.; BASAK, A. Evaluating deposits of SS316L powder and wire consolidated using co-axial laser directed energy deposition. **The International Journal of Advanced Manufacturing Technology**, Springer, v. 132, n. 3, p. 1627–1647, 2024. Cit. on pp. 45, 46.

- LALEH, M.; SADEGHI, E.; REVILLA, R. I.; CHAO, Q.; HAGHDADI, N.; HUGHES, A. E.; XU, W.; DE GRAEVE, I.; QIAN, M.; GIBSON, I.; TAN, M. Y. Heat treatment for metal additive manufacturing. **Progress in Materials Science**, v. 133, n. 1, p. 101051, 2023. Cit. on p. 24.
- LIANG, Z.; JINGLONG, L.; YI, L.; JINGTAO, H.; CHENGYANG, Z.; JIE, X.; DONG, C. Characteristics of metal droplet transfer in wire-arc additive manufacturing of aluminum alloy. **The International Journal of Advanced Manufacturing Technology**, Springer, v. 99, p. 1521–1530, 2018. Cit. on pp. 43, 46.
- LIU, C.; LE ROUX, L.; KÖRNER, C.; TABASTE, O.; LACAN, F.; BIGOT, S. Digital twin-enabled collaborative data management for metal additive manufacturing systems. **Journal of Manufacturing Systems**, p. 857–874, 2022. Cit. on pp. 20, 42.
- MALUKHIN, K.; EHMANN, K. Material Characterization of NiTi Based Memory Alloys Fabricated by the Laser Direct Metal Deposition Process. **Journal of Manufacturing Science and Engineering**, v. 128, n. 3, p. 691–696, 2005. Cit. on p. 26.
- MEDRANO, A.; FOLKES, J.; SEGAL, J.; PASHBY, I. Fibre laser metal deposition with wire: parameters study and temperature monitoring system. In: XVII International Symposium on Gas Flow, Chemical Lasers, and High-Power Lasers. 2009. Cit. on p. 31.
- MELTIO. **3D Printing reference manual: Meltio Technology, Slicing Strategies, and Slicing Software Evaluation**. Linares, Spain, 2022a. Available from: <<https://meltio3d.com>>. Cit. on pp. 33, 34, 36, 38.
- MELTIO. **Meltio partners with 12 leading software co.** 2022b. Available from: <<https://meltio3d.com/meltio-partners-12-leading-am-software-companies>>. Cit. on p. 42.
- MELTIO. **Meltio Space - Slicing Strategies**. 2024. Available from: <<https://academy.meltio3d.com/courses/take/meltio-space-general-training/lessons/52769479-3-1-slicing-workflow>>. Cit. on pp. 38, 39.
- MELTIO. **What is Laser Metal Deposition**. 2023. Available from: <<https://meltio3d.com/what-is-laser-metal-deposition>>. Cit. on p. 29.
- MELTIO. **Meltio Dashboard**. 2024. Available from: <<https://meltiodashboard.com>>. Cit. on p. 104.
- MELTIO. **Meltio Engine+Robot User Manual**. 2023a. Available from: <<https://meltio3d.com>>. Cit. on pp. 34, 35.
- MELTIO. **Wire-Laser Metal Deposition - Meltio Technology**. 2023b. Available from: <<https://youtu.be/PvnfrVNCVrw>>. Cit. on p. 34.

- MONTOYA-ZAPATA, D.; MORENO, A.; ORTIZ, I.; POSADA, J.; RUIZ-SALGUERO, O. Computer supported toolpath planning for LMD additive manufacturing based on cylindrical slicing. **The International Journal of Advanced Manufacturing Technology**, Springer, v. 128, n. 9, p. 4667–4683, 2023. Cit. on pp. 20, 44, 46.
- MORITZ, J.; SEIDEL, A.; KOPPER, M.; BRETSCHNEIDER, J.; GUMPINGER, J.; FINASKE, T.; RIEDE, M.; SCHNEEWEISS, M.; LÓPEZ, E.; BRÜCKNER, F., et al. Hybrid manufacturing of titanium Ti-6Al-4V combining laser metal deposition and cryogenic milling. **The International Journal of Advanced Manufacturing Technology**, Springer, v. 107, p. 2995–3009, 2020. Cit. on pp. 19, 43, 46.
- MOTTA, M.; DEMIR, A. G.; PREVITALI, B. High-speed imaging and process characterization of coaxial laser metal wire deposition. **Additive Manufacturing**, Elsevier, v. 22, p. 497–507, 2018. Cit. on pp. 21, 43, 46.
- NGO, T. D.; KASHANI, A.; IMBALZANO, G.; NGUYEN, K. T.; HUI, D. Additive manufacturing (3D printing): A review of materials, methods, applications and challenges. **Composites Part B: Engineering**, v. 143, n. 1, p. 172–196, 2018. Cit. on pp. 19, 24.
- RAMLAB. **File: -example/figuras/DED.png**. 2024a. Available from: <https://www.ramlab.com/wp-content/uploads/2021/04/RAMLAB-Charts_Dark-part-size-and-complexity.png>. Cit. on pp. 25, 26.
- RAMLAB. **File: -example/figuras/lmd.png**. 2024b. Available from: <https://www.ramlab.com/wp-content/uploads/2021/04/RAMLAB-ded_Dark-Laser-Metal-Deposition.svg>. Cit. on p. 29.
- RAO, K. V. Online modeling and prediction of weld bead geometry in robotic gas metal arc based additive manufacturing using grey prediction model. **Expert Systems with Applications**, Elsevier, v. 236, p. 121284, 2024. Cit. on pp. 44, 46.
- RASIYA, G.; SHUKLA, A.; SARAN, K. Additive manufacturing-a review. **Materials Today: Proceedings**, Elsevier, v. 47, p. 6896–6901, 2021. Cit. on pp. 20, 23.
- RIZA, S. H.; MASOOD, S.; WEN, C.; RUAN, D.; XU, S. Dynamic behaviour of high strength steel parts developed through laser assisted direct metal deposition. **Materials Design**, v. 64, n. 1, p. 650–659, 2014. Cit. on p. 26.
- RODRIGUEZ, E.; ALVARES, A.; RIANO, C. STEP-NC in additive manufacturing: a comprehensive review, architecture, and data model proposal. **The International Journal of Advanced Manufacturing Technology**, Springer, p. 1–37, 2025. Cit. on p. 23.
- RODRIGUEZ, N.; VÁZQUEZ, L.; HUARTE, I.; ARRUTI, E.; TABERNERO, I.; ALVAREZ, P. Wire and arc additive manufacturing: a comparison between CMT and TopTIG processes applied to stainless steel. **Welding in the World**, v. 62, n. 1, p. 1083–1096, 2018. Cit. on p. 25.

- SAMES, W. J.; LIST, F.; PANNALA, S.; DEHOFF, R. R.; BABU, S. S. The metallurgy and processing science of metal additive manufacturing. **International materials reviews**, v. 61, n. 5, p. 315–360, 2018. Cit. on p. [24](#).
- SEDIGHI, A. M.; NABAVI, S. F.; FARSHIDIANFAR, A. A Review on Effect of Cooling Rate on Metallurgical, Mechanical, Geometrical Characteristics and Defects of Laser Cladding Process. **Lasers in Manufacturing and Materials Processing**, p. 1–66, 2024. Cit. on p. [31](#).
- SHAIKH, M. O.; CHEN, C.-C.; CHIANG, H.-C.; CHEN, J.-R.; CHOU, Y.-C.; KUO, T.-Y.; AMEYAMA, K.; CHUANG, C.-H. Additive manufacturing using fine wire-based laser metal deposition. **Rapid Prototyping Journal**, Emerald Publishing Limited, v. 26, n. 3, p. 473–483, 2020. Cit. on p. [32](#).
- SHAO, G.; HELU, M. Framework for a digital twin in manufacturing: Scope and requirements. **Manufacturing letters**, p. 105–107, 2020. Cit. on pp. [19](#), [42](#).
- SHI, J.; ZHU, P.; FU, G.; SHI, S. Geometry characteristics modeling and process optimization in coaxial laser inside wire cladding. **Optics & Laser Technology**, v. 101, p. 341–348, 2018. Cit. on p. [31](#).
- SRIVASTAVA, M.; RATHEE, S.; PATEL, V.; KUMAR, A.; KOPPAD, P. G. A review of various materials for additive manufacturing: Recent trends and processing issues. **Journal of Materials Research and Technology**, Elsevier, v. 21, p. 2612–2641, 2022. Cit. on p. [23](#).
- WONG, K. V.; HERNANDEZ, A. A review of additive manufacturing. **International scholarly research notices**, v. 2012, n. 1, p. 208760, 2012. Cit. on p. [24](#).
- ZAPATA, A.; BERNAUER, C.; STADTER, C.; KOLB, C. G.; ZAEH, M. F. Investigation on the cause-effect relationships between the process parameters and the resulting geometric properties for wire-based coaxial laser metal deposition. **Metals**, MDPI, v. 12, n. 3, p. 455, 2022. Cit. on pp. [30](#), [32](#).

Appendix

APPENDIX A – Diagrams Associated with the Physical and Logical Integration of the RAMC

A.1 Safety System Connection Diagrams

Figures 68 and 70 illustrate the safety system's connections and electrical circuit. The system incorporates an emergency stop button, a reset button, an SRB 301MC safety relay, and four G7SA-4A2B relays, which manage signals to the DB9 cable and XG11.1 port of the KUKA robot. Figure 69 provides a detailed view of the XG11.1 safety interface, including its pin configuration and specifications. Additionally, these relays interact with the control buttons and the AZM150 SK-02 electronic lock, ensuring synchronized safety operations and compliance with industrial safety standards. The schematic in Figure 70 offers a comprehensive representation of the wiring and signal pathways, supporting seamless system integration, troubleshooting, and preventive maintenance.

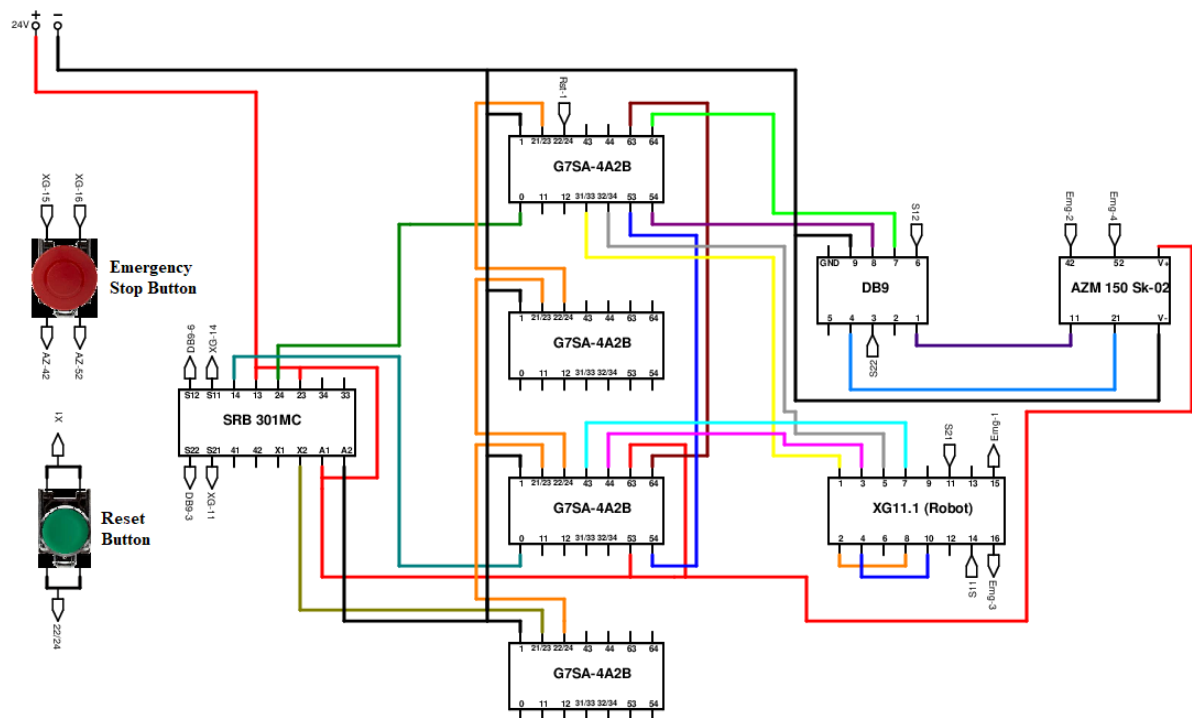


Figure 68 – Flowchart of Connections for Safety System.

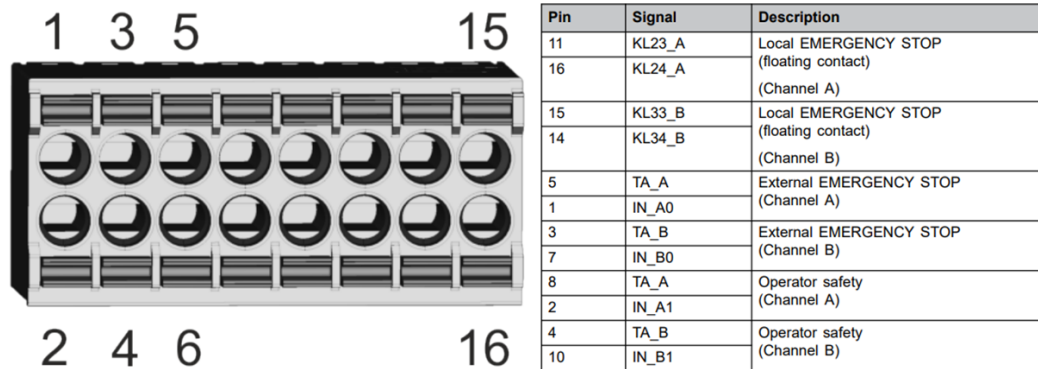


Figure 69 – XG11.1 Port Pinout and Description.

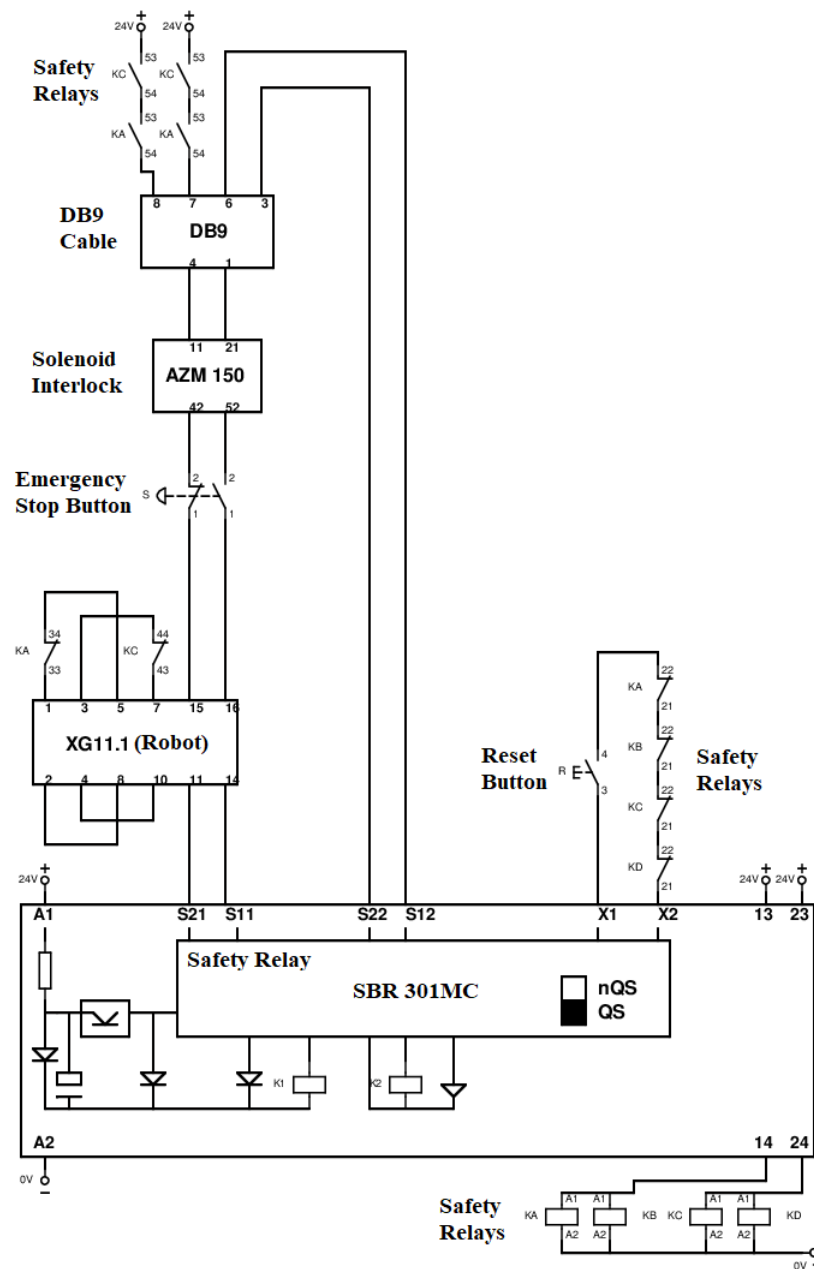


Figure 70 – Electrical Connection Diagram for Safety System.

A.2 DB15 Cable Connection Diagrams for Controllers

The integration of the KUKA robotic system with the Meltio controller was implemented using DB15 connectors to ensure accurate and reliable signal transmission. Figure 71 presents the detailed connection diagrams between the DB15 cables and the controllers. Figure 71 (A) illustrates the wiring configuration for robot outputs interfacing with Meltio inputs, where the male DB15 connector establishes connections with the Meltio controller via the XG12 port of the KUKA controller and an external 24V power supply. The robot output signals are identified with orange wiring. Figure 71 (B) depicts the wiring configuration for KUKA robot inputs connected to Meltio outputs, utilizing the female DB15 connector through the same XG12 port. The Meltio output signals are represented with blue wiring, maintaining integration with the external 24V power source. Figure 72 provides a detailed overview of the XG12 port, including its pin configuration and signal specifications, ensuring precise connectivity between the robotic system and the Meltio controller.

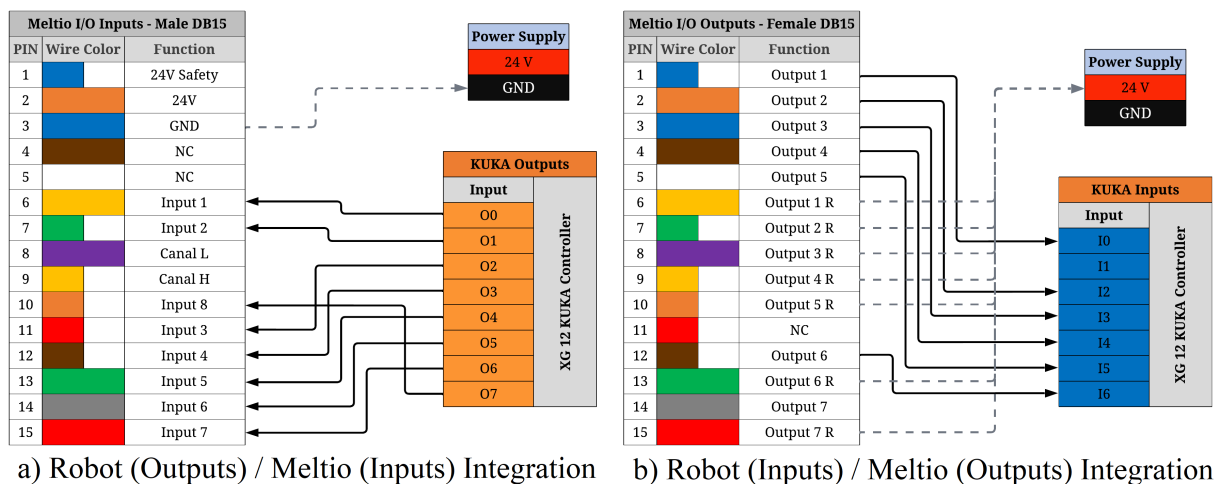


Figure 71 – Diagram of Connections for Robot/Meltio Integration.

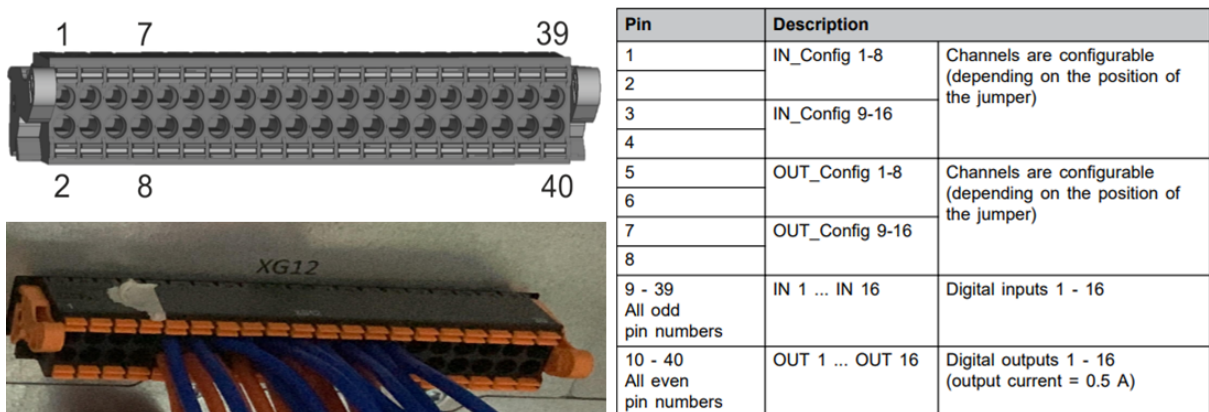


Figure 72 – XG12 Port Pinout and Description.

A.3 Safety Logic Integration for Deposition Modes

Figure 73 illustrates the safety logic implemented in the KUKA KR C5 controller using its internal PLC. The routine shown on the SmartPAD interface disables key digital outputs associated with the activation of the laser and wire feeder whenever the robot is set to T1 mode. Specifically, it blocks the activation of \$OUT[1], \$OUT[2], and \$OUT[4]—signals mapped to deposition hardware—by monitoring the robot's operational mode. This logic prevents unintended material deposition during programming or manual jogging, improving operator safety and avoiding process inconsistencies. Once the robot transitions to T2 or AUTOMATIC mode, the logic permits normal operation of the outputs, assuming all interlocks and system conditions are satisfied.

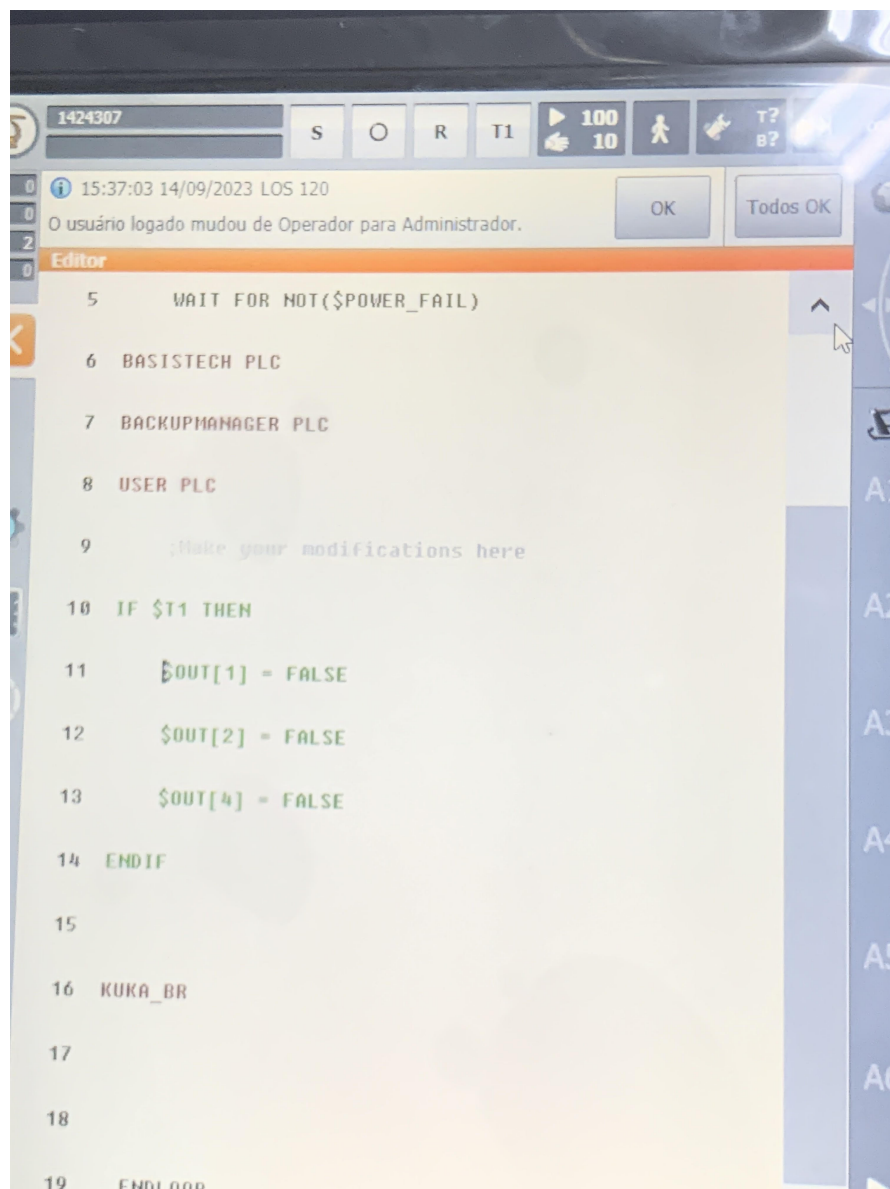
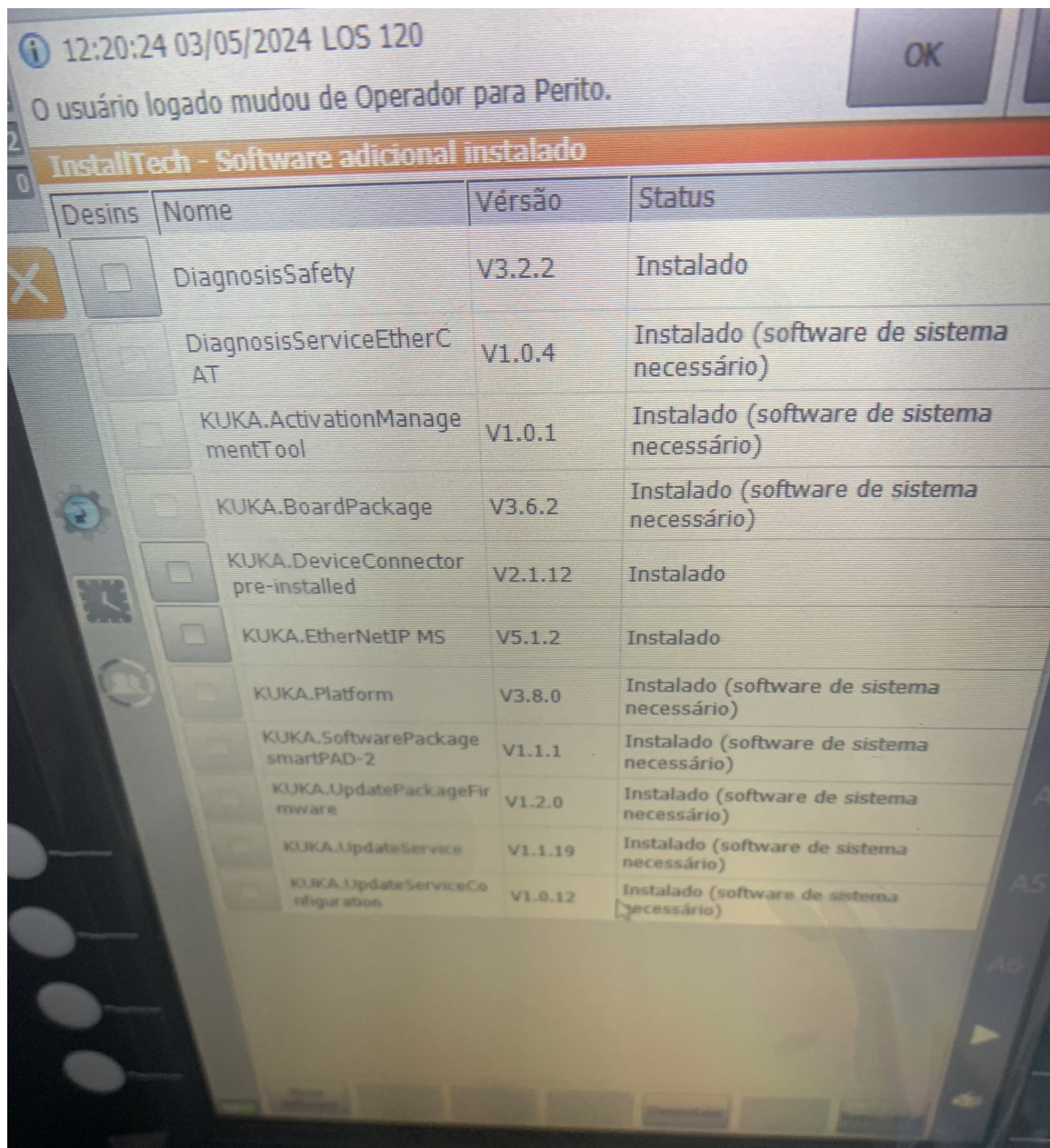


Figure 73 – PLC routine on KUKA SmartPAD to disable deposition outputs in T1 mode.

A.4 Installed Packages on the KUKA Controller

Figure 74 shows the software packages installed on the KUKA robot system, as displayed on the smartPAD interface. Key components include DiagnosisSafety, KUKA.DeviceConnector, and KUKA.EtherNetIP MS, among others, many of which are marked as essential system software. These packages enable communication, diagnostics, and safe operation, supporting features required for MQTT-based digital integration. The figure also highlights the presence of EthernetKRL, OPC UA, and MQTT client packages.



Desins	Nome	Versão	Status
<input type="checkbox"/>	DiagnosisSafety	V3.2.2	Instalado
<input type="checkbox"/>	DiagnosisServiceEtherCAT	V1.0.4	Instalado (software de sistema necessário)
<input type="checkbox"/>	KUKA.ActivationManagementTool	V1.0.1	Instalado (software de sistema necessário)
<input type="checkbox"/>	KUKA.BoardPackage	V3.6.2	Instalado (software de sistema necessário)
<input type="checkbox"/>	KUKA.DeviceConnector pre-installed	V2.1.12	Instalado
<input type="checkbox"/>	KUKA.EtherNetIP MS	V5.1.2	Instalado
<input type="checkbox"/>	KUKA.Platform	V3.8.0	Instalado (software de sistema necessário)
<input type="checkbox"/>	KUKA.SoftwarePackage smartPAD-2	V1.1.1	Instalado (software de sistema necessário)
<input type="checkbox"/>	KUKA.UpdatePackageFirmware	V1.2.0	Instalado (software de sistema necessário)
<input type="checkbox"/>	KUKA.UpdateService	V1.1.19	Instalado (software de sistema necessário)
<input type="checkbox"/>	KUKA.UpdateServiceConfiguration	V1.0.12	Instalado (software de sistema necessário)

Figure 74 – Installed packages on the KUKA KR C5 controller.

A.5 MQTT Configuration on the KUKA Controller

Figure 75 displays the configuration of the MQTT communication parameter on the KUKA robot controller interface. The variable KUKACONNECT_BROKER is modified by entering the broker IP address 164.41.45.153, establishing the connection between the controller and the MQTT message broker used for data transmission. The interface also includes options to update and set parameter values.

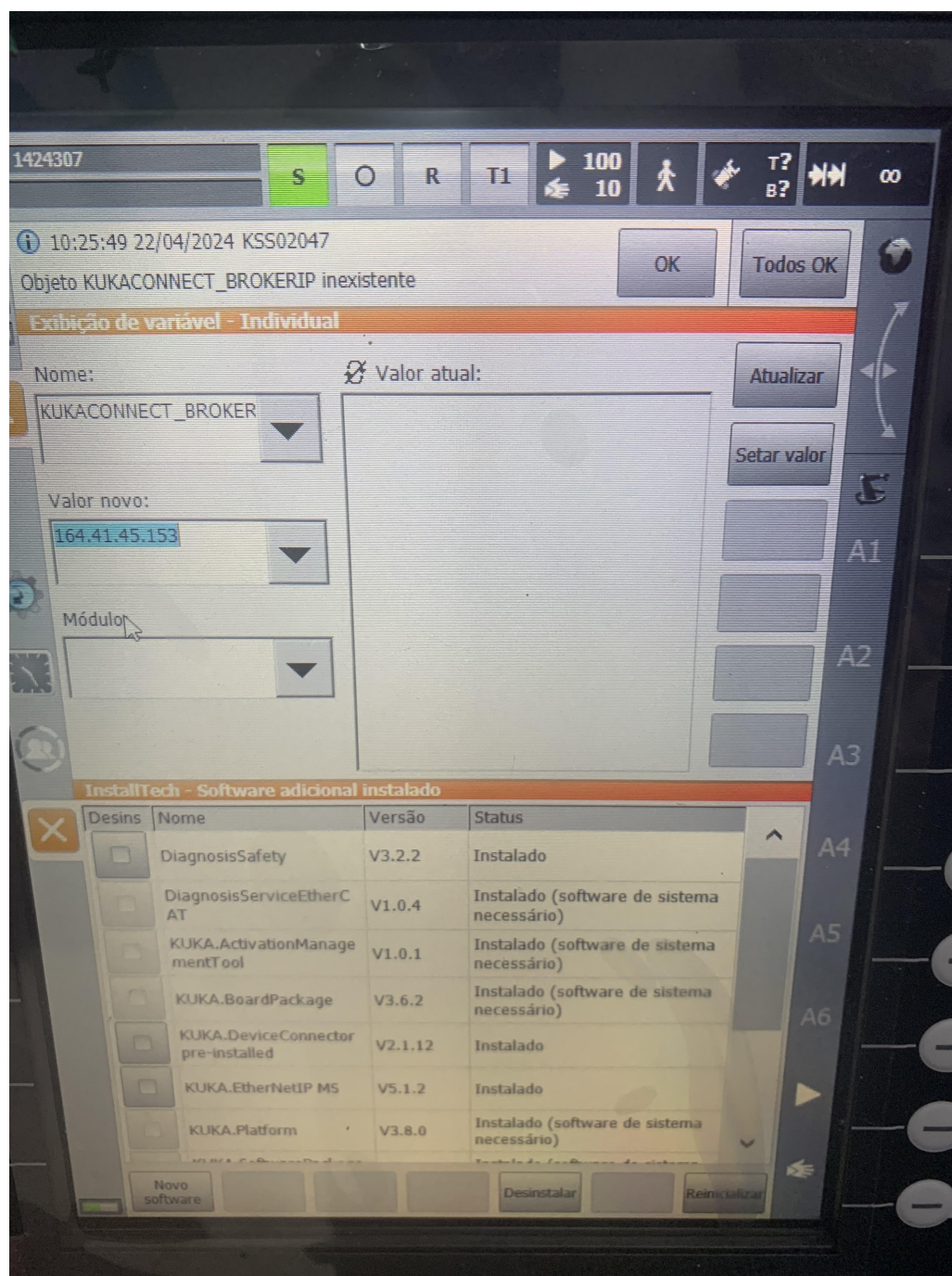


Figure 75 – Declaration of internal variables in the KUKA smartPAD interface for MQTT communication.

APPENDIX B – Codes for the Digital Twin System

B.1 MQTT Publisher

The file `mqttPublisher.pscj` functions as an MQTT socket, installed directly on the robot controller. It acts as a publisher, continuously extracting real-time operational data from the robot and transmitting it over the MQTT protocol. To ensure proper functionality, this file must be installed in the following directory on the robot controller:

```
C:\KRC\ROBOTER\Config\User\Common\OpcUa
```

This file is responsible for ensuring the reliable and consistent flow of data from the robotic system to other components that rely on this data for monitoring and simulation purposes. The file can be accessed at: <https://tinyurl.com/4h8x9f94>.

B.2 RoboDK 3D Environment

The file `roboDK3D.rdk` is the 3D environment file for RoboDK, which contains the 3D model of the robotic additive manufacturing cell available at <https://tinyurl.com/bddd4zdw>. Within RoboDK, there is a Python environment where the file `robodk_move.py` is used to subscribe to the MQTT data sent from the robot controller via Mosquitto, converting the data into the 3D simulation. The files can be accessed at: <https://tinyurl.com/56a4fb3c>.

B.3 Node-RED Flow

The file `nodered_flow.json` contains the Node-RED flow responsible for subscribing to the data via MQTT. This flow performs the data conversion, displays the dashboard graphics, and sends the data to the Firestore cloud storage. The file can be accessed at: <https://tinyurl.com/2xwe7z6h>.

APPENDIX C – Research Dissemination Through Peer-Reviewed Publications During the Master’s Program

The following peer-reviewed publications were developed from the results, methodologies, and academic activities carried out throughout this master’s program. These contributions reflect the scientific dissemination and impact of the research and are organized by type of publication.

C.1 Journal Articles

A. J. Álvares, B. S. Figueroa, J. V. A. Cabral and I. Lacroix, “Automated defect classification in additive manufacturing LMD-wire using deep learning”, *Journal of the Brazilian Society of Mechanical Sciences and Engineering*, vol. 47, p. 432, 2025. DOI: [10.1007/s40430-025-05740-5](https://doi.org/10.1007/s40430-025-05740-5).

A. J. Alvares, E. Rodriguez and B. S. Figueroa, “Digital Twin-enabled process monitoring for a robotic additive manufacturing cell using wire-based laser metal deposition”, *Processes*, vol. 13, no. 8, 2025. DOI: [10.3390/pr13082335](https://doi.org/10.3390/pr13082335)

A. J. Alvares, I. Lacroix, M. A. de Lima Maron and B. S. Figueroa, “Desenvolvimento de uma célula de manufatura aditiva robotizada baseada no processo deposição de metal à laser usando arame de soldagem”, *Peer Review*, vol. 5, no. 21, pp. 17–39, 2023. DOI: [10.53660/1102.prw2664](https://doi.org/10.53660/1102.prw2664).

A. Alvares, I. Lacroix, M. Maron and B. S. Figueroa, “Robotic additive manufacturing by laser metal deposition in the context of Industry 4.0”, *Concilium*, 2023. DOI: [10.53660/CLM-2571-23U13](https://doi.org/10.53660/CLM-2571-23U13).

C.2 Book Chapters

B. S. Figueroa, L. Araújo and A. Alvares, “Development of a digital twin for a laser metal deposition (LMD) additive manufacturing cell”, in *Advances in Automation and Robotics Research. LACAR 2023*, M. N. Cardona, J. Baca, C. Garcia, I. G. Carrera, and C. Martinez, Eds., *Lecture Notes in Networks and Systems*, vol. 940, Cham: Springer, 2024. DOI: [10.1007/978-3-031-54763-8_7](https://doi.org/10.1007/978-3-031-54763-8_7).

C.3 Conference Papers

B. S. Figueroa and A. Alvares, “Development of a robotic additive manufacturing cell based on the LMD-Wire process”, *Lecture Notes in Mechanical Engineering (LNME)*, Springer, 2025.

B. S. Figueroa and A. Alvares, “Methodological approach to the development of a robotic additive manufacturing cell based on LMD-Wire”, in *Proceedings of the XVI Ibero-American Congress of Mechanical Engineering (CIBIM)*, Springer, 2025.

B. S. Figueroa and A. Alvares, “Metodología para el desarrollo de una célula de manufactura aditiva robótica basada en el sistema de deposición de metal por láser (LMD)”, in *Actas del XVI Congreso Iberoamericano de Ingeniería Mecánica (CIBIM)*, 2024, <https://e-spacio.uned.es/bitstreams/950ddc4a-0564-4b7f-91f5-dfd96d18d083/download>

B. S. Figueroa, C. I. Riaño, C. A. Peña and A. Alvares, “Artificial vision system for digital inspection of dimensional and geometric measurements in closed-loop manufacturing architecture”, in *Proc. 2024 IEEE Latin American Conference on Computational Intelligence (LA-CCI)*, 2024, pp. 1, DOI: [10.1109/LA-CCI62337.2024.10814821](https://doi.org/10.1109/LA-CCI62337.2024.10814821)

A. Alvares, C. Zhu, L. S. da Silva, T. Tankova, I. Lacroix and B. S. Figueroa Betancourth, “Development of a robotic additive manufacturing cell based on laser metal deposition process at the University of Coimbra and University of Brasília”, in *Proc. 27th International Congress of Mechanical Engineering (COBEM)*, 2023, DOI: [10.26678/ABCM.COBEM2023.COB2023-0718](https://doi.org/10.26678/ABCM.COBEM2023.COB2023-0718)

A. Alvares, I. Lacroix, M. A. Maron, B. S. Figueroa Betancourth and L. S. D. A. Araújo, “Development of a digital twin for a robotic additive manufacturing system based on laser metal deposition (LMD) process”, in *Proc. 27th International Congress of Mechanical Engineering (COBEM)*, 2023, DOI: [10.26678/ABCM.COBEM2023.COB2023-0208](https://doi.org/10.26678/ABCM.COBEM2023.COB2023-0208)

APPENDIX D – Implementation Cost of the Robotic Additive Manufacturing Cell

Table 16 presents the estimated costs associated with the implementation of the Robotic Additive Manufacturing Cell (RAMC), including transportation and setup in Brasília. The values are given in Brazilian reais (BRL) and converted to U.S. dollars (USD) based on exchange rates of 1 USD = 5.5 BRL.

Table 16 – Implementation Costs of the RAMC (in BRL and USD)

Item	Cost (R\$)	Cost (USD)
Meltio system (including transport)	580,000.00	105,454.55
KUKA robot (including transport)	268,000.00	48,727.27
Safety relay, cables, 24V power supply, buttons, connectors	7,000.00	1,272.73
Galvanized steel cabin, doors, rails, locks, paint, and electrical installation	30,000.00	5,454.55
Computer with RTX 4850 GPU	20,000.00	3,636.36
Uninterruptible Power Supply (UPS)	4,000.00	727.27
Laser filters P1P10 for doors and camera	4,000.00	727.27
Infrared camera	4,000.00	727.27
Two USB cameras	1,500.00	272.73
Consumables (substrates, 300 kg of 316L wire, 500 kg of ER70S, 2 Ar cylinders)	40,000.00	7,272.73
Total	958,500.00	174,272.73

APPENDIX E – Resumo Estendido em Língua Portuguesa

Título: Desenvolvimento de uma Célula de Manufatura Aditiva Robotizada Baseada no Processo Deposição de Metal a Laser Usando Arame

Autor: Brayan Stiven Figueroa Betancourth

Orientador: Alberto José Alvares

Programa de Pós-Graduação em Sistemas Mecatrônicos

Brasília, 27 de Julho de 2025

Palavras-chave: Célula de Manufatura Aditiva. Robôs. Deposição de Metal à Laser. Gêmeo Digital.

Introdução

A manufatura aditiva (MA) tem transformado significativamente a produção industrial ao viabilizar a fabricação de componentes complexos por meio da deposição sequencial de material baseada em dados digitais ([RASIYA; SHUKLA; SARAN, 2021](#)). Essa tecnologia consolidou-se como um recurso estratégico em setores como o aeroespacial e o automotivo, nos quais o alto desempenho, a customização e a eficiência no uso de materiais são requisitos essenciais ([WONG; HERNANDEZ, 2012](#)). Ao permitir a produção de geometrias intrincadas e a minimização de desperdícios, a MA contribui para fluxos de trabalho mais ágeis e economicamente viáveis em ambientes de manufatura inteligente ([ZENISEK; WILD; WOLFARTSBERGER, 2021](#)).

Entre as técnicas de MA, o processo de Deposição de Metal a Laser com Alimentação por Arame (LMD-Wire) tem ganhado destaque devido à sua capacidade de fabricar estruturas metálicas de grande porte, com ligações metalúrgicas robustas e propriedades mecânicas adaptáveis ([MELTIO, 2023](#)). A utilização de um laser de alta potência para fundir o arame metálico durante a deposição torna o processo particularmente adequado para operações de reparo, reforço de peças e produção de componentes estruturais em aplicações críticas ([ARREGUI et al., 2018](#)). Além disso, a integração do LMD-Wire com sistemas inteligentes de manufatura aprimora a estabilidade e o controle do processo, por meio da aquisição de dados em tempo real e de mecanismos adaptativos de retroalimentação ([ZAPATA et al., 2022](#)).

A incorporação de robôs industriais na MA tem impulsionado o desenvolvimento de células robóticas de manufatura aditiva (CMAR) flexíveis e automatizadas, que combinam a precisão e repetibilidade dos sistemas robóticos com a versatilidade da MA (ALVARES et al., 2023). Essas células facilitam a produção de peças com geometrias complexas adaptadas a requisitos específicos, aumentando a eficiência, a segurança e a adaptabilidade dos processos de fabricação. Além disso, a automação robótica permite a implementação de estratégias avançadas de manufatura, como deposição em múltiplos eixos e otimização dinâmica de materiais, essenciais para alcançar sistemas produtivos eficientes e adaptáveis (GIBSON et al., 2022).

Gêmeos Digitais (GD) têm emergido como ferramentas fundamentais para a otimização e o controle de processos de MA em ambientes de manufatura inteligente. Os DTs possibilitam a simulação e o monitoramento em tempo real do comportamento da CMAR, por meio da integração de dados operacionais e parâmetros críticos, como velocidade de deposição, energia do laser e distribuição de material (SHAO; HELU, 2020). Essa capacidade de simular proativamente e ajustar o processo contribui não apenas para a melhoria da qualidade das peças fabricadas, mas também para a redução do tempo de produção e dos custos operacionais (LIU et al., 2022). A integração do processo LMD-Wire, da automação robótica e dos GD em uma arquitetura de Manufatura Inteligente representa uma solução robusta e eficiente para a produção de componentes metálicos avançados em ambientes industriais exigentes (FIGUEROA; ARAÚJO; ALVARES, 2023).

Este trabalho apresenta o desenvolvimento de uma Célula Robótica de Manufatura Aditiva (CMAR) que integra o processo LMD-Wire com automação robótica e tecnologias digitais. O sistema foi fisicamente construído com a coordenação de componentes, incluindo um manipulador robótico KUKA KR70 R2100 de seis eixos, a unidade de deposição Meltio Engine, mecanismos de segurança e uma plataforma de controle modular. A integração lógica permitiu a sincronização entre o robô e o cabeçote de deposição, possibilitando o controle preciso do movimento multieixos. Adicionalmente, foi desenvolvido um ambiente CAD/CAPP/CAM em conformidade com a norma ISO 23247 (ISO, 2021), permitindo o planejamento, a simulação e o monitoramento em tempo real do processo de fabricação. Uma arquitetura de GD foi empregada para aprimorar a rastreabilidade do sistema, a precisão da simulação e a supervisão automatizada do processo. A validação experimental foi conduzida por meio da fabricação de diferentes peças de estudo de caso. Posteriormente, os componentes impressos foram submetidos a análises dimensionais, exames metalográficos, caracterizações mecânicas e classificação de defeitos visuais, com o objetivo de avaliar a precisão da manufatura, a integridade estrutural e a qualidade superficial.

Materiais e Métodos

A Figura 76 apresenta a arquitetura da CMAR dentro de um sistema integrado CAD/CAPP/CAM, ilustrando o fluxo dos principais insumos e saídas críticas. O processo inicia-se com múltiplas entradas, incluindo parâmetros de impressão, sinais lógicos, gás argônio, peso de calibração do robô, líquido de resfriamento, arquivos STL e fio metálico de deposição. Esses insumos são processados no interior da CMAR, que consiste em uma cabine metálica segura contendo o sistema robótico KUKA KR70 R2100 de seis eixos e o módulo Meltio Engine, ambos gerenciados por um sistema de segurança e mesas de impressão de alta precisão. A arquitetura é responsável por transformar modelos digitais em comandos robóticos, seguindo estratégias de deposição alinhadas com a norma ISO 23247. As saídas do sistema incluem a peça final impressa, os dados do processo e os GD do robô KUKA, do software RoboDK e do sistema Meltio, os quais possibilitam o monitoramento em tempo real, a análise de dados e a otimização por meio de painéis 2D e serviços em nuvem, contribuindo significativamente para o controle e a eficiência operacional.

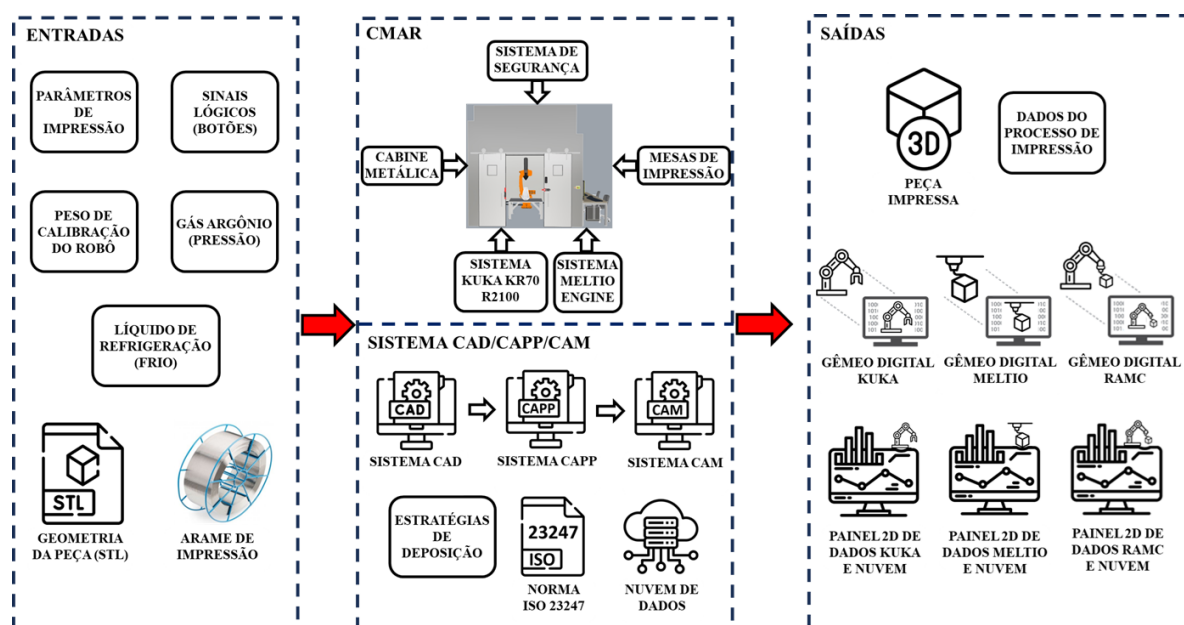


Figure 76 – Sistema Robótico de Manufatura Aditiva. Adapted from (FIGUEROA; ÁLVARES, 2025b).

A modelagem da CMAR foi realizada com base na metodologia IDEF0, proporcionando uma representação estruturada da integração física e lógica, juntamente com o sistema CAD/CAPP/CAM. Este modelo descreve os principais componentes, interações e fluxos de processo necessários para a operação da célula, assegurando conformidade com os padrões industriais. Os diagramas e a metodologia IDEF0 encontram-se disponíveis no repositório GitHub, acessível por meio do link: <https://tinyurl.com/5a286v7b>, servindo como referência para análise funcional e otimização do sistema.

Resultados e Discussões

A Figura 77 apresenta a arquitetura física e digital da CMAR. A Seção (A) exibe a célula física, composta pelo robô KUKA KR 70 R2100 de seis eixos, sistema Meltio Engine, controladores, sensores, sistema de segurança, cabine metálica e mesa de impressão. Essa configuração permite a coleta de dados em tempo real para o monitoramento do processo, proporcionando rastreabilidade e otimização da manufatura. Uma transmissão ao vivo da célula física durante o processo de impressão pode ser acessada em: <https://youtu.be/YS4s6kc01EY>.

A Seção (B) apresenta o GD, desenvolvido para simulação e monitoramento do sistema. Um modelo 3D é integrado ao ambiente RoboDK para replicar a cinemática do robô, enquanto o Node-RED gerencia a aquisição de dados, incluindo posições articulares, velocidades e temperaturas. As plataformas Meltio Dashboard e KUKA iiQoT otimizam o monitoramento da deposição e do estado operacional do robô, com os dados sendo armazenados na nuvem Google Firestore para análise posterior. O funcionamento do GD, que evidencia a sincronização entre simulação e realidade, está disponível em: <https://youtu.be/9YS4lmhMfYE>.

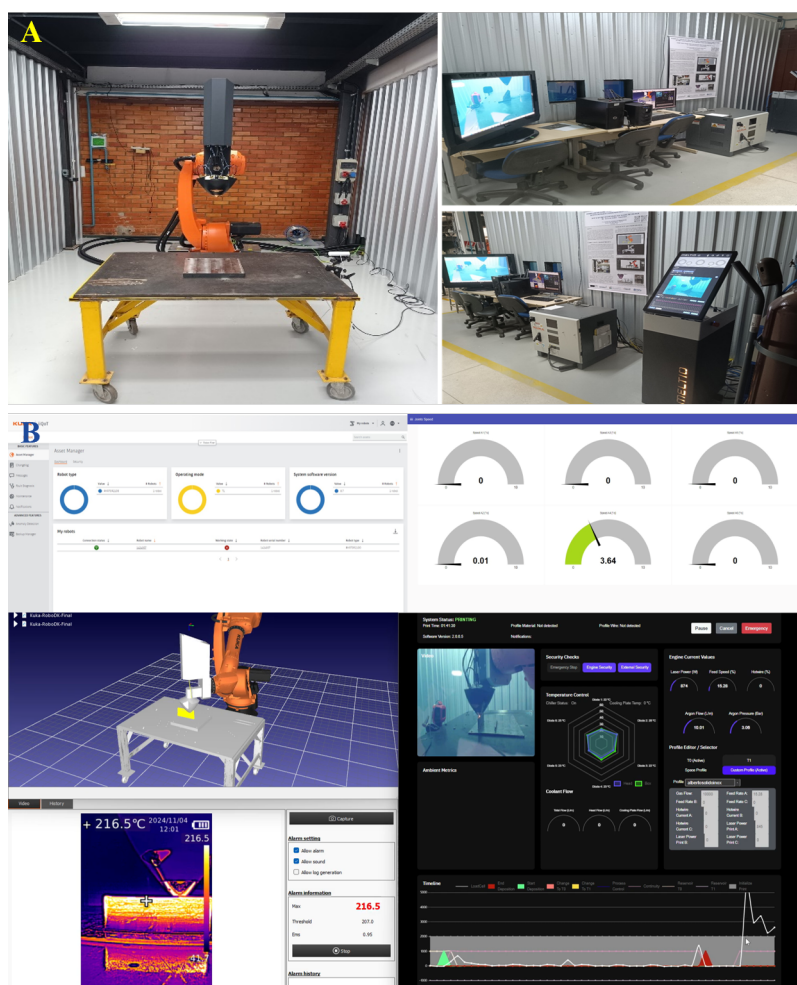


Figure 77 – Sistema Físico e Gêmeo Digital da RAMC.

Casos de estudo

A Figura 78 apresenta três casos de estudo considerados nesta pesquisa, nos quais se avaliam distintas estratégias de deposição e parâmetros de impressão no âmbito da manufatura aditiva a laser com alimentação por arame metálico. A Tabela 17 resume de forma estruturada os principais parâmetros empregados na produção das peças, incluindo a potência do laser, a velocidade do arame, o diâmetro de 1 mm do arame em aço inoxidável 316 LSi, a velocidade de impressão, a vazão do gás de proteção, a altura e a largura da camada, bem como o software de fatiamento 3D e a estratégia de deposição adotada.

Em todos os casos de estudo, utilizam-se os softwares Meltio Space e Rhino3D/Grasshopper para a importação das geometrias no formato STL, a definição das trajetórias de deposição e a geração do código em linguagem KUKA Robot Language (KRL), necessário à programação do robô industrial. Este fluxo metodológico assegura a correspondência entre os parâmetros de deposição e as características geométricas das peças, favorecendo a repetibilidade do processo e a adequação das condições operacionais ao perfil de cada amostra. Além disso, a integração entre parâmetros e estratégias de deposição contribui para o controle dimensional, a estabilidade do cordão fundido e a mitigação de defeitos, aspectos fundamentais para a confiabilidade e a consistência do processo de manufatura aditiva com arame.

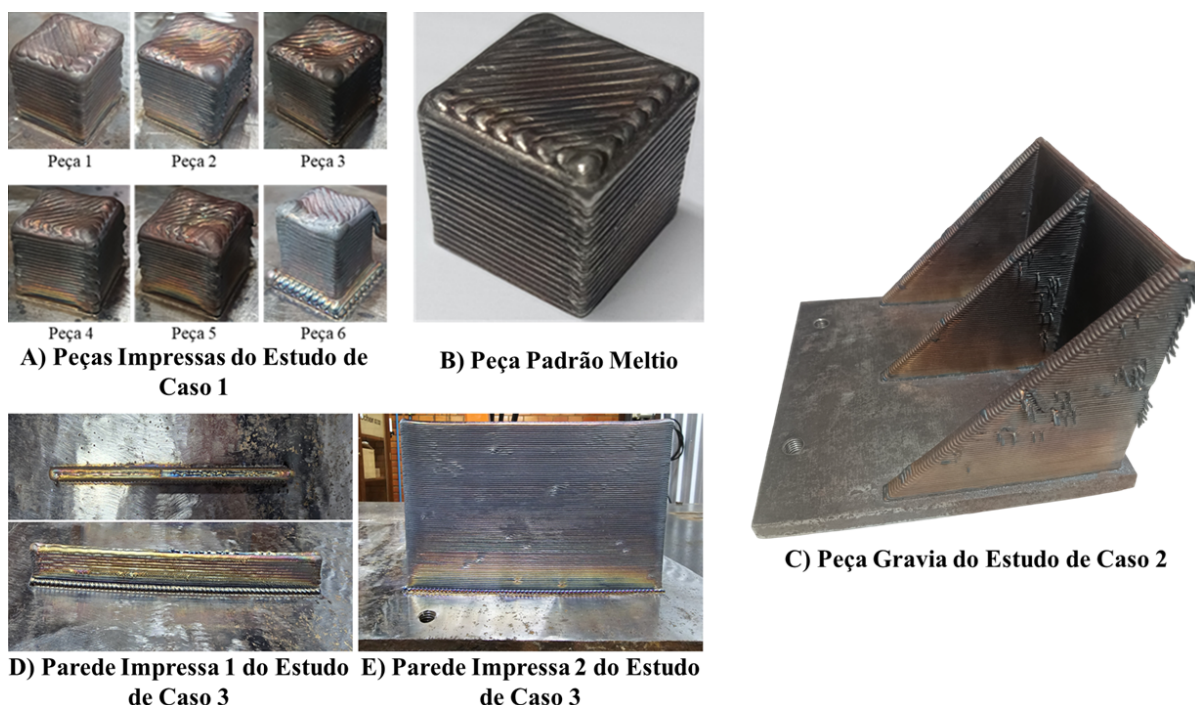


Figure 78 – Peças impressas dos casos de estudo. Adapted from (FIGUEROA; ÁLVARES, 2025a).

Table 17 – Parâmetros de deposição de todos os casos de estudo.

Peça	Potência Laser [W]	Veloc. Arame [mm/s]	Veloc. Im-pressão [mm/s]	Vazão de Gás [ml/min]	Altura Camada [mm]	Largura Camada [mm]	Software de Fatiamento 3D	Estratégia de Deposição
Part 1	860	15.3	10	12000	1.2	1	Grasshopper	Rectilinear in-fill
Part 2	860	15.3	10	12000	1.2	1	Grasshopper	Rectilinear in-fill
Part 3	860	15.3	10	12000	1.2	1	Grasshopper	Rectilinear in-fill
Part 4	860	15.3	10	12000	1.2	1	Grasshopper	Rectilinear + 0.1 mm Overlap
Part 5	860	15.3	10	12000	1.2	1	Grasshopper	Rectilinear + 0.2 mm Overlap
Part 6	845	15.28	10	10000	1.2	1	Meltio Space	Rectilinear in-fill + 2 mm Raft
Gravia	874	15.28	10	10000	1.2	1	Meltio Space	Linear infill
Wall 1	845	15.28	7.5	10000	1.2	1	Meltio Space	Linear infill + 2 mm Raft
Wall 2	845	15.28	10	10000	1.2	1	Meltio Space	Linear infill + 2 mm Raft

No Estudo de Caso 1, foram fabricados seis cubos com dimensões de 30 mm (altura) \times 30 mm (comprimento) \times 30 mm (largura), utilizando diferentes combinações de parâmetros de deposição, conforme apresentado na Tabela 17 (Peças 1 a 6) e ilustrado na Figura 78 (A). A peça padrão da Meltio (Figura 78 (B)) foi adotada como referência para a avaliação da qualidade da impressão, servindo como modelo comparativo do processo de deposição. A análise considerou o acabamento superficial, a precisão dimensional e a integridade da deposição. Com base em inspeções visuais e medições realizadas, foram identificados defeitos como formação de esferas (balling) e interrupções no fluxo de material, frequentemente associados à calibração inadequada do laser durante o processo de deposição.

No Estudo de Caso 2, foi produzido um suporte estrutural voltado para aplicações industriais, com dimensões de 99,6 mm (altura) \times 149,5 mm (comprimento) \times 104,2 mm (largura), destinado à empresa Gravia (Figura 78 (C)). O modelo foi desenvolvido no ambiente Rhino3D e fabricado com base nos parâmetros descritos na Tabela 17. De maneira semelhante ao primeiro estudo, foram avaliados o acabamento superficial, a precisão geométrica e a qualidade da deposição. Os resultados evidenciaram a presença de falhas recorrentes, como stubbing e balling, atribuídas principalmente a uma calibração inadequada do sistema de laser.

No Estudo de Caso 3, duas paredes com geometria idêntica de 100 mm (altura) \times 180 mm (comprimento) \times 3 mm (largura) foram impressas, adotando-se diferentes combinações de parâmetros de deposição (Figuras 78 (D) e (E)). Na peça mostrada na Figura 78 (D), a velocidade do robô provocou um desequilíbrio na deposição de material, impossibilitando a fusão adequada e levando à interrupção do processo. Em contrapartida, a peça representada

na Figura 78 (E) foi impressa com velocidades ajustadas e com nova calibração do sistema de laser, o que resultou em maior qualidade na deposição e mitigação dos defeitos anteriormente observados.

Conclusão

Esta pesquisa demonstrou o desenvolvimento e a validação bem-sucedida de uma CMAR baseada no processo LMD-Wire, integrando automação robótica, tecnologias de GD e sistemas CAD/CAPP/CAM para aprimorar a eficiência, a precisão e a automação do processo. A aplicação de uma metodologia estruturada com base no modelo IDEF0 permitiu a integração fluida dos componentes de hardware e software, enquanto a implementação de três modelos de GD contribuiu significativamente para o monitoramento em tempo real, o controle do processo e a capacidade preditiva. Os estudos de caso experimentais confirmaram a viabilidade, a repetibilidade e a confiabilidade do sistema proposto, evidenciando seu potencial para o avanço da MA inteligente e flexível, alinhada aos princípios da Indústria 4.0.

Referências

- ALVARES, A.; LACROIX, I.; MARON, M.; FIGUEROA, B. Robotic additive manufacturing by laser metal deposition in the context of industry 4.0: Manufatura aditiva robotizada por deposição de metal a laser no contexto da indústria 4.0. **Concilium**, v. 23, n. 23, p. 79–103, 2023. Cit. on p. 148.
- ARREGUI, L.; GARMENDIA, I.; PUJANA, J.; SORIANO, C. Study of the Geometrical Limitations Associated to the Metallic Part Manufacturing by the LMD Process. **Procedia CIRP**, v. 68, n. 1, p. 363–368, 2018. Cit. on p. 147.
- FIGUEROA, B. S.; ÁLVARES, A. Development of a robotic additive manufacturing cell based on the LMD-Wire process. In: LECTURE Notes in Mechanical Engineering (LNME). Springer, 2025a. Cit. on p. 151.
- FIGUEROA, B. S.; ÁLVARES, A. Methodological approach to the development of a robotic additive manufacturing cell based on LMD-Wire. In: PROCEEDINGS of the XVI Ibero-American Congress of Mechanical Engineering (CIBIM). Springer, 2025b. Cit. on p. 149.
- FIGUEROA, B. S.; ARAÚJO, L.; ALVARES, A. Development of a Digital Twin for a Laser Metal Deposition (LMD) Additive Manufacturing Cell. In: PROCEEDINGS of the Latin American Congress on Automation and Robotics. 2023. Cit. on p. 148.

- GIBSON, B. T.; MHATRE, P.; BORISH, M. C.; ATKINS, C. E.; POTTER, J. T.; VAUGHAN, J. E.; LOVE, L. J. Controls and process planning strategies for 5-axis laser directed energy deposition of Ti-6Al-4V using an 8-axis industrial robot and rotary motion. **Additive Manufacturing**, Elsevier, v. 58, p. 103048, 2022. Cit. on p. 148.
- ISO. **ISO 23247-1: Automation systems and integration—digital twin framework for manufacturing—Part 1: overview and general principles**. International Organization for Standardization Geneva, Switzerland, 2021. Cit. on p. 148.
- LIU, C.; LE ROUX, L.; KÖRNER, C.; TABASTE, O.; LACAN, F.; BIGOT, S. Digital twin-enabled collaborative data management for metal additive manufacturing systems. **Journal of Manufacturing Systems**, p. 857–874, 2022. Cit. on p. 148.
- MELTIO. **What is Laser Metal Deposition**. 2023. Available from: <<https://meltio3d.com/what-is-laser-metal-deposition>>. Cit. on p. 147.
- RASIYA, G.; SHUKLA, A.; SARAN, K. Additive manufacturing-a review. **Materials Today: Proceedings**, Elsevier, v. 47, p. 6896–6901, 2021. Cit. on p. 147.
- SHAO, G.; HELU, M. Framework for a digital twin in manufacturing: Scope and requirements. **Manufacturing letters**, p. 105–107, 2020. Cit. on p. 148.
- WONG, K. V.; HERNANDEZ, A. A review of additive manufacturing. **International scholarly research notices**, v. 2012, n. 1, p. 208760, 2012. Cit. on p. 147.
- ZAPATA, A.; BERNAUER, C.; STADTER, C.; KOLB, C. G.; ZAEH, M. F. Investigation on the cause-effect relationships between the process parameters and the resulting geometric properties for wire-based coaxial laser metal deposition. **Metals**, MDPI, v. 12, n. 3, p. 455, 2022. Cit. on p. 147.
- ZENISEK, J.; WILD, N.; WOLFARTSBERGER, J. Investigating the Potential of Smart Manufacturing Technologies. **Procedia Computer Science**, v. 180, p. 507–516, 2021. DOI: [10.1016/j.procs.2021.01.269](https://doi.org/10.1016/j.procs.2021.01.269). Cit. on p. 147.